UNIVERSIDADE FEDERAL DO RIO GRANDE DO SUL

INSTITUTO DE PESQUISAS HIDRÁULICAS

PROGRAMA DE PÓS-GRADUAÇÃO EM RECURSOS HÍDRICOS E SANEAMENTO AMBIENTAL

VINÍCIUS ALENCAR SIQUEIRA

MODELAGEM E PREVISÃO HIDROLÓGICA EM ESCALA CONTINENTAL PARA A AMÉRICA DO SUL

PORTO ALEGRE

2022

VINÍCIUS ALENCAR SIQUEIRA

MODELAGEM E PREVISÃO HIDROLÓGICA EM ESCALA CONTINENTAL PARA A AMÉRICA DO SUL

Tese apresentada ao Programa de Pós-graduação em Recursos Hídricos e Saneamento Ambiental da Universidade Federal do Rio Grande do Sul, como requisito parcial à obtenção do grau de Doutor.

Orientador: Walter Collischonn

Co-orientador: Rodrigo Cauduro Dias de Paiva

PORTO ALEGRE

2022

:

Siqueira, Vinícius Alencar
Modelagem e previsão hidrológica em escala continental para a América do Sul / Vinícius Alencar Siqueira. -- 2022.
263 f.
Orientador: Walter Collischonn.

Coorientador: Rodrigo Cauduro Dias de Paiva.

Tese (Doutorado) -- Universidade Federal do Rio Grande do Sul, Instituto de Pesquisas Hidráulicas, Programa de Pós-Graduação em Recursos Hídricos e Saneamento Ambiental, Porto Alegre, BR-RS, 2022.

1. Modelagem hidrológica. 2. Previsão de vazões. 3. América do Sul. 4. Previsão meteorológica. 5. Modelagem hidrodinâmica. I. Collischonn, Walter, orient. II. Cauduro Dias de Paiva, Rodrigo, coorient. III. Título.

VINÍCIUS ALENCAR SIQUEIRA

MODELAGEM E PREVISÃO HIDROLÓGICA EM ESCALA CONTINENTAL PARA A AMÉRICA DO SUL

Tese apresentada ao Programa de Pós-graduação em Recursos Hídricos e Saneamento Ambiental da Universidade Federal do Rio Grande do Sul, como requisito parcial à obtenção do grau de Doutor.

Aprovado em: Porto Alegre, 22 de fevereiro de 2022.

_____

Prof. Dr. Walter Collischonn – UFRGS
Orientador

_____

Prof. Dr. Rodrigo Cauduro Dias de Paiva – UFRGS
Co-orientador

_____

Prof. Dr. Carlos Henrique Ribeiro Lima – UNB
Examinador

_____

Prof. Dr. Eduardo Mario Mendiondo – USP
Examinador

_____

Prof. Dr. Juan Martin Bravo – UFRGS
Examinador

“The history of science, like the history of all human ideas, is a history of irresponsible dreams, of obstinacy, and of error. But science is one of the very few human activities perhaps the only one in which errors are systematically criticized and fairly often, in time, corrected. This is why we can say that, in science, we often learn from our mistakes, and why we can speak clearly and sensibly about making progress there.”

—Karl R. Popper

Agradecimentos

Agradeço primeiramente a meus pais Sílvio e Inês que, na humildade, muito batalharam para me proporcionar toda educação necessária e dar as condições para que fosse possível iniciar esta longa jornada universitária;

À Universidade Federal do Rio Grande do Sul (UFRGS), por ter disponibilizado toda a estrutura necessária para meu crescimento profissional e acadêmico, desde os meus primeiros contatos com os cursos de Engenharia Civil e Engenharia Ambiental até a conclusão no doutorado;

Ao CNPq e à CAPES pelo suporte financeiro da pesquisa;

À Adriana, por todos os ensinamentos ao longo dos últimos 14 anos, pelo companheirismo, por me proporcionar inúmeras experiências Brasil afora, pela coragem em enfrentar as distâncias impostas tanto por decisões profissionais que tomamos quanto pela pandemia do Covid-19, e pelo suporte físico e emocional nas horas que mais precisei. Você foi e sempre será um exemplo de afeto, lealdade, responsabilidade e sucesso acadêmico. Muito obrigado por fazer parte da minha vida;

Ao meu orientador e co-orientador, professores Walter Collischonn e Rodrigo Paiva, pela transferência de conhecimento, pelas ideias e soluções aportadas à tese, pela motivação, e por todo o apoio nos momentos de dificuldade e nas decisões que tiverem que ser tomadas ao longo do caminho. Tenho muita admiração pela postura profissional e humana de vocês, e por liderarem um grupo de pesquisa onde os alunos são ouvidos e tratados com igualdade e respeito independente de gênero e grau acadêmico. Com certeza vocês tiveram um papel muito importante para que este trabalho se tornasse realidade;

Aos demais membros do corpo docente do Instituto de Pesquisas Hidráulicas (IPH), em especial aos professores com quem tive a oportunidade de aprender nas disciplinas cursadas ao longo da pós-graduação (o que inclui o período de Mestrado) ou interagir em projetos de pesquisa: professores Joel, Fernando “Bike”, Olavo, Beatriz, Nilza, Louzada, Masato, André e Carlos André. Um agradecimento especial ao professor Juan Martín Bravo pelas contribuições feitas à tese (qualificação e banca final), pelos mais diversos auxílios, conselhos e conhecimentos que me foram passados ao longo da minha trajetória como estudante, e por ser esta pessoa humilde e íntegra para a qual tenho grande admiração;

Gostaria de agradecer especialmente aos professores membros do grupo de pesquisa em Hidrologia de Grande Escala (HGE) Fernando Fan e Anderson Ruhoff, e aos pesquisadores associados do grupo de pesquisa Paulo Pontes, Mino Sorribas e Adrien Paris, por me transmitirem conhecimento de hidrologia, pelas boas conversas, bom humor e pela colaboração direta em publicações ou projetos de pesquisa que originaram desta tese de doutorado;

Aos colegas do HGE: Alice, Aline, Anderson, Arthur, Ayan, Bibiana, Camila, Cléber, Erik, Gabriel, Germano, Gustavo, Hugo, Ingrid, Jéssica, João Paulo, Júlio, Katiúcia, Larissa, Leonardo, Lucas, Maria Eduarda, Maurício, Otávio, Pedro, Rafael(s), Renata, Sly, Sofia, Thainá, Thaís e Vinícius, pelas interações científicas ao longo do doutorado. Gostaria de direcionar um agradecimento especial ao colega e amigo Ayan pelo envolvimento de longa data em projetos de pesquisa, atividades de extensão e publicação de artigos, e também à Aline pelo auxílio durante a etapa inicial de coleta de dados para a tese. Agradeço ao João Paulo pela grande parceria e conversas técnico-filosóficas envolvendo o MGB–SA. Estendo também os meus agradecimentos a tod@s demais colegas do IPH — em especial ao pessoal dos grupos de pesquisa GPDEN e NESH — pelas inúmeras boas conversas, bom humor, parcerias musicais (violão, voz e cajón), viagens e partidas de vôlei, que certamente fizeram com que o desenvolvimento deste trabalho fosse um pouco menos árduo;

Aos amigos Ayan Fleischmann, Hugo Fagundes, Sly Wongchuig, João Paulo Brêda, Thiago (Zé) Tavares, Benício Monte, Cléber Gama, Jéferson Ferreira, Martha Weizenmann e Yara Breda por terem cedido um espaço em suas casas e me hospedado durante as minhas idas e vindas de Porto Alegre em função do doutorado. Sou muito grato por este apoio!

Ao professor Albrecht Weerts, que me recebeu e orientou durante o período de doutorado sanduíche realizado na Deltares, Holanda. Agradeço também à Jan Verkade e Bastian Klein pelo apoio no pós-processamento de previsões hidrológicas, além dos colegas da Deltares Rodolfo Montero, Bastiaan Vuyk e Yiqun Sun pela parceria e boas conversas. Agradeço também à *Technisiche Universiteit* (TU) Delft pela disponibilização da biblioteca, cujo ambiente foi muito propício para dar continuidade à tese de doutorado. Gostaria de deixar um agradecimento também à Thaine Assumpção, Victor Paca e Daniel Guzzo por terem me prestado importante auxílio no processo de acomodação em Delft.

À Maria-Helena Ramos pelas contribuições feitas à tese, pela boa disposição em sanar minhas dúvidas relacionadas ao tema de previsão hidrológica por conjunto, bem como por todo o suporte dado durante processos de publicação de artigo. Agradeço também ao Javier

Tomasella pelas importantes contribuições fornecidas na etapa de qualificação, e aos professores Carlos Henrique Ribeiro Lima e Eduardo Mario Mendiondo pelas críticas positivas, comentários e sugestões para pesquisas futuras que foram debatidos durante a defesa deste trabalho.

À *Universidad de Los Lagos* e à *Universitat de Barcelona* também pela disponibilização da infraestrutura das bibliotecas, as quais foram fundamentais para o avanço desta tese. Igualmente gostaria de agradecer ao Julien pela hospitalidade e por ceder inúmeras vezes um espaço e uma tomada para meu computador na cafeteria El Francés.

Resumo

A América do Sul (AS) possui uma área de ~17,8 milhões de km² e contribui com cerca de 30 % do volume total de água escoado para os oceanos. Gerenciar os recursos hídricos continentais na AS é uma tarefa desafiadora devido à heterogeneidade das características climáticas, suscetibilidade a cheias e secas, complexidade dos sistemas de rios e existência de usos múltiplos da água, em particular a produção de energia onde a hidroeletricidade corresponde por ~50 % da capacidade instalada na AS. Previsões de vazão, por exemplo, são essenciais para a operação de reservatórios e para melhorar a preparação contra eventos extremos, os quais podem ocorrer em múltiplas escalas espaciais e afetar extensas áreas inclusive para além de fronteiras políticas. Neste sentido, há necessidade de ferramentas que possibilitem quantificar fluxos hidrológicos com consistência espaço-temporal na AS, bem como prever a condição futura dos rios com estimativa de incerteza para dar suporte à tomada de decisão. O objetivo desta tese foi estabelecer uma base técnica para modelagem hidrológica com abrangência da América do Sul e dar contribuições para previsão de vazões em escala continental, no horizonte de médio prazo (até 15 dias). O modelo hidrológico MGB foi adaptado para simulação hidrológica–hidrodinâmica em múltiplas bacias sul americanas a partir de técnicas de geoprocessamento, produtos de sensoriamento remoto e outras bases de dados globais. O modelo desenvolvido, denominado MGB–SA, teve representação satisfatória de vazões em intervalo de tempo diário, apresentando acurácia superior à de modelos globais estado-da-arte. Também foram representados de forma adequada padrões de sazonalidade e magnitude de evapotranspiração e armazenamento terrestre de água nas principais bacias da AS, com desempenho razoável para os níveis simulados. Através de um experimento de previsão que assume o modelo hidrológico como livre de erros, foi identificado que previsões de chuva por conjunto (*ensemble*) com horizonte de médio prazo podem contribuir para a destreza das previsões de vazão com até 15 dias à frente. Na avaliação de desempenho geral das previsões de vazão, observou-se maior destreza para regiões situadas ao leste e sudeste da América do Sul, incluindo bacias como Uruguai, Alto Paraná, São Francisco, Parnaíba e Tocantins-Araguaia. Em relação à discriminação entre ocorrência e não ocorrência de eventos de vazão elevada, a destreza da previsão foi maior nos rios do sul do Brasil. Além disso, as previsões exibiram maior destreza para acurácia geral e discriminação em regiões de clima temperado e úmido (sub-tropical). Quando considerados ambos os erros do modelo hidrológico e da precipitação prevista, as previsões de vazão com horizonte de médio prazo demonstraram baixa ou nenhuma destreza na maioria das localidades analisadas além de um grande viés probabilístico, com a maior parte das observações situando-se fora dos limites do conjunto mesmo para antecedências mais longas após 1 semana à frente. Com aplicação de pós-processamento estatístico a destreza das previsões de vazão aumentou substancialmente, melhorando a consistência estatística e proporcionando largura de incerteza geralmente inferior ao da climatologia das vazões observadas. O desempenho de séries temporais de previsão por conjunto obtidas de distribuições preditivas pós-processadas também foi avaliado, demonstrando limitações principalmente em condições de baixo espalhamento do conjunto bruto. Por fim, os resultados deste trabalho sugerem que o modelo desenvolvido pode servir como uma ferramenta para dar suporte a pesquisas que contemplem os recursos hídricos da AS de forma integrada, e que previsões de vazão com destreza no horizonte de médio prazo podem ser obtidas na escala continental mesmo com dados in situ limitados.

Palavras chave: Modelagem hidrológica. Modelo MGB. América do Sul. Previsão. Conjunto.

Abstract

South America (SA) has an area of ~17.8 million km² and contributes around 30 % of the global runoff to the oceans. Managing the continental waters in SA is a challenge given the wide range of climatic characteristics, susceptibility to floods and droughts, complexity of river systems and existence of multiple water uses, in particular the energy production where hydropower accounts for ~50 % of the total installed capacity. Streamflow forecasts, for instance, are essential for reservoir operation and to improve preparedness against extreme hydrometeorological events, which can occur on multiple spatial scales and affect extensive regions including areas beyond the political boundaries. In this context, there is a need for tools that enable to quantify hydrological fluxes in SA with spatiotemporal consistency, as well as to predict future river conditions with uncertainty estimates to support decision making. The objective of this thesis was to establish a technical basis for hydrological modeling in the South America domain and contribute to medium-range (up to 15 days) streamflow forecasting at the continental scale. The MGB hydrological model was adapted for simulation of multiple South American basins by using hydrologic–hydrodynamic methods, geoprocessing techniques, remote sensing products and other global scale datasets. The developed model, named MGB–SA, showed a satisfactory representation of daily discharges and exhibited higher accuracy compared with state-of-the-art global models. Seasonality and magnitude of both evapotranspiration and terrestrial water storage were adequately represented at the scale of main SA basins, with a reasonable performance regarding the simulated water levels. Through a forecasting experiment that assumes the hydrological model as error-free, it was found that medium-range ensemble precipitation forecasts can contribute to the skill of streamflow forecasts up to 15 days ahead. Overall skill was higher in the eastern and southeastern SA regions, which include large basins such as Uruguay, Upper Paraná, São Francisco, Parnaíba and Tocantins-Araguaia. Skill in discrimination between the occurrence and non-occurrence of high flow events was mainly observed in rivers of southern Brazil. In addition, forecasts showed better skill in terms of overall quality and discrimination in warm temperate, fully humid regions. When the errors of both hydrological model and predicted precipitation were taken into account, medium-range streamflow forecasts exhibited low or no skill in most of the analyzed locations in addition to a large probabilistic bias, with most of the observations falling outside the ensemble limits even at longer lead times, after 1 week ahead. Statistical postprocessing substantially improved streamflow forecast skill, enhancing statistical consistency and generally providing lower uncertainty width compared with that of observed climatology. The performance of streamflow ensemble traces derived from postprocessed predictive distributions was also evaluated, showing limitations mainly in conditions for which the raw ensemble spread is low. Finally, the results of this work suggest that the developed model can be used to simulate the South American water resources in an integrated manner, and that skillful, medium-range streamflow forecasts could be obtained at the continental scale of SA even with limited in situ data.

Keywords: Hydrological modeling. MGB model. South America. Forecasting. Ensemble.

Lista de abreviações

ACF – *Autocorrelation Function*

ANA – Agência Nacional das Águas e Saneamento Básico

AROC – *Area under the ROC curve*

AS – América do Sul

AFFS – *African Flood Forecasting System*

BMA – *Bayesian Model Averaging*

CaMa-Flood – *Catchment-based Macro-scale Floodplain model*

CDF – *Cumulative Density Function*

CDR – *Climate Data Record*

CFL – *Courant-Friedrichs-Levy condition*

CMORPH – *Climate Prediction Center morphing method*

CRPS – *Continuous Ranked Probability Score*

CRPSS – *Continuous Ranked Probability Skill Score*

CR – *Coverage Rate*

CRU – *Climate Research Unit*

DGA – *Dirección General de Aguas*

DI – *Delay Index*

ECC – *Ensemble Copula Coupling*

ECC–T/Q/R (*ECC with Transformation / equally spaced Quantiles / Random sampling scheme*)

ECMWF – *European Center of Medium-range Weather Prediction*

EFAS – *European Flood Awareness System*

ENSO – *El Niño Southern Oscillation*

EM-DAT – *International Emergency Events Database*

EMOS – *Ensemble Model Output Statistics*

EPS – *Ensemble Prediction System*

ESP – *Ensemble Streamflow Prediction*

ERA-Interim – *Era Retrospective Analysis*

ET – *Evapotranspiration*

EWS – *Early Warning System*

FAO – *Food and Agriculture Organization*

FAR – *False Alarm Rate*

GDP – *Gross Domestic Product*

GEFS – *Global Ensemble Forecasting System*

GHM – *Global Hydrological Model*

GLDAS – *Global Land Data Assimilation System*

GloFAS – *Global Flood Awareness System*

GLOFFIS – *Global Flood Forecasting Information System*

GPCP – *Global Precipitation Climatology Project*

GRACE – *Gravity Recovery and Climate Experiment*

GRDC – *Global Runoff Database Center*

GSWP-2 – *Second Global Soil Wetness Project*

KGE – *Kling-Gupta Efficiency*

HAND – *Height Above the Nearest Drainage*

HEFS – *Hydrological Ensemble Forecast Service*

HEPEX – *Hydrological Ensemble Prediction EXperiment*

HG – *Hydraulic Geometry relationship*

HD – *Hydrodynamic*

HR – *Hit Rate*

HRU – *Hydrological Response Unit*

HTESSEL – *Tiled ECMWF Scheme for Surface Exchanges over Land incorporating land surface hydrology*

HydroSHEDS – *Hydrological data and maps based on SHuttle Elevation Derivatives at multiple Scales*

IDEAM – *Instituto de Hidrología, Meteorología y Estudios Ambientales*

IFS – *Integrated Forecast System*

INA – *Instituto Nacional del Agua*

ITCZ – *Intertropical Convergence Zone*

LAI – *Leaf Area Index*

LSM – *Land Surface Model*

MCS – *Mesoscale Convective System*

MDE – Modelo Digital de Elevação

MERIT-Hydro – *Multi-Error-Removed Improved-Terrain Hydrography dataset*

MERRA – *Modern-Era Retrospective analysis for Research and Applications*

MGB – Modelo de Grandes Bacias

MSWEP – *Multi-Source Weighted Ensemble Precipitation*

NOAA – *National Oceanic and Atmospheric Administration*

NSE – *Nash-Sutcliffe Efficiency*

NWP – *Numerical Weather Prediction*

ONS – Operador Nacional do Serviço Elétrico

ORE-HyBam – *Environmental Research Observatory for geodynamical, Hydrological and Biogeochemical control of erosion/alteration and material transport in the Amazon*

PDF – *Probability Density Function*

RC – *Runoff Coefficient*

RI – *Reliability Index*

RMSE – *Root Mean Square Error*

ROC – *Relative Operating Characteristic*

SACZ – *South Atlantic Convergence Zone*

SAMS – *South American Monsoon System*

SENAMHI – *Servicio Nacional de Meteorología y Hidrología*

SIN – Sistema Interligado Nacional

SRTM – *Shuttle Radar Topography Mission*

SS – *Sharpness skill*

TIGGE – *THORPEX Interactive Grand Global Ensemble*

TRMM – *Tropical Rainfall Measuring Mission*

TWS – *Terrestrial Water Storage*

VS – *Virtual Station*

WaterGAP – *Water - Global Assessment and Prognosis hydrological data model*

WCI – *Water Cycle Integrator*

WFDEI – *Watch Forcing Data applied to ERA Interim*

WRR – *Water Resources Reanalysis*

WSE – *Water Surface Elevation*

Sumário

CAPÍTULO 1: Introdução e contextualização

“Every new beginning comes from some other beginning’s end.”

—Seneca

1.1. **América do Sul: características e relevância do tema**

Os recursos hídricos continentais têm um papel importante no sistema terrestre, atuando nas trocas de água entre superfície, atmosfera e oceanos, bem como controle de ecossistemas e ciclos biogeoquímicos. A América do Sul (AS), com uma área de superfície de $17{,}8\times10^6$ km² que representa 12 % da massa continental da terra, contribui em média com 13.240 (± 2.430) km³ ano^{-1} de água doce para os oceanos, correspondendo a algo em torno de 30 % do escoamento total global (Clark *et al.*, 2015). Pelo fato de sustentar 6 dos 10 maiores rios do mundo em termos de vazão média anual (Tabela 1.1), a AS pode ser considerada como o "Continente das Águas" (Stevaux *et al.*, 2009), sendo drenada por bacias de enorme extensão geográfica como a do Amazonas (5,92 10^6 km²), Prata – Paraná/Paraguai/Uruguai (~3 10^6 km²), Orinoco (940 10^5 km²), Tocantins-Araguaia (775 10^5 km²) e São Francisco (654 10^5 km²).

Tabela 1.1. Lista dos rios com maior vazão média anual da América do Sul. Adaptado de Latrubesse *et al.* (2005).

#	Rio	Bacia	Vazão média anual (m³.s^{-1})[a]	Área de drenagem (km²)[b]	Escoamento médio anual (mm ano^{-1})
1	Amazonas	Amazonas	209.000	5.920.000	1.113
2	Orinoco	Orinoco	35.000	940.000	1.174
3	Madeira	Amazonas	32.000	1.370.000	737
4	Negro	Amazonas	28.400	716.000	1.251
5	Japurá	Amazonas	18.600	269.000	2.181
6	Paraná	Prata	18.000	2.600.000	218
7	Tapajós	Amazonas	13.500	495.000	860
8	Tocantins	Tocantins-Araguaia	11.800	775.000	480
9	Purus	Amazonas	11.000	379.000	915
10	Marañon	Amazonas	10.870	366.000	937
11	Xingu	Amazonas	9.700	515.000	594
12	Ucayali	Amazonas	9.544	355.000	848
13	Madre de Dios/Beni	Amazonas	8.920	283.000	994
14	Içá	Amazonas	8.800	122.000	2.275
15	Juruá	Amazonas	8.440	185.000	1.439
16	Mamoré	Amazonas	8.255	639.000	407
17	Guaviare	Orinoco	8.200	152.000	1.701
18	Magdalena	Magdalena	7.200	262.000	867
19	Araguaia	Tocantins-Araguaia	6.100	387.000	497
20	Caroní	Orinoco	5.000	92.000	1.714
21	Uruguai	Prata	4.660	352.000	417
22	Meta	Orinoco	4.600	109.000	1.331

[a]Latrubesse *et al.* (2005) e referências internas. As vazões médias anuais dos rios listados não correspondem necessariamente a um mesmo período de análise, portanto variações na posição desta lista são esperadas para médias calculadas com dados de vazões mais recentes.
[b]A área de drenagem aproximada dos rios foi atualizada com base no HydroSHEDS (Lehner *et al.*, 2008).

A distribuição da massa continental da AS sobre uma ampla faixa de latitudes (12º N–55º S), com vegetação variada e formas de relevo prominentes, favorece o desenvolvimento e atuação de diversos sistemas atmosféricos (Figura 1.1) e um clima com características tropical, subtropical e extratropical (Satyamurty *et al.*, 1998; Garreaud *et al.*, 2009; Reboita *et al.*, 2010). A Cordilheira dos Andes, maior cadeia montanhosa contínua do planeta com seus ~8.500 km de extensão meridional e áreas com mais de 4 km de altitude, atua como uma grande "parede climática" no lado oeste do continente, e juntamente com o Planalto Brasileiro, tendem a bloquear a circulação atmosférica em baixos níveis (Garreaud and Aceituno, 2007; Orme, 2007).

O clima na região tropical da AS é governado pela migração sazonal da Zona de Convergência Intertropical (ITCZ), uma faixa de baixa pressão em torno da linha do Equador associada a uma intensa atividade convectiva (Poveda *et al.*, 2006; Garreaud *et al.*, 2009). As variações sazonais no contraste térmico entre a AS e os oceanos adjacentes têm como resposta o desenvolvimento do Sistema de Monções Sul Americano (SAMS) (Vera *et al.*, 2006b), que possui pico de atividade durante o verão austral com mais de 50 % da precipitação anual caindo nesta estação (Marengo *et al.*, 2012a). Um importante componente do SAMS e que se estabelece no seu estágio de maturação é a Zona de Convergência do Atlântico Sul (SACZ) (Vera *et al.*, 2006a; Marengo *et al.*, 2012a), caracterizada por uma banda de alta nebulosidade e precipitação no sentido NO–SE desde o sul da Amazônia, passando pelo sudeste do Brasil em direção ao Atlântico (Liebmann *et al.*, 1999). A intensidade da SACZ é modulada por fluxos de umidade da Amazônia direcionados para a região subtropical (Nogués-Paegle and Mo, 1997; Liebmann *et al.*, 2004) por influência dos Andes e de um sistema de baixa pressão sobre o Chaco, os quais favorecem intensa atividade convectiva até a latitude de 35º S (Berbery and Barros, 2002; Vera *et al.*, 2006a; Garreaud *et al.*, 2009). Além disso, áreas no sul do Brasil, Uruguai e nordeste da Argentina são atingidas por sistemas frontais que atuam durante o inverno, em grande parte devido à interação entre massas de ar úmido provenientes do anticiclone do Atlântico Sul com massas de ar seco polar que atravessam a Patagônia (Paruelo *et al.*, 2007). Na região extratropical (> 35º S), há passagem de sistemas frontais vindos do Pacífico e efeitos orográficos que provocam chuva abundante na costa oeste dos Andes, com consequente perda de umidade nas massas de ar na travessia para o leste que ocorre em uma faixa mais estreita (< 150 km) e baixa (~1.500 m) da cordilheira (Garreaud, 2009; Viale *et al.*, 2019).

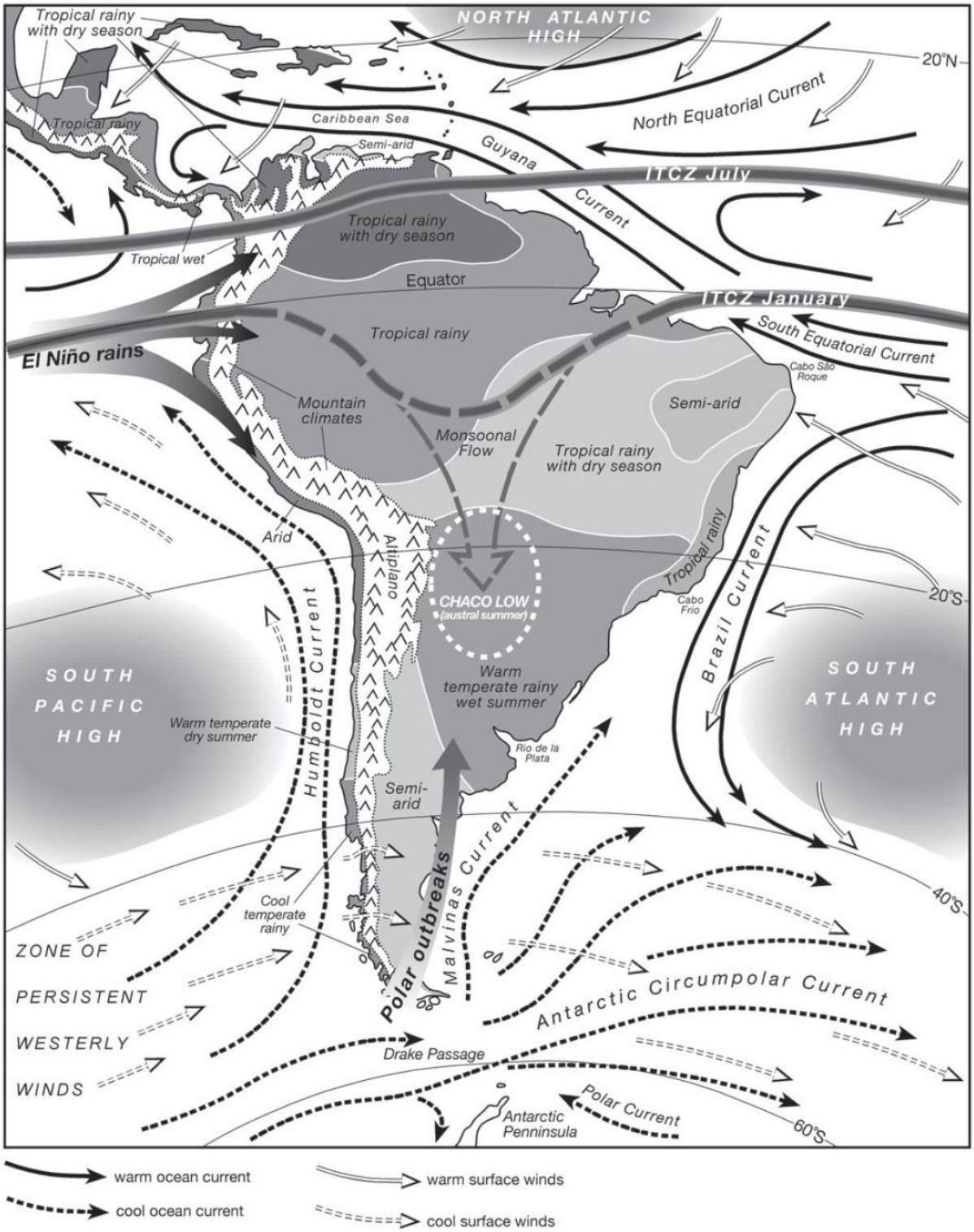

Figura 1.1. Regiões e influências climáticas sobre a América do Sul: Fonte: Adaptado de Orme (2009).

Em relação a volumes de precipitação na AS, as médias anuais chegam a variar entre < 1 mm ano^{-1} em algumas partes do deserto do Atacama ao norte do Chile (Houston, 2006), considerado o mais seco do mundo, até valores entre 8.000 e 13.000 mm ano^{-1} em Chocó na costa oeste da Colômbia (Poveda and Mesa, 2000). Na bacia Amazônica, são encontrados

médias anuais elevadas (superiores a 2.000 mm ano^{-1}) com um gradiente entre < 1.500 e > 3.000 mm ano^{-1} na direção sul-noroeste (Espinoza Villar *et al.*, 2009), abrigando a maior floresta tropical e um dos ecossistemas de maior biodiversidade do planeta. Já no Cerrado brasileiro, que possui precipitação em torno de 1.500 mm ano^{-1} e constitui a cabeceira de alguns dos maiores rios da AS (Oliveira *et al.*, 2014b), a sazonalidade é bastante marcante com estações seca (inverno) e chuvosa (verão) bem definidas, característica típica do SAMS (Marengo *et al.*, 2012a). Nas regiões para além das fronteiras a nordeste e sudoeste do Cerrado, i.e., semi-árido brasileiro e Chaco (Paraguai/Argentina), este comportamento sazonal é acompanhado de volumes de chuva anual menores, com média em torno de < 700 mm ano^{-1} e 700 a 1.400 mm ano^{-1}, respectivamente (Reboita *et al.*, 2010). No sul do continente, a precipitação anual pode alcançar volumes elevados na costa oeste dos Andes (> 4.000 mm) mas reduz exponencialmente com o afastamento da cordilheira na direção leste, resultando em volumes que chegam a ser inferiores a 200 mm ano^{-1} na região central da Patagônia (Paruelo *et al.*, 2007).

O clima da AS é periodicamente influenciado por interações oceano–atmosfera como o *El Nino Southern Oscillation* (ENSO), que dentre outros efeitos, provoca anomalias de sinais opostos (dependendo da fase quente/fria) sobre o volume e a frequência de extremos de precipitação em diferentes regiões do continente (Garreaud *et al.*, 2009; Grimm and Tedeschi, 2009). Os impactos do ENSO são ainda modulados por vários fatores, incluindo interações atmosfera–superfície, interações atmosfera–oceano na vizinhança da AS, interações entre os oceanos, bem como por modos de variabilidade climática natural que ocorrem em escalas interdecenais a multidecenais (Cai *et al.*, 2020). Além destes fenômenos cíclicos, projeções climáticas alertam para mudanças significativas nos extremos de temperatura e precipitação na AS para o futuro (Marengo *et al.*, 2009), as quais podem ser ainda intensificadas quando observadas do ponto de vista dos recursos hídricos continentais (Hirabayashi *et al.*, 2013; Zhao and Dai, 2015).

Considerando que a água é um recurso indispensável para a vida, para a manutenção dos ecossistemas e para o desenvolvimento econômico, quantificar os recursos hídricos continentais da AS frente a estas condicionantes climáticas possui um valor imensurável para a sociedade. A hidroeletricidade, por exemplo, corresponde por mais da metade da capacidade instalada na AS e possui muito potencial ainda inexplorado (Rudnick *et al.*, 2008), sendo que novos barramentos estão planejados para serem construídos principalmente nas bacias Amazônica e do Prata, apesar dos impactos ambientais associados (Zarfl *et al.*, 2015). O setor

agrícola, que corresponde por cerca de 70 % do uso consuntivo de água[1], aumentou a produção cerca de 50 % entre os anos de 2000 a 2012 (incluindo América Central) e mais de 70 % apenas no Brasil (Mekonnen *et al.*, 2015), o que inevitavelmente gera pressão sobre os recursos hídricos. Em paralelo, secas severas que têm atingido várias regiões da AS nos últimos anos (Erfanian *et al.*, 2017) provocaram colapso hídrico sem precedentes no abastecimento do sudeste brasileiro (Melo *et al.*, 2016), no transporte de insumos na Amazônia (Marengo *et al.*, 2008), além de graves problemas na produção agrícola do nordeste brasileiro (Marengo *et al.*, 2017) e da Argentina (Naumann *et al.*, 2019).

Especificamente sobre o tema de inundações, o continente sul americano é uma das regiões mais vulneráveis do mundo a desastres naturais originados por eventos hidrometeorológicos (Golnaraghi *et al.*, 2014). Através de uma consulta ao *International Disaster Database* da *Université Catholique de Louvain* (EM-DAT), durante o período de 1980 a 2021 foram identificados 292 registros de inundações ribeirinhas na América do Sul, responsáveis por aproximadamente 30 bilhões de dólares em danos econômicos, 38 milhões de pessoas afetadas e mais de 1 milhão de desabrigados. Alguns eventos extremos em grandes rios foram as cheias excepcionais de 1983, 1992 e 1998 na bacia do Paraná (Camilloni and Barros, 2000; Antico *et al.*, 2016), as cheias de 2010–2011 na bacia do Magdalena na Colômbia (Hoyos *et al.*, 2013); 2007 e 2008 nas bacias do Mamoré/Beni na Bolívia (Ovando *et al.*, 2016); 2009 (Marengo *et al.*, 2012b), 2012, 2013 (Marengo and Espinoza, 2016), 2014 (Espinoza *et al.*, 2014), e 2021 (Espinoza *et al.*, 2022) em diversas partes da Amazônia; e na bacia do Prata (rios Paraguai e Uruguai) em dezembro de 2015, que teve forte repercussão internacional com mais de 150.000 pessoas afetadas[2].

Uma característica que merece destaque neste contexto é a própria natureza transfronteiriça de alguns rios sul americanos (Figura 1.2). Em um estudo baseado nas estatísticas do EM-DAT e do *Dartmouth Flood Observatory* nos anos entre 1985–2005, Bakker (2009) destacou que, embora 10 % das cheias ribeirinhas tenham atravessado fronteiras entre países no período, foram responsáveis por cerca de 60 % dos afetados em todo o globo. Isso ocorre por diversas razões e que são amplificadas por discrepâncias entre países (menos

[1] FAO – Food and Agriculture Organization of the United Nations. Water Uses. Disponível em: http://www.fao.org/nr/water/aquastat/countries_regions/americas/indexesp4.stm. Acesso em 16/06/2017.

[2]Disponível em: http://www.bbc.com/news/world-latin-america-35184793. Acesso em 22/06/2017.

desenvolvidos), envolvendo diferenças na disponibilidade de recursos financeiros e humanos para implantação de redes de monitoramento e sistemas de previsão hidrológica; dificuldades em extrapolar previsões em localidades específicas para áreas geográficas mais amplas, incluindo trechos de rio não monitorados; limitações quanto ao compartilhamento de dados; falta de padronização e controle de qualidade das informações em tempo real; entre outros (Pagano *et al.*, 2014; Emerton *et al.*, 2016; Lavers *et al.*, 2019).

Figura 1.2. Bacias hidrográficas com caráter transfronteiriço na América do Sul. Fonte: Adaptado de UNEP (2002).

Paralelamente, a AS é muito dependente dos recursos hídricos para geração de energia (Popescu *et al.*, 2012; Rudnick *et al.*, 2012; Varas *et al.*, 2013). Especialmente no Brasil, o maior país da AS e que possui dimensões continentais (cerca de 50 % da área territorial da AS), a hidroeletricidade foi responsável por 80 % da geração total no ano de 2017 (EPE, 2018). Atualmente existem mais de 1.300 aproveitamentos hidrelétricos no Brasil, dentre os quais 218

são usinas de grande porte (> 30 MW) (Dias *et al.*, 2018b) instaladas em mais de 150 reservatórios que integram um Sistema Interligado Nacional (SIN), coordenado pelo Operador Nacional do Serviço Elétrico (ONS). A previsão de vazões afluentes naturais aos reservatórios do SIN, em múltiplas escalas temporais, é um fator chave para o planejamento da operação do sistema, que busca atender a demanda e maximizar a eficiência global através da minimização de perdas por vertimento e redução de custos adicionais com combustíveis (Costa *et al.*, 2007; Guilhon *et al.*, 2007; Oliveira and Lima, 2016). Além disso, decisões operativas devem ser ainda tomadas de forma conjunta com os agentes de geração para se adaptar às condições atuais da bacia (e.g., vazão dos rios em situação de atenção, alerta ou emergência), tendo em vista a manutenção de volumes de espera para controle de cheias a jusante dos reservatórios e garantia da segurança das barragens (Oliveira *et al.*, 2014a; Fan, 2015). Na maioria dos casos, a previsão é realizada através de modelos estatísticos que levam em conta apenas o histórico passado das vazões afluentes, de forma independente para cada reservatório (Oliveira and Lima, 2016).

A complexidade do sistema hidrológico em um continente como a AS, aliado ao fato de que eventos extremos podem ocorrer em múltiplas escalas espaciais e não respeitar fronteiras políticas, torna necessário o desenvolvimento de estratégias para quantificar fluxos hídricos com consistência espaço-temporal e prever a condição futura dos rios em regiões mais abrangentes que uma localidade ou bacia hidrográfica. Neste contexto, nas próximas seções será apresentado um apanhado geral sobre os tópicos relacionados à presente tese de doutorado, seguido do objetivo geral da pesquisa e das questões técnico-científicas abordadas no trabalho.

1.2. **Modelagem hidrológica continental a global**

Os desafios crescentes relacionados aos recursos hídricos, seja pela carência de monitoramento em áreas de difícil acesso, ou pelo caráter transfronteiriço dos rios e dificuldade de compartilhamento de informações entre diferentes países, têm impulsionado a implementação de modelos hidrológicos para domínios continentais e globais (Archfield *et al.*, 2015; Bierkens, 2015; Sood and Smakhtin, 2015). Conceitualmente, modelos hidrológicos são representações matemáticas que descrevem, fisicamente ou de forma simplificada através de parametrizações, os processos que ocorrem em uma bacia hidrográfica. Estes modelos podem ser utilizados para fins como: (i) Quantificação das variações espaço-temporais dos fluxos e estoques hidrológicos; (ii) Produção de informações para locais com pouco ou nenhum monitoramento; (ii) Avaliação da resposta do sistema hidrológico a condições adversas, como

mudanças no uso da terra ou no clima e seus efeitos sobre a disponibilidade hídrica e a ocorrência de eventos extremos; (iv) Previsão de vazão em tempo real.

Quando aplicados em escala global, os modelos hidrológicos geralmente são classificados em modelos de superfície (*Land Surface Models* — LSMs) ou modelos hidrológicos globais (*Global Hydrological Models* — GHMs). Os LSMs foram desenvolvidos para atuar como o componente terrestre de modelos atmosféricos, ou seja, com foco no cálculo de fluxos verticais de água e energia (interface solo-planta-atmosfera), enquanto que os GHMs são focados na avaliação de impactos antrópicos sobre os recursos hídricos e no transporte do escoamento gerado (ao longo da rede de drenagem). Os modelos LSM, por exemplo, têm sido bastante utilizados nos últimos anos para produção de reanálises, que são estimativas de variáveis do ciclo hidrológico (e.g., escoamento, fluxos de energia, umidade do solo, evapotranspiração, etc) para um período no passado com integração de modelos atmosféricos e técnicas de assimilação de dados. Alguns exemplos de projetos destinados a este fim são o *Global Land Data Assimilation System* (GLDAS) (Rodell *et al.*, 2004), o *Second Global Soil Wetness Project* (GSWP-2) (Dirmeyer *et al.*, 2006), o *Modern-Era Retrospective analysis for Research and Applications* (MERRA-Land) (Reichle *et al.*, 2011), o ERA-Interim/Land (Balsamo *et al.*, 2015) e mais recentemente o ERA5-Land (Muñoz-Sabater *et al.*, in preparation). Alguns modelos globais incluem também processos relacionados à evolução de vegetação e ciclo de carbono, e podem ser enquadrados em classificações adicionais. A Figura 1.3 apresenta uma linha do tempo de desenvolvimento destes modelos.

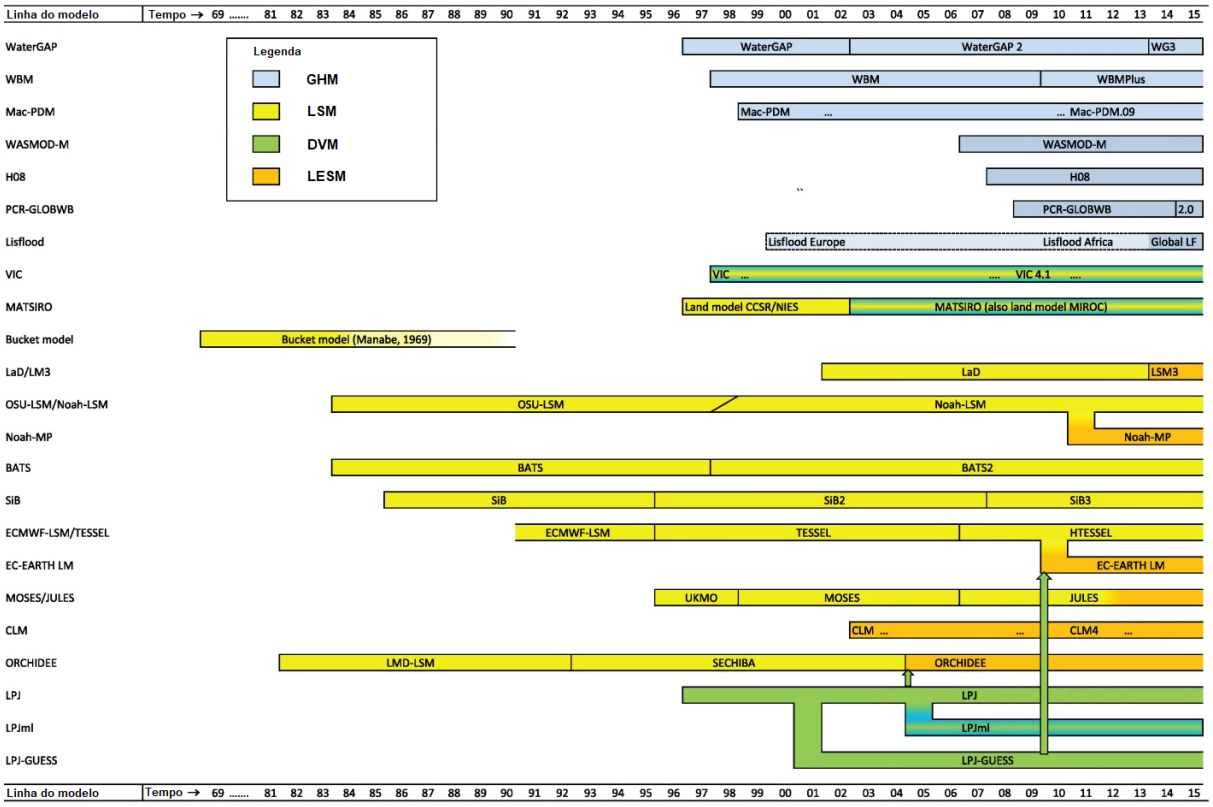

Figura 1.3. Linha do tempo relacionada ao desenvolvimento de modelos globais até o ano de 2015. GHMs: modelos hidrológicos globais; LSMs: modelos de superfície; DVM: modelos de vegetação dinâmica, incluem processos de ciclo de carbono; LESM: modelos do sistema terrestre. Adaptado de Bierkens (2015).

O desenvolvimento de reanálises consistentes no espaço e no tempo, com abrangência multidecenal (geralmente de 1979 até a atualidade), tem sido de grande auxílio para contornar a carência de dados e fornecer estimativas de fluxos hidrológicos para todo o globo. Isso têm motivado inclsuive a comparação entre LSMs e GHMs para destacar suas habilidades e deficiências (e.g., Haddeland *et al.*, 2011; Beck *et al.*, 2017b), bem como a produção de reanálises hidrológicas que incluem estimativas de vazão propagada nos rios (e.g., Schellekens *et al.*, 2017). Apesar dos inúmeros avanços, há um consenso de que modelos globais ainda são bastante limitados em representar os processos envolvidos na transformação chuva-vazão, devido a problemas de parametrização e elevada heterogeneidade das características físicas e climáticas das bacias (Haddeland *et al.*, 2011; Gudmundsson *et al.*, 2012; Archfield *et al.*, 2015; Sood and Smakhtin, 2015; Beck *et al.*, 2017b). Além das limitações no balanço hídrico, há também aquelas relacionadas ao transporte de água ao longo da rede de drenagem. Em regiões da AS como a Amazônia e o Pantanal, por exemplo, sistemas de rios complexos com baixa declividade, extravasamento de água do canal para extensas planícies inundáveis e efeitos de remanso muitas vezes governam o escoamento dos rios, resultando em atenuação do pico e

atraso dos hidrogramas de cheia (Trigg *et al.*, 2009; Paz *et al.*, 2011; Bravo *et al.*, 2012; Paiva *et al.*, 2013a; Paz *et al.*, 2014; Pontes *et al.*, 2017). Geralmente, as simplificações empregadas no módulo de propagação de modelos hidrológicos globais (Bierkens, 2015; Kauffeldt *et al.*, 2016; Schellekens *et al.*, 2017) acabam prejudicando o tempo de ocorrência (*timing*) e a magnitude das vazões, conforme demonstrado por um estudo comparativo de vários destes modelos em diversas regiões do mundo (Zhao *et al.*, 2017). Portanto, métodos de propagação que possuam maior representação física do escoamento em rios devem ser incorporados em simulações que envolvem a AS, o que pode ser conseguido através do acoplamento de modelos hidrodinâmicos que resolvem as equações clássicas unidimensionais (1D) de Saint-Venant.

Apesar desta abordagem possuir maiores limitações em termos de informações de entrada e custo de processamento, os avanços recentes na capacidade computacional e na disponibilidade de dados globais de sensoriamento remoto têm proporcionado grandes perspectivas para estudos de modelagem hidrológica-hidrodinâmica. Atualmente, existem modelos digitais de elevação (MDEs) gerados a partir do *Shuttle Radar Topography Mission* - SRTM (Farr *et al.*, 2007) que possuem pós-processamento, correção de vazios (e.g., Jarvis *et al.*, 2008) e tratamento de efeitos da vegetação (e.g., O'Loughlin *et al.*, 2016; Yamazaki *et al.*, 2017), além de bases de dados hidrologicamente consistentes que permitem rápida extração de redes de drenagem e que são derivadas do SRTM, como o HydroSHEDS (Lehner *et al.*, 2008) e o MERIT–Hydro (Yamazaki *et al.*, 2019). De forma complementar aos dados de vazão in situ, também é possível calibrar e validar modelos de grande escala através de produtos variados, incluindo altimetria espacial (e.g., Paiva *et al.*, 2013a), áreas inundadas (e.g., Revilla-Romero *et al.*, 2015), evapotranspiração (e.g., Lopez *et al.*, 2017) e armazenamento terrestre de água (e.g., Alkama *et al.*, 2010; Werth and Guntner, 2010). Outros parâmetros chave, como largura e profundidade de rios, tradicionalmente vistos como um grande obstáculo ao uso de modelos hidrodinâmicos (Hodges, 2013), já possuem estimativas globais a exemplo de relações geomorfológicas baseadas em vazão média anual (e.g., Andreadis *et al.*, 2013), ou valores estimados a partir de máscaras de água do SRTM combinadas com mapas de direção de fluxo (e.g., Yamazaki *et al.*, 2014).

Além de bases de dados para preparação e validação dos modelos de grande escala, é importante citar também algumas técnicas desenvolvidas para reduzir o custo computacional da propagação hidrodinâmica. Um avanço importante dos últimos anos e que merece destaque é a formulação inercial explícita da equação dinâmica de Saint-Venant (Bates *et al.*, 2010), que

se mostra como uma alternativa interessante a esta última devido sua relativa eficiência, facilidade de implementação e paralelização de código (Yamazaki *et al.*, 2013; Pontes *et al.*, 2017). Este método de propagação já foi aplicado com sucesso tanto em estudos regionais (e.g., Paz *et al.*, 2011; Neal *et al.*, 2012; Getirana *et al.*, 2017b; Pontes *et al.*, 2017; Fleischmann *et al.*, 2018) como globais (e.g., Yamazaki *et al.*, 2013; Zhao *et al.*, 2017), demonstrando assim um enorme potencial para aplicações continentais que requerem equilíbrio entre custo computacional e representação de processos hidrológicos.

1.3. **Previsão hidrológica em escalas continental a global**

Conforme mencionado anteriormente, modelos hidrológicos são ferramentas que, dentre outras finalidades, podem ser utilizadas para previsão de vazões. Quando acoplados a saídas de modelos atmosféricos, que fornecem previsões quantitativas de precipitação e outras variáveis de interesse (e.g., temperatura), se torna possível estender a previsão de vazão em relação àquela que poderia ser feita somente com a resposta da chuva observada.

Inspirado na mudança de paradigma da meteorologia na década de 90 (Tracton and Kalnay, 1993; Molteni *et al.*, 1996), as previsões hidrológicas vêm se movendo de uma abordagem determinística, que fornece apenas um valor único para cada instante futuro, em direção a uma abordagem probabilística com geração de múltiplos cenários de vazão. Esta última, também conhecida como previsão hidrológica por *ensemble* – ou por conjunto (Cloke and Pappenberger, 2009), se justifica pela propagação de incertezas que tendem a crescer na medida em que a antecedência da previsão é ampliada. Tais incertezas estão associadas a diversos fatores como dados de entrada (e.g., forçantes meteorológicas), estrutura do modelo (e.g., simplificações de equações físicas), condições iniciais (e.g., umidade antecedente no solo) e parâmetros utilizados no cálculo de processos hidrológicos. A Figura 1.4 mostra um exemplo de previsão por conjunto, onde cada membro representa uma possível evolução futura da vazão a partir do instante em que a previsão é iniciada.

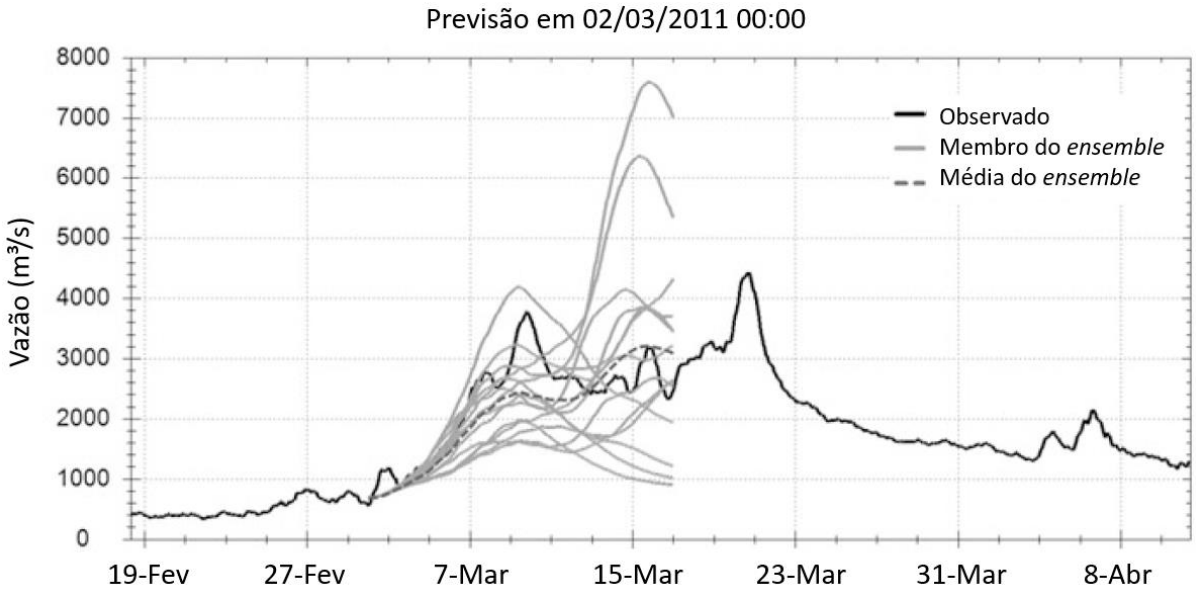

Figura 1.4. Exemplo de uma previsão por conjunto lançada para o reservatório de Três Marias, na estação úmida de 2010/2011. No gráfico são mostrados os membros da previsão relacionados aos diferentes cenários da previsão meteorológica (linha cinza, contínua), além de uma previsão determinística dada pela média do conjunto (linha cinza, tracejada). Adaptado de Tucci *et al.* (2019).

Atualmente, existe um consenso de que a incerteza nos sistemas de previsão hidrológica deve ser tratada em diferentes escalas temporais, desde horas (*nowcasting*) até meses à frente, e escalas espaciais, variando de local a global (Thielen *et al.*, 2009b; Alfieri *et al.*, 2012; Pagano *et al.*, 2014; Emerton *et al.*, 2016; Arnal *et al.*, 2018). Assim, as previsões devem evoluir de uma indicação geral (em grande escala) da probabilidade de ocorrência de eventos extremos com maior antecedência no tempo, onde se admitem maiores incertezas, para uma estimativa precisa da magnitude e do *timing* das vazões em localidades específicas (WMO, 2011). Para antecedências mais longas, as previsões de precipitação são geralmente consideradas como a fonte dominante de incertezas (Pappenberger *et al.*, 2005; Roulin and Vannitsem, 2005; Cloke and Pappenberger, 2009; Zappa *et al.*, 2011) pela alta sensibilidade às condições iniciais da atmosfera e sua evolução caótica (Lorenz, 1963), e devido à parametrização de processos de formação de chuva que ocorrem em escalas muito menores que a grade numérica dos modelos atmosféricos (Buizza *et al.*, 1999; Stensrud *et al.*, 2000).

Em algumas partes do mundo, principalmente no Hemisfério Norte (Cloke and Pappenberger, 2009; Wu *et al.*, 2020), a aplicação de previsões meteorológicas por conjunto em modelos hidrológicos já vem sendo estudada desde o inicio do século passado. Um dos grandes motivadores deste tema de pesquisa tem sido o projeto *Hydrological Ensemble Prediction EXperiment* (HEPEX) iniciado no ano de 2004, que visa o compartilhamento de experiências entre meteorologistas, hidrológos e previsores para resolver questões científicas

relacionadas ao tema e acelerar o desenvolvimento de sistemas de previsão por conjunto (Schaake *et al.*, 2007). Em geral, os estudos têm demonstrado que as previsões probabilísticas possuem desempenho superior às determinísticas mesmo quando a resolução espacial é mais baixa (e.g., Jaun and Ahrens, 2009; Velázquez *et al.*, 2009; Boucher *et al.*, 2011), agregam valor ao indicar sobre a possível ocorrência eventos críticos (e.g., Gouweleeuw *et al.*, 2005; Younis *et al.*, 2008; Hopson and Webster, 2010), propiciam maior benefício econômico para produção de energia ou redução de prejuízos em sistemas de alerta (e.g., Roulin, 2007; Muluye, 2011; Verkade and Werner, 2011a; Boucher *et al.*, 2012), e implicam em melhores decisões quanto a restrições operativas em reservatórios (e.g., Wang *et al.*, 2012a). Já na América do Sul, mais precisamente no Brasil, uma maior atenção para o tópico de *ensemble* tem sido dada somente a partir de meados da última década. Na literatura, são encontrados trabalhos com avaliação do desempenho de previsões de curto prazo (< 3–4 dias) voltadas a sistemas de alerta contra cheias (Calvetti and Pereira Filho, 2014; Meller *et al.*, 2014; Siqueira *et al.*, 2016a; Casagrande *et al.*, 2017; Tomasella *et al.*, 2019), avaliação de previsões de médio prazo (3 a 15 dias) para tomada de decisão em usinas hidrelétricas (Fan *et al.*, 2014; Fan *et al.*, 2015b; Fan *et al.*, 2016a) ou de curto prazo para otimização operacional de reservatórios (Raso *et al.*, 2014; Schwanenberg *et al.*, 2015; Fan *et al.*, 2016c). Entretanto, estes estudos avaliam apenas resultados pontuais em bacias específicas, ou seja, o conhecimento sobre o desempenho de previsões hidrológicas por conjunto quando estas são avaliadas espacialmente — e em grandes domínios espaciais como a AS — ainda é bastante limitado.

O sucesso das pesquisas no exterior, aliado aos avanços na capacidade de processamento, estimativa de precipitação por satélite em tempo (quase) real, e modelagem atmosférica, tem favorecido a rápida expansão de sistemas de previsão hidrológica por conjunto para escalas continental e global (Emerton *et al.*, 2016). Alguns sistemas mais focados em cheias, por exemplo, já funcionam operacionalmente (ou estão em fase de protótipo) na escala continental como o *European Flood Awareness System* (EFAS) (Thielen *et al.*, 2009a), o *African Flood Forecasting System* (AFFS) (Thiemig *et al.*, 2015), o *Latin America Flood and Drought Monitor* (Wood *et al.*, 2018) e o *Hydrological Ensemble Forecast Service* (HEFS) para todo o território dos Estados Unidos (Demargne *et al.*, 2014), enquanto outros operam com abrangência global como o GloFAS (Alfieri *et al.*, 2013) e o GLOFFIS (Weerts, 2018) (Figura 1.5). Recentemente, a NOAA nos Estados Unidos anunciou um sistema denominado *National*

Water Model[3], que roda em um supercomputador e fornece previsões de vazões horárias até um mês à frente para 2,7 milhões de trechos de rio nos Estados Unidos, incluindo partes do México e Canadá (Snow *et al.*, 2016).

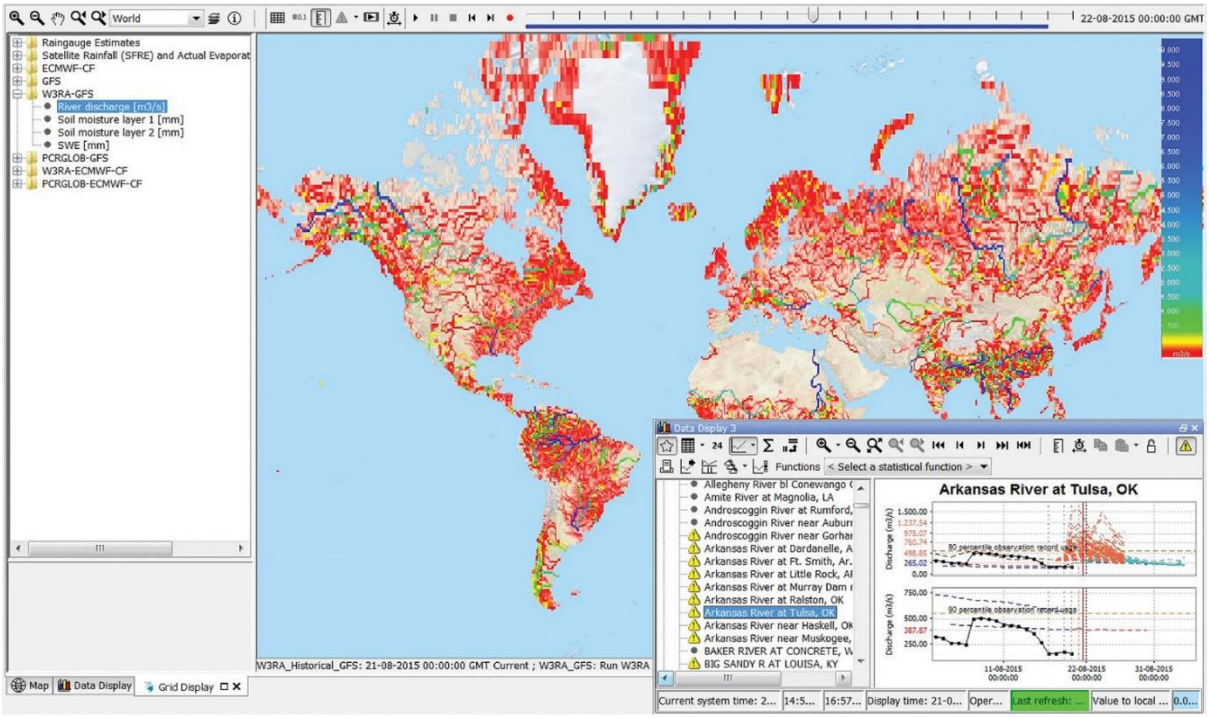

Figura 1.5. Interface do sistema global de previsão de vazões por conjunto GLOFFIS, operado dentro da plataforma Delft-FEWS. Adaptado de Emerton *et al.* (2016).

A implantação de sistemas continentais ou globais se justifica por diversos motivos. Por exemplo, sistemas de previsão por conjunto requerem elevada capacidade computacional e altos investimentos para operação, que se torna mais economicamente viável na escala continental (ou global). Isso porque a ociosidade do sistema tende a ser muito menor do que em escalas regionais ou locais pela maior ocorrência de eventos extremos, já que diferentes regiões climáticas e grandes áreas passam a ser contempladas. Além disso, se torna possível gerar informações com semanas de antecedência para regiões/países que não possuem qualquer sistema de previsão, que podem ser úteis para bacias transfronteiriças ou até servir como uma informação complementar para sistemas locais focados em bacias específicas e em menores antecedências. Quanto mais cedo o planejamento puder ser iniciado, melhores serão as ações preparatórias, de coordenação e compartilhamento de informações para redução dos impactos

[3]Disponível em: http://water.noaa.gov/about/nwm, Acesso em 31/07/2017.

de eventos extremos (Thielen *et al.*, 2009a; Alfieri *et al.*, 2012; Alfieri *et al.*, 2013; Pappenberger *et al.*, 2015a; Emerton *et al.*, 2016).

1.4. **Pós-processamento de previsões hidrológicas**

A disponibilidade de previsões de vazão por conjunto com informação probabilística, seja na escala regional ou continental, é fundamental para que os usuários finais possam tomar decisões sob a incerteza dos acontecimentos hidrológicos futuros. Entretanto, é muito comum representar a incerteza das previsões de vazão apenas por um número finito de membros atrelados ao *ensemble* de chuva prevista, principalmente pela dificuldade em quantificar a incerteza relacionada aos modelos hidrológicos de forma adequada e também por limitações computacionais, que é um critério importante para previsão em tempo real. Além disso, a própria previsão meteorológica, que inevitavelmente possui viés devido a erros sistemáticos na resolução das equações físicas, resulta da integração de uma amostra pequena do espectro de condições iniciais possíveis, o que normalmente leva a uma falta de espalhamento (dispersão) na previsão por conjunto. Isso significa que o *ensemble* no final das contas é apenas uma representação parcial das incertezas, e que uma incerteza residual ainda vai permanecer após o conjunto de chuva prevista ser propagado ao longo do componente hidrológico da previsão.

Krzysztofowicz (1999) destaca que a tomada de decisão "*requer que a incerteza total sobre um preditando seja quantificada em termos de uma distribuição de probabilidade, condicionada a todo o conhecimento e informação disponível*". Para o caso específico da vazão, "o conhecimento" pode ser encapsulado em uma ou mais previsões geradas por um modelo hidrológico, no sentido em que as previsões são utilizadas como uma forma de reduzir a incerteza preditiva, e não como estimativas do valor futuro da variável de interesse (Todini, 2008; Coccia and Todini, 2011). A Figura 1.6 mostra um exemplo de previsão cuja incerteza é expressa por uma função densidade de probabilidade.

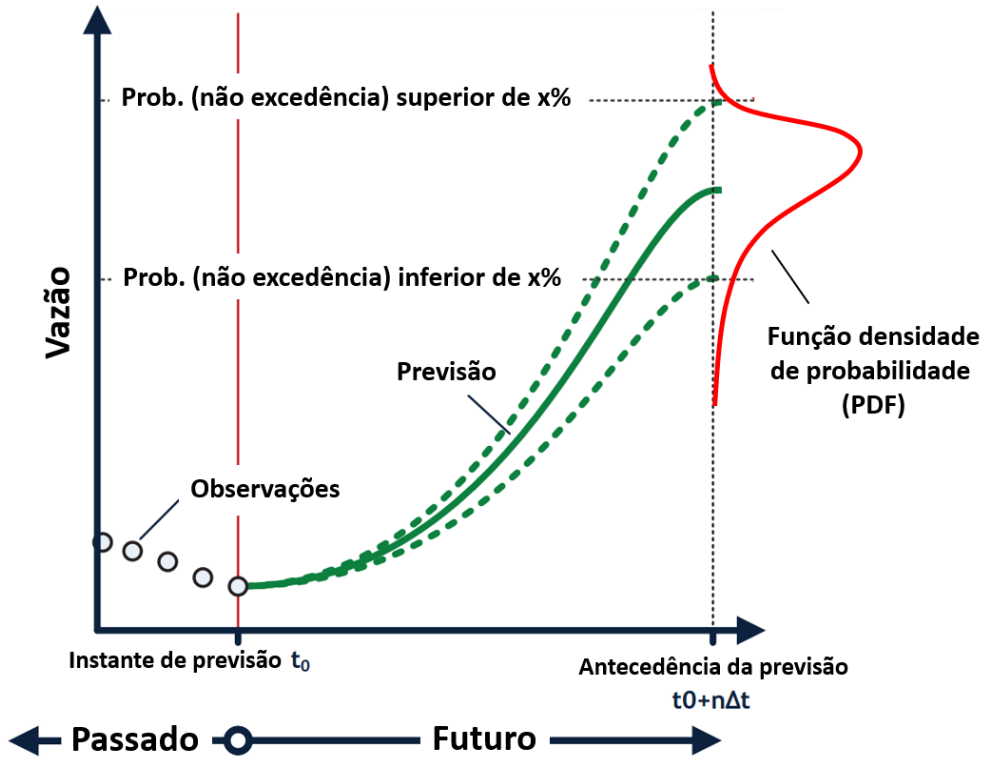

Figura 1.6. Representação esquemática da incerteza preditiva condicional a uma previsão de vazão. Adaptado de Verkade (2015).

O pós-processamento, no contexto da previsão por conjunto, é utilizado com o propósito de simultaneamente corrigir viés e erros de dispersão do *ensemble* (Boucher *et al.*, 2018). Mais precisamente, ele busca produzir densidades preditivas cuja banda de incerteza seja a mais estreita quanto possível, desde que as probabilidades previstas para um determinado evento ou condição sejam consistentes com as suas respectivas frequências observadas (Gneiting *et al.*, 2005; Raftery *et al.*, 2005; Wilks, 2018). Para isso, séries longas de previsões realizadas para o passado e observações correspondentes são usadas para ajustar um modelo estatístico, que fornece uma distribuição de probabilidade condicional válida para uma dada localidade e antecedência (i.e., univariadas) (Li *et al.*, 2017). Ter esta informação em mãos permitiria aos tomadores de decisão se concentrar apenas nas decisões *per se*, sem a necessidade de fazer julgamentos adicionais sobre a qualidade das previsões (Bennett *et al.*, 2014). A Figura 1.7 mostra uma representação esquemática do procedimento típico de pós-processamento de previsões hidrológicas.

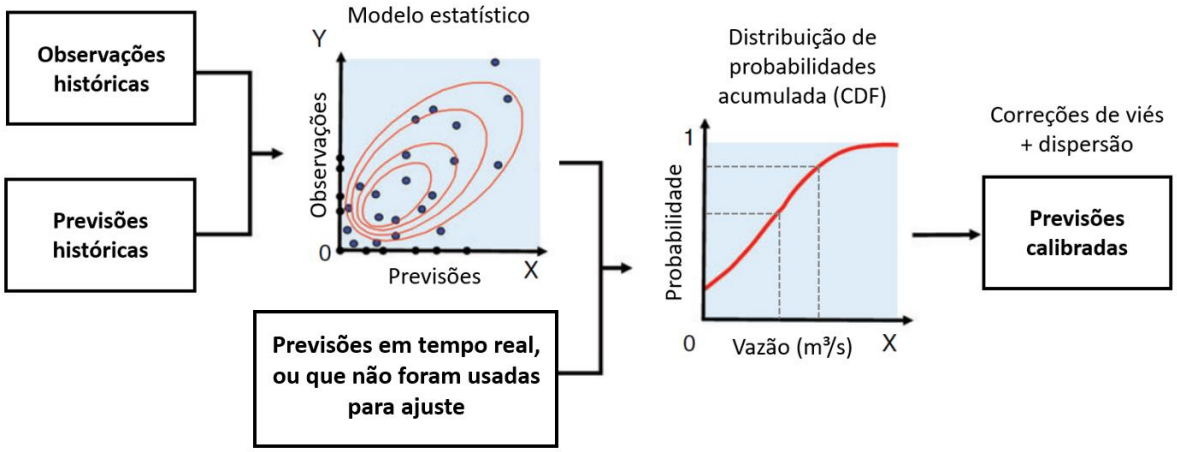

Figura 1.7. Procedimento típico de pós-processamento de previsões hidrológicas. A vazão prevista condiciona uma distribuição de probabilidade cumulativa (CDF), da qual são amostrados quantis de interesse. Adaptado de Li *et al.* (2017).

Na literatura atual podem ser encontrados diversos trabalhos que utilizam pós-processamento de previsões hidrológicas com horizontes de curto a médio prazo (até 15 dias). Grande parte dos esforços têm sido destinados para propor ou adaptar abordagens de pós-processamento sobre variáveis como vazão ou nível (e.g., Krzysztofowicz and Kelly, 2000; Seo *et al.*, 2006; Duan *et al.*, 2007; Todini, 2008; Reggiani *et al.*, 2009; Bogner and Pappenberger, 2011; Weerts *et al.*, 2011; Pagano *et al.*, 2013; Regonda *et al.*, 2013; Madadgar *et al.*, 2014; Hemri *et al.*, 2015; Klein *et al.*, 2016), comparar diferentes técnicas de pós-processamento ou múltiplas configurações destas (e.g., López López *et al.*, 2014; Boucher *et al.*, 2015; Dogulu *et al.*, 2015; Verkade *et al.*, 2017), bem como verificar ganhos de desempenho do pós-processamento em relação a previsões com representação parcial da incerteza ou determinísticas (Van den Bergh and Roulin, 2016; Siddique and Mejia, 2017). Em geral, os resultados apontam que o pós-processamento estatístico traz melhorias para a acurácia e confiança das previsões probabilísticas, cujos aspectos têm sido relacionados com benefícios econômicos principalmente em sistemas de reservatórios (e.g., Boucher *et al.*, 2012; Matte *et al.*, 2017; Cassagnole *et al.*, 2021).

Outro aspecto que merece destaque e que depende das necessidades dos usuários é a forma como as previsões probabilísticas são emitidas. Por exemplo, distribuições preditivas são úteis para indicar um intervalo de confiança para a vazão prevista ou a probabilidade de ultrapassar um limiar crítico (Reggiani *et al.*, 2009; Weerts *et al.*, 2011; Bogner *et al.*, 2016), ao passo que a evolução temporal dos cenários futuros de vazão (e.g., os traços do *ensemble* na Figura 1.4) pode ser necessária para a operação e otimização de reservatórios (e.g., Raso *et al.*,

2014; Schwanenberg *et al.*, 2015). Entretanto, a grande maioria dos pós-processadores estatísticos não preserva a dependência espacial (ao longo da rede de drenagem) e temporal (ao longo das antecedências), pois a densidade preditiva é estimada individualmente para uma localidade, antecedência e variável específica (Schefzik *et al.*, 2013; Li *et al.*, 2017). Técnicas de pós-processamento multivariadas têm sido desenvolvidas buscando reconstruir esta dependência espaço-temporal, as quais podem ser categorizadas em dois grupos (Schefzik, 2016): i)métodos paramétricos moldados para configurações específicas, geralmente de baixa dimensão (i.e., nº de antecedências, localidades, etc); ii)métodos de reordenamento do tipo não-paramétricos, baseados em um *template* de dependência aplicável sobre as densidades pós-processadas. Neste ultimo grupo são encontradas as técnicas *Schaake Shuffle* (Clark *et al.*, 2004) e o *Ensemble Copula Coupling* (Schefzik *et al.*, 2013), que têm como vantagem o baixo custo computacional e o fato de serem adequadas para qualquer dimensão.

Tais abordagens, por exemplo, têm sido usadas para produzir trajetórias realísticas de precipitação prevista a partir de densidades preditivas como pré-requisito a modelos hidrológicos, dado que a resposta na vazão depende muito da distribuição espacial e temporal da chuva da bacia (e.g., Clark *et al.*, 2004; Robertson *et al.*, 2013; Verkade *et al.*, 2013; Bennett *et al.*, 2014; Demargne *et al.*, 2014; Bellier *et al.*, 2017a; Scheuerer *et al.*, 2017). Paralelamente, a combinação de métodos de pós-processamento univariados e multivariados para aplicação direta na vazão (Figura 1.8) é um campo de pesquisa que vem ganhando espaço na literatura (e.g., Hemri *et al.*, 2015; Bellier *et al.*, 2018; Cassagnole *et al.*, 2021), especialmente porque trajetórias de previsão coerentes podem ser derivadas após as incertezas de ambos componentes meteorológico e hidrológico terem sido levadas em consideração.

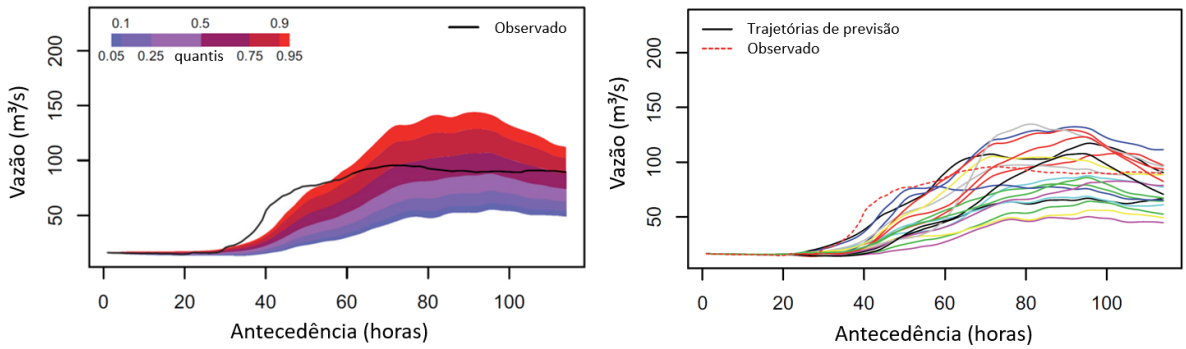

Figura 1.8. Trajetórias realísticas de previsão derivadas de densidades preditivas, a partir de *Ensemble Copula Coupling*. Adaptado de Hemri *et al.* (2015).

1.5. **Objetivo de pesquisa**

Nas seções anteriores foi apresentada uma visão geral da AS, discutindo sobre a necessidade de quantificar fluxos hidrológicos com consistência espacial e temporal, bem como prever a condição futura dos rios juntamente com estimativas de incerteza para uma ou mais semanas à frente. Este cenário dá condições para que sejam criadas novas oportunidades de pesquisa, uma vez que: (i) Não se sabe se o desempenho e eficiência de um modelo hidrológico–hidrodinâmico para a AS justifica o esforço necessário para sua preparação, dado que já existem modelos globais que podem ser utilizados para esta finalidade; (ii) Pouco se sabe sobre o ganho potencial em se usar previsões meteorológicas por conjunto para a geração de previsões de vazão, principalmente quando o foco não é a avaliação em localidades específicas na AS; (iii) Ainda não existem estudos com avaliação de pós-processamento estatístico na previsão de vazão por conjunto no contexto da AS. Soma-se a isso os inúmeros desafios técnicos trazidos pela própria escala continental a ser abordada, heterogeneidade das características hidroclimáticas da AS, e limitação de dados observados especialmente em tempo quase real, cuja disponibilidade é menor do que em regiões com países desenvolvidos.

Neste contexto, o objetivo geral desta tese de doutorado é estabelecer uma base técnica para modelagem hidrológica com abrangência da América do Sul e dar contribuições para a previsão de vazões diárias em escala continental, considerando um horizonte de médio prazo (até 15 dias). Para alcançar este objetivo, buscou-se responder as seguintes questões técnico-científicas:

- Qual o desempenho esperado de um modelo hidrológico–hidrodinâmico continental quanto à representação de variáveis hidrológicas nas diferentes regiões da AS? Como o desempenho das vazões simuladas se compara ao de modelos de escala global na AS? (Capítulo 2)

- O uso de previsões meteorológicas por conjunto pode contribuir para o ganho de desempenho (destreza) nas previsões de vazão com horizonte de médio prazo? Como a destreza da previsão varia geograficamente e nas principais bacias da AS? Como a destreza da previsão se relaciona com características climáticas e tamanho da bacia? (Capítulo 3)

- Qual é o desempenho esperado de previsões de vazão pós-processadas em relação a previsões por conjunto brutas (cruas), na escala continental? Como o desempenho destas previsões de vazão se compara ao de previsões mais simples, como climatologia e persistência das vazões observadas? É possível gerar trajetórias realísticas de previsão de vazão a partir de distribuições preditivas pós-processadas, considerando limitação de dados em tempo (quase) real? (Capítulo 4)

1.6. **Organização da tese**

O capítulo 1, apresentado até este momento, trouxe uma visão introdutória sobre os principais conceitos e estado-da-arte nos temas abordados, além dos objetivos que norteiam este trabalho. O capítulo 2 apresenta o desenvolvimento do modelo hidrológico para a AS, dando enfoque para as bases de dados e técnicas de modelagem, estratégias de validação e comparação com resultados de modelos globais. Já o capítulo 3 foca na avaliação do potencial de previsões meteorológicas por conjunto em contribuir para a destreza das previsões de vazão na AS, onde são consideradas apenas as incertezas da chuva prevista que são propagadas através do modelo hidrológico desenvolvido. Na sequência, no capítulo 4 é avaliado o desempenho das previsões de vazão emitidas na escala continental considerando não só as incertezas da previsão meteorológica como também aquelas oriundas do modelo hidrológico e demais componentes da cadeia de previsão, investigando sobre os potenciais benefícios — em termos de qualidade da previsão — em se usar pós-processamento estatístico. Os capítulos 2, 3 e 4, que são o núcleo desta pesquisa, estão organizados em prólogo, que é basicamente uma prévia sobre o que é tratado e discutido no capítulo, seguido de introdução, informações sobre a área de estudo, métodos utilizados, análise de resultados, discussão e conclusões parciais. Estes capítulos foram escritos na forma de artigos científicos (em idioma inglês) que atualmente se encontram publicados em periódicos internacionais. Finalmente, no capítulo 5 são apresentadas as principais conclusões desta pesquisa, juntamente com as limitações e recomendações para trabalhos futuros. A Figura 1.9 mostra um fluxograma da organização geral da tese e a relação entre os tópicos aqui abordados.

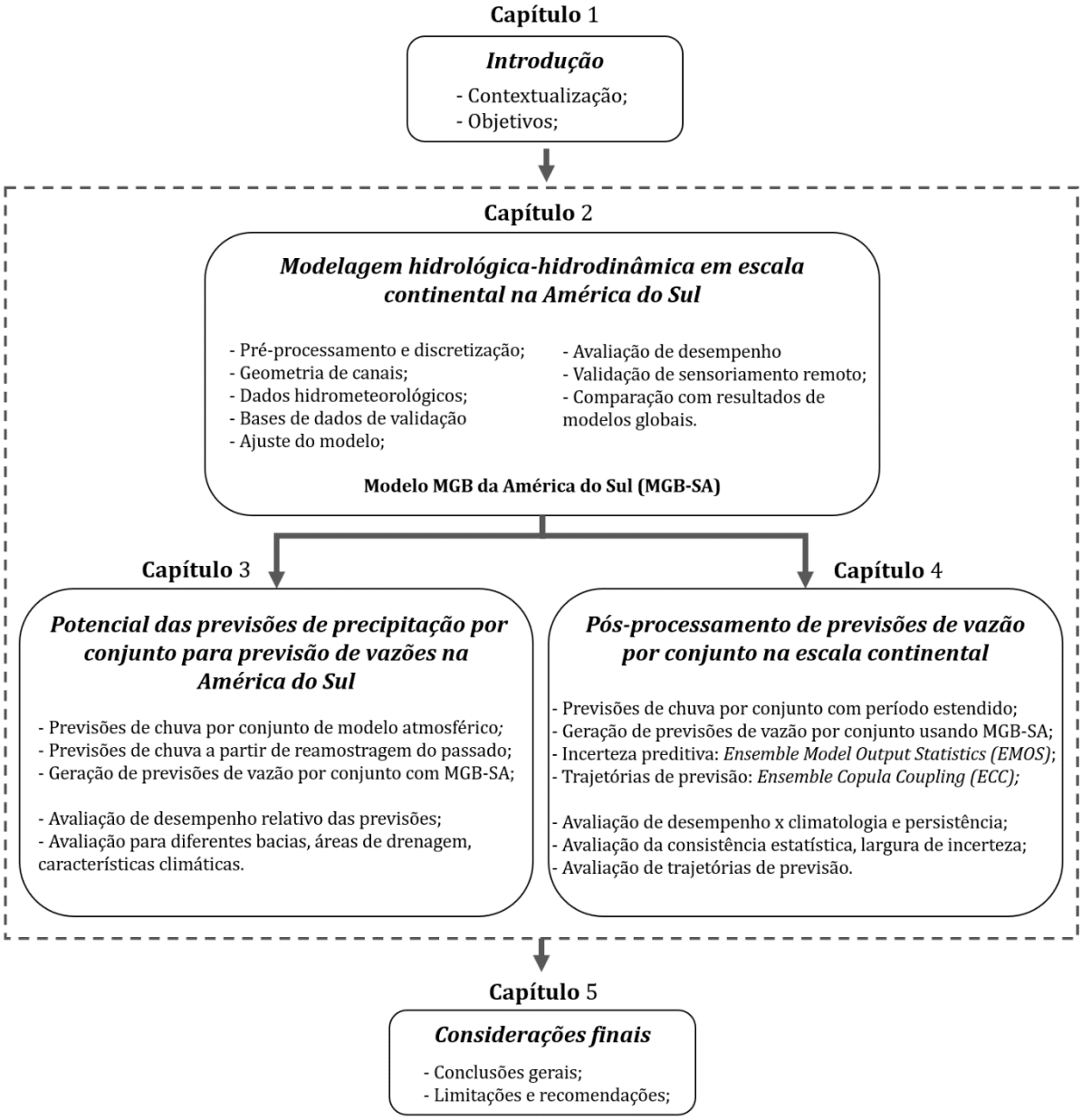

Figura 1.9. Organização da tese e relação entre os temas abordados

CAPÍTULO 2: Modelagem hidrológica–hidrodinâmica em escala continental na América do Sul

"It seems to us that in an increasingly interconnected, globalized world, water management is going to be much more complex than before. Water security challenges and other societal problems related to water are going to be addressed through multilateral approaches, including interbasin (or international) transfers of real water and regional and global exchanges of virtual water […] Failure to address water shortages is likely to generate not only local problems but also regional and global problems, including border conflicts, migration and global political instability."

—M. Sivapalan e G. Blöschl[4]

[4] Retirado de: Sivapalan, M., Blöschl, G. (2017) The growth of hydrological understanding: technologies, ideas, and societal needs shape the field. **Water Resources Research**, vol. 53, p.8137–8146.

Prólogo

Este capítulo apresenta o desenvolvimento de um modelo hidrológico–hidrodinâmico com abrangência da América do Sul, sua validação, e comparação com modelos hidrológicos que são aplicados na escala global. Utilizou-se aqui o Modelo de Grandes Bacias (MGB) (Collischonn, 2001) buscando aproveitar experiências de aplicações anteriores em bacias do continente sul americano, tanto de simulação hidrológica com propagação não hidrodinâmica (e.g., Allasia *et al.*, 2006; Collischonn *et al.*, 2007a) e hidrodinâmica (e.g., Paiva *et al.*, 2013a; Pontes, 2016; Pontes *et al.*, 2017). Uma descrição detalhada da estrutura e equacionamento do modelo MGB podem ser encontrados no **Anexo A.1.1 e A.1.2**, presente ao final desta tese.

Inicialmente foi realizada uma coleta extensiva de informações necessárias à modelagem a partir de estudos e fontes de dados regionais e globais, incluindo dados de vazão de diversas agências e institutos responsáveis por redes de monitoramento na AS, dados climáticos, geometria de rios, MDE com correção do efeito de vegetação, mapa de direções de fluxo hidrologicamente consistente, bem como informações de uso e tipo do solo. Também foram adaptadas técnicas de geoprocessamento para lidar com aspectos relacionados à propagação hidrodinâmica, como discretização de trechos de rio, batimetria de planície e perfis longitudinais dos rios, relatadas com detalhe no **Anexo A.1.3 – A.1.6**. O modelo, definido aqui como MGB–SA em homenagem ao seu domínio continental, foi forçado com uma base de dados global de precipitação que resulta de uma combinação de reanálises atmosféricas, observações in situ e informação de satélites. O MGB–SA foi calibrado manualmente através de um ajuste por etapas na direção de montante para jusante, para cada bacia individualmente, e considerando métricas como a eficiência de Kling-Gupta (KGE), Nash-Sutcliffe (NSE), logaritmo do NSE, viés, índice de atraso das vazões (*delay index* - DI), e concordância visual entre os hidrogramas simulado e observado. Os resultados foram avaliados de forma pontual através de observações de vazão e nível (este último com dados in situ e altimetria por satélite), bem como espacialmente através de dados de variações de armazenamento terrestre de água observada pelo satélite GRACE, e evapotranspiração estimada através de múltiplas fontes.

Para fins de comparação das vazões simuladas pelo MGB–SA com aquelas simuladas por modelos globais (i.e., GHMs e LSMs), utilizou-se a base de dados de reanálise hidrológica global do projeto eartH2Observe (Dutra *et al.*, 2017; Schellekens *et al.*, 2017), que era a mais recente até o momento em que o trabalho foi realizado. A reanálise do eartH2Observe tem como vantagem a disponibilidade de saídas de vazão em rios, ou seja, considerando propagação de

vazão na rede de drenagem e não só o escoamento gerado no balanço hídrico vertical, além de possuir maior resolução espacial que outras bases similares, permitindo a comparação dos resultados em um maior número de postos fluviométricos. No contexto deste estudo foram selecionados 3 modelos globais: WaterGAP3, LISFLOOD, e HTESSEL/CaMa-Flood (LSM acoplado a um modelo de propagação hidrodinâmica).

Os resultados obtidos para as simulações indicaram que houve uma representação satisfatória das vazões e razoável para os níveis observados, e que o modelo continental foi capaz de capturar padrões de sazonalidade e magnitude de evapotranspiração e armazenamento terrestre de água especialmente nas grandes bacias da AS. Notou-se um desempenho inferior do MGB–SA em áreas cuja qualidade dos dados de precipitação potencialmente é mais baixa, a exemplo de regiões com orografia complexa, como os Andes, e em climas mais secos onde a estrutura do modelo aparenta ter menor capacidade em representar os processos hidrológicos. Erros pronunciados nos níveis simulados foram em grande parte atribuídos a fatores como incertezas no coeficiente de manning e geometria dos canais, bem como limitações do MDE (acurácia, resolução) para definição de perfis longitudinais dos rios e topografia de planície. Em relação à sazonalidade de ET, foram detectadas diferenças de *timing* entre as estimativas de múltiplas fontes e as estimativas do modelo em bacias com regiões semi-áridas (Parnaíba e São Francisco), que poderiam estar conectadas a uma má representação da dinâmica da água no solo por parte do MGB, que utiliza apenas uma camada, como também por limitações dos produtos de ET que dependem de dados de reanálise e parametrização de equações. Maiores dificuldades em capturar a amplitude do GRACE ocorreram na bacia do Orinoco, potencialmente por deficiências na calibração do armazenamento do solo do MGB–SA, e nas regiões mais áridas, especialmente aquelas em que variações na água estocada em neve / geleiras podem estar influenciando significativamente o sinal do GRACE.

Na comparação com os modelos globais, foi observado que estes últimos possuem grandes limitações na representação de vazões em escala de tempo diária, com tendência de superestimativa principalmente no Nordeste brasileiro e grande número de postos com NSE < 0, e que o MGB–SA teve desempenho mediano superior em todas as métricas avaliadas. A avaliação individual dos modelos globais indicou que o LISFLOOD de maneira geral possui um elevado viés positivo, além de causar atraso nos hidrogramas simulados na região da Amazônia; o WaterGAP3 demonstrou menor viés absoluto dentre os globais porém tendência de adiantamento dos hidrogramas, possivelmente devido à representação simplificada da propagação de vazão; enquanto que o HTESSEL/CaMa-Flood também apresentou tendência

de adiantamento dos hidrogramas, o que poderia estar relacionado à falta de ajuste da geometria dos rios no modelo hidrodinâmico, como também a limitações no escoamento gerado pelo HTESSEL (que não possui qualquer calibração). Também foi demonstrada a influência da calibração e da propagação hidrodinâmica sobre a simulação de vazões diárias na AS, através de experimentos que levaram em conta a ausência e a operação conjunta/isolada destes dois fatores no MGB–SA. Outras fontes potenciais de erros relacionados à modelagem de escalas continental e global na AS foram discutidas ao longo deste capítulo.

Este capitulo é baseado no seguinte artigo publicado no periódico *Hydrology Earth System Sciences (HESS)*:

SIQUEIRA, V. A., PAIVA, R. C. D., FLEISCHMANN, A. S., FAN, F. M., RUHOFF, A. L., PONTES, P. R. M., PARIS, A., CALMANT, S., COLLISCHONN, W. Toward continental hydrologic–hydrodynamic modeling in South America. **Hydrology and Earth System Sciences**, v. 22, n. 9, p. 4815-4842, DOI: 10.5194/hess-22-4815-2018, 2018.

2.1. **Introduction**

Reliable estimates simulations of streamflow dynamics and related processes are vital to support water resources management regarding water security, natural hazards, navigation, agriculture and energy production. Therefore, improved predictions of the hydrological system can aid policymakers and stakeholders in making better decisions, also fostering actions to reduce risk and impacts on water resources under current and future conditions. In South America, recent important floods (Marengo *et al.*, 2012b; Hoyos *et al.*, 2013; Ovando *et al.*, 2016) and droughts (Melo *et al.*, 2016; Erfanian *et al.*, 2017), together with uncertainties about the potential effects of climate change (Marengo *et al.*, 2009) are encouraging new strategies for meeting social, economic and environmental water demands in large river basins all over the continent, some of them extending beyond political borders.

In this context, large-scale hydrological models arise as important tools for simulating the terrestrial phase of the water cycle. Despite limitations related to observed (in situ) data, especially in developing countries, advances in computational resources and remote sensing technologies are pushing such models toward continental and global scales with increasing resolution (Wood *et al.*, 2011; Bierkens, 2015; Bierkens *et al.*, 2015; Sood and Smakhtin, 2015). Currently, estimates of water fluxes at these scales are usually obtained using two modeling frameworks, namely global hydrological models (GHMs) and land surface models (LSMs) (Haddeland *et al.*, 2011). While GHMs are more concerned with water resources assessment and lateral transfer of water, thus enabling quantification of human impacts and water scarcity/stress (Doll *et al.*, 2009; Wada *et al.*, 2011), LSMs were primarily developed to provide lower boundary conditions for atmospheric circulation models, i.e., having a particular focus on vertical fluxes of heat and water (Balsamo *et al.*, 2009). The latter are often coupled (i.e., in offline mode) to global river routing models designed for transporting water along drainage networks (Decharme *et al.*, 2008; Zaitchik *et al.*, 2010; Yamazaki *et al.*, 2011; Getirana *et al.*, 2012), which also enables the conversion from surface and groundwater runoff into river discharge and other surface water variables (e.g., flood extent, water level).

Although global-scale models can provide valuable spatiotemporal estimates of water fluxes and projections of those estimates (Sood and Smakhtin, 2015), their ability to reproduce discharge observations at basin scale and to address practical water management issues is still limited (Archfield *et al.*, 2015; Hattermann *et al.*, 2018). Inaccuracies in runoff estimation from GHMs and LSMs may be first attributed to the uncertainty in global satellite precipitation

products (Tian and Peters-Lidard, 2010; Sperna Weiland *et al.*, 2015), but several studies have shown considerable differences between model outputs even when using the same meteorological forcing, given the lack of knowledge about runoff generation processes and deficiencies in parameter estimation (Haddeland *et al.*, 2011; Gudmundsson *et al.*, 2012; Zhou *et al.*, 2012; Beck *et al.*, 2017b). In particular, calibration has been found to have the largest impact on storage fluxes, evapotranspiration and discharge in comparison to variations in model structure and forcing data (Muller Schmied *et al.*, 2014), which is a reason to call for efforts on this exercise as many of the GHMs and LSMs are not calibrated (Sood and Smakhtin, 2015; Zhang *et al.*, 2016; Beck *et al.*, 2017b).

An alternative to overcome some limitations of GHMs and LSMs is to expand the spatial domain of hydrological models that were initially developed for catchment to regional scales. Applying these models at national (Crooks *et al.*, 2014) to continental domains (Abbaspour *et al.*, 2015; Pechlivanidis and Arheimer, 2015; Donnelly *et al.*, 2016) translates into a better use of local expert knowledge and country-specific datasets that may be difficult to reach globally. At the same time, it is possible to focus on regionally relevant processes that are usually not included or not well resolved in global models. In South America, for example, several previous studies suggested that lateral water fluxes in large lowland rivers should be resolved using hydrodynamic routing (Paiva *et al.*, 2011; Paz *et al.*, 2011; Yamazaki *et al.*, 2011; Paiva *et al.*, 2013a; Paz *et al.*, 2014; Pontes *et al.*, 2017; Zhao *et al.*, 2017), while GHMs generally apply methods based on constant/variable velocity or a kinematic simplification of the St. Venant equations (see the overview by Kauffeldt *et al.* (2016) and Bierkens (2015)). Even if LSMs can be coupled offline to more physically based global river routing models (Yamazaki *et al.*, 2011; Getirana *et al.*, 2017b), calibration in the latter is likely to compensate for errors in runoff generation (Pappenberger *et al.*, 2010; Getirana *et al.*, 2013; Hodges, 2013) and lack of relevant vertical hydrological processes linked to river–floodplain dynamics (Pedinotti *et al.*, 2012; Paz *et al.*, 2014; Fleischmann *et al.*, 2018). In turn, fully coupled large-scale hydrologic–hydrodynamic models (Paiva *et al.*, 2013a) can handle the above interactions while using one single modeling framework, and are now feasible for using in continental domains because recent routing schemes (Bates *et al.*, 2010) have proved to be computationally efficient for both regional (Getirana *et al.*, 2017b; Pontes *et al.*, 2017; Fleischmann *et al.*, 2018) and global simulations (Yamazaki *et al.*, 2013).

Over the past decades, skill in streamflow prediction has been emphasized in catchment- to regional-scale modeling (Archfield *et al.*, 2015), but there is a growing opportunity to

perform further spatial analyses rather than just relying on point measurements. Currently, a wide range of remote sensing products can be used to assess other variables than discharge, such as terrestrial water storage (Tapley *et al.*, 2004; Watkins *et al.*, 2015), evapotranspiration (Miralles *et al.*, 2011; Zhang *et al.*, 2018), soil moisture (Kerr *et al.*, 2012) or water surface elevation derived from satellite altimetry (Santos da Silva *et al.*, 2010). Previous studies have shown the utility of the aforementioned datasets not only to validate hydrological/routing models (Alkama *et al.*, 2010; Getirana *et al.*, 2012; Paiva *et al.*, 2013a) but also as an interesting tool to constrain and estimate model parameters (Getirana, 2010; Werth and Guntner, 2010; Lopez *et al.*, 2017). Therefore, remote sensing products can be helpful for continental-scale modeling in assessing regions where streamflow data are scarce, as well as to outline areas in which future model improvements are potentially needed.

In parallel, the interest in building catchment/regional models up to continental domains, together with global models trying to be locally relevant through hyper-resolution (Wood *et al.*, 2011), fosters the need to reduce the gap between these two modeling communities (Archfield *et al.*, 2015; Bierkens *et al.*, 2015). If the primary goal of a continental model is to provide estimates of river discharge to support regional water management practices, the results can also be compared with outputs of global models to assess both the performance and potential shortcomings of these models under a regional perspective. In recent years, there has been an increasing number of studies assessing outputs of LSMs through multimodel intercomparison (Zaitchik *et al.*, 2010; Gudmundsson *et al.*, 2012; Zhou *et al.*, 2012), sometimes in conjunction with GHMs (Haddeland *et al.*, 2011; Beck *et al.*, 2017b). Other recent studies focused on intercomparison of regional models in large basins around the world, usually relating overall performance to a single gauge station and having a particular interest in monthly statistics (Huang *et al.*, 2016; Eisner *et al.*, 2017; Krysanova *et al.*, 2017). Moreover, little attention has been given to the intercomparison of global and regional-scale models, and the existing studies only focused on monthly to annual flows (Zhang *et al.*, 2016) and projection of climate change impacts using a small number of gauge stations (Gosling *et al.*, 2011; Hattermann *et al.*, 2018). As streamflow is highly variable over space and at short timescales (i.e., daily), model performance should be assessed with spatially distributed data within large basins and at sub-monthly intervals (Wu *et al.*, 2014; Beck *et al.*, 2017b; Zhao *et al.*, 2017), but to our knowledge, no cross-scale (i.e., regional/continental × global models) intercomparison with a comprehensive evaluation of daily river discharge has been carried out over South America.

In this paper, we aim to start bridging this gap by (i) extending a regional-scale, fully coupled hydrologic–hydrodynamic model to the entirety of South America, assessing its ability to represent discharge and other hydrological variables across the continent; (ii) exploring how discharge estimates from continental-scale modeling perform when compared to those estimated with state-of-the-art global models and (iii) identifying the issues that should be addressed for improving continental-/global-scale modeling in this continent. The next sections provide a brief description of (i) the major river systems of South America, (ii) modeling approaches, (iii) datasets selected for validation, (iv) calibration procedures, (v) global models selected for discharge comparison and (vi) metrics used for assessment of results.

2.2. **Overview of the major South American river systems**

South America is one of the most freshwater-abundant regions on Earth, contributing around 30 % of the global runoff to the oceans (Clark *et al.*, 2015) despite only having 12 % of the total land area. Because of a combination of wide latitudinal extent (10º N–55º S), major orographic features and strong oceanic influences (Garcia and Mechoso, 2005; Vera *et al.*, 2006a; Garreaud *et al.*, 2009), the continent is subject to a diverse climate that feeds 6 out of the 10 largest basins in the world in terms of mean annual discharge, 4 of them only within the Amazon (Latrubesse *et al.*, 2005). In particular, the Amazon is probably the most relevant hydrological system of the world, which attracts great scientific attention due to its ecological importance and role in local to global climate (Werth and Avissar, 2002; Vera *et al.*, 2006a).

Figure 2.1 presents general information about South America, including hydroclimatic characteristics, major wetlands and hydrological regions. According to classifications of the Food and Agriculture Organization (FAO) and Brazilian National Water Agency (ANA), the continent is partitioned into 27 major hydrological divisions, with the largest ones (Amazon, La Plata and Orinoco basins) sharing much of their water between different countries. Because almost 80 % of the territory lies between the tropics, the continent is dominated by an equatorial (tropical) climate that drives high amounts of rainfall especially near the equator, but extreme conditions also exist and range from very arid (such as the Atacama desert in northern Chile) to polar areas over the Andes Cordillera and south of Patagonia (southern Argentina and Chile). As a result, water availability is subject to be highly variable with large discrepancies in mean annual flows, for example, 8.7 mm yr^{-1} at Desaguadero River in the Colorado basin (Canalejas gauge station, 1.8 10^5 km^2) compared with 2100 mm yr^{-1} at Japura River (Puerto Cordoba gauge station, 1.5 10^5 km^2), the latter located in the Amazon basin

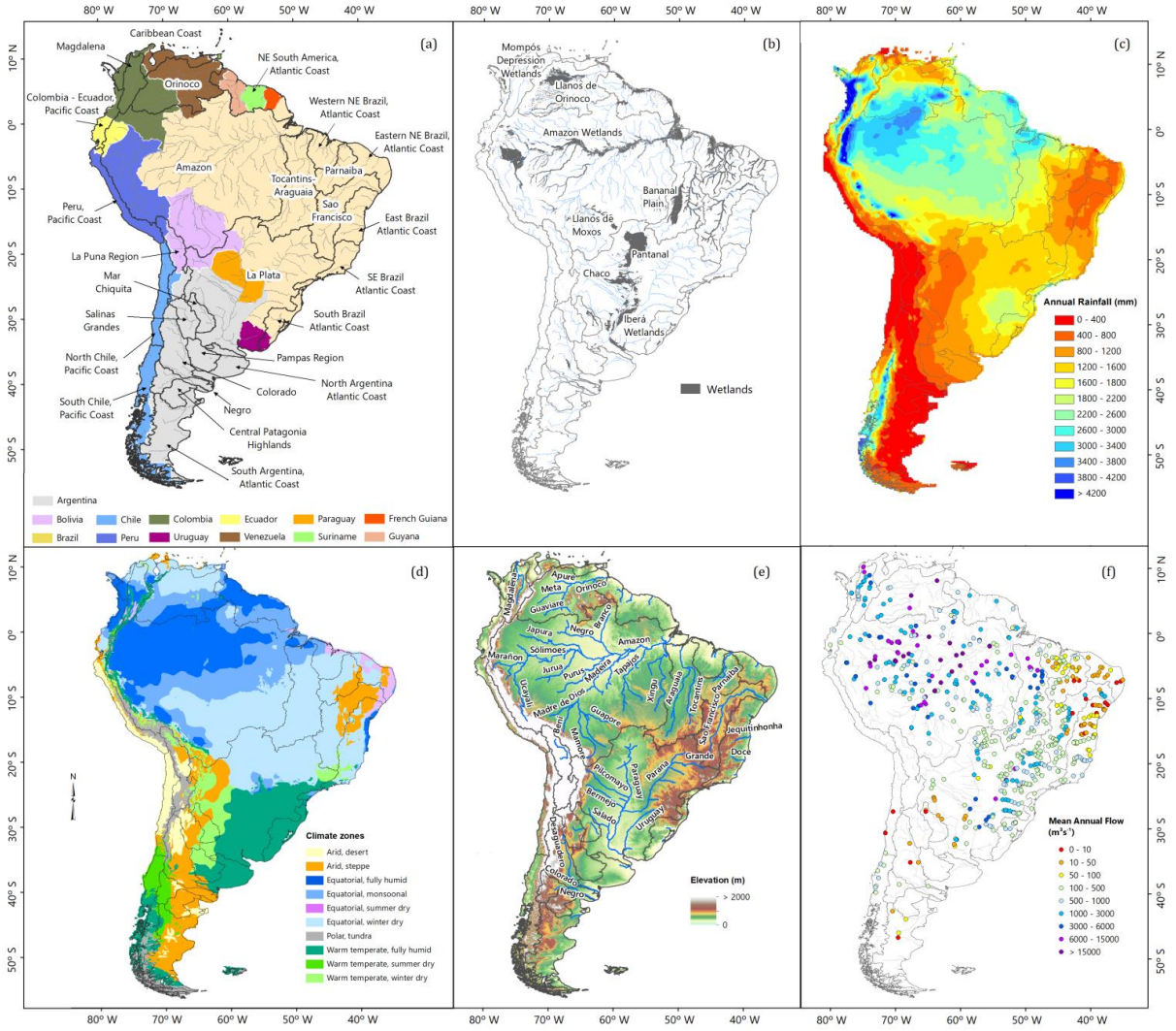

Figure 2.1. South America maps showing: (a) countries and major hydrological regions according to FAO and ANA classifications, (b)Major wetlands and lowland regions, adapted from (Lehner and Döll, 2004), (c) mean annual precipitation derived from the MSWEP dataset (Beck *et al.*, 2017c), (d) Köppen–Geiger updated climate classification from Kottek *et al.* (2006), (e) relief map based on the Bare-Earth SRTM (O'Loughlin *et al.*, 2016), including main rivers and (f) mean annual flow at discharge gauge stations used in this study.

Regarding river dynamics, flows in the Amazon are largely affected by floodplains over extensive flat terrains, causing significant flood peak delay and attenuation (Richey *et al.*, 1989; Alsdorf *et al.*, 2007; Yamazaki *et al.*, 2011; Paiva *et al.*, 2013a). Because flood waves have travel times in the order of a few months, sometimes out of phase because of the seasonal differences in precipitation (Richey *et al.*, 1989), rivers are subject to strong backwater effects that extend for several hundred kilometers upstream of the river mouth or the confluence of its tributaries (Meade *et al.*, 1991; Getirana and Paiva, 2013; Paiva *et al.*, 2013a), existing in both high- and low-water periods (Trigg *et al.*, 2009). To the north, the Orinoco basin shares some characteristics of the Amazon, such as a unimodal flood pulse and low interannual variability of floodplain inundation, especially in the Llanos region (Hamilton *et al.*, 2002). In addition,

the high amplitude of the mainstem water level — 14 to 16 m — produces backwater effects in its tributaries with strong hydrological gradients (Rosales *et al.*, 2002).

At the heart of South America, the La Plata basin plays a major role in terms of agriculture, hydroelectricity and the economy in general, corresponding to almost 70 % of the combined gross domestic product (GDP) in countries such as Argentina, Paraguay, Bolivia and Brazil (Barros *et al.*, 2006; Vera *et al.*, 2006a). La Plata is mainly composed of the Paraná and Paraguay Rivers and, to a lesser extent, the Uruguay River, which are completely different with respect to flow conditions. For example, the upper Paraná is largely regulated by reservoirs (about 50 % of mean annual flow, according to Su and Lettenmaier (2009)) and provides around 75 % of discharge up to the confluence with Paraguay River, despite the similar drainage area of both basins (~10^6 km²) (Barros *et al.*, 2006). The Paraguay basin, on the other hand, is largely influenced by one of the largest wetlands in the world — the Pantanal —, a complex anabranching river–floodplain system characterized by very gentle slopes that can be less than 1.5 cm.km^{-1} (Tucci and Clarke, 1998; Berbery and Barros, 2002; Paz *et al.*, 2011; Bravo *et al.*, 2012). Much of the water stored in the floodplain at high water does not return to the channels during the drying phase and become available for evaporation and infiltration (Paz *et al.*, 2014), so flood waves are lagged by about 4–6 months (Tucci and Clarke, 1998; Hamilton *et al.*, 2002), up to 60 % water volume can be lost (Goncalves *et al.*, 2011), and the shape of downstream hydrographs is strongly modified (Bravo *et al.*, 2012). Moreover, huge areas on the right overbank of the Paraguay River (Chaco Plain) have poorly defined drainage networks associated with alluvial megafans (Latrubesse, 2015), which makes this basin one of the most challenging regions for hydrological modeling in South America.

The headwaters of La Plata also border important hydrological systems such as the Tocantins–Araguaia and São Francisco in a tropical wet–dry biome called Brazilian Cerrado (i.e., Brazilian savanna). The former is composed of Tocantins and Araguaia rivers, flowing parallel northwards until joining approximately 550 km upstream of the basin mouth near the Amazon delta. While the Tocantins is marked by a cascade of large dams, the Araguaia River is much less altered and hosts the huge Bananal plain, which contributes up to 30 % of reduction in peak discharge due to floodplain inundation (Lininger and Latrubesse, 2016). Regarding São Francisco, two-thirds of the runoff is generated at the upper part of the basin (Allasia *et al.*, 2006) and the main stem crosses a semiarid region known as the “drought polygon,” which affects several parts of Northeast Brazil including the Parnaíba basin. At the south of the continent, rivers flowing to the Atlantic Ocean correspond to less than 40 % of the area (i.e., >

60 % is related to endorheic basins) (Pasquini and Depetris, 2007) and their annual cycles usually show two maxima, one associated with the winter rainfalls and another with snowmelt during spring and early summer (Rivera *et al.*, 2018).

2.3. **Methods**

2.3.1. MGB model

2.3.1.1. Model description

The MGB, *Modelo hidrológico de Grandes Bacias* (Large-Scale Hydrological Model) is a conceptual, semi-distributed, large-scale hydrological model first presented by Collischonn *et al.* (2007a). The choice of MGB for this study was motivated by several past applications in South America (Allasia *et al.*, 2006), which encompassed rapid response (Collischonn *et al.*, 2005; Siqueira *et al.*, 2016a) to markedly seasonal and often slow response basins (Bravo *et al.*, 2012; Paiva *et al.*, 2013a; Fan *et al.*, 2016a; Pontes *et al.*, 2017). In its most recent version, basins are divided into unit-catchments (Paiva *et al.*, 2011; Pontes *et al.*, 2017), each one containing a single river reach with an associated floodplain and hydrological vertical water balance. Combinations of soil type and land use within each unit-catchment are categorized as Hydrological Response Units (HRUs). Water and energy budgets are computed independently for each HRU of each unit-catchment, and soil is depicted as a bucket model with a single layer. Canopy interception is represented in terms of leaf area index (LAI) and evapotranspiration (soil, plant transpiration and open water evaporation) is calculated using the Penman–Monteith equation. Surface runoff is produced using the variable contribution area concept following the Arno model (Todini, 1996), while groundwater and subsurface flows are computed, respectively, with linear and nonlinear functions according to water availability in the soil layer. Runoff from each one of the components (surface, subsurface and groundwater) is propagated to the stream network using linear reservoirs (i.e., hillslope routing). As MGB was primarily developed for tropical regions, snow processes are not represented in the current model version.

Flow routing in river channels can be computed using the Muskingum–Cunge method (Collischonn *et al.*, 2007a), a one-dimensional full hydrodynamic method (Paiva *et al.*, 2013a) or the local inertial method (Pontes *et al.*, 2017). In this work, the MGB was applied with the inertial routing as described by Pontes *et al.* (2017), which uses the 1D version of the explicit local inertial approximation proposed by Bates *et al.* (2010). The routing structure of MGB is similar to that described by Yamazaki *et al.* (2011) and Yamazaki *et al.* (2013), i.e., the volume

of water stored in a given unit-catchment is the only prognostic variable, while other variables such as flow depth and flooded area are diagnosed from the stored volume using floodplain profiles derived using sub-grid topography. The floodplain is treated as a simple storage model and the water level for a given time step is assumed to be constant along the entire unit-catchment. In addition, the model accounts for evaporation in floodplains and infiltration from flooded areas to the unsaturated soil (Fleischmann *et al.*, 2018), thus feedbacks between hydrological and hydrodynamic modules can also be represented (i.e., a two-way coupling approach). Further details on model water balance and flow routing equations are presented in the **Annex A**.

2.3.1.2. GIS Processing

All geoprocessing steps were conducted using an adapted version of the IPH-Hydro Tools package (Siqueira *et al.*, 2016b), using the 15 arcsec HydroSHEDS flow direction map (Lehner *et al.*, 2008) as the main input. We chose the latter because it has received extensive corrections to address topological problems in flat areas and endorheic regions (Lehner *et al.*, 2008) and has been successfully applied for river routing in other studies (Yamazaki *et al.*, 2013; Zhao *et al.*, 2017). An upstream area threshold of 1000 km² was adopted for the onset of drainage networks, while unit-catchments and river reaches were delineated using a fixed-length vector-based discretization of Δx = 15 km (see **Annex A.1.3** for details). This length threshold was selected to ensure a balance between model stability and efficiency, resulting in an improved resolution when compared with configurations used by Yamazaki *et al.* (2013) and Getirana *et al.* (2017b) for river routing with the local inertial method at global and Amazon domains (grids with 0.25º resolution), respectively.

To estimate sub-grid floodplain topography, we first computed the Height Above Nearest Drainage (HAND) map (Renno *et al.*, 2008) using flow directions and drainage networks derived from HydroSHEDS together with the Bare-Earth SRTM version 1 digital elevation model (DEM) (O'Loughlin *et al.*, 2016), and further a floodplain profile was created at each unit-catchment relating HAND value, flooded area and water volume similarly to that done by Yamazaki *et al.* (2013). The Bare-Earth SRTM, resampled from 3 to 15 arcsec to match the HydroSHEDS resolution, was adopted to account for vegetation biases in floodplains since the C-band radar used by the original SRTM is not able to penetrate fully through the canopy (Carabajal and Harding, 2005; Berry *et al.*, 2007). Channel bed elevation at a given unit-catchment was estimated subtracting channel bankfull depth from river bank height (i.e., the elevation at bankfull depth) (Yamazaki *et al.*, 2011; Paiva *et al.*, 2013a), the latter also derived

from Bare-Earth SRTM. However, one of the drawbacks of using an unconditioned DEM such as the Bare-Earth SRTM is the high level of noise affecting channel bank elevations, which need to be attenuated to avoid excessive inundation in low-relief areas. Instead of applying smoothing algorithms that modify the original DEM values (Paiva *et al.*, 2011), a simple linear regression was fitted to DEM pixels located over drainage networks within each unit-catchment (river reach). Channel bank heights were set as the smoothed elevation associated with the center pixel of each river reach, while the original DEM values remained unchanged, for example, when computing the HAND model and associated floodplain profiles (see **Annex A.1.5 and A.1.6**, for more details).

2.3.1.3. River hydraulic geometry

Because flow routing is very sensitive to river geometry (Yamazaki *et al.*, 2011; Getirana *et al.*, 2012; Paiva *et al.*, 2013a), channel parameters such as bankfull width and depth must be properly defined. However, detailed information about channel geometry is usually not available for large-scale basins and a very common approach is to adopt classic hydraulic geometry relationships (HGs) (Leopold and Maddock, 1953) for specific sites according to drainage area or discharge (Decharme *et al.*, 2008; Yamazaki *et al.*, 2011; Getirana *et al.*, 2012; Paiva *et al.*, 2013a; Luo *et al.*, 2017; Pontes *et al.*, 2017). Here, the global database of Andreadis *et al.* (2013) was used to set initial values of bankfull widths and depths, which were derived from 2-year return period flows using the Global Runoff Database Center (GRDC) data and universal HGs obtained from several rivers around the world. In addition, regional HGs (Beighley and Gummadi, 2011; Paiva *et al.*, 2011; Paiva *et al.*, 2013a; Pontes, 2016) and width estimates based on satellite imagery from Pontes (2016) were included to improve the global channel geometries of Andreadis *et al.* (2013) for Amazon and La Plata basins.

2.3.1.4. Model forcing

The Multi-Source Weighted Ensemble Precipitation — MSWEP v1.1 (Beck *et al.*, 2017c) — was used as precipitation input to the rainfall-runoff module of the MGB model. This is a 3-hourly, global-scale dataset (0.25º resolution) that optimally combines satellite, reanalysis and daily gauge data, and it has been evaluated with satisfactory results in a recent comparison of several precipitation datasets (Beck *et al.*, 2017d). Regarding climate variables used to compute evapotranspiration, mean monthly data for the period 1961–1990 were retrieved from the Climate Research Unit (CRU) Global Climate v.2 (New *et al.*, 2002), which provides long-

term climatologies of temperature, pressure, radiation and wind speed for all land areas at 10′ resolution.

2.3.1.5. Land use and soil data

Herein, we used the 400-m resolution HRU merged product (soil + land use) for South America (Fan *et al.*, 2015a), which is available at https://www.ufrgs.br/lsh. Basically, the soil map is a combination of the Brazilian database RADAMBrasil and the FAO Digitized Soil Map of the World and Derived Soil Properties, the latter included to account for areas lying outside of Brazil. Land use classification was retrieved from the Global Land Cover map, which was generated using Envisat MERIS fine-resolution (300 m) satellite imagery over the year 2009. Regional land use maps of some Brazilian states were further included in the HRU merged product to improve level of detail.

2.3.2. Validation datasets

2.3.2.1. Discharge and water level data

Daily records of discharge were collected from several national hydrological services including Agência Nacional de Águas (ANA/Brazil: http://www.snirh.gov.br/hidroweb/), Operador Nacional do Serviço Elétrico (ONS/Brazil, Reservoir naturalized flows: http://ons.org.br/), Instituto Nacional del Agua (INA/Argentina: http://bdhi.hidricosargentina.gob.ar/), Instituto de Hidrología, Meteorología y Estudios Ambientales (IDEAM/Colombia: http://www.ideam.gov.co/solicitud-de-informacion), Servicio Nacional de Meteorología y Hidrología (SENAMHI/Peru and Bolivia), Dirección General de Aguas (DGA/Chile: http://snia.dga.cl/BNAConsultas/) and other databases such as the Environmental Research Observatory for geodynamical, Hydrological and Biogeochemical control of erosion/alteration and material transport in the Amazon (ORE-HyBam: http://www.ore-hybam.org) and the GRDC (http://www.bafg.de/GRDC/, for Ecuador and NE South America). Based on expert knowledge, we masked out gauges heavily influenced by upstream reservoirs and included only gauges with more than 10 000 km² of drainage area. In a few cases, however, this threshold was lowered to include, at least, a small number of gauges due to the lack of available data. Short time series with less than five years of records were also excluded from analysis. The complete list of discharge gauge stations can be found in the **Annex B.**

Satellite altimetry data were obtained from the THEIA/Hydroweb website (http://hydroweb.theia-land.fr/). Within this database, time series of water surface elevation (WSE) were extracted manually using the methodology presented in (Santos da Silva *et al.*, 2010) and are provided at virtual stations (VSs) where the satellite ground track forms a crossover with the river network (~10–40 cm of water level accuracy). A total of 841 VSs were found over the Amazon basin, 10 over the Orinoco basin and 29 over the La Plata basin. Data are derived from the observations of Envisat and Jason-2 for the period of 2002–2010 (35-day repeat orbit) and 2008–2010 (10-day repeat orbit), respectively. In situ stage data from ANA gauge stations were also obtained for the Brazilian territory and were filtered using the same criteria as discharge data.

2.3.2.2. Terrestrial water storage (TWS)

Launched in 2002, the Gravity Recovery and Climate Experiment (GRACE) measures temporal changes in the Earth's gravity field (Tapley *et al.*, 2004). Several studies have shown the ability of GRACE to detect continental water storage variations at large spatial scales (Wahr *et al.*, 1998; Ramillien *et al.*, 2004; Tapley *et al.*, 2004), which can provide insights into hydrological modeling about potential deficiencies in process description, parameters and input data (Schmidt *et al.*, 2008). Here, we used the Release 05 JPL RL05M v2 mass concentration (mascon) estimates available on the GRACE Tellus website (https://grace.jpl.nasa.gov). The JPL RL05M mascon solution solves for monthly gravity anomalies in terms of 3º × 3º equal-area spherical cap mascons, while using a Coastline Resolution Improvement (CRI) filter to discriminate between land and ocean mass portions of each mascon that spans coastlines (Wiese *et al.*, 2016). Regarding the traditional spherical harmonic approach (SH), which has been widely used in the last decade for global studies (Wahr *et al.*, 1998; Landerer and Swenson, 2012), mascon solutions can also be applied to regional scales (Scanlon *et al.*, 2016) and do not require the user to apply any postprocessing filters to the data, lowering the dependence on using scale factors to recover signal loss (Watkins *et al.*, 2015). Uncertainties in GRACE mascon solutions (3º × 3º) over South America are around 10–15 mm of equivalent water thickness, and have been found to be similar or slightly lower in relation to SH solutions (Scanlon *et al.*, 2016).

Despite the native resolution (3º × 3º), mascon grids are provided with a spatial sampling of 0.5º × 0.5º. We kept the original resolution computing a simple average of 0.5º grid pixels located inside 3º × 3º mascon locations, as signals at sub-mascon resolution cannot be

considered independent of each other. Time series of simulated TWS were first derived by summing water stored in all hydrological compartments, including rivers, floodplains, soil, groundwater and vegetation canopy, in each time step. Similar to Paiva *et al.* (2013a), the modeled TWS was then resampled as the weighted mean of TWS of all unit-catchments within each 3º × 3º equal-area mascon cell, using the former drainage area as weight. To ensure agreement with GRACE data, anomalies of simulated TWS were obtained by subtracting the long-term mean computed for the period between 2004 and 2009.

2.3.2.3. Evapotranspiration (ET)

Reference values of ET were extracted from the Climate Data Record (CDR) (Zhang *et al.*, 2018), which is available at http://stream.princeton.edu:8080/opendap/MEaSUREs/. Within this dataset, 10 gridded global ET products estimated from satellite (five), reanalysis (two) and LSMs (three) were optimally combined at 0.5º resolution using weighted averaging and a Bayesian merging technique. The weight of each product is related to the inverse of the ensemble spread and the deviation from the ensemble mean is assumed as a proxy of the uncertainty/error in individual products. Together with other optimally merged variables provided by the CDR dataset (precipitation, runoff and TWS), estimates of ET were further adjusted with a Constrained Kalman Filter to ensure terrestrial water budget closure at each 0.5º grid cell (Zhang *et al.*, 2018). For comparison purposes, the modeled ET was spatially aggregated into cells of 0.5º resolution using the unit-catchment drainage area as weight.

2.3.3. Model adjustment

Model calibration is commonly performed to improve agreement between observations and model results. However, the traditional gauge-by-gauge calibration used in regional hydrological modeling is not very common in continental to global domains (Archfield *et al.*, 2015; Bierkens, 2015; Mizukami *et al.*, 2017; Samaniego *et al.*, 2017) because it can lead to spatial discontinuities of parameters (i.e., patchwork patterns) and overfitting to account for limitations in data and model structure. In other words, good results of discharge may not reflect a suitable depiction of the underlying hydrological processes, so modelers are more likely to "get the right answers for the wrong reasons" (Kirchner, 2006).

In an attempt to reduce the only dependency of river gauges during calibration, regions of parameter sets were derived by intersecting the global map of lithology/geology of Durr *et al.* (2005) with large South American basins/hydrological regions, the latter shown in Figure

2.1a. The Amazon and La Plata basins were further divided into their main tributaries prior to intersection due to their large spatial extent. As parameter sets do not correspond to a single gauge station, but rather to regions defined by geological characteristics, multiple gauges were calibrated at the same time using the same parameter set. It is worth mentioning that calibration still remains a challenge for hydrological modeling with respect to large-scale domains (Mizukami *et al.*, 2017) and assessing the suitability of emerging parameter regionalization techniques (Samaniego *et al.*, 2017) may be investigated in the future because it is beyond the scope of this paper.

The set of parameters used for model calibration is listed in Table 2.1, including their respective typical ranges of values. Other parameters used to compute energy balance and evapotranspiration (e.g., LAI, superficial resistance, albedo and canopy height) were defined a priori for each HRU vegetation type according to Collischonn (2001, and references within). Automatic calibration was not used herein to keep coherent values according to soil type and land cover, thus aiding to reduce model overparameterization. Therefore, sensitivity analysis of rainfall-runoff parameters was continuously performed as part of the manual calibration process. Regarding the hydrodynamic module, downstream boundary condition at oceans and lakes (endorheic basins) was set to a constant water level for simplification. Manning coefficient values were globally set to 0.03, with adjustments in specific rivers of the Amazon basin according to Paiva *et al.* (2013a). Infiltration from floodplains to the soil column was considered and only calibrated for Pantanal region (Kinf = 10 mm day^{-1}) since previous studies showed that vertical hydrological processes largely influence model results in this area (Paz *et al.*, 2014). It is worth mentioning that model sensitivity to river geometry and infiltration parameters were previously assessed by Paiva *et al.* (2013a) and Fleischmann *et al.* (2018), respectively.

Table 2.1. Parameters of the rainfall-runoff module of MGB-IPH used for calibration.

Parameter	Description	Unit	Min	Max
Wm	Maximum water storage	mm	50	2000
b	Controls the distribution of water storage capacity of the soil	-	0.01	1.6
Kbas	Percolation rate from soil to groundwater	mm Δt^{-1}	0.1	4
Kint	Saturated soil hydraulic conductivity	mm Δt^{-1}	4	40
Kinf	Infiltration rate from floodplains when soil is completely dry	mm Δt^{-1}		
XL	Soil porosity índex	-	Default = 0.67	
Cb	Groundwater reservoir residence time	hours	800	8000
Ci	Adjustment factor for subsurface reservoir residence time	-	50	200
Cs	Adjustment factor for surface reservoir residence time	-	1	30

As a result of the calibration procedure, several model parameter sets were manually adjusted and can be summarized into the following median values and percentile ranges (p5–p95): Wm = 500 (50–1500) mm; b = 0.2 (0.02–1.5); Kbas = 0.2 (0.01–3.0) mm day^{-1}, Kint = 2 (0.1–50) mm day^{-1}, XL = 0.67 (0.1–0.67), Cs = 15 (5–35), Ci = 120 (20–200) and Cb = 1200 (800–6000) h.

2.3.4. River discharge from GHMs and LSMs

Discharge outputs from state-of-the-art global models were acquired through the eartH2Observe Water Cycle Integrator (WCI: ftp://wci.earth2observe.eu). The WCI hosts multidecadal global water resources reanalysis datasets produced by 10 GHMs and LSMs, providing multi-scale (regional, continental and global) estimates of meteorological and hydrological water balance variables. We selected outputs from the 0.25º resolution Water Resources Reanalysis run 2 (WRR-2) baseline, which is an improved dataset over the WRR-1 (0.5º) produced by the initial project run (Schellekens *et al.*, 2017). Models in the WRR-2 baseline are forced with MSWEP precipitation (1979–2014) and bias-corrected ERA-Interim data using the WFDEI correction methodology (see Dutra *et al.* (2017)). Among the global models in WRR-2, river discharge at 0.25º resolution was only available for one LSM, the HTESSEL offline coupled to CaMa-Flood (Balsamo *et al.*, 2009; Yamazaki *et al.*, 2011), and two GHMs, namely, LISFLOOD (Van Der Knijff *et al.*, 2010) and WaterGAP3 (Doll *et al.*, 2009). The latter two have some degree of calibration and performed relatively well in terms of runoff in a recent model intercomparison (Beck *et al.*, 2017b), while the former is uncalibrated but uses a state-of-the-art hydrodynamic routing model. Within the eartH2Observe project, LISFLOOD and WaterGAP3 were run at, respectively, 0.1º and 0.08333º resolutions, and discharge was then resampled to 0.25º for WRR-2 (Dutra *et al.*, 2017). A brief overview of the structure of these models is shown in Supplement Table S.2.1, at the end of this chapter.

Because these models are grid-based, we followed a similar procedure to that in Zhao *et al.* (2017) to match grid cells to corresponding river gauge stations. First, we applied an automatic routine to find the cell coordinates nearest to the gauge locations. Cells were selected when the difference in the upstream area was within 5 %; otherwise, the surrounding cell with minimum upstream area difference was selected. Gauges associated with cells whose drainage area differed more than 15 % were excluded from the analysis. This procedure was performed separately for each global model to deal with differences between their respective drainage networks. Moreover, due to the spatial resolution mismatch of LISFLOOD and WaterGAP3,

flow accumulation grids were recomputed using their respective flow direction maps (at 0.1º and 0.08333º) and were resampled to the same resolution of discharge grids (0.25º). The corresponding cells were then extensively validated with a thorough, GIS-assisted visual inspection, supported by long-term mean annual discharge grids (derived from each global model) to minimize errors of gauge mislocation.

2.3.5. Model evaluation

MGB simulation was carried out between 01–Jan–1990 and 31–Dec–2009 using a daily time step and a warmup period of 2 years to eliminate the influence of initial conditions. Model results were assessed in terms of discharge, water levels, ET and TWS, while simulated river discharge was further compared with the output of global models. Table 2.2 lists all efficiency metrics used for assessment of model results. Statistics such as the Kling–Gupta efficiency and delay index were the same as used in Kling *et al.* (2012) and Paiva *et al.* (2013a), respectively.

Table 2.2. Efficiency metrics used in this study.

Metric	Abbreviation	Assessment	Variables	Equation
Pearson's Correlation Coefficient	r	Linear correlation	Discharge, Water level, TWS	$\frac{\sum[(x_{sim}-\mu_{sim})(x_{obs}-\mu_{obs})]}{\sqrt{\sum(x_{sim}-\mu_{sim})^2}\sqrt{\sum(x_{obs}-\mu_{obs})^2}}$
Modified Kling-Gupta Efficiency	KGE	Overall Performance	Discharge	$1-\sqrt{(1-r)^2+\left(1-\frac{\mu_{sim}}{\mu_{obs}}\right)^2+\left(1-\frac{CV_{sim}}{CV_{obs}}\right)^2}$
Nash-Sutcliffe Efficiency	NSE	High Flows	Discharge, Water level, TWS	$1-\frac{\sum(x_{sim}-x_{obs})^2}{\sum(x_{obs}-\mu_{obs})^2}$
Log-transformed Nash-Sutcliffe Efficiency	NSE Log	Low Flows	Discharge	$1-\frac{\sum[Log(x_{sim})-Log(x_{obs})]^2}{\sum[Log(x_{obs})-Log(\mu_{obs})]^2}$
Overall BIAS (%)	BIAS	Under- and overestimation (volume)	Discharge,	$\left(\frac{\sum x_{sim}-\sum x_{obs}}{\sum x_{obs}}\right).100$
BIAS in standard deviation (%)	σBIAS	Under- and overestimation (anomalies)	Water levels, TWS	$\left(\frac{\sigma_{sim}-\sigma_{obs}}{\sigma_{obs}}\right).100$
Delay Index (days)	DI	Timing errors	Discharge	$\max r_{xy}[x_{sim};x_{obs}],\quad \text{lag}\,[-100;+100]$
Root Mean Square Error	RMSE	Deviation of predicted values	ET, TWS	$\sqrt{\frac{\sum(x_{sim}-x_{obs})^2}{n}}$

Where: x_{sim}= simulated variable; x_{obs}= observed variable; μ_{sim} = mean of simulated variable; μ_{obs} = mean of observed variable; CV = coefficient of variation, equal to σ/μ; r_{xy} = cross-correlation

2.4. **Results and discussion**

2.4.1. Model Validation

2.4.1.1. River Discharge

Simulated daily discharge was compared with in situ observations and results were presented in maps of performance metrics (*r*, KGE and NSE) at each gauge station (Figure 2.2). In addition, the runoff coefficient ($RC = Q_{mean}/P_{mean}$) was calculated for each gauge station and was plotted against its respective KGE and drainage area (Figure 2.3). There is a good agreement between simulated and observed flows in several regions of South America, as NSE and KGE values are larger than 0.6 in 55 % and 70 % of the cases, respectively. Model performance is clearly higher in the southern and southeastern regions of Brazil, including central Amazon. On the other hand, performance decreases in regions marked by semiarid to arid climates, such as in Northeast Brazil, west and southwest of the La Plata basin, most parts of Argentina and northern Chile. For instance, a poor correlation ($r < 0.2$) is observed in a semiarid region covered by the Colorado basin, where snowmelt/glacier melt contribute a large amount to total runoff and corresponds to the main source of water for human activities (Rivera *et al.*, 2017). Other locations with lower performance (NSE < 0.2) usually refer to regions strongly influenced by orography (around Andes Cordillera), which are expected due to larger uncertainties of satellite-derived precipitation in these areas (Tian and Peters-Lidard, 2010; Paiva *et al.*, 2013a). River discharge at gauge stations with the RC ranging between 0.3 and 0.6 is generally well represented in all spatial scales, while performance tends to be lower for RC < 0.3 and highly variable for rivers with lower drainage areas.

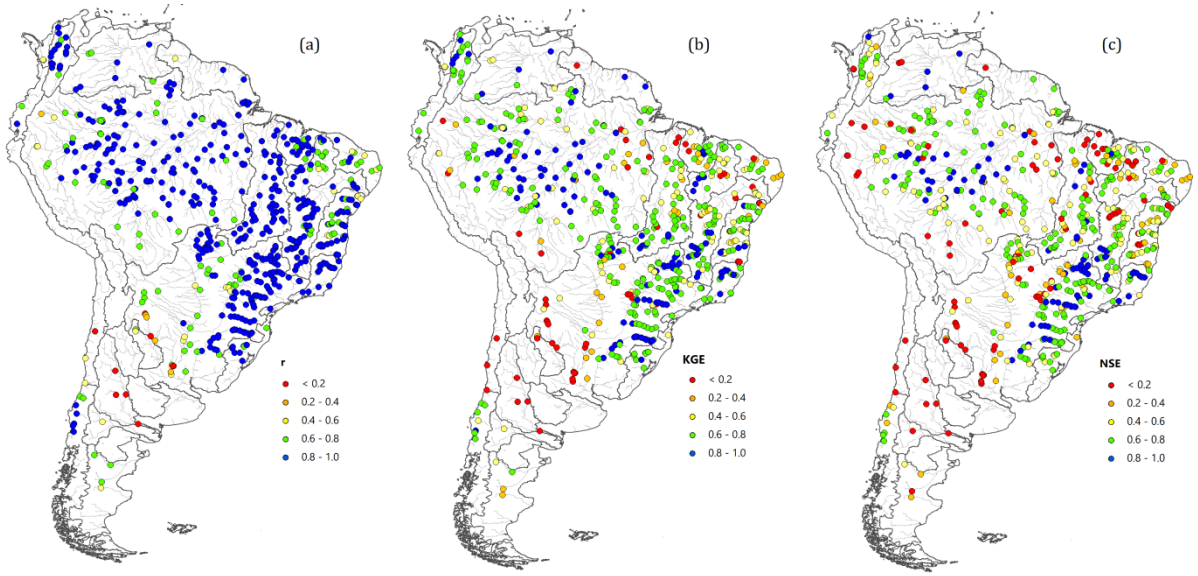

Figure 2.2. Discharge performance over South America in terms of (a) correlation (*r*), (b) Kling–Gupta efficiency (KGE) and (c) Nash–Sutcliffe (NSE).

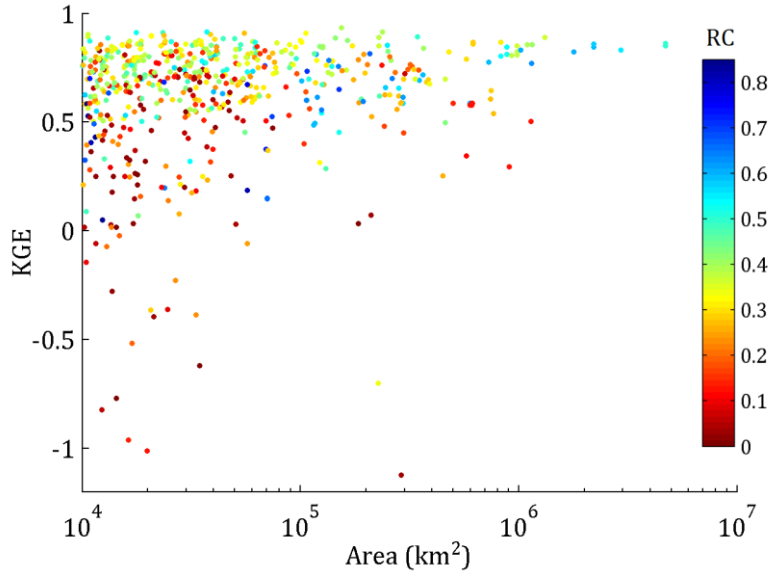

Figure 2.3. MGB model performance (KGE) versus RC and drainage area over South America.

Figure 2.4 shows daily simulated discharge for some of the large South American rivers. The agreement between simulated and observed discharge is notable for both high and low flows in most of the cases, which indicates the model's ability to simulate regional- to continental-scale rivers (10^5 km² to 4.7 10^6 km²) with different flow regimes. Results in the Amazon basin (e.g., Obidos, NSE_{HD} = 0.89) are comparable to other regional studies (e.g., Getirana et al., 2012; Paiva et al., 2013; Luo et al., 2017) while better performance is found over several of its tributaries (e.g., Purus, Madeira and Japura rivers). Figure 2.4 also highlights the improvements of MGB using a hydrodynamic (HD) model over a non-hydrodynamic (noHD) routing method. In the Paraguay River, peak flows are dramatically reduced at the

Amolar gauge station when using the HD routing (up to –75 %), and a similar behavior can be seen at Puerto Bermejo (NSE_{noHD} = –5.8 to NSE_{HD} = 0.42) located about 1600 km downstream near the confluence with the Paraná River. Previous attempts of regional hydrological modeling in this basin that did not account for the floodplain inundation in the Pantanal (e.g., using the calibrated VIC model; see Su and Lettenmaier (2009)) reported negative NSE values for Puerto Bermejo, even at the monthly timescale. Differences in performance between noHD and HD are also quite remarkable (especially in terms of NSE) at gauge stations of Conceicao do Araguaia and Calamar in the lower Magdalena, where a pronounced attenuation effect is observed. On the other hand, in some rivers such as the Uruguay at Garruchos (NSE_{noHD} = 0.85; NSE_{HD} = 0.82), Paraná at Itaipu (NSE_{noHD} = 0.91; NSE_{HD} = 0.87) and Tocantins at Descarreto (NSE_{noHD} = 0.72; NSE_{HD} = 0.70) the routing method has a minor impact. In the case of Orinoco at Ciudad Bolivar, both hydrographs look similar, but the NSE suggests that results are improved when HD routing is used (NSE_{noHD} = 0.83; NSE_{HD} = 0.9).

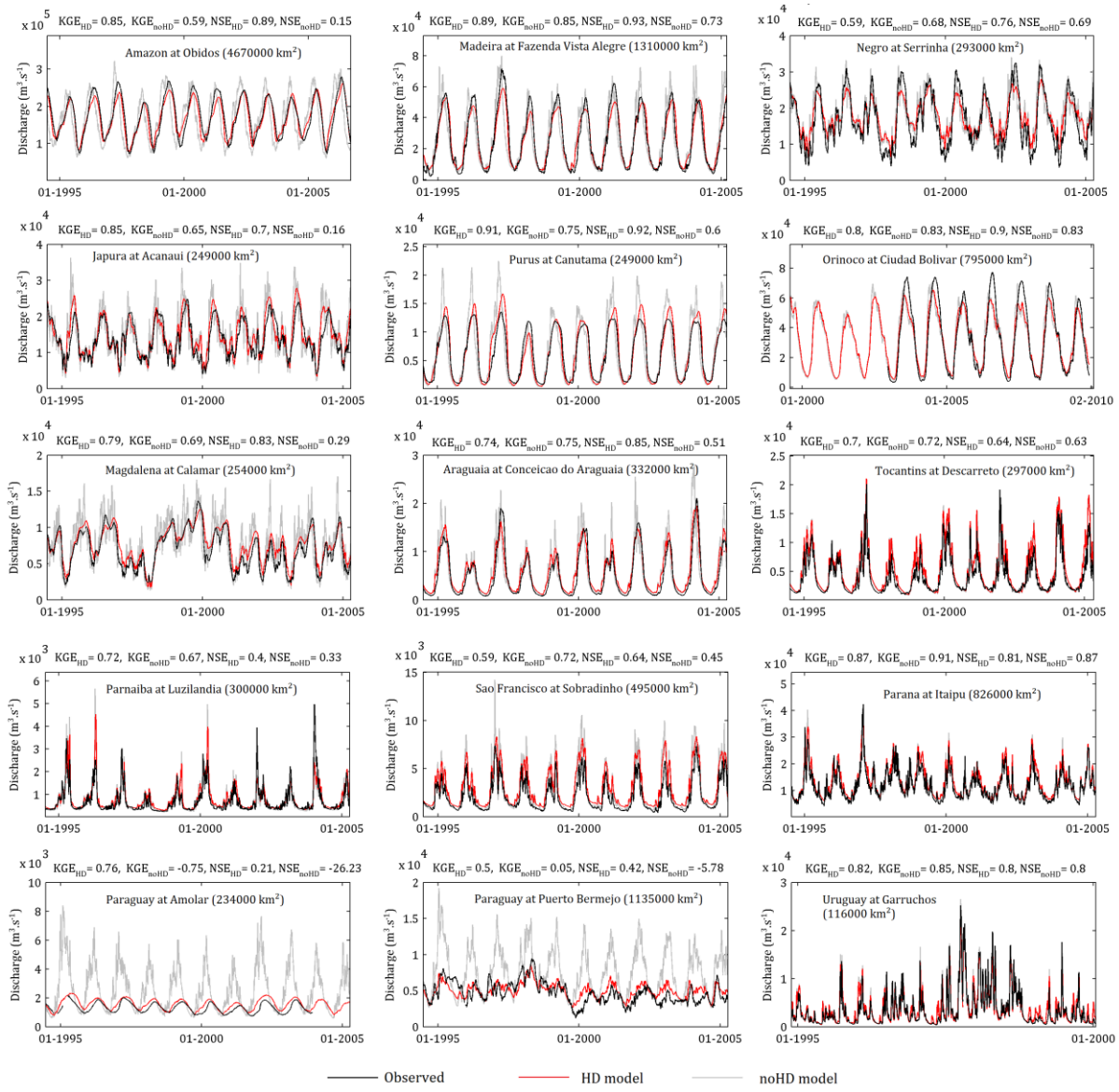

Figure 2.4. Comparison between observed (black) and simulated discharge for major South American rivers. Model results are shown considering both hydrodynamic (HD; red color) and non-hydrodynamic (noHD; gray color) routing methods.

2.4.1.2. Water levels

Results of performance metrics regarding water levels are presented in Figure 2.5. For a suitable comparison, observed data and modeled WSE were first converted into anomalies (i.e., by subtracting their respective long-term mean $\left(h_{new} = h - \bar{h}\right)$ to keep values with the same reference. In addition, Figure 2.6 shows time series of simulated water level anomalies (hereafter referred to as water levels) for some of the large rivers of South America, which were plotted against in situ water levels and satellite altimetry. In general, the results obtained for the assessed gauges and VSs are considered satisfactory in terms of correlation ($r \geq 0.8$ in 80 % of cases) and Nash–Sutcliffe (NSE ≥ 0.6 in 60 % of cases), with a reasonable performance for

amplitudes (–30 % < σBIAS < 30 % in 50 % of the cases). Like prior studies in the same region (Getirana *et al.*, 2012; Paiva *et al.*, 2013a; Getirana *et al.*, 2017b), water levels are well represented in central Amazon, where a good performance is observed at tributaries and along the main river down to its mouth in the Atlantic Ocean. Amplitudes are overestimated (σBIAS > 30 %) in southeast tributaries such as Madeira, Xingu and Tapajos, as well as in headwaters located in the northwest part of the basin. Outside the Amazon, there are acceptable results in the Orinoco (e.g., lower Meta), Uruguay and Tocantins–Araguaia basins, where the model generally performs well in all assessed metrics. Large overestimations in the standard deviation (σBIAS > +50 %) are systematically found over the São Francisco main stem, which are reflected by very low values of NSE (< 0.2). On the Paraguay River, a reasonable agreement between observed and simulated water levels is observed at Amolar, but performance significantly reduces in both correlation and σBIAS for downstream regions (e.g., at Porto Murtinho). In the latter case, model results are clearly advanced in time and do not capture rapid variations of water level originating from lateral contributions of tributaries.

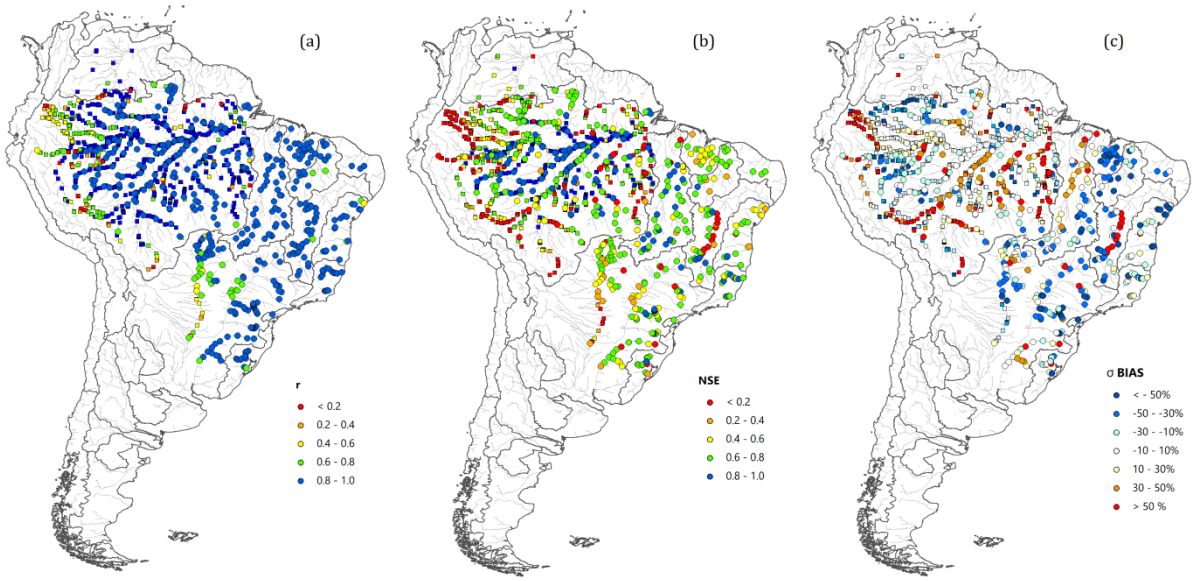

Figure 2.5. MGB performance for simulated water levels over South America in terms of (a) correlation (*r*), (b) Nash–Sutcliffe (NSE) and (c) bias in standard deviation (σBIAS). In situ and satellite altimetry locations are shown by circle and square symbols, respectively.

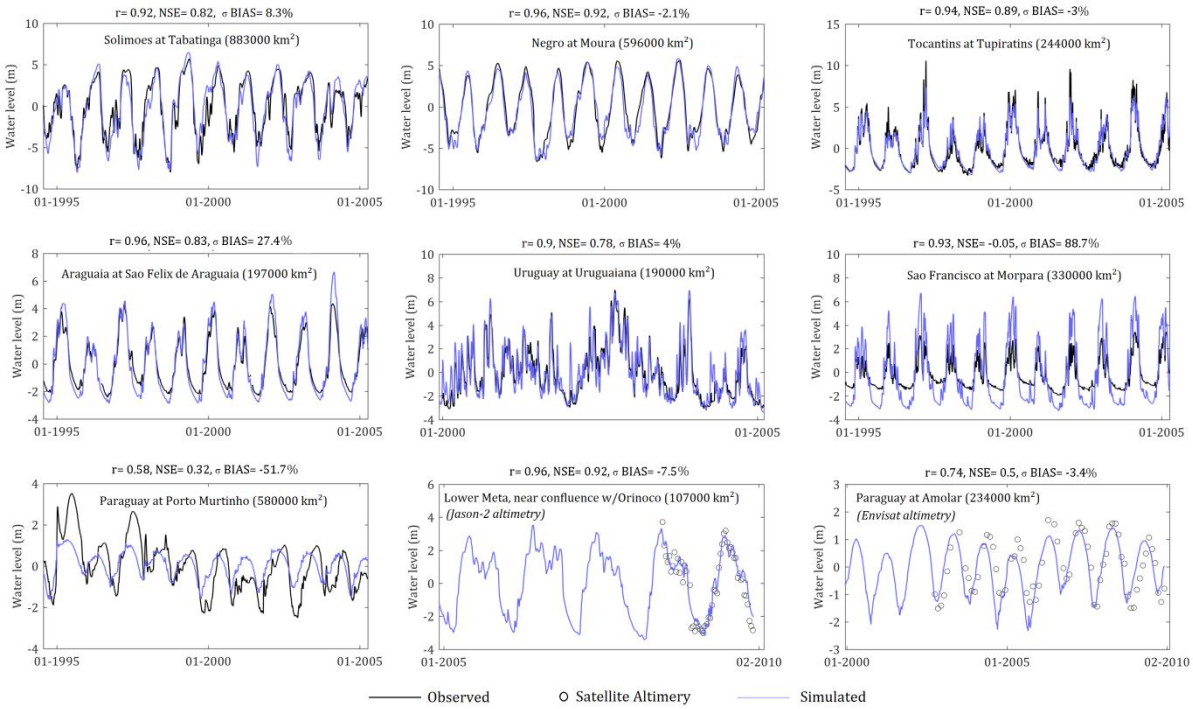

Figure 2.6. Comparison between simulated (blue) and observed (black) water level anomalies in major South American rivers for in situ gauges (continuous lines) and satellite altimetry (circles) at virtual stations (VSs).

Performance in water levels is directly related to the agreement between simulated and observed discharge. On the other hand, even if discharge is well represented, there are uncertainties related to Manning values and also to river widths and depths derived from HGs, which do not reflect singularities of cross sections such as narrowing or widening of rivers at both gauge and VS locations. Previous studies have demonstrated the large influence of channel geometry and roughness on both amplitude and timing of water levels, especially over the Amazon basin (Yamazaki *et al.*, 2011; Paiva *et al.*, 2013a; Paris *et al.*, 2016; Luo *et al.*, 2017). Moreover, riverbed profiles are subject to DEM errors that can hardly be reduced through simple profile-smoothing procedures. For example, datasets used to remove the vegetation bias in Bare-Earth SRTM (IceSAT, vegetation height maps, uncorrected SRTM) have different spatial resolutions that lead to artifacts around the edges of vegetation patches (O'Loughlin *et al.*, 2016), producing additional noise on riverbed elevations. In addition to vegetation, other SRTM error sources such as stripe noise (Rodriguez *et al.*, 2006) significantly affect large flat areas on the La Plata basin (Yamazaki *et al.*, 2017), which can ultimately impact model results. Model resolution and the ability to route discharge in downstream multi-directions (e.g., rivers with bifurcations and anabranching networks) can affect simulated water levels and flooded areas (Mateo *et al.*, 2017), which has been taken into account in recent studies with MGB (Pontes *et al.*, 2017; Fleischmann *et al.*, 2018) but not in this continental model application.

Other simplifications in the model may also affect results, like the assumption of rectangular cross-sections and zero velocity of water stored on floodplains.

2.4.1.3. Evapotranspiration (ET)

Figure 2.7 shows the magnitude and seasonality of ET averaged for major basins in South America, as well as the magnitude of errors (RMSE) comparing modeled values to the optimal estimate of the CDR dataset. The ratio of the RMSE to the CDR uncertainty ($RMSE_{unc}$) was calculated to outline regions where simulated ET tends to deviate from the optimal CDR value, i.e., values above unity indicate that the model error is larger than the mean deviation of all datasets (used in CDR) from their ensemble mean.

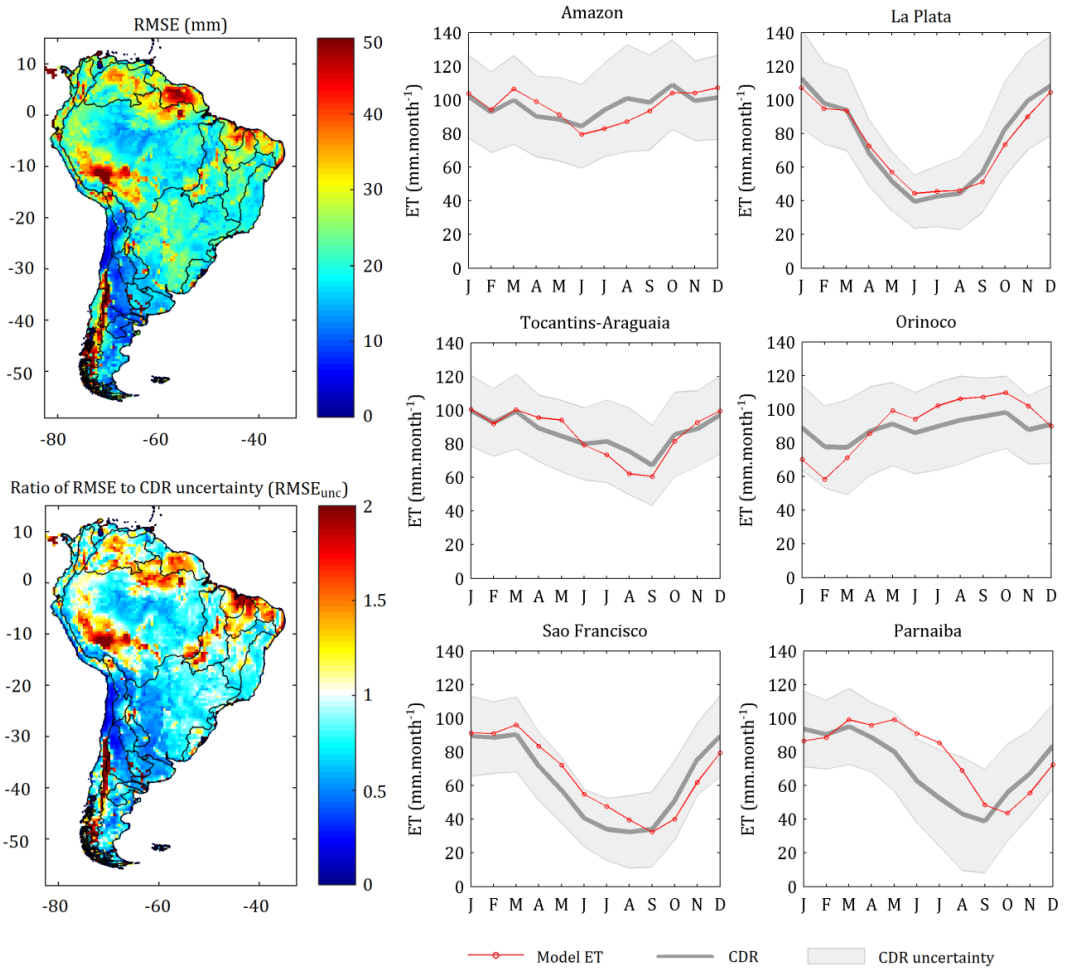

Figure 2.7. Comparison between MGB and CDR ET estimates in terms of RMSE (left) and seasonality for major South American basins (right). The light gray area represents the proxy of the CDR uncertainty, i.e., the mean deviation of all datasets (within CDR) from the ensemble mean (Zhang et al. 2018).

Results show that MGB can capture patterns of ET over the South America region. Simulated ET values are within the CDR uncertainty range in most of the continent ($RMSE_{unc}$ < 1), with errors varying between 10 and 30 mm $month^{-1}$. A good agreement in terms of

magnitude and seasonality of ET is observed for the Amazon, Tocantins–Araguaia and mainly for La Plata basin, but the model also performs reasonably well in Sao Francisco. Conversely, larger deviations ($RMSE_{unc} > 1$) are found at low latitudes (20º S–10º N) where RMSE values reach up to 50 mm $month^{-1}$. ET is underestimated during the dry season in basins such as Orinoco (DJF), Amazon and Tocantins–Araguaia (JJA), while it is largely overestimated from the onset to the end of the dry (wet) season in São Francisco and Parnaíba (Orinoco). The latter two are clearly affected by a temporal lag in ET seasonality, where simulated values are delayed by approximately 1 month with respect to CDR estimations. At midlatitudes (> 20º S), large RMSE values (above 50 mm $month^{-1}$ and $RMSE_{unc} > 2$) are only observed in a narrow N–S range over the southern Andes.

Regarding issues about the timing and magnitude of simulated ET, meteorological forcing probably has an influence on model performance because long-term mean climate data are used for ET computations. Another possible reason is the lack of spatial variability of moisture in the MGB soil column. Guswa *et al.* (2002) compared a simple bucket (one layer) to a physically based Richards model, showing that large discrepancies can occur with respect to the relationship between ET and average root-zone saturation, as well as in timing and intensity of transpiration, especially for water-limited conditions. Moreover, Wang *et al.* (2006) found that timescales of evapotranspiration can differ significantly between a single-layer and multi-layer soil scheme due to nonlinear interactions that occur in the latter. Indeed, ET is expected to respond quickly at the beginning of the rainy season due to an increase of water availability at the soil surface layer, which cannot be well represented with a single-layer, bucket-type model like MGB. In contrast to some of the datasets used in CDR (e.g., reanalysis and LSMs), the MGB does not account for snow processes, which may explain the large RMSE values over the southern Andean region.

Although it is beyond the scope of this study for a full assessment of ET estimations derived from hydrological models and other sources, it is important to note that errors presented here correspond to the difference between both estimates (MGB and CDR). ET is one of the most uncertain water balance variables due to its high spatial and temporal variability, thus it is difficult to validate given the lack of ground observations (Miralles *et al.*, 2011; Zhang *et al.*, 2018). Even accounting for ~70 % of the weight in CDR dataset in comparison to LSM and reanalysis (Zhang *et al.*, 2018), remote sensing products of ET are based on Penman–Monteith or Priestley–Taylor equations that depend on vegetation indices and meteorological forcing derived from satellite/reanalysis data, which are associated with many uncertainties (Miralles

et al., 2011; Vinukollu *et al.*, 2011). Christoffersen *et al.* (2014) and Maeda *et al.* (2017) showed that most remote sensing and land surface models are unable to consistently reproduce ET seasonal cycles in tropical areas (across the Amazon basin) when compared with eddy covariance measurements and ET estimates from water balance. In the Amazon, for example, ET seasonality is regulated by radiation, rainfall and how vegetation assimilates water and energy (Restrepo-Coupe *et al.*, 2013; Maeda *et al.*, 2017). Other limitations are also associated with the vegetation cover fraction and how ET is partitioned between transpiration, soil and canopy evaporation (Miralles *et al.*, 2011).

2.4.1.4. Terrestrial water storage (TWS)

Figure 2.8 shows the performance of simulated TWS anomalies in comparison to observations from GRACE mascon solutions. To evaluate the ability of MGB to reproduce monthly variations of TWS, both simulated and observed time series of TWS were averaged to the scale of large basins in South America and are presented in Figure 2.9.

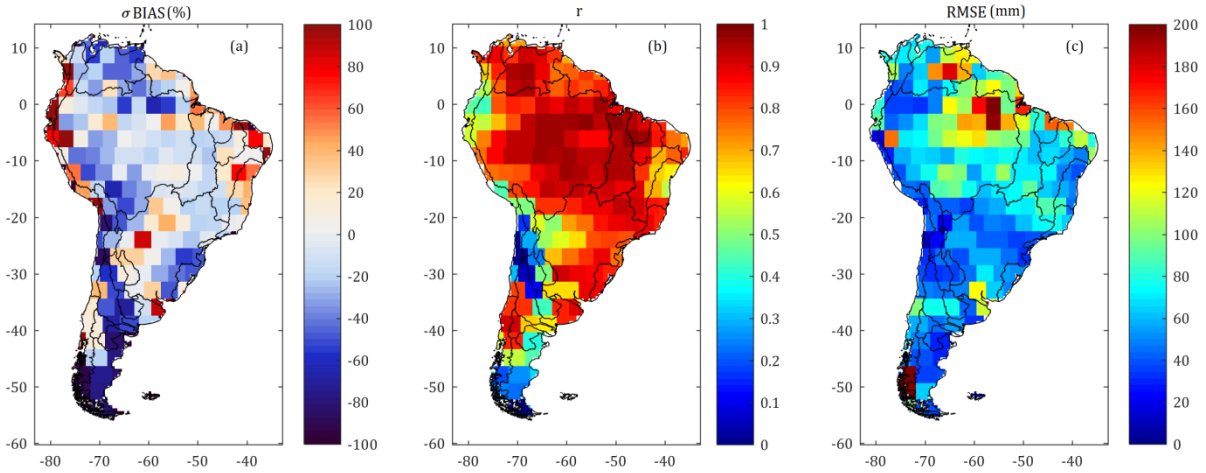

Figure 2.8. Comparison between MGB and GRACE (JPL RL05 v2 mascon solution) TWS anomalies in terms of (a) bias in standard deviation, (b) correlation and (c) RMSE.

In general, the results show that MGB has the ability to represent TWS anomalies over the continent. There is a good temporal correlation in most parts of tropical South America (r > 0.75), as well as in temperate regions with dry summer between latitudes of 30º S and 40º S. Amplitudes of TWS are reasonably well simulated (–20 % < σBIAS < 20 %) mainly in central Brazil, parts of the northeast, south of La Plata and areas of southern Chile. On the other hand, performance typically decreases in semiarid to arid climates, as can be seen in regions such as northern Chile, Colorado basin, west of La Plata and southern Argentina. High negative bias with large RMSE (> 150 mm) is observed in the northeast Amazon and west of the Orinoco,

whereas large overestimations are found mainly over coastlines at low latitudes in the Southern Hemisphere (0–20º S). Moreover, in some regions characterized by polar climate, at the extreme south or in areas over the Andes, modeled TWS anomalies are markedly underestimated (σBIAS < –80 %).

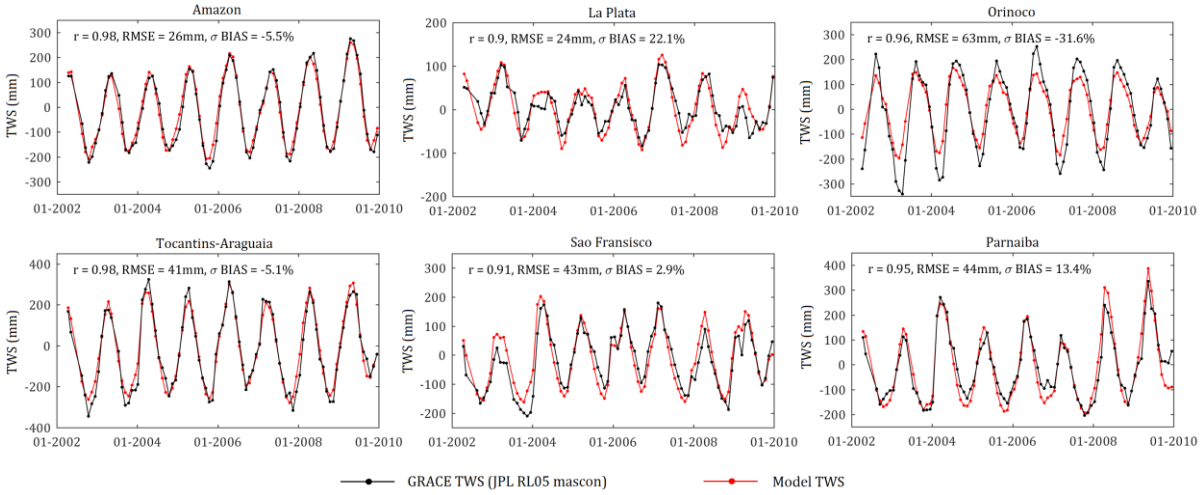

Figure 2.9. Comparison between MGB and GRACE (JPL RL05 v2 mascon solution) monthly TWS anomalies for major South American basins.

Modeled TWS is in good agreement with GRACE observations over the Amazon, Tocantins–Araguaia, São Francisco and Parnaíba basins (r > 0.9, |σBIAS| < 15 % and RMSE < 45 mm), capturing both the interannual variability and amplitude of TWS anomalies for the analyzed period. MGB is also successful in representing annual changes of TWS in the La Plata basin, but with an overestimation (σBIAS = 22 %) probably caused by high positive σBIAS in the Paraguay and Chaco regions. Errors in the La Plata basin (RMSE = 24 mm) are in the same order as those in the Amazon (RMSE = 26 mm). In addition, larger amplitude differences clearly occur in the Orinoco (σBIAS = –32 %), but with a pronounced RMSE (> 60 mm) that mainly originates from the eastern part of the basin.

The good agreement found in the Amazon basin can be attributed to the explicit representation of surface water reservoirs (channels and floodplains), which has been demonstrated to play an important role in both the magnitude and timing of TWS (Alkama *et al.*, 2010; Paiva *et al.*, 2013a; Getirana *et al.*, 2017a). Other authors have pointed out that the contribution of surface storage to TWS is also potentially high in the Orinoco (~45 %) (Frappart *et al.*, 2014), suggesting a large underestimation of the soil storage (in the eastern part of the basin) because anomalies of water level were reasonably well simulated. Indeed, surface storage has been understood as a major component of TWS variability over tropical regions of South America, and may also be relevant for large rivers crossing semiarid areas such as the São

Francisco (Getirana *et al.*, 2017a). In the case of La Plata, the TWS amplitude is likely to be amplified if surface water is anticipated in time (Getirana *et al.*, 2017a), which is probably occurring due to the low correlation of water levels previously simulated for the Paraguay River. In addition, the absence of a well-defined river system due to very flat terrains (e.g., Chaco region, in the west part of La Plata) potentially favors the dominance of the groundwater dynamics over TWS, as already reported by Kuppel *et al.* (2015) in the western Pampas more in the south.

It is worth mentioning that, for regions of South America located in midlatitudes, TWS is dominated by interannual variability rather than the seasonal cycle (Humphrey *et al.*, 2016), where TWS amplitudes are generally lower and errors more apparent. Previous studies showed a strong negative trend in GRACE mascon solutions in the Colorado basin (Scanlon *et al.*, 2016) that can be associated with a decrease in snow water equivalent over the dry Central Andes (Rivera et al., 2017). Moreover, negative variations in glacier mass have been reported in southern Argentina/Chile over the Patagonia Icefields (Chen *et al.*, 2007), which is probably the main responsible for the large RMSE observed in the extreme south of the continent. TWS in nearby semiarid areas is potentially affected by snowmelt/glacier melt because the latter is an important water source of Patagonian rivers flowing to the Atlantic Ocean (Pasquini and Depetris, 2007; Rivera *et al.*, 2018). Inconsistencies along coastlines are also expected because of the smaller size of land mascons that increase uncertainty in GRACE estimates (Wiese *et al.*, 2016). Finally, in addition to issues related to model parameterization and depiction of hydrological processes (e.g., snowmelt), artificial reservoirs (dams) and lakes are not included in the current version of the South America MGB model, leading to additional uncertainties in TWS estimation.

2.4.2. Cross-scale comparison of river discharge from continental × global models

This section presents an assessment of MGB simulated discharge in comparison to the outputs from HTESSEL/CaMa-Flood, LISFLOOD and WaterGAP3 models, extracted from WRR-2 in the context of the eartH2Observe project (Dutra *et al.*, 2017; Schellekens *et al.*, 2017). This offers an interesting opportunity to evaluate to what extent discharge estimates can be improved at the continental scale of South America, as well as to identify the major shortcomings that should be addressed. To provide a concise spatial analysis, discharge from global models was reduced to their ensemble mean (Ensemble GM) and results are presented in terms of the difference of each metric (indicated by "d_metric"), i.e., by subtracting the

performance of MGB from the performance of the Ensemble GM (Figure 2.10). Bias and DI values are given in terms of absolute differences (d_Abs(metric)) to make both under- and overestimations comparable. Therefore, positive values indicate that MGB outperforms the ensemble mean of global models and vice versa. Detailed performance metrics of each model can be found in supplementary material S.2.2, at the end of this chapter.

The continental model presents improvements for all metrics over most of the South America regions when compared with the global ensemble mean. In relative terms, a better agreement of simulated and observed discharge (d_KGE > 0.8) is observed over semiarid regions (e.g., east/northeastern Brazil and most parts of Argentina), which are strongly impacted by bias in the Ensemble GM (d_Abs (BIAS) > 60 %). In tropical regions with marked seasonality and dry winter (e.g., upper Paraná headwaters), differences in bias are lower (–10 % < d_Abs (BIAS) < 20 %), which indicates that KGE performance mainly depends on the variability of flows that is not captured by the Ensemble GM. Correlation is considerably higher over the Paraguay River (d_r > 0.4), highlighting the strong influence of hydrodynamic effects and complex processes in the Pantanal and Chaco regions, as documented by regional studies (Paz *et al.*, 2011; Bravo *et al.*, 2012; Paz *et al.*, 2014; Pontes, 2016). There is also a clear correlation improvement in rivers such as the Araguaia, Amazonas and lower Magdalena, which are also affected by river–floodplain interactions with consequent flood peak attenuation (Paiva *et al.*, 2013a; Lininger and Latrubesse, 2016; Pontes *et al.*, 2017; Angarita *et al.*, 2018). A similar performance is observed for timing (d_Abs (DI)) with absolute differences being larger than 20 days, which also occur in the main stem of the Orinoco basin. In terms of NSE, the largest differences in performance previously observed for the KGE now extend to the main Amazon River, to its tributaries in the eastern region (i.e., Tapajos and Xingu) and also to both Magdalena and Tocantins–Araguaia basins, with values of d_NSE ≥ 0.8. With respect to low to medium flows (d_NSElog), there is a similar pattern to d_KGE (except for eastern Brazil), although with more pronounced differences in the Amazon and Magdalena regions.

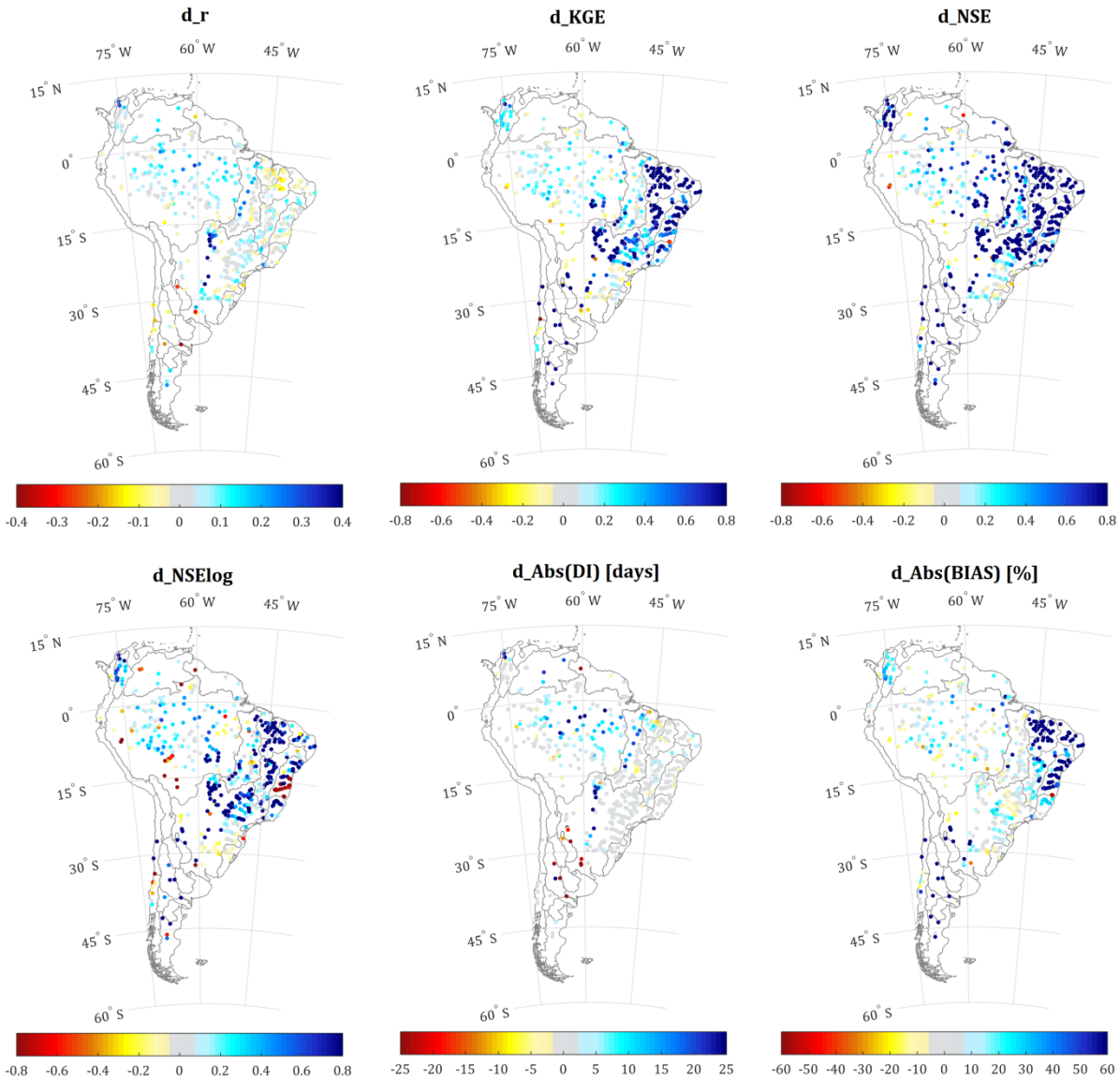

Figure 2.10. Difference between performances of MGB and the Ensemble GM for discharge metrics. Values considered as not significant (gray) are within the ranges –0.05 to +0.05 (d_r, d_KGE, d_NSE and d_NSElog), –5 % to 5 % (d_Abs(BIAS)) and –2 to +2 days (d_Abs(DI)).

The Ensemble GM performs relatively well in all statistics over temperate regions with the absence of lowland rivers (e.g., southern Brazil and southern Chile), and outlines specific locations where the continental approach may be somewhat limited. For example, correlation is slightly reduced for the continental model (–0.1 < d_r < –0.2) in areas over the Parnaíba basin and Chile, while a marked decrease in timing performance (d_Abs (DI) < –20 days) is observed in dry Argentinian rivers like Salado (southwest of La Plata basin) and Desaguadero (Colorado basin). Poor estimates of river geometry and large overestimation of flows in these regions may be causing excessive flooded areas and consequent peak attenuation. Regarding intermediate to low flows, considerable differences in model performance are mainly observed over specific rivers in eastern Brazil and parts of the Amazon basin near the Andes Cordillera (d_NSElog <

–0.8), as well as in regions over southern Chile (–0.2 < d_NSElog < –0.6) that are potentially affected by snowmelt.

Table 2.3 shows differences in median discharge statistics for each global model and also for the Ensemble GM in comparison to the MGB continental model. Because LISFLOOD and WaterGAP3 account for reservoir impacts in their model structure, gauge stations with naturalized discharge data (n = 98) were excluded from the analysis to provide a fair assessment. Except for the Ensemble GM, differences in performance regarding each pair of models (i.e., difference between continental and global) are quite similar for KGE (~0.45) and NSElog (~0.5), while being highly variable for both NSE (~1 to ~1.8) and bias (~4 % to ~30 %). Differences in median DI are between 1 and 2 days, which can be important for cases where flood timing is around this order of magnitude. Among the estimates from global models only, the Ensemble GM outperforms four out of the six metrics analyzed (KGE, NSE, NSElog and DI) with correlation (d_r = 0.03) equivalent to the best of global models for this metric (LISFLOOD, d_r = 0.02). A reduction in performance only occurs when bias is evaluated, where 50 % of the gauge stations have an absolute difference equal to or greater than 11 % compared with differences in HTESSEL/CaMa-Flood (d_Abs (BIAS) ≈ 8 %) and WaterGAP3 (d_Abs (BIAS) ≈ 4 %). In the assessment by Beck *et al.* (2017b) for basins < 10 000 km² around the world, LISFLOOD also had an advantage in correlation when compared with other global models, while WaterGAP3 demonstrated problems related to baseflow index, which may be indicated here by the largest difference of NSElog (d_NSElog ≈ 0.6).

Table 2.3. Median values of discharge metrics for South America, computed as the performance difference between continental and global models. Lower values show better performance for a given model in comparison to MGB continental hydrologic–hydrodynamic model. Gauge stations with naturalized flows were removed from the analysis to provide a fair comparison.

Model difference	d_r	d_KGE	d_NSE	d_NSElog	d_abs(BIAS) (%)	d_abs(DI) (days)
MGB – HTESSEL/CaMa-Flood	0.11	0.48	1.35	0.53	8.3	1
MGB – LISFLOOD	0.02	0.44	1.86	0.48	32.5	1.5
MGB – WaterGAP	0.16	0.44	1.05	0.57	3.8	2
MGB – Ensemble GM	0.03	0.26	0.91	0.27	11.0	0

The set of box plots shown in Figure 2.11 summarizes the individual performance of continental and global models. Results are presented for some of the representative South America basins and for the entire continental region, using a subset of metrics (KGE, NSE, BIAS and DI). In addition, a further analysis of the continental model performance was carried

out using a few degraded configurations: hydrodynamic routing with calibrated rainfall-runoff parameters, i.e., the reference simulation (MGB_HD_calib), hydrodynamic routing with uncalibrated rainfall-runoff parameters (MGB_HD_noCalib), non-hydrodynamic routing with calibrated rainfall-runoff parameters (MGB_noHD_calib) and non-hydrodynamic routing with uncalibrated rainfall-runoff parameters (MGB_noHD_noCalib). For the uncalibrated MGB versions (noCalib), a single set of parameters was adopted corresponding to the median values resulting from model adjustment (as shown in section 2.3.3). It is important to note that only rainfall-runoff parameters were reduced to their median values, while river routing parameters (Manning coefficient and river geometries) remained unchanged.

Results indicate that global models have important limitations in representing daily discharge in South America. In absolute terms, more than 40 % (60 %) of the gauge stations show KGE (NSE) values that are negative or close to zero. These models tend to overestimate discharge in the continent, with median bias ranging between +10 % and +50 %. In general, the performance among global models is variable according to the analyzed region and metric, which is supported by the large box plot ranges. None of the models has a clear advantage with respect to all statistics, and this is especially valid for NSE and KGE. In the Amazon, KGE values present a more uniform pattern than in other regions with a median value close to 0.5, while models agree in a reasonable number of positive KGE and NSE values. Performance in the La Plata basin is highly variable between models, and this is the only region in which both systematic underestimation (HTESSEL/CaMa-Flood with median BIAS ≈ –20 %) and overestimation (LISFLOOD with median BIAS ≈ +20 %) is observed. Moreover, performance of the global models in basins with semiarid regions (e.g., Sao Francisco and Parnaiba) is extremely poor for KGE and NSE (median < –1 and < –2 respectively), which is probably associated with a dramatic overestimation of flows in these regions. WaterGAP3 shows a lower bias for all basins, but simulated peak flows occur too early according to DI for South America (percentile 25 % of DI ≈ –10 days). On the other hand, LISFLOOD appears to have a systematic delay in flow timing with more pronounced values over the Amazon (median DI ≈ +10 days), and a strong wet bias. For instance, median values of bias in LISFLOOD are larger than 40 % for the entire continent and exceed 100 % in basins such as São Francisco and Parnaíba. Absolute DI values are generally lower for HTESSEL/CaMa-Flood (median DI closer to 0) and this model usually shows an intermediate performance with respect to other metrics in comparison to LISFLOOD and WaterGAP3. Furthermore, the Ensemble GM shows a better

overall performance when compared with each of these models alone, but still produces a similar number of negative KGE and NSE values (33 % and 60 % of the gauges, respectively).

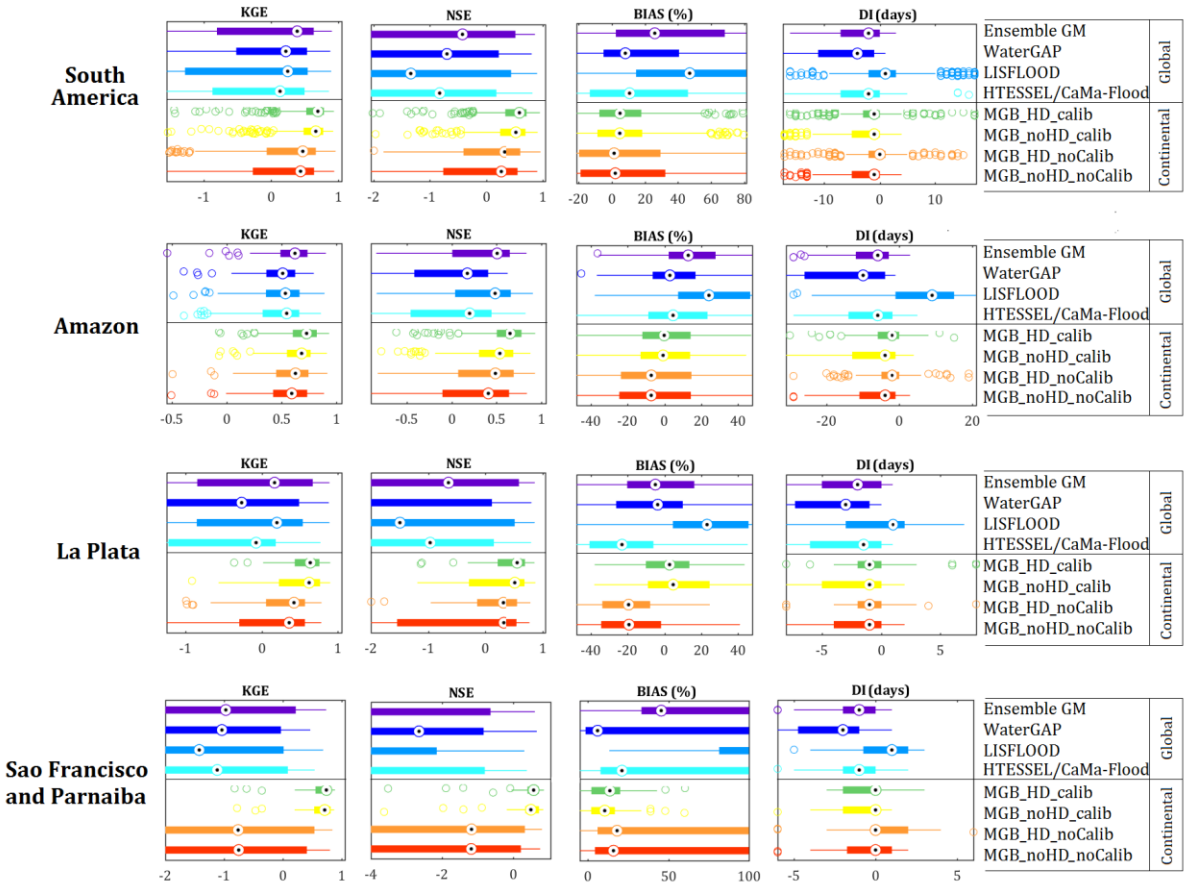

Figure 2.11. Box plots of global (above center line) and continental (below center line) model performances for different South American regions. MGB model configurations: hydrodynamic routing with calibrated rainfall-runoff parameters (MGB_HD_calib), hydrodynamic routing with uncalibrated rainfall-runoff parameters (MGB_HD_noCalib), non-hydrodynamic routing with calibrated rainfall-runoff parameters (MGB_noHD_calib) and non-hydrodynamic routing with uncalibrated rainfall-runoff parameters (MGB_noHD_noCalib). Gauge stations with naturalized flows were removed from the analysis to provide a fair comparison.

Simulated discharge after setting MGB with a single set of rainfall-runoff parameters (MGB_noHD_noCalib) results in positive values for both KGE and NSE median values, varying between 0.3 and 0.6 for the entire continent. The uncalibrated version of the continental model outperforms global models in South America except for basins with semiarid regions (e.g., São Francisco and Parnaíba), where performances seem to be very dependent on parameter adjustment. The introduction of hydrodynamic routing (MGB_HD_noCalib) causes a slight improvement in NSE and KGE but this effect is more evident in the Amazon and especially over the La Plata basin (percentile 25 % of NSE changes from –1.5 to 0). Improvements in flow timing (DI) for both Amazon and La Plata are also observed after including the HD routing method, although excessive delays occur in São Francisco and

Parnaíba because of the large bias that leads to an excess of floodplain attenuation (see MGB_HD_noCalib × MGB_HD_Calib). Furthermore, boxplot ranges are considerably smaller for KGE, NSE and bias in the default MGB simulation (MGB_HD_Calib) with respect to global models, and this reduction can be mostly seen in both MGB calibrated versions.

Our results agree with other studies from the literature, highlighting the large influence of model structure and parameterization in addition to meteorological forcing (Haddeland *et al.*, 2011; Gudmundsson *et al.*, 2012; Zhou *et al.*, 2012; Beck *et al.*, 2017b). Regarding global models, other studies also stress the large number of negative NSE values resulting from LSMs and GHMs in many basins around the world (Zhang *et al.*, 2016; Beck *et al.*, 2017b), including South America (Wu *et al.*, 2014). In particular, WaterGAP3 is expected to produce a lower bias because it is calibrated in terms of mean annual flow (Doll *et al.*, 2009; Muller Schmied *et al.*, 2014), and the systematic advance in timing is probably caused by the simple variable velocity equation (based on Manning) used for computing flow routing. In the case of LISFLOOD, large overestimation of flows in comparison to other global models has already been reported in the context of the eartH2Observe project (Beck *et al.*, 2017b), where it showed the lowest estimate of potential evaporation (Schellekens *et al.*, 2017). Indeed, this excessive wet bias is one of the possible reasons for the observed delay in flows, but this is not the only factor because large overestimations are concomitantly found in regions where DI is negative. This is the case for eastern Amazon tributaries located downstream of Obidos, such as the Tapajos and Xingu (see Figure S.2.6). The interplay between the Manning coefficient and groundwater parameters and their influence on flow timing of LISFLOOD has been shown in recent studies (Revilla-Romero *et al.*, 2015; Zajac *et al.*, 2017), and here may compensate for limitations of the double kinematic wave (channel + floodplain) used for river routing, especially in the Amazon. This suggests that calibrating large basins with lowland river systems using few downstream stations (e.g., Obidos) should be taken with care if hydrodynamic routing is not accounted for in the model structure.

Although some authors pointed to a clear (and general) underestimation of HTESSEL (Haddeland *et al.*, 2011; Beck *et al.*, 2017b), our results showed that it only occurs in the La Plata Basin and not in other regions, which may be related to the precipitation forcing used in WRR-2 (MSWEP). With respect to model performances, the relatively better flow timing of HTESSEL can be attributed to CaMa-Flood routing, but the advantages of this coupling were below the expected ones when looking at other statistics. It is worth mentioning that default parameters for river routing were used within WRR-2 simulations, i.e., the CaMa-Flood model

was not calibrated (Dutra *et al.*, 2017). This could be one of the reasons that low values of NSE are found over the Amazon main stem for this model (see Figure S.2.3). Characteristics such as timing and magnitude of flood waves in the hydrodynamic routing are very sensitive to channel geometry and roughness (Yamazaki *et al.*, 2011; Paiva *et al.*, 2013a), but also to DEM vegetation effects (Baugh *et al.*, 2013) that can impact the subgrid floodplain profiles (Yamazaki *et al.*, 2011; Paiva *et al.*, 2013a). Furthermore, Zhao *et al.* (2017) emphasize that the benefit of CaMa-Flood highly depends on the runoff fields simulated by the coupled LSM. Our results showed that discharge estimates of an uncalibrated model are improved over Amazon and (mainly) La Plata basins after inclusion of hydrodynamic routing (MGB_HD_noCalib), provided that channel geometry and floodplain topography are reasonably well estimated. Apart from the particular issues of WaterGAP3, LISFLOOD and HTESSEL/CaMa-Flood over South America, our findings reinforce the conclusion of other authors who recommend the ensemble mean of global models as the most reliable estimate (Haddeland *et al.*, 2011; Gudmundsson *et al.*, 2012; Schellekens *et al.*, 2017; Hattermann *et al.*, 2018), and it occurs even when discharge of a small number of models is averaged (three in the present case).

As outlined by many studies (Haddeland *et al.*, 2011; Gudmundsson *et al.*, 2012; Pechlivanidis and Arheimer, 2015; Zhang *et al.*, 2016; Krysanova *et al.*, 2017), performance of both regional and global models generally reduces when there is a transition from wet to dry conditions. In semiarid regions, satellites have several limitations in capturing rainfall intensities due to the local, convective nature of the precipitation, and they often overestimate the occurrence of rainfall because raindrops are likely to evaporate (i.e., sub-cloud evaporation) before reaching the surface (Dinku *et al.*, 2010a; Sunilkumar *et al.*, 2015; Beck *et al.*, 2017d). In addition, runoff generation mechanisms are strongly nonlinear and depend too much on storage processes, which are parameterized with large uncertainty (Gudmundsson *et al.*, 2012). For instance, there is little knowledge about the influence of transmission losses, their partitioning between its main components (e.g., infiltration/evaporation from channels or floodplains) (Jarihani *et al.*, 2015) and the dominant mechanisms of losing/gaining water according to different periods of the wet season (Costa *et al.*, 2013). Processes such as reinfiltration of surface runoff, lateral redistribution of subsurface runoff and hydraulic-connected stream–aquifer interactions have been shown to be necessary for hydrological modeling in Northeast Brazil (Guntner and Bronstert, 2004; Costa *et al.*, 2012; Costa *et al.*, 2013), but are not explicitly accounted for in any structure of the assessed models. Therefore,

a systematic underestimation of continental ET and consequent overestimation of flows is expected in dry regions (Alkama *et al.*, 2010; Haddeland *et al.*, 2011; Zhang *et al.*, 2016). Uncertainties about human interferences in water resources (i.e., small ponds and reservoirs, water abstractions) may also play an important role (Hanasaki *et al.*, 2018), especially in regions where data are scarce. Nevertheless, the complexity of the global models assessed herein makes it difficult to explain the real factors that impact discharge estimates.

Model resolution can partially explain performances in headwater catchments or in areas with complex orography. In addition to issues related to the quality of satellite products (Tian and Peters-Lidard, 2010), aspects that potentially affect these regions are the shape (grid or unit-catchment) and size of computational elements, as well as the downscaling method of rainfall fields to force the hydrological models (Rahman *et al.*, 2009), which is in our case a simple inverse distance weighting interpolation. It is worth noting that we have used a drainage area threshold of 1000 km² for headwater catchments (i.e., the onset of drainage networks), while this same area for global models varies between ~100 and ~625 km² according to their respective grid resolutions (between 0.08333º and 0.25º). In addition, results of discharge were evaluated at gauges monitoring at least 10 000 km², meaning that at these points the continental model has at least ~20 unit-catchments forced by ~16 MSWEP pixels. On the other hand, response to precipitation at these smaller basins may occur at an hourly scale, while model forcing and analyses were performed at a daily scale.

2.5. **Summary and conclusions**

For the first time, a regional-scale, fully coupled hydrologic–hydrodynamic model (MGB) was applied to a continental domain (South America). Model results were assessed using observed discharge and water levels from both in situ/satellite altimetry in an unprecedented gauge network over the continent, together with estimates of TWS and ET from remote sensing and other data sources. In addition, a cross-scale assessment (i.e., regional/continental × global models, the latter acquired from the eartH2Observe project) was conducted with the novelty of using spatially distributed, daily discharge data for model comparison.

Regarding continental modeling, analyses showed a satisfactory agreement between simulated and observed discharge, with NSE (KGE) > 0.6 in more than 55 % (70 %) of the gauges. The performance was generally better in large rivers and humid regions, but worse in areas with semiarid to arid climates, influence of snowmelt or draining complex orography such

as the Andes Cordillera. Similar results were found for water levels (both in situ and satellite altimetry), despite 50 % of the gauges showing large under- and overestimation of amplitudes (> |30 %|). The model was able to capture patterns of seasonality and magnitude of ET and TWS in many parts of the continent, especially when results were averaged to the scale of large South American basins (e.g., Amazon, La Plata, Orinoco, Tocantins–Araguaia, São Francisco, Parnaíba). In addition, model errors in simulating discharge were also found in other hydrological variables, which demonstrates the importance of assessing model results using multiple data sources. Uncertainties were attributed to deficiencies in process representation and simplifications in parameterization, as well as to limitations of the datasets used as model input and validation.

The cross-scale comparison shed light on the extent to which is possible to improve discharge estimates in South America. Global models (HTESSEL/CaMa-Flood, LISFLOOD and WaterGAP3) presented negative NSE values in a large number of gauges (> 60 % of streamflow gauges) and showed highly variable performances when evaluated over multiple gauges within large basins. A considerable improvement was found when the continental model was compared with individual global models, reaching median differences of around 0.45 for both KGE and NSElog, being larger than unity for NSE. By using the ensemble mean of global models as their best estimate, large differences in absolute bias (> 60 %) were detected mainly in eastern/northeastern Brazil and regions over Argentina, as well as in São Francisco, Parnaíba and Magdalena basins. Differences in timing of more than 20 days were found in rivers with floodplain effects, such as the Amazon, La Plata, Tocantins–Araguaia, Orinoco and lower Magdalena. Nevertheless, global models demonstrated a good ability to predict daily discharges over temperate, humid regions with the absence of lowland rivers (e.g., southern Brazil and southern Chile), while performing reasonably in the Amazon basin.

The analyses also showed that model calibration and hydrodynamic routing cannot be neglected if simulation of daily discharge in this continent is desired. Calibration was found to be a key factor to model performance in most regions but mainly in drier basins (e.g., Parnaíba and São Francisco), where models generally fail to represent the underlying hydrological processes. In addition, a hydrodynamic routing module was essential to achieve a suitable representation of both magnitude and timing in major river systems, especially in cases where flows are dramatically attenuated by floodplains (e.g., the Paraguay River). However, the expected benefit of coupling hydrodynamic and hydrological models occurs when river geometries are reasonably well represented and calibration of rainfall-runoff parameters is

performed together. This must be conducted by looking to different flow signatures (low and high flows, bias, timing of hydrographs) in a spatially distributed way, i.e., not considering only a single downstream gauge of large basins to reduce potential issues related to parameter compensation. As many of the approaches used in this study are applicable to global models, our findings suggest that large improvements on estimated discharge can be achieved by the latter even without a significant increase in the number of computational elements.

Regardless of the scale (global or continental), limitations still remain in some regions of South America and can be explored as "stress tests" in model evaluation studies. For instance, characteristics of the La Plata basin such as complex floodplains, extensive rivers with mild slopes, significant reservoir regulation and existence of several climatic zones make it a unique test bed for model assessments. In addition, large basins with semiarid conditions located in Northeast Brazil (e.g., Parnaíba) or also with snowmelt-driven regimes in the south of the continent (e.g., Colorado) are interesting examples of stress model performance. Despite the cross-scale assessments conducted herein only encompassed river discharge, we recommend that other studies should also include in situ water levels and observation-inferred variables (e.g., TWS from GRACE, ET from remote sensing/global datasets, and satellite altimetry) when possible. To facilitate access to in situ data, we call for cooperation among South American countries to produce a continental dataset that can be used by a broader audience, thus contributing to reduce the gap between regional and global modeling communities.

Finally, this study shows that extending a regional, fully coupled hydrologic-hydrodynamic model to the whole South American continent is feasible. This underscores the importance of regional expert knowledge, which can indicate relevant hydrological processes and datasets to be included in continental/global model simulations. We hope that moving from regional toward continental hydrologic–hydrodynamic modeling will bring new opportunities for operational practices such as real-time hydrological forecasting, which is the topic of ongoing research. Nevertheless, several improvements should be carried out in the model structure not only to achieve a better understanding of the underlying processes but also to provide further insights about human impacts on South American water resources. This includes the representation of reservoirs, lakes and water abstractions. It is also important to address uncertainties in model parameters, and these should be investigated further.

Acknowledgments

The first author would like to acknowledge the Brazilian National Council for Scientific Research (CNPq) for the financial support under the grant numbers 141450/2015-0 and 422422/2016–9 (Project: “South America Flood Awareness System – SAFAS”); the institutions ANA, SENAMHIs, IDEAM, DGA, INA, HyBAM, GRDC and ONS for providing in situ discharge and water stage data; the LEGOS–HydroWeb for both Envisat and Jason-2 satellite altimetry data; the Jet Propulsion Laboratory (JPL) for GRACE mascon data; Princeton University for the CDR–ET data; the eartH2Observe project for WRR-2 discharge from global models (WaterGAP3, LISFLOOD and HTESSEL/CaMa-Flood); Martina Floerke, Gabriel Fink, Ad de Roo, Emanuel Dutra and Gianpaolo Balsamo for their kind support with the global models used herein; and Guy Schumann and other anonymous reviewer who helped to improve this manuscript.

Supplementary material

S.2.1. Structure of models (continental and global) evaluated in this study

General information about the structure of MGB continental model, as well as the global models HTESSEL/CaMa-Flood, LISFLOOD and WaterGAP3 is summarized in Table S.2.1.

Table S.2.1. Summary of the structure of models used in this study, acquired from eartH2Observe Water Resources Re-analysis run 2 (WRR-2) (Dutra *et al.*, 2017).

Component/Model	MGB	HTESSEL/CaMa-Flood	LISFLOOD	WaterGAP3
Interception	Single reservoir, potential evaporation	Single reservoir, potential evaporation	Single reservoir, potential evaporation	Single reservoir
Evaporation	Penman–Monteith	Penman–Monteith	Penman–Monteith	Priestley–Taylor
Snow	No	Energy balance, single layer (5 layers)	Degree-day, single layer	Degree-day, single layer
Soil layers	Single layer	9 layers	3 layers	Single layer
Groundwater	Yes	No	Yes	Yes
Runoff generation	Saturation excess	Saturation excess	Saturation and infiltration excess	Beta function
Reservoir/Lakes	No	No	Yes	Yes
Routing	1D inertial routing (Channel), floodplain as a storage	CaMa-Flood (1D inertial routing)	1D Double Kinematic wave (Channel + Floodplain)	Manning–Strickler
Vertical processes in floodplains	Evaporation and infiltration	No	No	No
Water use	No	No	Yes	Yes
Time step	1 day water and energy balance, CFL for routing	1 h	1 day	1 day
Grid/Sub-basin	Sub-basin (unit-catchments)	Grid	Grid	Grid
Model resolution	Fixed-length (15 km)	0.25º	0.1º	0.0833º (5 arc minutes)

S.2.2. Metrics for individual continental and global models

Figures S.2.1–S.2.6 show the performance metrics computed for each individual model and for the ensemble of global models, for each analyzed gauge station.

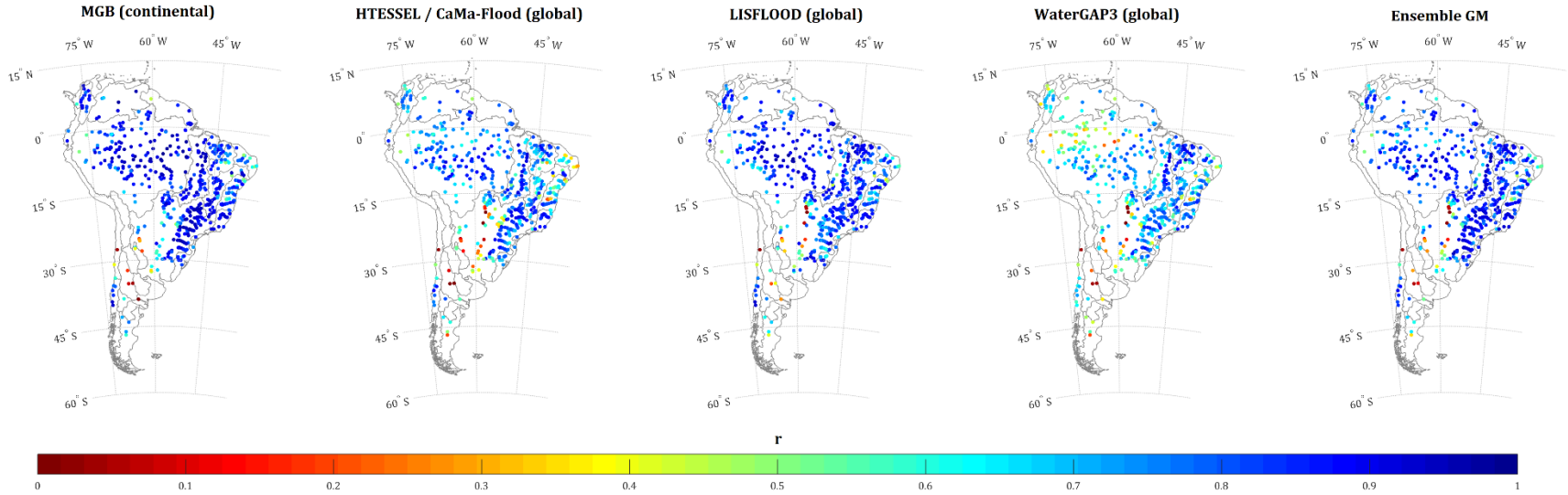

Figure S.2.1. Correlation of simulated discharges obtained from MGB and global models. The Ensemble GM relates to the mean discharge of global models.

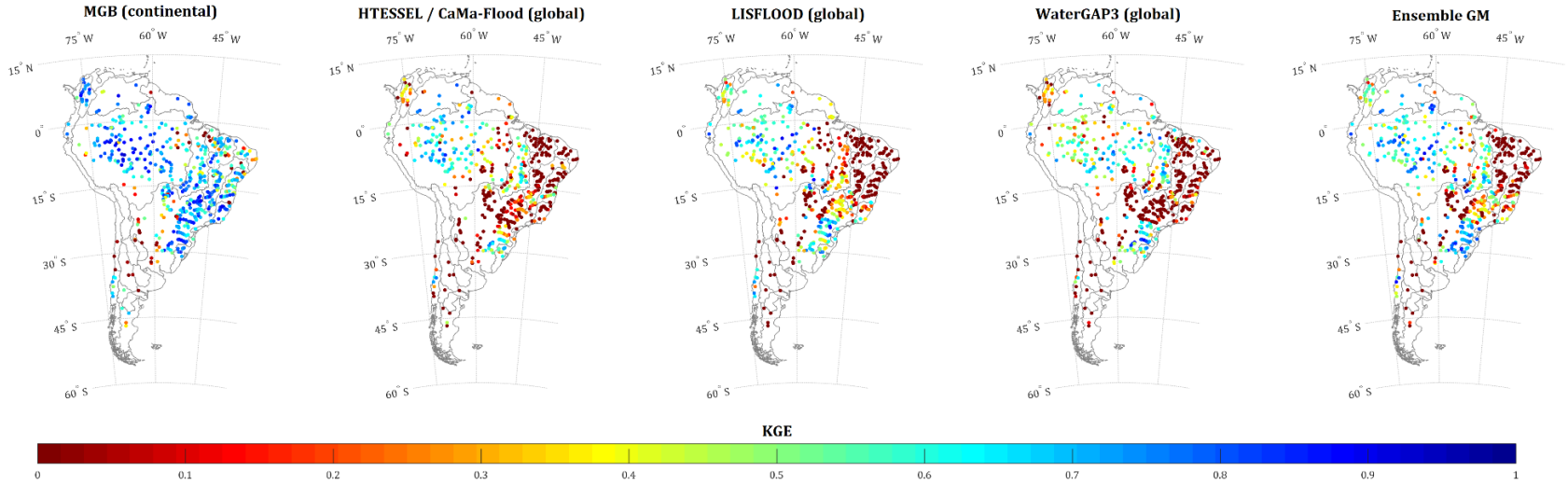

Figure S.2.2. KGE of simulated discharges obtained from MGB and global models. The Ensemble GM relates to the mean discharge of global models.

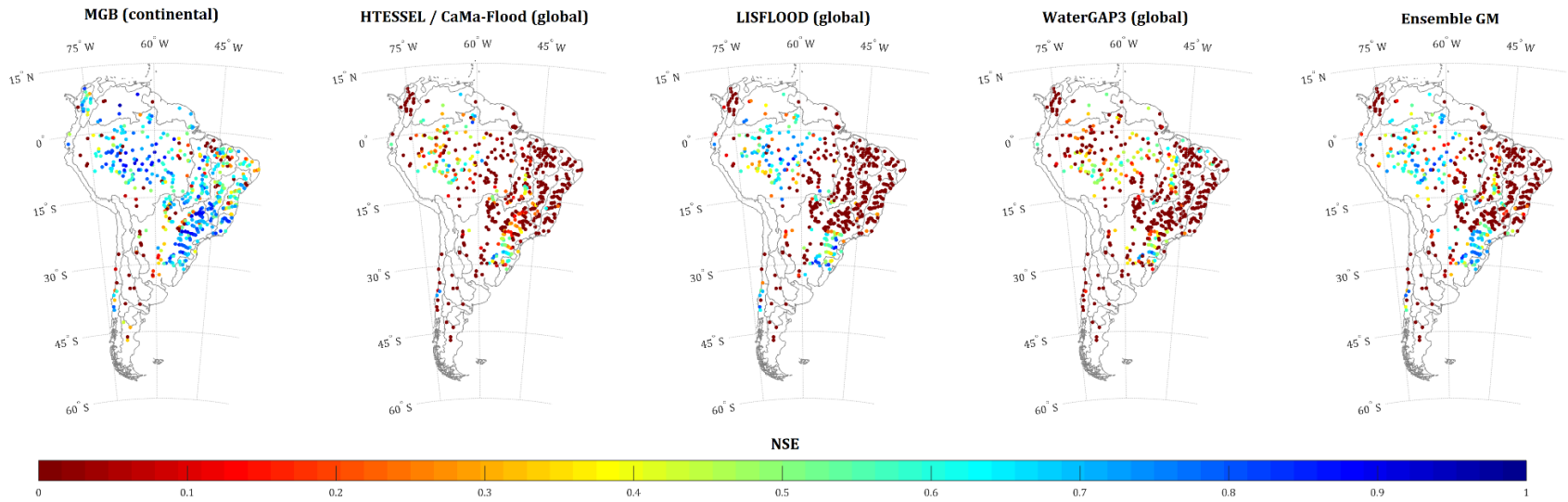

Figure S.2.3. NSE of simulated discharges obtained from MGB and global models. The Ensemble GM relates to the mean discharge of global models.

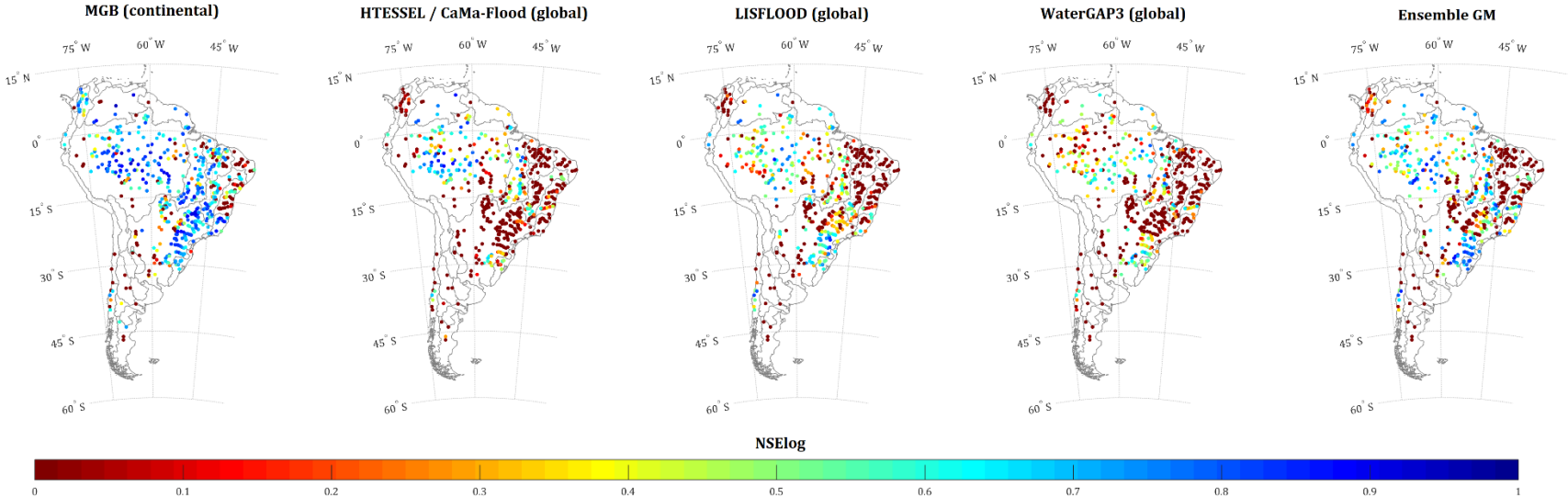

Figure S.2.4. NSElog of simulated discharges obtained from MGB and global models. The Ensemble GM relates to the mean discharge of global models.

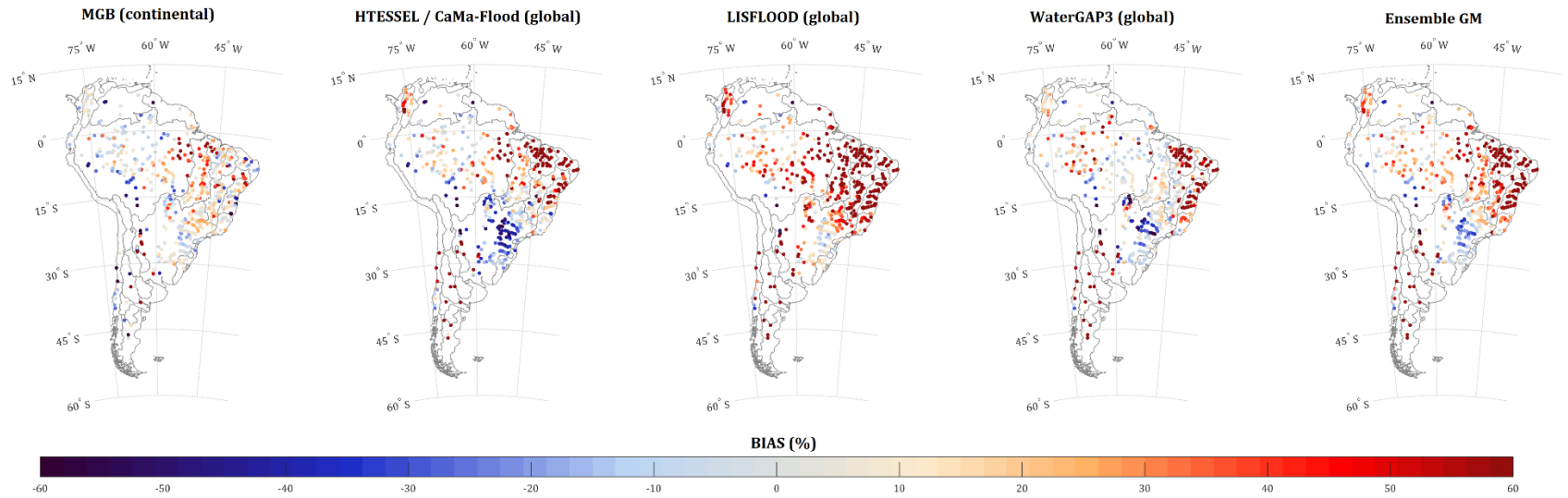

Figure S.2.5. Bias (%) of simulated discharges obtained from MGB and global models. The Ensemble GM relates to the mean discharge of global models.

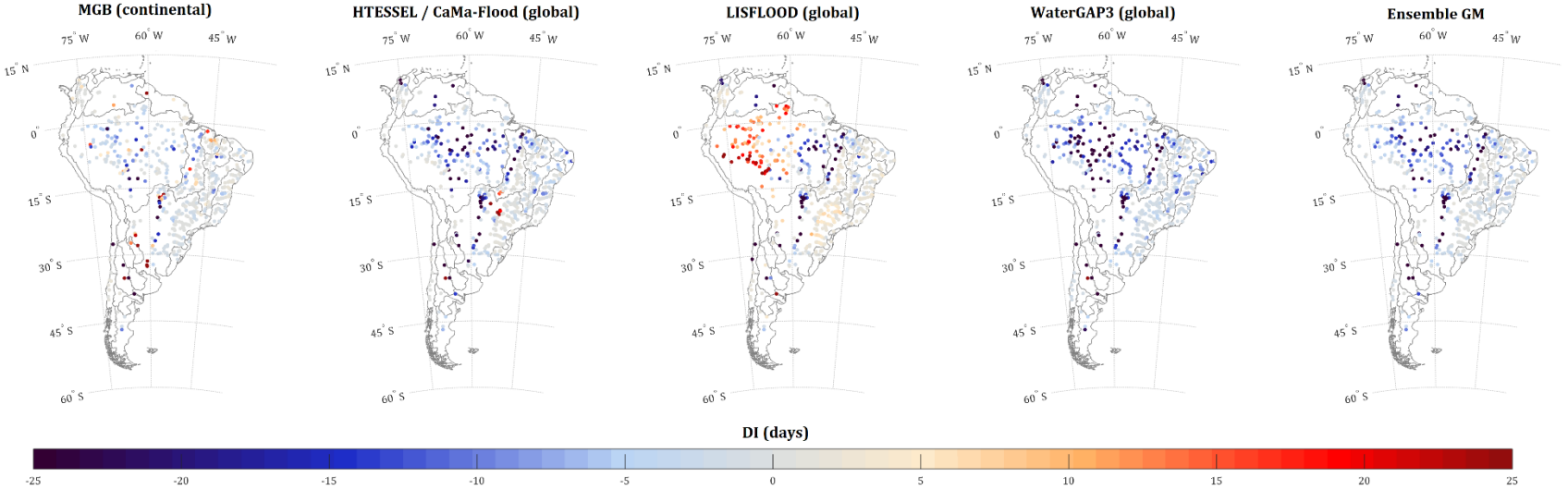

Figure S.2.6. Delay Index (days) of simulated discharges obtained from MGB and global models. The Ensemble GM relates to the mean discharge of global models.

CAPÍTULO 3: Potencial de previsões de precipitação por conjunto para previsão de vazões na América do Sul

"A way to make bad predictions useful"

—Holger Kantz, resumindo a essência da previsão por conjunto.[5]

[5] Retirado de Siegert, S. (2012). Rank statistics of forecast ensembles. Tese de Doutorado. Technical University of Dresden. 136pp.

Prólogo

No capítulo anterior, foi apresentado o desenvolvimento de um modelo de simulação com escala continental (MGB–SA) e analisou-se a sua capacidade de representar variáveis do ciclo hidrológico em grandes bacias sul americanas. Em particular, os resultados indicaram uma representação satisfatória das vazões em passo de tempo diário, em geral superiores em comparação a outros modelos que possuem capacidade de gerar informação para o domínio da AS. Estes resultados sugerem que o MGB–SA pode ser utilizado também como plano de fundo para experimentos de previsão de vazões em escala continental, cujo tópico de pesquisa é iniciado no presente capítulo.

Buscou-se aqui investigar sobre a capacidade de previsões de precipitação por conjunto em contribuir para a destreza da previsão de vazão na escala continental, para um horizonte de médio prazo (até 15 dias à frente). A destreza, ou simplesmente *skill*, é um termo que foi derivado da meteorologia para informar sobre o ganho (ou não) de desempenho em relação a um sistema de previsão de referência (*benchmark*). Tipicamente se utiliza como previsão de referência a climatologia da variável a ser prevista, o valor da última observação recente disponível (também chamado de persistência), ou mesmo uma previsão aleatória para avaliar a destreza. Nesse sentido, as principais fontes de destreza de uma previsão de vazão (considerando um horizonte de 2 semanas) são as previsões meteorológicas, a estimativa das condições iniciais hidrológicas, e a representação dos processos de transformação chuva-vazão e propagação nos canais de drenagem por parte dos modelos hidrológicos, geralmente atribuída a sua estrutura e parametrização (Schaake *et al.*, 2007; Pagano *et al.*, 2014). Neste capítulo 3, foi dado enfoque em avaliar apenas a contribuição das previsões de precipitação para a destreza das previsões de vazão, mais especificamente para previsão de cheias em grandes rios da AS.

Em relação à metodologia, o MGB–SA foi inicialmente forçado com a chuva observada do MSWEP efetuando-se uma rodada contínua em modo simulação, onde para cada dia do período de disponibilidade de previsões de precipitação (indicado a seguir), as variáveis de estado do modelo — i.e., as condições iniciais — como volume de água subterrânea, no solo, em rios e planícies, além de níveis, vazões, etc, foram gravadas para posterior leitura em modo previsão. Na sequência, foram adquiridas previsões de precipitação por conjunto (50 membros) operacionais com frequência diária e horizonte de 15 dias ao longo de um período de 4 anos (Nov/2010–Out/2014), a partir do sistema de previsão atmosférica do *European Center of Medium-Range Weather Forecasting* (ECMWF). Estas previsões foram processadas e

utilizadas como dado de entrada ao MGB–SA em modo previsão, onde o modelo realiza repetidamente a leitura das condições iniciais e de cada membro da chuva prevista para gerar previsões de vazão por conjunto. Adicionalmente, sequências de observações de chuva do MSWEP foram reamostradas do passado com o intuito de criar uma previsão meteorológica alternativa, baseada na climatologia diária da precipitação. Estas previsões de chuva alternativas também alimentaram o modelo MGB–SA em modo previsão, gerando previsões de vazão por conjunto que atuaram como *benchmark* para avaliação da destreza. Ao invés de avaliar as previsões com dados in situ observados, estas foram comparadas às vazões simuladas pelo próprio modelo hidrológico continental. Esta metodologia permite isolar a contribuição da chuva prevista para a destreza — i.e., a destreza teórica ou potencial —, dado que qualquer ganho ou redução de desempenho da previsão de vazão (baseada no ECWMF) em relação ao *benchmark* se deve apenas à previsão de precipitação.

Em resumo, as previsões de vazão baseadas no ECMWF exibiram destreza potencial no quesito desempenho geral (acurácia) principalmente nas regiões mais próximas ao leste e sudeste da AS, porém se observou pouca ou nenhuma destreza em grandes rios que drenam a região Andina. Para a discriminação entre a ocorrência e não ocorrência de eventos com vazões elevadas, considerando um limiar equivalente ao percentil 90 % de não-excedência da série histórica em cada trecho do modelo, a destreza foi geograficamente mais restrita, indicando maior ganho relativo de desempenho principalmente na região sul do Brasil. Ainda, as previsões de vazão baseadas no ECMWF tiveram maior destreza tanto em termos de desempenho geral e discriminação em regiões de clima temperado quente com baixa sazonalidade (sub-tropical). Verificou-se também o desempenho de previsões de vazão para eventos de cheia selecionados em algumas localidades da AS, porém através de análises de caráter visual. Na discussão do capítulo foi destacado o elevado viés positivo da chuva prevista do ECMWF sobretudo nas áreas próximas da Cordilheira dos Andes, o que pode estar associado à redução da destreza para desempenho geral nas bacias que drenam estas áreas montanhosas. Este viés potencialmente afeta as probabilidades previstas, que tendem a superestimar a frequência de superação dos limiares para ocorrência de eventos com vazões elevadas. Também se observou um padrão em algumas bacias como Alto Paraná, Uruguai, São Francisco, Parnaíba, e Tocantins-Araguaia onde a destreza para desempenho geral ao longo do horizonte de médio prazo tende a ser maior para áreas de drenagem maiores, ao passo que a destreza para capacidade de discriminação tende a ser maior para áreas de drenagem menores (com exceção do Uruguai cujo desempenho do *benchmark* reduz mais rapidamente devido a ausência de sazonalidade). Limitações quanto

às analises efetuadas e dados utilizados, além de comparações com estudos de previsão hidrológica em escala regional a global no contexto da América do Sul também foram discutidos ao final deste capítulo.

Este capitulo é baseado no seguinte artigo publicado na revista *Journal of Hydrology*:

SIQUEIRA, V. A., FAN, F. M., PAIVA, R. C. D., RAMOS, M-H., COLLISCHONN, W. Potential skill of continental-scale, medium-range ensemble streamflow forecasts for flood prediction in South America. **Journal of Hydrology**, v. 590, 125430, DOI: 10.1016/j.jhydrol.2020.125430, 2020.

3.1. **Introduction**

Floods are among the most common water-related disasters worldwide, causing several impacts including human losses, issues on public health and damages to property and infrastructure. According to EM–DAT database (Guha-Sapir *et al.*, 2018), riverine floods alone were responsible for at least US$ 20 billion in economic losses, 38 million affected people and 1 million homeless in South America (SA) between 1980–2017, partly because of the rapid population growth, urban expansion and occupation of riparian zones in the last century with consequent exposition to risk (Tucci and Bertoni, 2003; Nunes, 2011; Vorosmarty *et al.*, 2013). Recent extreme, large-scale flood events have been documented in scientific literature for the Amazon region (Marengo *et al.*, 2012b; Espinoza *et al.*, 2013; Espinoza *et al.*, 2014), Colombia (Hoyos *et al.*, 2013), Southeastern Brazil (Tomasella *et al.*, 2019) and also in international headlines (e.g., 2015 floods in Paraguay, Argentina, Uruguay and Southern Brazil) due their widespread effects and great repercussion. Besides, projected impacts of climate change point to an increase of the frequency of current 100-yr flood magnitude over much of SA (Hirabayashi *et al.*, 2013; Arnell and Gosling, 2016). Therefore, there is a need to improve adaptation measures and preparedness through feasible and cost-effective solutions, especially in less developed regions where financial resources are often limited.

Provision of flood forecasting and early warning systems (EWSs) can bring considerable benefits to anticipate flood events. EWSs can trigger preparedness actions among civil defense organizations, local governments, and people in potentially affected areas, allowing them to respond timely in order to reduce emergency costs (Moore *et al.*, 2005; Jacks *et al.*, 2010; Rogers and Tsirkunov, 2011; Alfieri *et al.*, 2018). To extend the lead time of forecasts issued by EWSs and consequently enable more effective actions, one solution is to force hydrological models with precipitation outputs from numerical weather prediction systems (NWPs). The ability to predict river flows with longer lead times comes, however, with the drawback that such forecasts are subject to large uncertainties. For instance, small errors on the initial conditions of NWPs may rapidly evolve — in a chaotic manner — into large discrepancies on future states of the atmosphere (Kalnay, 2003; Leutbecher and Palmer, 2008), while fine-scale processes related to rainfall such as cloud microphysics or deep convection need to be resolved with parameterization schemes due to their extreme complexity and relatively coarse resolution of numerical grids (Mesinger *et al.*, 2012; Song *et al.*, 2012). Similarly, hydrological models suffer from errors in input data, simplification of model

equations, and deficiencies in parameter estimation, thus amplifying the uncertainty in streamflow (Velázquez *et al.*, 2011; Zappa *et al.*, 2011). The use of ensemble techniques, originally from the meteorology field (Kalnay, 2003), makes it possible to account for the uncertainties of distinct components of the forecasting chain (Schaake *et al.*, 2007; Cloke and Pappenberger, 2009), where the most common approach is to force a hydrological model with multiple forecast scenarios from Ensemble Prediction Systems (EPS). By enabling a probabilistic assessment of the forecasts, such as the likelihood of occurrence of a given flood magnitude, ensemble hydrological predictions are generally more useful than deterministic ones that rely on a single forecast outcome (e.g., Roulin, 2007; Jaun and Ahrens, 2009; Schellekens *et al.*, 2011; Verkade and Werner, 2011b; Boucher *et al.*, 2012; Ramos *et al.*, 2013), and are recognized as the only way to achieve skillful predictions for longer lead times (Pappenberger *et al.*, 2011).

Advances in computational power, atmospheric prediction (Buizza and Leutbecher, 2015) and large-scale hydrological/river routing modeling (Yamazaki *et al.*, 2013; Bierkens, 2015) are encouraging ensemble flood forecasting systems to be applied not only at regional scale but also at the continental and global domains. Some operational examples are the European Flood Awareness System (EFAS) (Thielen *et al.*, 2009a), the Hydrological Ensemble Forecasting System (HEFS) (Demargne *et al.*, 2014), the Global Flood Awareness System (GloFAS) (Alfieri *et al.*, 2013; Emerton *et al.*, 2018) and its derivatives (e.g., Snow *et al.*, 2016), which are currently providing early warning information and future river conditions for the next weeks or even months ahead (see Emerton *et al.* (2016) for an overview about this topic). Continental to global-scale forecasting systems can foster knowledge about flood conditions beyond the catchment boundaries, increase awareness and support coordination at international level (Thielen *et al.*, 2009a; Alfieri *et al.*, 2013; Alfieri *et al.*, 2014; Thiemig *et al.*, 2015; Emerton *et al.*, 2016), as long as the massive information produced by ensemble predictions is properly communicated to end users (Ramos *et al.*, 2010). The use of state-of-the-art atmospheric and hydrological modeling techniques have leveraged the monetary benefit of these systems (Pappenberger *et al.*, 2015a), thus aiding to narrow the gap between research and operational activities (Pagano *et al.*, 2014; Emerton *et al.*, 2016).

The benefits of coupling hydrological models with atmospheric EPSs have been widely explored over the past decade, mostly in developed countries (see the review by Cloke and Pappenberger, 2009), but in SA this topic has received attention only in the last years. For

instance, ensemble forecasting approaches have been increasingly tested at short- to medium range (3–15 days) in order to assess the potential of supporting early warning systems (e.g., Meller *et al.*, 2014; Siqueira *et al.*, 2016a; Casagrande *et al.*, 2017; Tomasella *et al.*, 2019) and to optimize reservoir operations under multiple objectives (e.g., Fan *et al.*, 2014; Raso *et al.*, 2014; Fan *et al.*, 2015b; Schwanenberg *et al.*, 2015; Fan *et al.*, 2016c; Quedi and Fan, 2020). However, there is currently no integrated ensemble forecasting of national and transnational basins in SA from local institutions due to the complexity in simulating large South American rivers (Paiva *et al.*, 2013a; Siqueira *et al.*, 2018), challenges in handling multiple model runs and processing large amounts of data, and low coverage of real-time hydrometeorological monitoring for forecasting needs (Fan *et al.*, 2014; Fan *et al.*, 2015b; Salio *et al.*, 2015; Fan *et al.*, 2016a; Tomasella *et al.*, 2019). Efforts toward continental hydrologic–hydrodynamic modeling in SA (Siqueira *et al.*, 2018) and new precipitation datasets that can be obtained in real time (Beck *et al.*, 2017a; Beck *et al.*, 2017c) may be the starting point to overcome such limitations and to expand hydrological forecasting initiatives in the region also to broader scales.

Routinely issuing ensemble hydrological forecasts at the continental scale requires considerable institutional and technical developments, so there must be a prior knowledge about the skill of these forecasts to outline potential strengths and deficiencies. In general, the streamflow forecast skill depends on the relative importance of each source of forecast error (Paiva *et al.*, 2012b; Greuell *et al.*, 2019; Sharma *et al.*, 2019). It may be useful to isolate one of the major sources of uncertainty (e.g., Olsson and Lindström, 2008; Pappenberger *et al.*, 2011; Greuell *et al.*, 2019), for example, if one wants to assess whether the rainfall from the meteorological ensemble is able to provide skillful predictions after propagated through the hydrological system (e.g., Thirel *et al.*, 2008; Bartholmes *et al.*, 2009; Voisin *et al.*, 2011; Alfieri *et al.*, 2013; Alfieri *et al.*, 2014). This is sometimes treated as a potential (or theoretical) skill, in which a hydrological model run is used as the "truth" to neglect the associated model biases (van Dijk *et al.*, 2013; Candogan Yossef *et al.*, 2017; Greuell *et al.*, 2019). Forecast skill may be evaluated by checking attributes like the agreement of the ensemble distribution to the corresponding observations (or a historical model run) and the ability to warn about the occurrence of floods by detecting the exceedance of critical flow thresholds (Bartholmes *et al.*, 2009; Alfieri *et al.*, 2013), in terms of how the performance would be compared with simpler alternative systems (Pappenberger *et al.*, 2015b). Besides, many studies evaluating hydrological

forecasts over large domains or multiple basins have indicated that forecast skill has a close relationship with catchment size and geographic location (e.g., Thirel *et al.*, 2008; Pappenberger *et al.*, 2011; Alfieri *et al.*, 2013; Alfieri *et al.*, 2014; Bennett *et al.*, 2014; Pappenberger *et al.*, 2015b; Quedi and Fan, 2020). As the continental extent of SA encompasses a wide range of climate types and hydrological conditions, understanding the spatial patterns of forecast skill becomes important to highlight regional differences and to provide insights on how the skill in a given point of interest can be linked to different areas within a same basin.

While some studies have evaluated the performance and skill of hydrological ensemble forecasts from continental scale operational systems (e.g., Bartholmes *et al.*, 2009; Alfieri *et al.*, 2014; Bennett *et al.*, 2014; Brown *et al.*, 2014), in SA this has been done only under a global perspective (e.g., Alfieri *et al.*, 2013) and through a few number of regional studies focusing on specific basins where monitoring is a priority or data are available from hydropower companies (e.g., Fan *et al.*, 2014; Fan *et al.*, 2016a; Fan *et al.*, 2016c; Siqueira *et al.*, 2016a; Tomasella *et al.*, 2019), with few exceptions (e.g., Bischiniotis *et al.*, 2019). Today, there are still knowledge gaps on how the forecast skill varies across different geographic locations, basins, catchment areas and climates of SA. In this context, the aim of this study is to assess the potential skill of medium-range ensemble streamflow forecasts in South America, with a particular focus on flood prediction. This paper is structured as follows. Section 2 provides a brief description about the hydroclimatic characteristics of SA. Section 3 describes the hydrological model and meteorological inputs, methods of producing ensemble streamflow forecasts, strategy of forecast skill evaluation, and verification metrics. Results and discussion are presented in sections 4 and 5, respectively. Finally, the key conclusions are presented in section 6.

3.2. **Hydroclimatic features of South America**

South America (SA) features unique tropical, subtropical and extratropical weather and climate patterns (Satyamurty *et al.*, 1998), with an average annual precipitation ranging from less than 1 mm yr^{-1} in the Atacama Desert (Houston, 2006) to around 10 000–13 000 mm yr^{-1} in the Chocó region in Colombia (Poveda and Mesa, 2000). In a nutshell, the atmospheric phenomena are strongly influenced by the adjacent oceans and topographic barriers such as the Brazilian Plateau and the complex, prominent Andes Cordillera, which extends along the western side of the continent between the northern and southern tips (10º N–55º S) with altitudes exceeding 4 km in some areas (Garreaud *et al.*, 2009). Much of the precipitation over tropical and subtropical SA emerges from deep or wide convective cores that can evolve to

broad stratiform regions (Romatschke and Houze Jr, 2010), whereas deep stratiform clouds that develop along cold and warm fronts play a major role in the extratropics (Garreaud et al., 2009). Within northern SA the annual cycle of precipitation follows the meridional migration of the Intertropical Convergence Zone (ITCZ), producing a variety of unimodal and bimodal patterns (Poveda *et al.*, 2006). Besides, the seasonality of rainfall in most areas between the equator and 25º S is connected to the South American Monsoon System (SAMS), exhibiting more than 50 % of annual precipitation in austral summer (DJF) and less than 5 % in austral winter (JJA) (Marengo *et al.*, 2012a). An important feature of the regional climate is that significant amounts of moisture from tropical latitudes (i.e., Amazon Basin) are transported to the southeastern SA throughout the year (Vera *et al.*, 2006a), which makes the latter region absent of a distinct rainy season due to the passage of cold fronts producing abundant precipitation during the winter (Vera *et al.*, 2002). This moisture flow also contributes to the development of spatially extensive, long-lasting Mesoscale Convective Systems (MCSs) east of the Andes in regions like northern Argentina, southern Brazil and Uruguay, featuring some of the most extreme convective systems on Earth (Salio *et al.*, 2007 and references therein; Romatschke and Houze Jr, 2010). In southern SA precipitation is markedly asymmetric; frontal systems act in conjunction with orographic processes in the western Andean slopes, exhibiting a wet JJA in both sides of the Cordillera (it gradually changes to fully-humid south of ~35º S), but with drastic reductions of annual precipitation in Argentinean Patagonia (Garreaud *et al.*, 2009; Viale *et al.*, 2019).

In terms of continental hydrology, SA holds large transnational basins such as the Amazon, La Plata and Orinoco, as well as other basins with national relevance including the São Francisco, Tocantins-Araguaia, Parnaíba and Magdalena. Some large rivers like the Paraguay, the Amazon and its tributaries are highly influenced by floodplain effects, with long lasting floods that can extend from weeks to months (Paz *et al.*, 2011; Paiva *et al.*, 2012b; Paiva *et al.*, 2013a). An overview of the hydroclimatic characteristics of SA is shown in Figure 3.1.

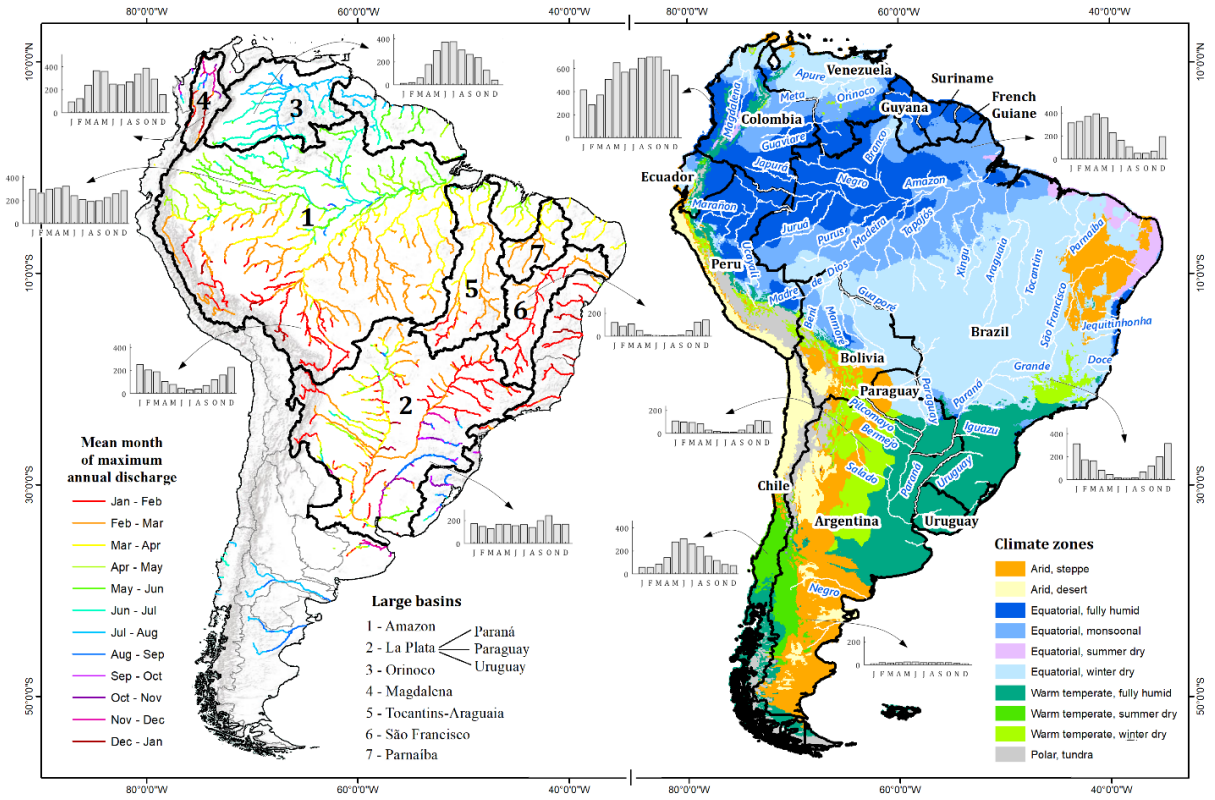

Figure 3.1. Hydroclimatic characteristics, political divisions (right) and large basins of South America (left). Histograms represent the annual cycle of precipitation (mm), derived from the MSWEP dataset (Beck *et al.*, 2017c). The mean month of maximum annual discharge of South American large rivers was computed using the simulated discharge dataset available from Siqueira *et al.* (2018).

3.3. Data and Methods

3.3.1. MGB hydrologic-hydrodynamic model

The MGB - *Modelo Hidrológico de Grandes Bacias* (acronym of Large-Scale Hydrological Model) (Collischonn *et al.*, 2007a; Pontes *et al.*, 2017) is a conceptual, semi-distributed, large-scale hydrological model developed for tropical regions. It has been applied in several past forecasting experiments in South American basins, encompassing both deterministic (e.g., Collischonn *et al.*, 2005; Collischonn *et al.*, 2007b; Fan *et al.*, 2017) and ensemble approaches (Paiva *et al.*, 2012b; Fan *et al.*, 2014; Meller *et al.*, 2014; Fan *et al.*, 2015b; Fan *et al.*, 2016a; Fan *et al.*, 2016c; Siqueira *et al.*, 2016a). Here we used the South America MGB model version presented in Siqueira *et al.* (2018), hereafter named as MGB–SA. The model uses a vector-based river network divided in reaches of constant length (Δx = 15 km), and basin discretization is obtained by defining the direct catchment area to the individual reaches (i.e., in the form of unit-catchments). Combinations of land use and soil type within each unit-catchment are categorized as Hydrological Response Units (HRU), where

water budget and energy balance are computed independently at a daily time step. Propagation of surface, subsurface and groundwater runoff to the main channel is computed with linear reservoirs in order to represent catchment delay and attenuation. Flow routing in the river network and associated discharge, water surface elevation and flood extent are simulated using a 1D local inertia hydrodynamic model based on Bates *et al.* (2010) with an adaptive time step (few minutes) (Pontes *et al.*, 2017). Hydrodynamic routing has been shown to be important to simulate flood delay in many large rivers of SA (Paiva *et al.*, 2013c; Siqueira *et al.*, 2018).

MGB–SA was manually calibrated with hundreds of in situ observations focusing on a well-balanced simulation, i.e., a reasonable depiction of high and low flows. The model was validated using river water levels, evapotranspiration and terrestrial water storage from multiple data sources, being able to reproduce daily discharges satisfactorily over several regions of South America (70 % [55 %] of the gauges with KGE [NSE] > 0.6) (Figure 3.2). MGB–SA also compared favorably to state-of-the-art global hydrological models with respect to several performance metrics (Siqueira *et al.*, 2018). In this study, no additional modifications were made to the original MGB–SA, and for further details about model setup, parameterization and validation results the reader is referred to Siqueira *et al.* (2018).

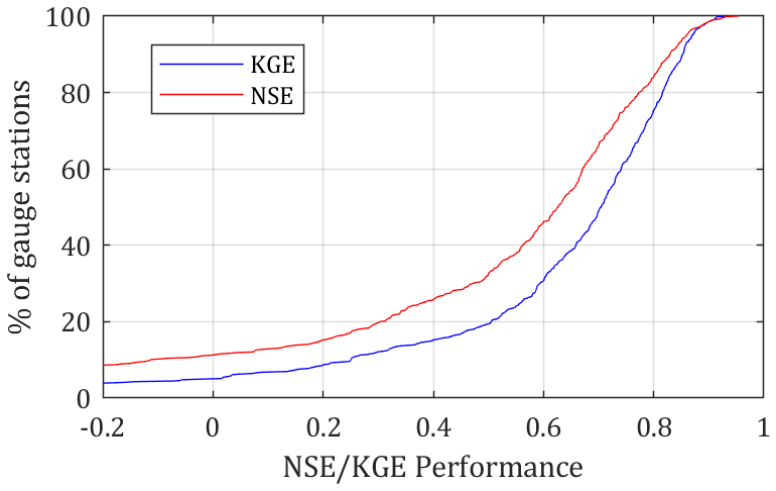

Figure 3.2. Cumulative distribution of NSE and KGE performances of MGB–SA in 604 gauge stations across South America, computed for the model calibration period (1990–2010).

3.3.2. Meteorological input

3.3.2.1. Observed rainfall and climate data

The Multi-Source Weighted Ensemble Precipitation (MSWEP) v1.1 (Beck *et al.*, 2017c) was used as the input forcing to initialize forecasts. This is a global-scale dataset (0.25º

resolution) that optimally combines precipitation from satellite, reanalysis and in situ gauges. This dataset was chosen because it performed well compared to 22 other satellite-based estimates (Beck *et al.*, 2017d) and was successfully used for MGB–SA calibration (Siqueira *et al.*, 2018). Other meteorological variables needed by the model to compute evapotranspiration (ET) were retrieved from the CRU Global Climate v.2 (New *et al.*, 2002), which provides long-term monthly means (1961–1990) of temperature, pressure, radiation and wind speed for all land areas at 10' resolution. In order to match these meteorological fields to the irregular computational elements of the hydrological model, data from MSWEP and CRU were interpolated to the unit-catchments of MGB–SA using the inverse-distance-weighted method and nearest neighbor approach, respectively.

3.3.2.2. Predicted rainfall: ECMWF ensemble data

Precipitation forecasts from the ECMWF Ensemble Prediction System (ECMWF EPS) were acquired between Nov/2010–Oct/2014 through the THORPEX Interactive Grand Global Ensemble (TIGGE) repository (Bougeault *et al.*, 2010). The ECMWF EPS is a 51-member ensemble composed by a control run and 50 perturbed forecasts, produced after perturbing the initial conditions and physical parameterizations of the atmospheric model using the Singular Vectors technique and a stochastic approach (Leutbecher *et al.*, 2017). Forecasts are issued twice a day (00 UTC and 12 UTC) and provided with 6-h accumulated intervals and a forecast horizon up to 15 days ahead. The operational EPS runs with a variable horizontal grid resolution of 32 km up to day 10 and 63 km for days 10–15, but outputs in TIGGE database are freely available to the general public with a 0.5º resolution (it ranges from ~55 km at the equator to ~32 km at the southern tip of SA). The ECMWF EPS has demonstrated relatively good performance in South America with respect to other similar systems (Medina *et al.*, 2019), even when predicted precipitation is propagated to the hydrological forecasts (Fan *et al.*, 2015b; Tomasella *et al.*, 2019). Only the 50 ECMWF perturbed members were used in this study.

3.3.3. Forecasting setup

3.3.3.1. Producing hydrological ensemble forecasts

Here, ensemble streamflow forecasts were issued daily by cascading only uncertainties from numerical weather prediction to the hydrological outputs. This was performed within a four-year hindcasting period from 01/11/2010 to 31/10/2014. Although more recent ECMWF

forecasts are available in TIGGE repository, we chose to limit our hindcasting period due to computational constraints and to keep coherence with the MSWEP v1.1 precipitation used to calibrate MGB–SA (see Siqueira *et al.*, 2018). MSWEP data from 2015 onwards are available only for more recent versions of this dataset, which include major upgrades (Beck *et al.*, 2019) that would require model recalibration.

To match resolutions of both meteorological and hydrological models, 6-h accumulated precipitation from ECMWF EPS forecasts were temporally aggregated to daily input data and were spatially disaggregated to the centroids of unit-catchments in the same way as done with the observed rainfall. Model state variables were updated by a long-term run using MSWEP data, starting from 01/01/1990 up to each forecast day in order to account for antecedent conditions such as soil moisture and water stored in rivers and floodplains. To produce the ensemble of streamflow forecasts (hereafter named as ECMWF-based forecasts), rainfall from each of the 50 perturbed members of ECMWF EPS was then used to force the MGB-SA model using the updated hydrological states, while other meteorological variables used to compute ET (temperature, wind speed, relative humidity, radiation and pressure) were kept equal to their long-term monthly means along the forecast horizon, similarly to previous approaches in South American basins (e.g., Fan *et al.*, 2014; Meller *et al.*, 2014; Fan *et al.*, 2015b; Fan *et al.*, 2016a; Siqueira *et al.*, 2016a).

3.3.3.2. Deriving flow thresholds and proxies of in-situ observations

Early warning systems are often evaluated in terms of exceeding or not a critical threshold level (Bartholmes *et al.*, 2009; Thielen *et al.*, 2009a; Hirpa *et al.*, 2016). Although thresholds should be ideally linked to predefined return periods (e.g., 2-yr, 5-yr or 25-yr), floods are relatively rare so that having extreme discharges as a reference may result in capturing a relatively small number of events, especially in short analyzed periods (Bartholmes *et al.*, 2009; Cloke and Pappenberger, 2009). Moreover, information about warning and alert levels might be only available locally and at specific gauge stations. A feasible solution is to consider simulated discharges as a proxy of in situ observations and to derive thresholds by using predefined quantiles of these proxies (e.g, Olsson and Lindström, 2008; Thirel *et al.*, 2008; Bartholmes *et al.*, 2009; Pappenberger *et al.*, 2011; Voisin *et al.*, 2011; Cloke *et al.*, 2017). The main advantage of this approach is that it does not take into account errors associated with deficiencies in the hydrological model structure, also enabling to evaluate forecast performance over the entire model domain instead of using only a limited number of gauge stations (e.g.,

Thielen *et al.*, 2009a; Alfieri *et al.*, 2013; Alfieri *et al.*, 2014; Hirpa *et al.*, 2016; Bischiniotis *et al.*, 2019). The above strategy relies on the assumption of a perfect hydrological model, i.e., that errors in streamflow predictions are reflected only by inaccuracies in the predicted precipitation. This is far from true in our case, therefore results derived here have to be seen only as a *potential* forecast skill.

Long-term discharge climatologies (observed proxies) were first extracted for each river location by running the MGB–SA model with MSWEP data from 01/01/1990 to 31/12/2014. To capture a reasonable number of events and conduct a meaningful statistical analysis, reference thresholds equivalent to the 90th percentile (Q_{90}) of non-exceedance flows (i.e., 90 % of simulated discharges lying below this value) were derived from the long-term discharge climatology, which is in agreement with other similar studies (e.g., Thirel *et al.*, 2008; Pappenberger *et al.*, 2011; Alfieri *et al.*, 2013).

3.3.3.3. Using ESP forecasts for benchmarking

Hydrological forecasts are often compared with a reference benchmark in order to evaluate the relative performance (the forecast skill), since a similar outcome sometimes can be achieved by a less computationally expensive method (Pappenberger *et al.*, 2015b). The most common examples of benchmarks used for this purpose are the streamflow climatology and the persistence of the last observed discharge, especially for the assessment of flood forecasting systems at continental to global scales (e.g., Bartholmes *et al.*, 2009; Pappenberger *et al.*, 2011; Alfieri *et al.*, 2013; Alfieri *et al.*, 2014). Selecting the appropriate benchmark is not a straightforward task because benchmarks that are too naïve can easily result in apparent high skill, so the benchmark should be preferably the "hardest to beat" alternative (Pappenberger *et al.*, 2015b). The Ensemble Streamflow Prediction (ESP) technique commonly used to produce or assess the skill of seasonal streamflow forecasts (Wood and Lettenmaier, 2006; Crochemore *et al.*, 2017; Arnal *et al.*, 2018) was selected as the benchmark for this study. Moreover, it has been shown that the ESP (also known as meteorological benchmark) can suit well evaluations of forecasting skill also at the medium-range (Bennett *et al.*, 2014; Pappenberger *et al.*, 2015b). In this approach, an ensemble of meteorological variables (e.g., precipitation) for the same calendar day are retrieved from historical observations and are used to force the hydrological model, considering the state variables updated for the current forecast day.

Taking the first day of the hindcasting period (01/11/2010) as an example, the ensemble of predicted precipitation for the first lead time is obtained by resampling MSWEP data in all years between 1990 and 2009 for the target day (i.e., 01/11/1990, 01/11/1991... 01/11/2009). This is repeated for all lead times and initialization dates. To produce the corresponding ESP forecast, MGB–SA is forced with each one of these precipitation scenarios resampled from past observations, using the updated model states computed for the forecast initialization day (01/11/2010). The resampled precipitation data were extracted from a retrospective period spanning from 01/01/1990 to 31/12/2009, which is independent of the hindcasting one and corresponds to the same calibration period of MGB–SA (Siqueira *et al.*, 2018). Therefore, 20-member ESP forecasts were produced as a benchmark system, similarly to the experiment carried out by Pappenberger *et al.* (2015b). Although the potential effects of ensemble size were not evaluated in this study, we recognize that using a different number of members regarding ECMWF-based and ESP forecasts may affect the skill scores, as discussed by Ferro *et al.* (2008). For example, a previous study has shown that reducing the ensemble size from 51 to 20 members led to reductions in CRPSS metric by around 2–3 % for lead times up to 5 days (Junk *et al.*, 2015). Figure 3.3 summarizes the methods used to produce ensemble streamflow forecasts.

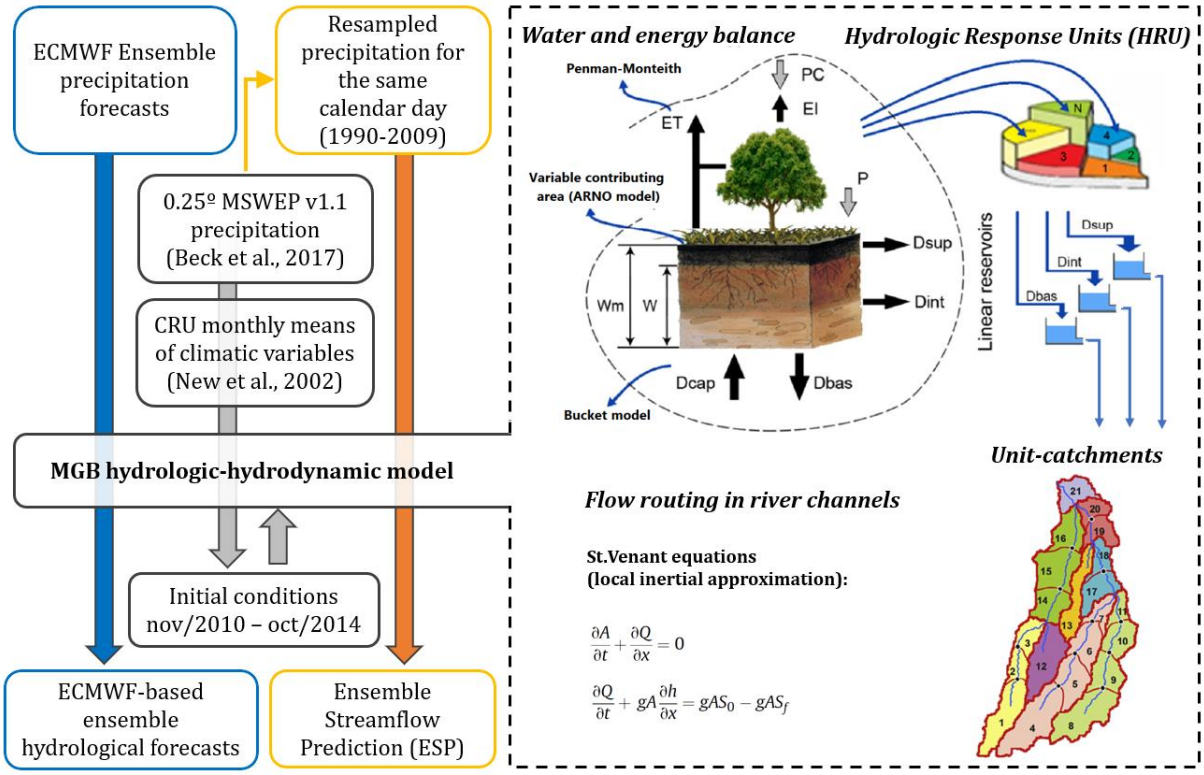

Figure 3.3. Scheme of the forecasting setup for producing hydrological ensemble forecasts.

We reinforce that the term "observations" used for precipitation and discharge in the next sections refer to the MSWEP data and streamflow proxies, respectively.

3.3.4. Forecast assessment

There are many scores and graphical tools to measure the performance of probabilistic forecasts, most of them based on standard methods used in meteorology (e.g., Wilks, 2011; Jolliffe and Stephenson, 2012). For instance, the Continuous Ranked Probability Score (CRPS) (Hersbach, 2000) is a widely-known metric to evaluate the performance of forecasting systems and is often published in official reports (Pappenberger *et al.*, 2015b). CRPS summarizes the overall quality of a probabilistic forecast by comparing its cumulative distribution function (CDF) to a Heaviside step function at the observed value. It is computed as an average of all individual CRPS for a given forecast lead time, according to:

$$\overline{\mathrm{CRPS}} = \frac{1}{\mathrm{N}}\sum_{\mathrm{i}=1}^{\mathrm{N}}\int_{-\infty}^{\infty}[\mathrm{F_i(y)} - \mathrm{F_i^0(y)}]^2\mathrm{dy} \quad (3.1)$$

$$\mathrm{F^0(y)} = \begin{cases} 0, & \mathrm{y} \leq \text{observed value} \\ 1, & \mathrm{y} > \text{observed value} \end{cases} \quad (3.2)$$

Where $F_i(y)$ is the CDF of the forecast ensemble y, computed for the forecast day i; $F^0(y)$ is the Heaviside step function that equals to 1 when forecast values are greater than the observed value and is zero otherwise; N is the number of forecasts issued.

$\overline{\mathrm{CRPS}}$ is finally converted into a skill score as follows:

$$\mathrm{CRPSS} = 1 - \frac{\overline{\mathrm{CRPS}}_{\mathrm{fcst}}}{\overline{\mathrm{CRPS}}_{\mathrm{benchmark}}} \quad (3.3)$$

Where $\overline{CRPS}_{fcst}$ is the $\overline{CRPS}$ computed for the ECMWF-based forecasts, and $\overline{CRPS}_{benchmark}$ is the $\overline{CRPS}$ computed for the ESP forecasts as the benchmark system. The ECMWF-based system is skillful if CRPSS > 0 and maximum skill occurs when CRPSS = 1.

The ability to discriminate between the occurrence and no occurrence of an event is assessed with Relative Operating Characteristic (ROC) curves. Both forecasts and observations are transformed into a set of binary events according to the exceedance or non-exceedance of the reference flow threshold (we used Q_{90} as the threshold, as described earlier in Sect 3.3.3.2).

A 2 × 2 contingency table (Table 3.1) is computed for different forecast probabilities derived from the ensemble, where an event is forecasted if at least X % (i.e., 10 %, 20 %, …) of the ensemble members lie above the threshold. ROC curves are then constructed by plotting the corresponding pairs of hit (HR) and false alarm (FAR) rates obtained from the contingency tables:

Table 3.1. Contingency table for a given forecast probability and lead time. Forecasts and observations are considered as binary events according to the exceedance or non-exceedance of the reference flow threshold Q_{90}.

		Observed	
		Yes	No
Forecast	Yes	a (Hit)	b (False alarm)
	No	c (Miss)	d (Correct negative)

$$HR_j = \frac{a_j}{a_j + c_j} \tag{3.4}$$

$$FAR_j = \frac{b_j}{b_j + d_j} \tag{3.5}$$

Where *j* is the index that denotes the forecast probability.

The tradeoff between hit rate and false alarms can be summarized into a single scalar score given by the area under the ROC curve (AROC). A perfect forecasting system would have an area equal to unity. Using a similar approach to Emerton *et al.* (2019) we computed the dAROC as a measure of skill, which is defined as the difference between the AROC of ECMWF-based forecasts and the AROC of the ESP benchmark:

$$dAROC = AROC_{fcst} - AROC_{benchmark} \tag{3.6}$$

Reliability diagrams are diagnostic tools used to evaluate whether the forecast is reliable. A perfectly reliable system would produce forecast probabilities X_i that are consistent with the corresponding frequencies Y_i at which the event (e.g., a threshold being exceeded) is observed. Such diagrams are constructed by plotting *X* against *Y*, with the forecast probability values often grouped into bins of equal width (e.g., 10–20 %, 20–30 %, ...) (Bröcker and Smith,

2007). The reliability diagram is conditioned on the forecasts; therefore, the observed frequency for a given forecast probability bin (X_k) and lead time is computed according to:

$$X_k = \frac{O_k}{O_k + NO_k} \quad (3.7)$$

Where O_k is the number of times the event has occurred for the probability bin k (observed proxy exceeding the reference flow threshold Q_{90}); and NO_k is the number of times the event has not occurred for the probability bin k (observed proxy not exceeding the reference flow threshold Q_{90}).

If precipitation forecasts persistently over- or underestimate the rainfall used to initialize the hydrological model, discharge forecasts and consequently the prediction of flood alerts will be consequently biased, which may lead to over- or under-prediction of flood alerts (Alfieri *et al.*, 2014). As large precipitation volumes accumulated over several days are usually the main trigger of floods in large basins, we computed the average difference between the accumulated ensemble mean and the accumulated observed rainfall in order to assess the forecast bias:

$$\text{Bias} = \frac{1}{N}\sum_{i=1}^{N}[P_{fcst} - P_{obs}] \quad (3.8)$$

Where P_{fcst} and P_{obs} are, respectively, the ensemble mean of the accumulated precipitation forecast and the accumulated observed rainfall for the lead time in analysis and forecast day i; N is the number of forecasts issued. Bias in precipitation was computed for accumulation periods of 5 and 15 days.

We first performed an analysis of the predicted precipitation before assessing the hydrological forecasts. Rainfall metrics were computed after averaging pixels of ECMWF (0.5º) and MSWEP (0.25º) in grids of 1.0º × 1.0º to minimize position errors between the observed and predicted rainfall fields. Regarding hydrological forecasts, as we have a particular focus on flood prediction, the computation of skill (CRPSS and dAROC) was carried out only for moderate to high flows. This was performed by selecting only the verification pairs (forecasts/observations) for which the observed discharge exceeds the median of flows (Q_{50}) in the hindcasting period (i.e., the subset of flows < Q_{50} was not included in the computation of $\overline{CRPS}$ and contingency tables). We reinforce that Q_{50} differs from the reference threshold Q_{90}

used for ROC curves since the former is used to select a subset from the entire verification data. Table 3.2 summarizes the forecasting setup and the verification metrics adopted in this study.

Table 3.2. Summary of the forecasting setup and metrics/diagrams used for the assessment of forecasts.

Information	Evaluated system	Benchmark
Precipitation ensemble	Daily precipitation forecasts from the 0.5º resolution, ECMWF EPS	Daily resampled MSWEP precipitation from the past (1990–2009), for the same calendar day
Hydrological model	Hydrologic–hydrodynamic model (MGB–SA): *ECMWF-based forecasts*	Hydrologic–hydrodynamic model (MGB–SA): *ESP forecasts*
Number of ensemble members	50	20
Forecast horizon	15 days	15 days
Verification scores / diagrams	Discharge and Precipitation: CRPSS* Discharge only: dAROC* and Reliability diagrams. The reference flow threshold is the Q_{90} (90^{th} percentile of non-exceedance flows) Precipitation only: Bias	
Hindcasting period	Nov/2010–Oct/2014 (4 years)	
Discharge Observations	Observed proxies: Simulated discharges of MGB–SA using daily MSWEP precipitation data as the model forcing.	

*For discharge, the computation of skill scores was performed only for moderate to high flows, i.e., using the subset of verification data for which observed proxies > Q_{50}.

3.4. **Results**

3.4.1. Analysis of predicted rainfall

Figure 3.4 and Figure 3.5 show the performance maps of precipitation in terms of CRPSS and cumulative bias, respectively. Results are presented separately according to the season of the year (DJF, MAM, JJA and SON) and for the lead times of 5 and 15 days. Large basins and hydrological regions of South America are also displayed to aid visualization. Areas shown in blue in Figure 3.4 indicate skillful precipitation forecasts, whereas gray and red areas demonstrate no added skill and lower overall performance than the reference, respectively. As observed, ensemble precipitation forecasts from the ECMWF have skill over climatology in many regions of SA. The skill is higher at shorter leads (i.e., 5 days) but decreases along the forecast horizon, resulting in values predominantly close to 0 after 15 days. Higher values of CRPSS are mainly observed at eastern and southeastern SA regions, while in the subtropics and midlatitudes north of 50º S positive CRPSS values can be found all year round, such as in the south of La Plata basin and central Chile. On the other hand, in large areas located at central SA (e.g., Amazon, Tocantins–Araguaia, north of La Plata basin) and also north of the equator like the Orinoco basin (Venezuela), the CRPSS values are notably lower in the wet than the dry season. In most of these areas ECMWF forecasts show little or no added skill even at shorter lead times (5 days), except for the dry season. Interestingly, negative values of CRPSS are markedly seen along a narrow stripe at the western part of the continent (close to the Andes Cordillera), thus indicating a lower performance of predicted precipitation in comparison to daily rainfall climatology in such regions.

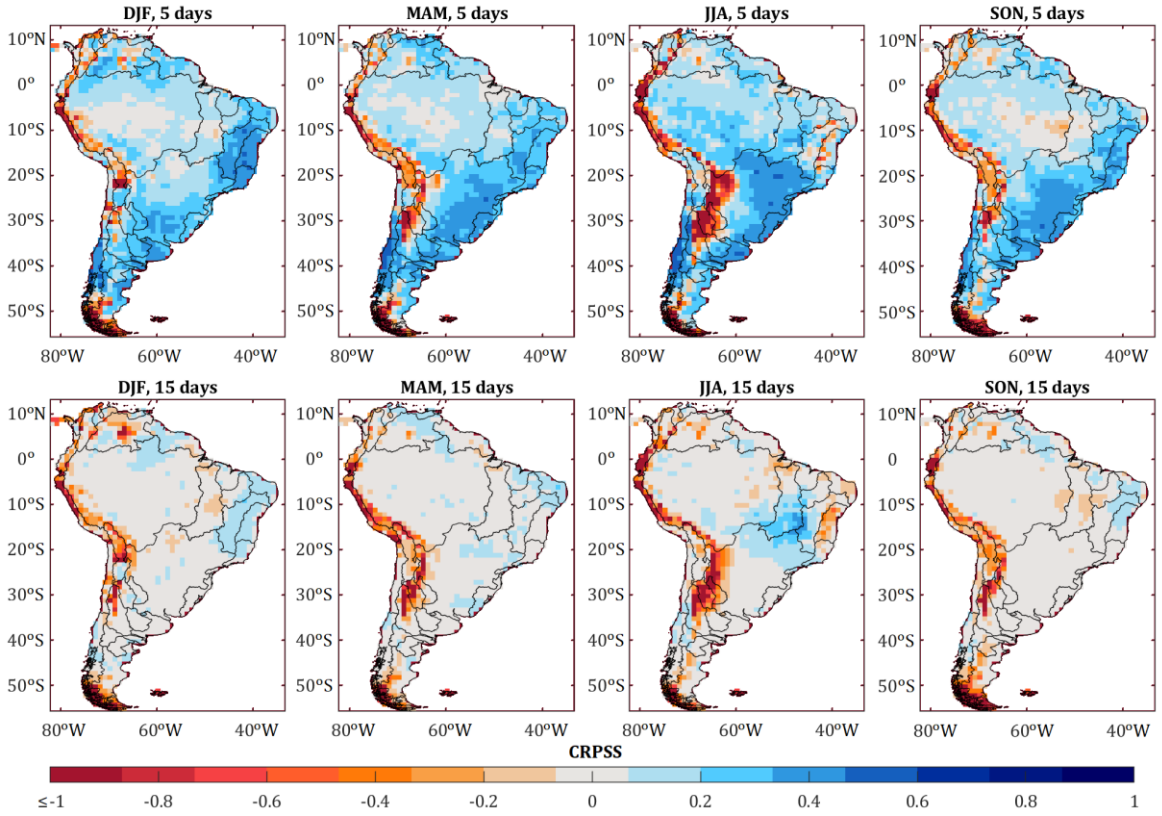

Figure 3.4. CRPSS maps of ECMWF predicted precipitation for lead times of 5 (top) and 15 days (bottom). Results are computed for each season of the year, using the resampled daily climatology from MSWEP as the reference benchmark.

The mean cumulative bias in Figure 3.5 also exhibits spatial and seasonal variations. ECMWF overestimates precipitation in most of La Plata basin, but mainly in the southwestern Amazon and northwestern SA with bias generally ranging from 10 to 20 mm for 5-day accumulated rainfall (reaching > 30 mm in the case of 15 days). Overestimation in some areas near the tropical Andes and central Orinoco is expressive even for shorter lead times (> 30 mm for 5-day accumulated rainfall), although such regions have abundant precipitation along the year. In turn, predicted precipitation is underestimated in northern SA, central part of Tocantins–Araguaia basin (and to some extent in the Parnaíba basin), as well as in Chile between latitudes of 30º S and 40º S (–20 < bias < –10 mm for 5-day accumulated rainfall). As expected, bias is notably higher in the wet season peak (e.g., Orinoco in JJA, Northern SA in MAM, La Plata in DJF), while in the Tocantins–Araguaia it is also perceptible in the onset of the rainy season (SON). In southeastern La Plata (Uruguay basin), precipitation is overestimated in the summer (DJF) but underestimated in the winter (JJA) for longer lead times (15 days).

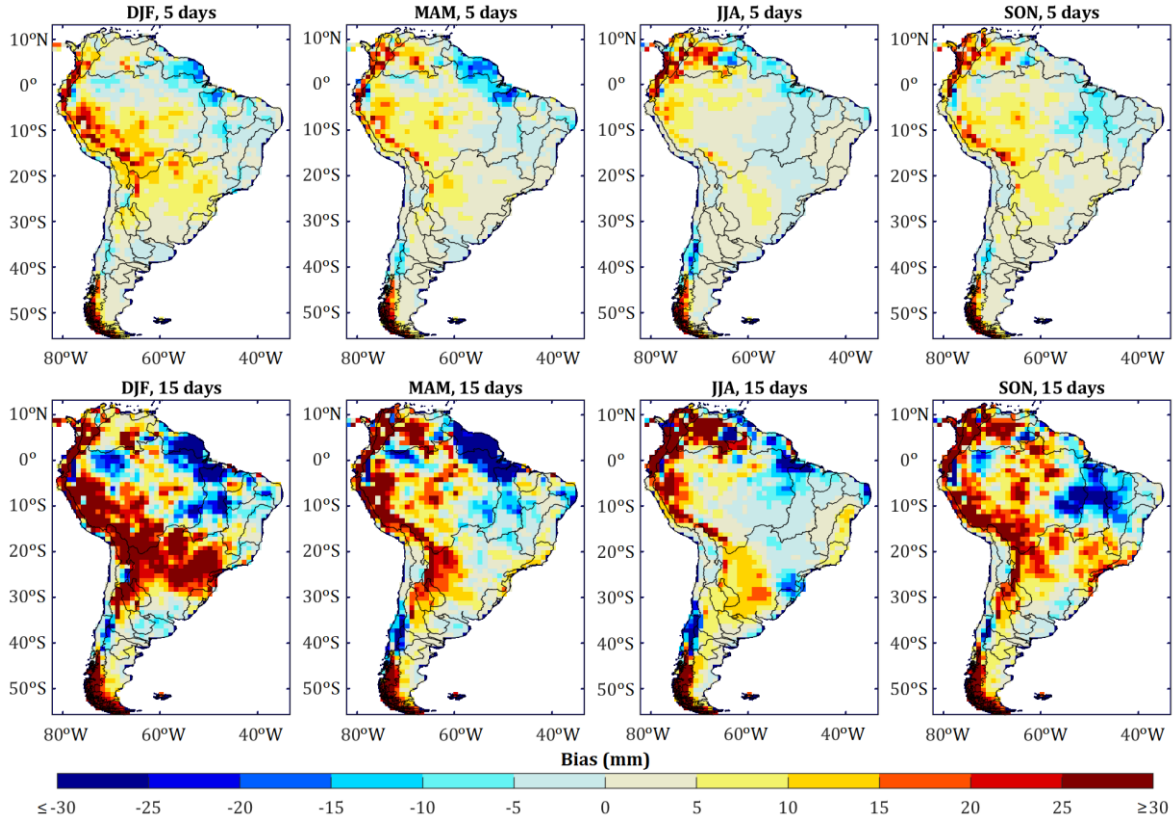

Figure 3.5. Maps of mean cumulative bias (in mm) of ECMWF predicted precipitation in comparison with MSWEP data, for accumulation periods of 5 (top) and 15 days ahead (bottom). Results are computed for the ensemble mean and are separated for each season of the year.

3.4.2. Assessment of hydrological ensemble forecasts

Performance maps of CRPSS and dAROC for ensemble streamflow forecasts are shown in Figure 3.6 and Figure 3.7, respectively. Metrics were computed for each river segment within the model domain, albeit results are shown only for those with upstream drainage area larger than 10 000 km² for visualization purposes. CRPSS is positive in central SA including the north of the Amazon, and increases at the eastern and southeastern part of the continent. ECMWF-based forecasts generally exhibit higher skill at lead time of 5 days, but are still skillful 15 days in advance especially for large rivers. In turn, negative values of CRPSS occur systematically in areas such as central Orinoco, southwest of the Amazon and west of La Plata basins. Except for Orinoco, the lack of skill is observed next to the headwaters at shorter leads and propagates downstream along the forecast horizon. Regarding dAROC (Figure 3.7), skill is substantially higher in both southern and eastern Brazil than in other regions. Some rivers draining the Andes have positive dAROC values up to around 10 days, showing a contrasting pattern to CRPSS. Conversely, a considerable fraction of large rivers shows no or little dAROC skill for ECMWF-

based forecasts in comparison with the ESP ones. This is broadly observed in the Amazon, but also in the main stem of Orinoco, Araguaia, Paraguay and lower Paraná basins.

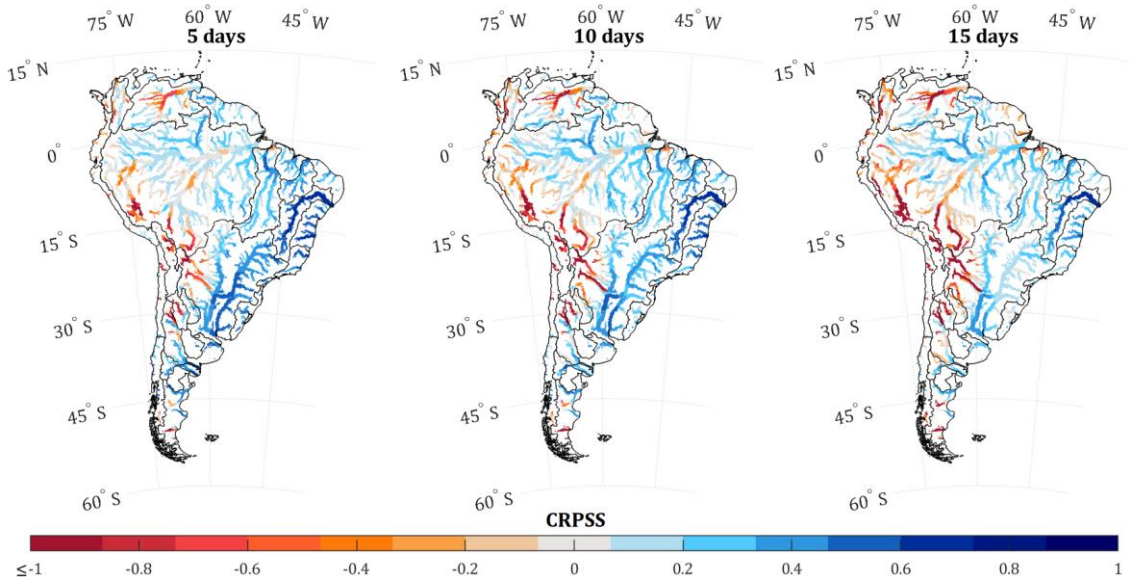

Figure 3.6. CRPSS maps of ECMWF-based streamflow forecasts for lead times of 5, 10 and 15 days, using ESP as the reference benchmark. CRPSS is shown only for rivers with drainage area > 10 000 km².

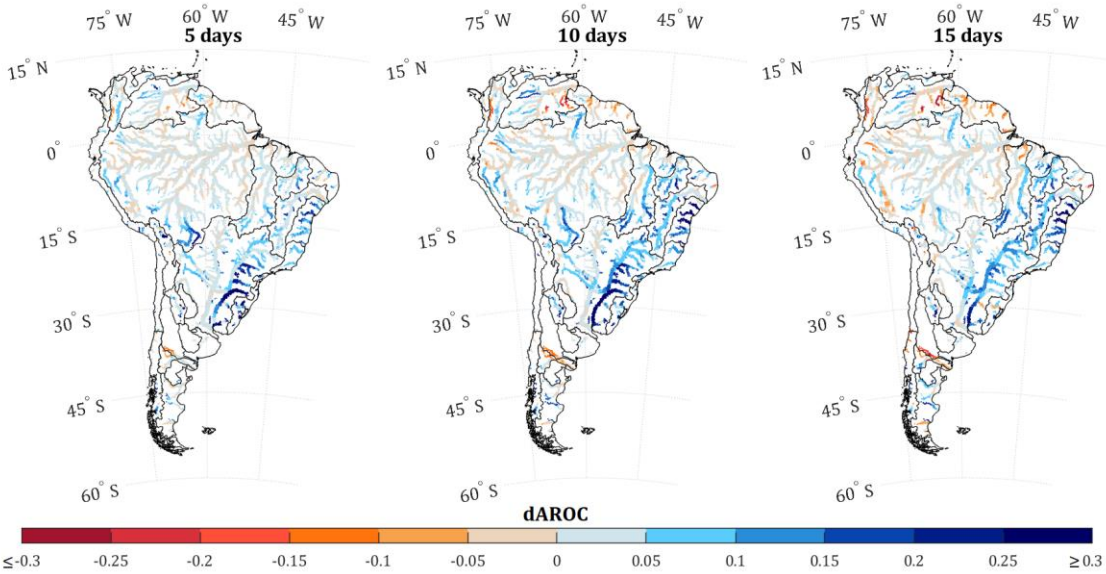

Figure 3.7. dAROC maps for ECMWF-based streamflow forecasts for lead times of 5, 10 and 15 days, using ESP as the reference benchmark. Discrimination is computed using the Q_{90} of non-exceedance flows as the reference threshold and is shown only for rivers with drainage area > 10 000 km².

To provide a more detailed, regional analysis about the performance of ECMWF-based forecasts, both metrics (CRPSS and dAROC) were plotted against the forecast lead time and basin size for a selection of large basins of the continent (Figure 3.8 and Figure 3.9, respectively). Median values of CRPSS (Figure 3.8) are close to 0 (no skill) in basins such as Magdalena, Orinoco, Madeira and Paraguay. A large dispersion of forecast performance is

observed in these cases. While the upper 5th percentile (p_5) line is mostly limited to a skill around +0.2, the 95th percentile (p_{95}) reaches values below –1.0 for lead times between 5 to 10 days in advance. Especially for Magdalena, Orinoco and Madeira, there is no clear pattern that relates forecast added skill, drainage area and lead time. Indeed, the signal of skill (positive or negative) is not evenly distributed at the tributaries, which can be visually confirmed in the spatial analysis (Figure 3.6). On the other hand, the median of CRPSS is positive in all lead times in Upper Paraná, Uruguay, Parnaíba, São Francisco and Tocantins-Araguaia. Maximum CRPSS (median) is achieved at lead times around 3–5 days because part of the streamflow forecast skill at shorter lead times comes from observed precipitation, reducing to median values close to +0.2 at the end of the forecast horizon. Only in the latter basins, skill is higher for larger drainage areas, reaching values slightly over +0.5 in the best case (São Francisco).

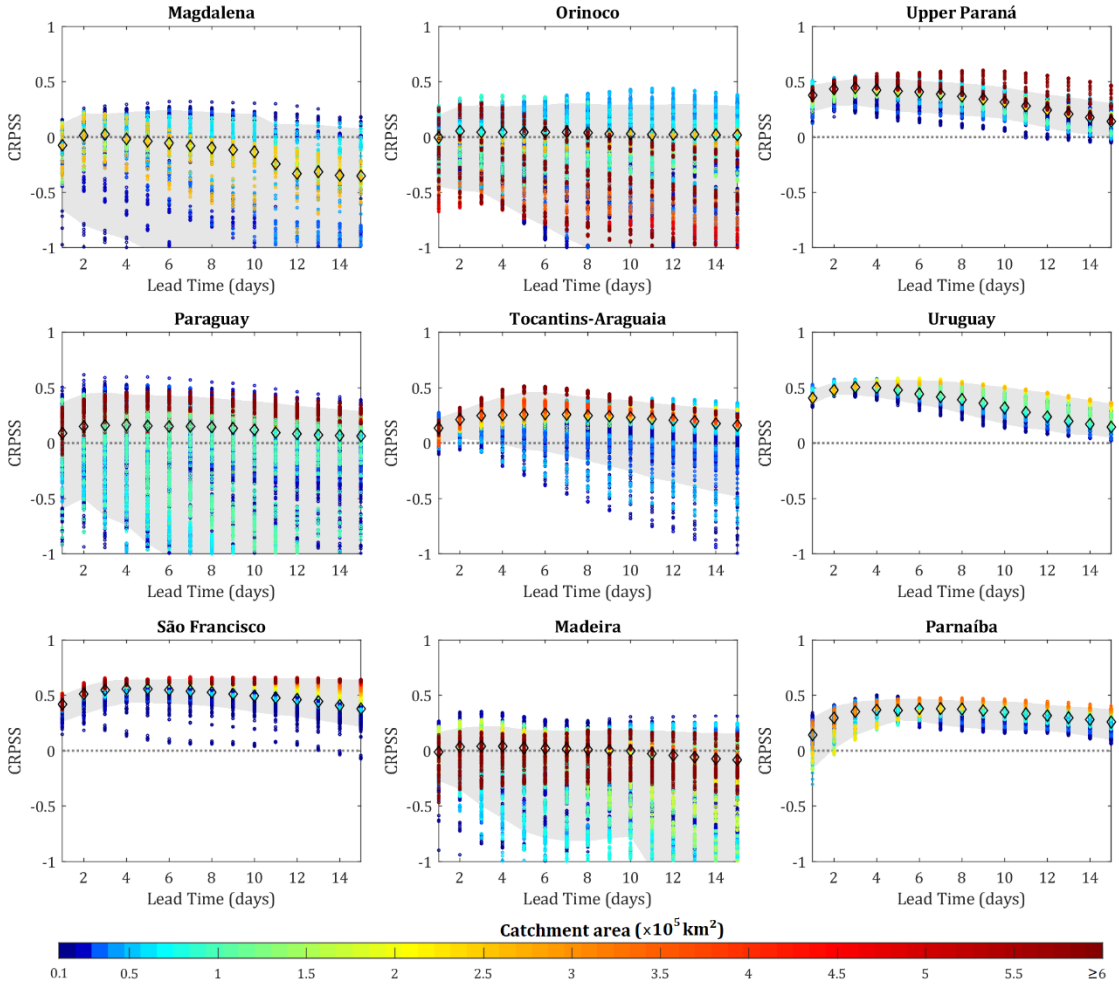

Figure 3.8. Relationship between CRPSS, lead time and basin size for different river basins of South America. Colors indicate the drainage area of MGB–SA river segments within each basin. The light gray area represents the interval between the 5th and 95th percentile, whereas the diamond symbols refer to the median of CRPSS values. The dark gray dotted line at 0 corresponds to the no skill threshold.

According to Figure 3.9, a relatively symmetric dispersion of dAROC occurs around the no skill line in large basins located in the northern hemisphere (Magdalena and Orinoco), with most of the values ranging between –0.2 and +0.2. In the other cases, the p_5 boundary is close to 0 for almost all lead times, which indicates that ECMWF-based forecasts usually tend to be at least as skillful as the ESP regarding the detection of high flow events. For the Upper Paraná, Parnaíba, São Francisco and Paraguay, dAROC skill is better for smaller drainage areas than larger ones, thus exhibiting an inverted pattern in relation to CRPSS. In the Uruguay, values of dAROC are higher (lower) for smaller (larger) drainage areas at shorter lead times but start to reduce (increase) along the forecast horizon, resulting in an inverted pattern around 5–10 days in advance.

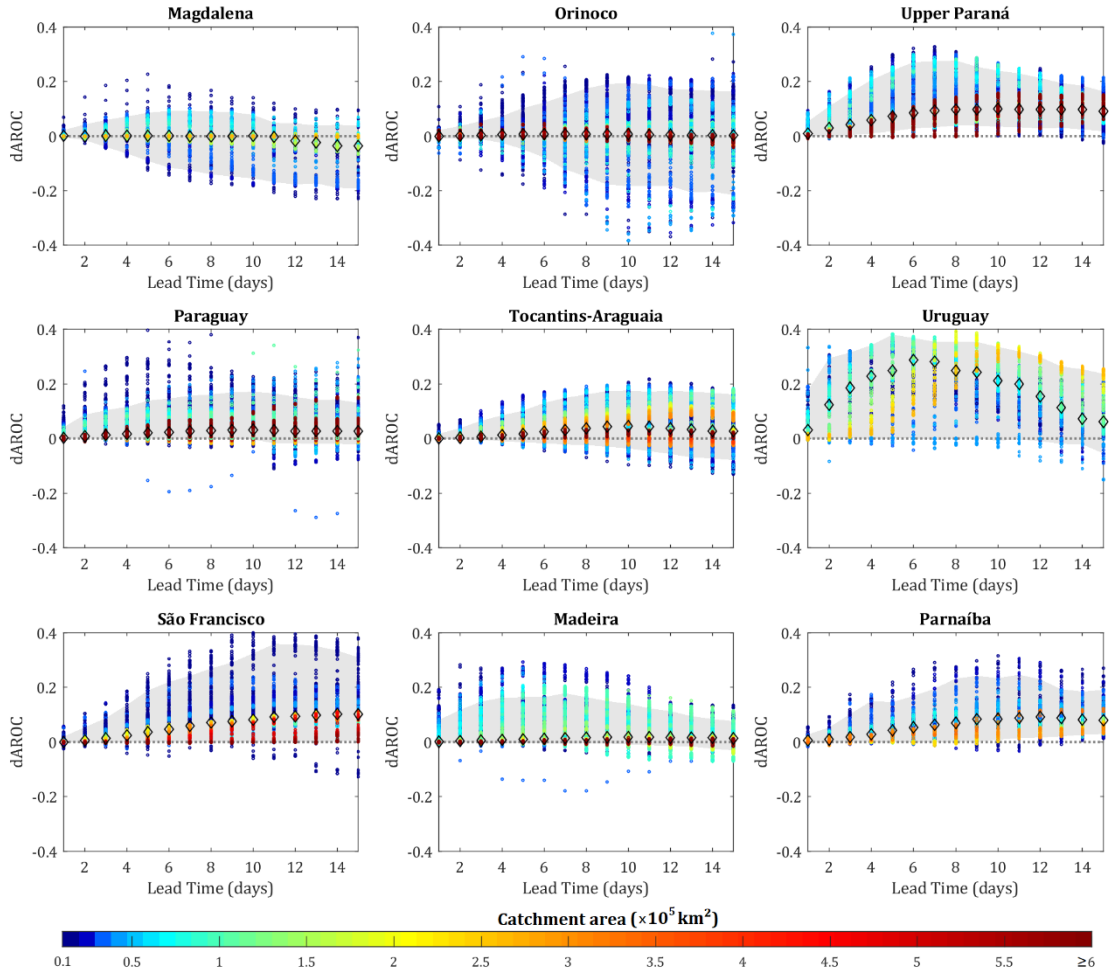

Figure 3.9. Relationship between dAROC, lead time and basin size for different river basins of South America. Colors indicate the drainage area of MGB–SA river segments within each basin. The light gray area represents the interval between the 5th and 95th percentile, whereas the diamond symbols refer to the median of dAROC values. The dark gray dotted line at 0 corresponds to the no skill threshold.

The boxplots in Figure 3.10 summarize the performance metrics (CRPSS and dAROC) in terms of climatic characteristics, considering a fixed lead time of 5 days. The locations of each unit-catchment centroid were categorized according to its corresponding climate region, and results are shown only for drainage areas < 50 000 km² to reduce the influence of large rivers that potentially cross multiple climates. Desert and polar regions, which are both concentrated at the western part of South America (Figure 3.1), were not included in the analysis as the model does not account for snowmelt processes that may be important for these areas (Siqueira *et al.*, 2018). As observed, interquartile ranges of CRPSS are notably above the no skill line in equatorial with summer or winter dry climates, as well as in warm temperate with fully humid and dry summer regions. For dAROC, skill tends to be higher along areas characterized by a fully humid, warm temperate climate but also in arid (steppe) zones, where the variability of performance is also larger.

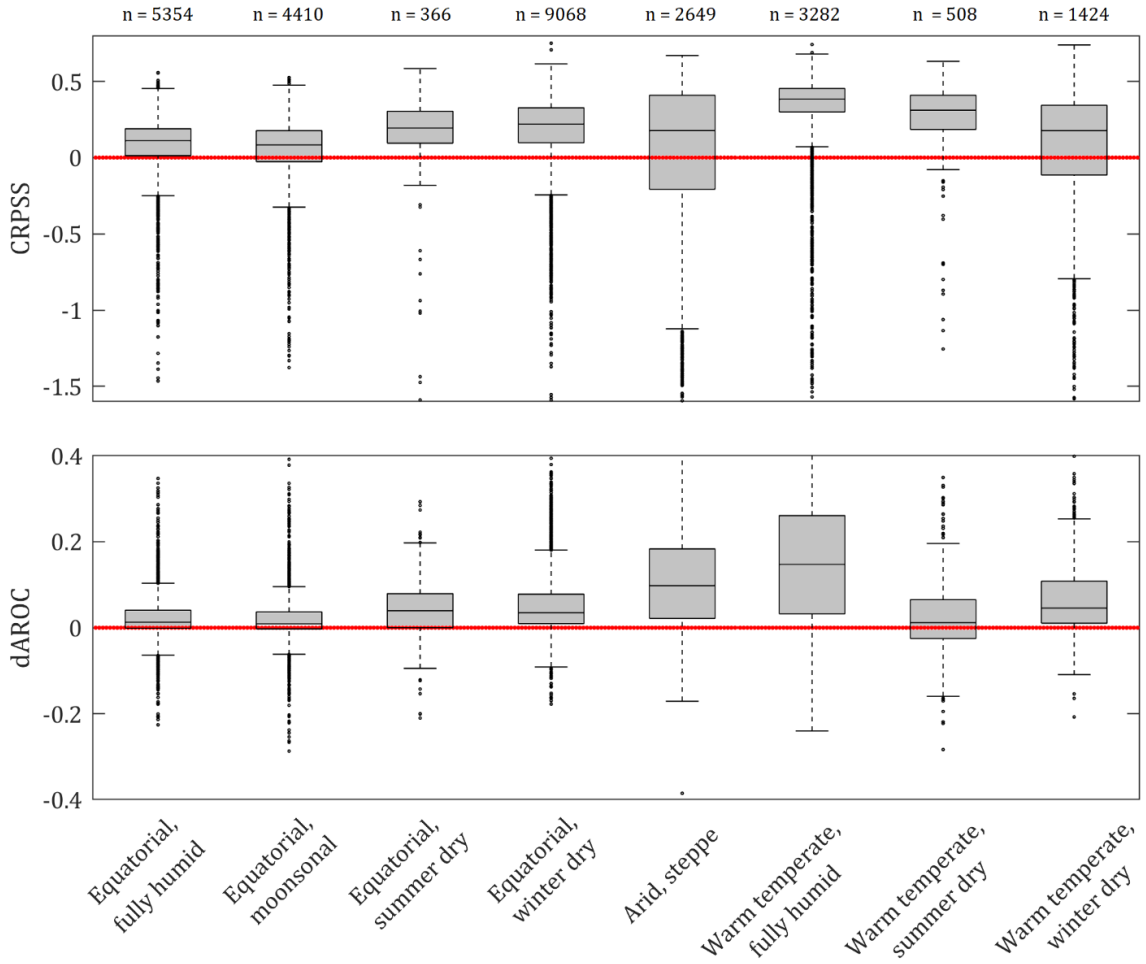

Figure 3.10. Skill scores for different climate types in South America considering a lead time of 5 days. Values at the top indicate the number of unit-catchments inside each boxplot. Results are shown for drainage areas < 50 000 km².

To assess the conditional biases of the ECMWF-based forecasts, the reliability diagrams for selected basins and different lead times are shown in Figure 3.11. Probabilities of exceeding the Q_{90} threshold are given in bins of deciles (e.g., 10–20 %, 20–30 %, …) and were plotted in the arithmetic center of the bin. Reliability diagrams were constructed by pooling the ensemble forecasts over the entire basins to increase the sample size in each bin, and the number of times each probability was predicted is shown in the bar charts at the upper left corner of diagrams. In general, the reliability curve expressed by the points over the diagrams tends to fall below the diagonal line. This pattern can be clearly seen in the Magdalena, Orinoco, Paraguay and Madeira basins, suggesting that the ECMWF-based forecasts highly overpredict the probability of exceedance of the reference threshold in these cases. For instance, events for which forecasts are predicting ~80 % of chance to occur would be observed around 40 % of the times (or even less), and this ratio is also noted in intermediary probabilities. In turn, the consistency between forecast probabilities and observed frequencies is better at the scale of other basins, especially in the São Francisco, Tocantins-Araguaia and Parnaíba. A change in the pattern of reliability diagrams over different lead times is generally unnoticeable, being more visible in the highest probabilities and, in particular, in the Uruguay basin for 15 days in advance. The shape of the histograms (note the log scale of y-axis) indicates that ECMWF-based forecasts tend to predict very low probabilities of exceedance of the Q_{90}, albeit a large number of predictions demonstrate probabilities near 100 %. This means that the ensemble streamflow forecasts are relatively sharp for the analyzed threshold.

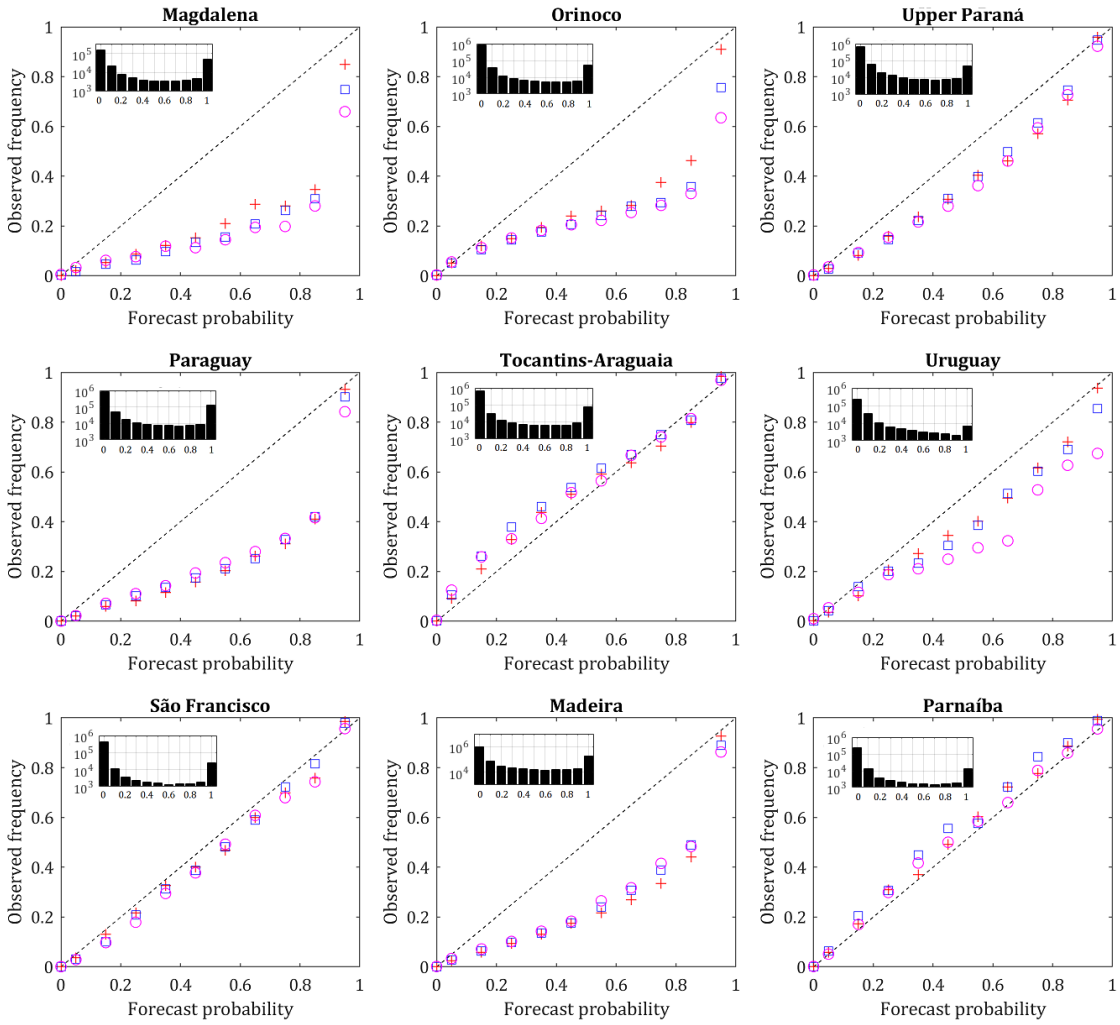

Figure 3.11. Reliability diagrams of ECMWF-based streamflow forecasts for different South American basins. Diagrams were constructed by pooling the ensemble forecasts over each basin and are shown for lead times of 5 (red cross), 10 (blue square) and 15 days (magenta circle). The diagonal dashed line represents a condition with perfect reliability. The sharpness histograms show the sample size (log scale) in each bin and are presented for the lead time of 5 days.

3.4.3. Event-based analysis

In this section we conduct a visual analysis of selected flood events at Uruguay, Iguazu, Doce, Magdalena and Beni rivers using sequences of ensemble streamflow forecasts (Figure 3.12). These were the largest floods within the hindcasting period (Nov/2010–Oct/2014) for the corresponding rivers, and were selected based on relevance or available documentation in the scientific literature. Table 3.3 provides additional details for the selected locations and their respective flood events according to in situ observations. Critical thresholds (5- and 25-yr return period) used as a reference for flow magnitudes in Figure 3.12 were calculated using Gumbel distribution considering the years 1990–2014 to keep coherence between simulated and observed data. As the ECMWF-based forecasts (gray lines) and ESP (not shown) share the

same initial conditions of the model reference run (blue line), it is normal that they follow the same path along forecast dates, which sometimes differ considerably from in situ observed discharges (black line).

Table 3.3. Characteristics of the selected flood events based on in situ observations.

Location	River	Basin	Peak date	Maximum daily observed discharge (m^3s^{-1})
Uruguaiana[1] (190 000 km²)	Uruguay	Uruguay (La Plata)	06/07/2014	23 190
Salto Caxias dam[2] (57 100 km²)	Iguazu	Upper Paraná (La Plata)	09/06/2014	17 970 (reservoir naturalized flows)
Colatina[1] (77 000 km²)	Doce	Doce (Southeast Brazil – Atlantic Coast)	25/12/2013	9196
Arrancaplumas[3] (54 600 km²)	Magdalena	Magdalena	21/04/2011	5070
Rurrenabaque[4] (68 900 km²)	Beni	Madeira (Amazon)	double peak, 31/01/2014 (1st), 12/02/2014 (2nd)	22 130 (1st), 25 000 (2nd)

Data sources: [1]ANA(Brazil), [2]ONS (Brazil), [3]IDEAM (Colombia) and [4]ORE-HyBam (Amazon/Orinoco).

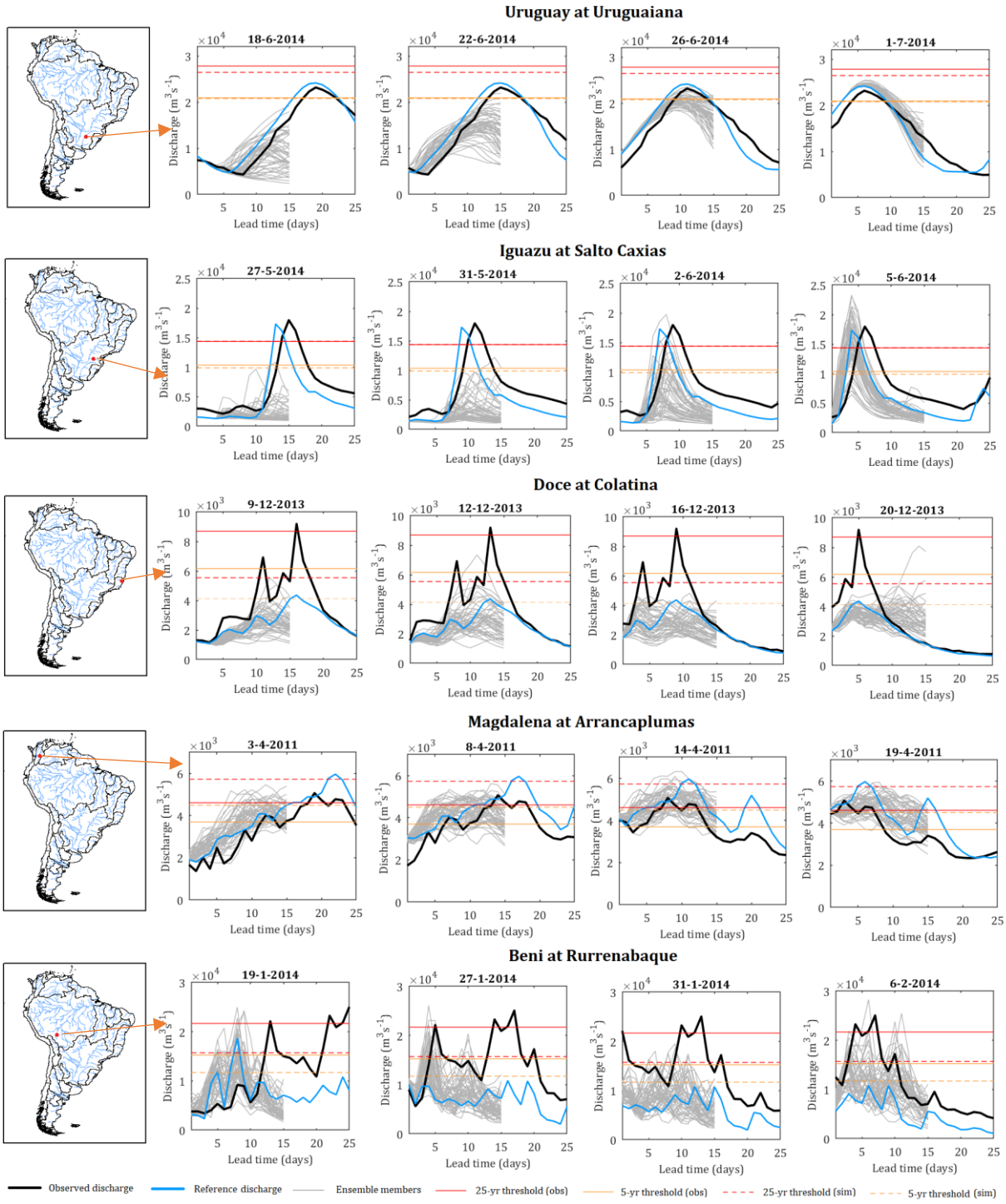

Figure 3.12. ECMWF-based forecasts issued for selected flood events. Black and blue thick lines represent the observed and reference discharge (*proxy*), respectively, whereas gray thin lines represent the forecast ensemble members. Dates at the top of figures indicate the day for which the forecast was issued, starting at lead time 0. Flow thresholds correspond to return periods of 5 (orange) and 25 years (red) and were computed for in situ observations (solid line) and simulated discharge (dashed lines) using Gumbel fit and data from 1990 to 2014.

The selected flood event of the Uruguay river occurred in July 2014, with the peak reaching around 23 000 m^3s^{-1} between return periods of 5 and 25-yrs. ECMWF-based forecasts

were successful in predicting the rising, magnitude and also the flood recession for this particular event. Another flood, in the Iguazu river, reached a maximum daily flow of ~18 000 m^3s^{-1} at Salto Caxias dam (57 100 km^2) in June 2014, and was classified as one of the most catastrophic floods after 1970 in upstream locations (Steffen and Gomes, 2018). High discharges in Iguazu river were predicted with increasingly higher probabilities along the forecast dates, and both peak timing and magnitude were relatively well predicted at shorter lead times.

In Doce river (Southeastern Brazil) at Colatina (77 000 km^2), forecasts are shown for the December 2013 flood event (peak of ~9200 m^3s^{-1}). It was the second-most severe flood in the period of 1939–2014 that occurred in the basin, affecting more than 54 000 people and causing 45 fatalities (Tomasella *et al.*, 2019 and references therein). As noted, the simulated discharges for this event were largely underestimated by the MGB–SA forced with MSWEP data. Some ensemble members predicted flows near the simulated 25-yr threshold only at longer lead times (for instance, the forecast issued at 12/12/2013), but probabilities of very high discharges reduced for forecast dates closer to the second peak date. For the Magdalena river (Colombia), streamflow forecasts are issued at Arrancaplumas station (56 400 km^2) and refer to a flood that occurred during the extreme 2010–2011 La Niña. That year was characterized by multiple hydrometeorological events (floods, landslides, windstorms, etc) that caused losses of more than US$ 7.8 billion (Hoyos *et al.*, 2013). According to Figure 3.12, gradually increasing discharges in Magdalena river have exceeded the 5-yr reference threshold over many days, thus producing a relatively long-lasting flood. ECMWF-based forecasts predicted the streamflow increase in a persistent manner several days in advance, however with considerable ensemble spread.

Finally, forecasts in the Beni river (Bolivia) at Rurrenabaque (68 900 km^2) are shown for the extreme January 2014 floods, which were dramatic for both local and downstream Amazonian communities. According to Espinoza *et al.* (2014), around 68 000 families and more than 40 000 ha of agriculture were severely affected by the flood event. It was characterized by two main peaks with around 10 days of difference, with discharges above 20 000 m^3s^{-1} in both cases. Streamflow forecasts were marked by a very large ensemble spread in all dates and lead times, thus reflecting a very low predictability in this location. Although the simulated discharges were not in agreement with the observed ones, very high discharges exceeding the

simulated 25-yr threshold were sequentially forecasted by a considerable number of ensemble members, which indicated high probabilities of extreme events during the analyzed period.

3.5. **Discussion and limitations**

The analysis carried out in the previous section suggests that medium-range (up to 15 days) ensemble streamflow forecasts based on the ECMWF EPS are skillful over many regions of South America, when compared to ESP forecasts that rely on resampled rainfall from historical observations as the model forcing. The assessment was performed in a 4-year period between Nov/2010 and Oct/2014 using a continental-scale hydrologic-hydrodynamic to produce hydrological forecasts, which was specifically developed for large-scale hydrological analysis in this continent (Siqueira *et al.*, 2018).

We first compared the precipitation forecasts from the ECMWF EPS to the resampled rainfall predictions that were both used to force the hydrological model. The ECMWF EPS performs well in the east side and southern regions of SA, but has little or no added skill over climatology in the central-north part of the continent and particularly along the Andes. By comparing ECMWF EPS and GEFS precipitation forecasts in Brazilian territory, Medina *et al.* (2019) also highlighted the former as being skillful at east and southern regions, with a lack of skill in the Amazon basin. Indeed, the forecast skill of atmospheric models is known to be lower at the tropics than midlatitudes (Zhu *et al.*, 2014; Dias *et al.*, 2018a), since rainfall in the former mostly occurs through deep convection activity that is highly parameterized and one of the major sources of uncertainty in NWPs. In addition, the low CRPSS in areas close to the Andes Cordillera comes together with a positive bias, which was observed systematically over all seasons. Kidd *et al.* (2013) compared predictions from the ECMWF model to TRMM rainfall data and found a similar pattern of overestimation over the Andes, especially during the austral summer. Janowiak *et al.* (2010) also found a substantial overestimation in both north and central parts of SA, when assessing forecasts from the ECMWF model against GPCP and CMORPH rainfall estimates. Results are also in agreement with those from Bischiniotis *et al.* (2019), who evaluated the performance of GloFAS in Peru and stated that ECMWF EPS tends to forecast higher precipitation than the forcing (ERA-Interim reanalysis) used to initialize the hydrological model.

Notwithstanding, there are important remarks on the MSWEP data used as the observation. The latter is a good option to ensure consistent rainfall fields in both space and

time over the continental domain, since the availability of gauge stations greatly varies from one region to another. In turn, MSWEP largely depends on the anomalies derived from satellite rainfall estimates over South America (Beck *et al.*, 2017c), for which the associated shortcomings are documented for many countries of the continent (e.g., Dinku *et al.*, 2010b; Blacutt *et al.*, 2015; Mantas *et al.*, 2015; Salio *et al.*, 2015). Particularly in the Andes, where the largest discrepancies between MSWEP and ECMWF EPS were found, the spatial variability of precipitation can be quite impressive. Interesting examples are the rainfall hot spots in the Bolivian and Peruvian foothills where annual gradients can reach up to 190 mm km^{-1} (Espinoza *et al.*, 2015), which are certainly misrepresented in the coarse resolution precipitation grids. A common drawback of satellite products in this region is that they typically overestimate light precipitation and underestimate high precipitation rates (Blacutt *et al.*, 2015; Mantas *et al.*, 2015; Salio *et al.*, 2015; Zambrano-Bigiarini *et al.*, 2017). Besides, the detection accuracy of satellites has been found to deteriorate in altitudes between 500–2000 m as a potential effect of the orographic uplift of moist air moving towards the Andean slopes (Dinku *et al.*, 2010b; Mantas *et al.*, 2015), often related to warm rain processes for which the infrared threshold (of cloud top temperature) may be too low to detect precipitation (Dinku *et al.*, 2010b; Satgé *et al.*, 2016; Hobouchian *et al.*, 2017). Heavy rainfall that develops in such mountainous regions may also lack a vertical structure with densely populated frozen hydrometeors, resulting in weak scattering signals for microwave retrievals (Hobouchian *et al.*, 2017). Large areas in the central Andes, like the Altiplano in Bolivia and northern Chile, are very arid and sometimes located in very high altitudes (> 3500 m), and may be affected by sub-cloud evaporation and presence of snow-covered regions that can lead to overestimation (Salio *et al.*, 2015; Satgé *et al.*, 2016; Zambrano-Bigiarini *et al.*, 2017). Although these shortcomings make it difficult to evaluate the actual skill of predicted precipitation and related biases, satellite estimates are still expected to be more correlated with in situ data when compared to NWPs (Lu *et al.*, 2010).

As expected, the geographical distribution of CRPSS regarding the streamflow forecasts is akin to that observed in predicted rainfall. On the other hand, while overall skill in precipitation decreases to values close to zero for a 15-day range in almost all regions, streamflow forecast skill is still positive two weeks in advance in many rivers due to the delay produced by the processes that transform rainfall into runoff and river discharge, moreover in large river basins. This suggests that ECMWF-based forecasts could perform better than ESP even at longer lead times (i.e., sub-seasonal ranges), which may be relevant also for hydropower

and water management purposes. This is highlighted for the Upper Paraná basin in the study of Quedi and Fan (2020), who found that ECMWF-based forecasts are skillful when compared to ESP for lead times up to 3–4 weeks ahead.

At the regional scale, the ECMWF-based forecasts are potentially more skillful in basins such as Uruguay, Upper Paraná, São Francisco, Tocantins-Araguaia and Parnaíba, albeit less in Magdalena, Orinoco, Madeira and Paraguay. The former ones showed a similar pattern of overall skill, for which the performance declines for longer lead times and tends to be better for larger drainage areas, similarly to general findings from other studies (e.g., Alfieri *et al.*, 2014; Bischiniotis *et al.*, 2019; Quedi and Fan, 2020). This seems, however, not to be valid for all cases, as such relationship was not found in Magdalena, Orinoco and Madeira basins due to distinct forecast performances at their tributaries. Moreover, forecast probabilities in the latter basins were consistently too large relative to the corresponding conditional event frequencies, which is linked to the positive bias in the predicted rainfall that occurs mainly on the wet season. This overprediction would probably lead to a high number of alerts being issued and, consequently, a high number of false alarms considering the analyzed reference threshold (Q_{90}). One should note that a positive bias in forecast probabilities also increases detection. The area under the ROC curve is more sensitive to hit rate than false alarms (because correct negatives of high flow events occur most of the time) and this could be one of the reasons for which a positive dAROC was found in rivers draining the Andes. It is important, however, to keep in mind the potential issues related to rainfall observations used herein.

The relation between basin size and discrimination skill is also spatially dependent. In large SA basins located north of the equator we found no relationship probably due to biases and low precipitation skill. For some other basins, however, the discrimination skill was found to decrease with drainage area, even for longer lead times. This may be explained by the fact that large rivers are often dominated by initial conditions, that is, the predicted rainfall only becomes important to the streamflow forecasts after a certain number of days. Propagation of floods tends to be very slow in regions with mild slopes that are often regulated by floodplains, as typically observed in large South American basins like the Paraguay (Paz *et al.*, 2011), Amazon (Paiva *et al.*, 2013a), Araguaia (Pontes *et al.*, 2017) and Magdalena (Angarita *et al.*, 2018). For instance, Paiva *et al.* (2012b) clearly show that, for the first weeks (and months in some cases), the relative importance of rainfall forecasts is negligible in comparison with hydrological initial conditions in tributaries at the Central Amazon. Our results provide

additional information to those obtained by Alfieri *et al.* (2013) when evaluating the GloFAS system, who found that in large rivers of SA (such as the Amazon and Paraná) values of area under ROC curve remain high (> 0.7) over several days in advance. It is worth mentioning that Alfieri *et al.* (2013) adopted random forecasts (AROC = 0.5) as a reference for discrimination ability. This may limit the assessment of discrimination skill because even ESP forecasts can have high levels of detection in such rivers at shorter lead times, due to the little influence of predicted precipitation with respect to the hydrological initial conditions.

Notably, both overall and discrimination skill had a better performance in the fully-humid, temperate climate, which in turn coincides with southern Brazil, Uruguay and northeast Argentina (southeastern SA). The absence of seasonality potentially makes the ESP benchmark less useful, thus enhancing the relative performance of ECMWF-based forecasts regarding the former. In Australia, Bennett *et al.* (2014) also found the forecasting system performing better in temperate regions than in other climate types, especially the arid ones with intermittent flows. Moreover, even though severe hydrometeorological events in southeastern SA may be related to MCSs (Salio *et al.*, 2007; Demaria *et al.*, 2011), floods in larger rivers in this region are often triggered by frontal systems during the cold season (Berbery and Barros, 2002; Vera *et al.*, 2002) that can be reasonably well predicted by atmospheric models (Zhu *et al.*, 2014).

The scale of our study indicates to which extent the findings from hydrological forecasting studies in specific regions of SA may be applicable to other parts of the continent. Fan *et al.* (2015b) reported good performance of streamflow forecasts in the Tocantins, Doce (East Brazil) and Upper São Francisco basins when conducting experiments with ECMWF and other precipitation ensembles from TIGGE dataset. Tomasella *et al.* (2019) found that streamflow forecasts based on the ECMWF EPS were comparable to those obtained from a regional, high-resolution (Eta) EPS for drainage areas larger than 20 000 km² in Doce basin, while Siqueira (2015) showed that ECMWF EPS performed similarly to the same Eta model tested by Tomasella *et al.* (2019) at the short-term range in Southern Brazil. Although these studies focused in comparing the performance of different ensemble forecasting systems rather than skill to a benchmark, one should note that such studies were carried out in locations at east and southeastern South America where the ECMWF EPS was found here to perform reasonably well. However, our results indicate that such forecast performances may not be transposable to the western areas of the continent (e.g., rivers draining the tropical Andes region).

It is worth mentioning again that our results were obtained by assuming simulated discharges as surrogate of observed data (proxies), which were produced by forcing a hydrological model with precipitation estimates from MSWEP. While this is an interesting way to assess which regions ensemble precipitation forecasts might be useful for hydrological forecasting (e.g., Bartholmes *et al.*, 2009; Alfieri *et al.*, 2014), predicted flows are likely to exhibit large deviations from the observed hydrographs. In fact, hydrological models can significantly contribute to the total uncertainty for both short- (Seo *et al.*, 2006; Velázquez *et al.*, 2011; Zappa *et al.*, 2011) and medium forecast ranges (Pappenberger *et al.*, 2011; Paiva *et al.*, 2012b; Sharma *et al.*, 2019), and this can be even more important for large-scale hydrological models with simplified calibration (as the MGB–SA) that are forced by other sources than in situ precipitation (Sperna Weiland *et al.*, 2015; Siqueira *et al.*, 2018). Future studies should advance by making use of in situ data where possible or producing better estimates of discharge as a proxy, for instance, through data assimilation methods that have demonstrated promising results in the region (e.g., Paiva *et al.*, 2013b; Wongchuig *et al.*, 2019).

We understand that there are potential impacts of using quite old precipitation forecasts (2010–2014). These are likely to be improved in more recent ECMWF model versions. However, significant improvements are not expected in regions close to the tropical Andes and Amazon basin where results were found here to be relatively poor, given the convective nature of rainfall and its very high spatial variability, as well as the lack of observations that are needed for data assimilation in the atmospheric model. Another limitation is that we did not perform bias correction in ensemble precipitation forecasts. Indeed, bias correction could improve the skill of streamflow forecasts relative to the ESP to some extent, but the known existing uncertainties in the MSWEP product, especially in the west side of SA where the relative bias is high, do not allow to reliably calibrate bias correction techniques in these areas. In addition, bias correction methods usually rely on long and homogeneous time series of both observed and predicted precipitation, while operational forecasts such as the ones from TIGGE repository (as used here) continuously improve over time as atmospheric models are updated. Potential benefits of bias correction strategies with the support of long series of retrospective precipitation forecasts from the same model cycle (i.e., reforecasts) should be investigated in a future work.

The use of a threshold corresponding to the Q_{90} of non-exceedance flows is here justifiable, as the 4-year hindcasting period is relatively short to capture relevant flood events

in a single river location. Selecting fixed quantiles from simulated discharges to discriminate between the occurrence and non-occurrence of an event is a common practice at national to global-scale forecasting (e.g., Bartholmes *et al.*, 2009; Alfieri *et al.*, 2013; Alfieri *et al.*, 2014; Bischiniotis *et al.*, 2019), but are not expected to represent flood conditions equally well in the whole South America. For instance, the Q_{90} threshold may be low in rivers with large variability of flows (e.g., Uruguay), albeit high in others where the flood pulse is very slow and unimodal (e.g., Amazon, Orinoco). Besides, the ECMWF forecasts were shown to be biased compared with the MSWEP data used as the model forcing to derive flow thresholds, which may cause a negative effect in forecast exceedance probabilities. Producing reference thresholds based on a long-term model run with reforecast data rather than observed precipitation (e.g., Hirpa *et al.*, 2016) and defining them according to the lead time in analysis (e.g., Alfieri *et al.*, 2019) may allow further improvements on forecast detection skill.

While the assessment of hydrological forecast skill should be continuously evaluated over time (e.g., Pappenberger *et al.*, 2011; Alfieri *et al.*, 2014), it is also important to outline potential research directions based on recent experiments on large-scale (i.e., continental to global) operational forecasting systems. For example, some studies are currently testing multimodel frameworks (e.g., Kauffeldt *et al.*, 2016) and combining multiple forecasts through postprocessing methods (e.g., Zsoter *et al.*, 2016) in order to better represent the inherent uncertainties. Data assimilation of other variables than in situ discharge such as flood extent maps (e.g., Revilla-Romero *et al.*, 2016) or soil moisture from remote sensing products (e.g., Wanders *et al.*, 2014) may be promising to update state variables and initial conditions of the hydrological model, as streamflow records are often limited in terms of spatial coverage. Furthermore, downscaling and routing the predicted runoff from well-established global forecasting systems (like GloFAS) through a high-resolution river network (e.g., Perez *et al.*, 2016; Snow *et al.*, 2016) could be interesting to reduce computational costs while improving the local relevance of warnings.

3.6. **Conclusions**

This work presented a comprehensive evaluation of the potential skill of medium-range ensemble streamflow forecasts (up to 15 days ahead) for flood prediction in large basins of South America (SA). Raw ensemble precipitation forecasts issued by the ECMWF EPS were used as input to a continental-scale, fully coupled hydrologic–hydrodynamic model to identify regions where the predicted precipitation is expected to produce skillful streamflow forecasts,

i.e., after the former is propagated through a perfect hydrological system (namely ECMWF-based forecasts). The assessment of potential skill was carried out having Ensemble Streamflow Prediction (ESP) forecasts as the benchmark, which resamples past rainfall observations (here from the MSWEP dataset) to drive the same hydrological model. Our main findings can be summarized as follows:

- ECMWF-based forecasts are skillful up to 15 days in advance mainly in eastern and southeastern SA. On the other hand, overall skill is considerably lower in large rivers draining the Andean region (at western SA regions), where ECMWF-based forecasts often have lower performance than the ESP;

- ECMWF-based forecasts show skill in discrimination between occurrence and non-occurrence of events compared to the ESP mainly over southern Brazil;

- Both overall and discrimination skill of ECMWF-based forecasts is higher in warm temperate, fully-humid regions than other climate types;

- A global relation between basin size and overall forecast skill was not identified. Although in large basins such as Uruguay, Upper Paraná, São Francisco, Tocantins–Araguaia and Parnaíba the skill of ECMWF-based forecasts reduces with lead time and is generally higher for larger catchment areas compared to the ESP, in others like Magdalena, Orinoco and Madeira the overall skill does not follow the same behavior since it varies geographically along basin tributaries;

- The relation between basin size and discrimination skill is also spatially dependent. In Upper Paraná, Parnaíba, São Francisco and Paraguay basins it is generally higher for smaller drainage areas, whereas for larger basin sizes it tends to increase with lead time as an effect of hydrological initial conditions. On the other hand, in large basins of SA north of the equator no relationship was found;

- Forecast probabilities are highly overestimated in Magdalena, Orinoco, Paraguay and Madeira basins, as an effect of wet biases in predicted precipitation (in relation to MSWEP) that occur mainly during the rainy season.

Our findings also reinforce previous statements that ensemble precipitation forecasts can be valuable to drive continental hydrological models, thus providing large-scale

hydrological predictions to complement existing systems or to encompass regions where no forecasts are currently available (Thielen *et al.*, 2009a; Alfieri *et al.*, 2013; Thiemig *et al.*, 2015; Emerton *et al.*, 2016). Although the results presented herein offer a broad picture about the potential skill of streamflow forecasts based on meteorological EPS, important technical challenges are posed. Given the low coverage of hydrometeorological gauge stations providing real-time data in the context of SA, the use of satellite estimates (or satellite-based products that merge data from multiple sources) is — and will be — of paramount importance to initialize the hydrological states before precipitation forecasts can be used as model input. The known limitations of such estimates combined to the model errors (Siqueira et al., 2018) undoubtedly lead to significant hydrological uncertainties, and these must be accounted for in order to shed light on the actual skill of the forecasting system. Therefore, there are major opportunities of postprocessing and data assimilation techniques at the continental domain of SA to make the best use of available in situ observations and remote sensing data. Nonetheless, as the topic of ensemble hydrological prediction is still incipient in SA, we expect that our results can also encourage regional forecast experiments in SA locations where hydrological forecasts may benefit from a meteorological EPS (such as the ECMWF).

Acknowledgments

The authors would like to acknowledge the Brazilian National Council for Scientific Research (CNPq) for funding this research under the grant numbers 141450/2015-0 and 422422/2016-9 (Project: “South America Flood Awareness System – SAFAS”); the European Center of Medium-Range Weather Forecasting (ECMWF) for making available the ensemble precipitation forecasts used in this study; Princeton University for the MSWEP precipitation data; and the two anonymous reviewers for their useful contributions which helped us to improve the manuscript.

CAPÍTULO 4: Pós-processamento de previsões de vazão por conjunto na escala continental

"All those whose duty it is to issue regular daily forecasts know that there are times when they feel very confident and other times when they are doubtful as to the coming weather. It seems to me that the condition of confidence or otherwise forms a very important part of the prediction, and ought to find expression."

—W.E. Cooke (1906) [6], ex-meteorologista do governo Australiano.

[6] Retirado de: Krzyzstofowicz, R. (1998). Probabilistic Hydrometeorological Forecasts: Toward a new era in operational forecasting. **Bulletin of the American Meteorological Society**, vol. 79, n.2, pp 243–252.

Prólogo

No capítulo 3 foi discutido sobre a capacidade das previsões meteorológicas por conjunto em contribuir para a destreza das previsões de vazão. Os resultados obtidos para diferentes regiões e bacias da AS permitiram inferir apenas sobre o *skill* potencial (ou teórico) que poderia ser obtido através do uso das previsões de precipitação oriundas do ECMWF, uma vez que os erros do modelo hidrológico continental e da própria forçante usada para inicializar o modelo no instante de previsão foram negligenciados. Entretanto, conforme apontado nos capítulos anteriores (2 e 3), existem importantes incertezas relacionadas ao MGB–SA que, juntamente com aquelas remanescentes da previsão meteorológica por conjunto, precisariam ser tratadas com o intuito de estimar e avaliar a incerteza total da cadeia de previsão.

No presente capítulo, buscou-se investigar a respeito do uso de pós-processamento estatístico sobre previsões de vazão por conjunto emitidas na escala continental, no horizonte de médio prazo. Para isso, foi realizada uma extensão do período de dados das previsões de precipitação por conjunto do ECMWF a partir da aquisição de *reforecasts* (abreviação para previsões retrospectivas), totalizando um período de ~19 anos (mar/1996–dez/2014) porém com frequência de emissão de duas vezes por semana. Diferente das previsões operacionais que foram utilizadas no capítulo 2, cujo modelo atmosférico tende a sofrer atualizações frequentes ao longo do tempo, as *reforecasts* são amostras para um período geralmente multidecenal e consistentes com um mesma versão do modelo operacional. Assim, elas podem ser entendidas como a climatologia do modelo de previsão, cujos dados são bastante úteis para fins de calibração estatística de previsões.

As *reforecasts* de precipitação, aqui compostas por 10 membros perturbados e uma previsão de controle, foram processadas e utilizadas como dado de entrada ao MGB–SA (em modo previsão) para geração de previsões de vazão por conjunto. As previsões de vazão brutas (i.e., não pós-processadas) foram pareadas com observações do passado em aproximadamente 490 localidades da AS, sendo que posteriormente foi aplicada a técnica *Ensemble Model Output Statistics* (EMOS) com treinamento/validação cruzada para gerar densidades preditivas condicionais no horizonte de médio prazo. Estas distribuições, válidas para uma dada localidade e antecedência específica, foram ainda processadas com a técnica *Ensemble Copula Coupling* (ECC), buscando derivar trajetórias de previsão realísticas com dependência temporal. Por fim, as previsões brutas e pós-processadas foram avaliadas entre si usando tanto a climatologia como a persistência das ultimas vazões observadas como *benchmarks*.

Em resumo, os resultados mostraram que, na escala continental e para um horizonte de 15 dias, apenas incluir as incertezas da previsão meteorológica muitas vezes não é condição suficiente para gerar previsões mais acuradas do que a climatologia ou a persistência. Ficou evidente que as incertezas do MGB–SA não podem ser negligenciadas e que o pós-processamento estatístico tem um papel importante para garantir destreza e melhorar a consistência estatística (calibração) das previsões de vazão. Apesar das previsões corrigidas com o EMOS resultarem, de forma geral, em maior dispersão do que as previsões brutas (i.e., menos agudas), as primeiras ainda mantiveram-se com menor largura média de incerteza quando comparadas àquela da climatologia. Mostrou-se também que séries de vazão prevista pós-processadas que preservam a dependência temporal (i.e., ao longo das antecedências) poderiam ser obtidas na escala continental, principalmente na região leste da bacia do Prata onde a representação da autocorrelação das séries demonstrou ser, na maioria dos casos, adequada. Em contrapartida, as trajetórias de previsão de vazão tendem a ser menos realísticas, isto é, com menor representação da autocorrelação em condições de baixo espalhamento do conjunto bruto, especialmente quando este é associado a distribuições preditivas pós-processadas com grande largura de incerteza. Na discussão do capítulo foi destacado um maior aumento da dispersão das previsões pós-processadas em relação à climatologia em regiões como Amazônia e oeste da bacia do Prata, que poderiam estar associadas a uma maior incidência de erros aleatórios nas previsões brutas. Estes erros podem ter relação com a menor destreza da precipitação prevista nestas áreas (Capítulo 3), baixo espalhamento das previsões brutas — no caso de rios com maior influência da condição inicial para a previsibilidade de vazões —, e potenciais erros de *timing* do MGB–SA (Capítulo 1). Em relação às trajetórias derivadas com ECC, uma análise de sensibilidade de parâmetros indicou que as autocorrelações das séries de vazão prevista podem ser melhor capturadas a um custo de redução de calibração das previsões. Limitações relacionadas aos métodos aplicados e abordagens existentes na literatura que poderiam reduzir tais limitações também foram discutidos ao final deste capítulo.

Este capitulo é baseado no seguinte artigo publicado na revista *Journal of Hydrology*:

SIQUEIRA, V. A., WEERTS, A. H., KLEIN, B., FAN, F. M., PAIVA, R. C. D., COLLISCHONN, W. Postprocessing continental-scale, medium-range ensemble streamflow forecasts in South America using Ensemble Model Output Statistics and Ensemble Copula Coupling. ***Journal of Hydrology***, 126520, DOI: 10.1016/j.jhydrol.2021.126520, 2021.

4.1. **Introduction**

Medium-range hydrological forecasts (up to 15 days) play a key role in decision-making on water resources management and planning. In South America (SA), such forecasts may help to increase awareness and anticipate extreme hydrometeorological events in large national and transnational basins (e.g., Siqueira *et al.*, 2020), to optimize energy production in reservoirs subject to flood control (e.g., Fan *et al.*, 2014; Schwanenberg *et al.*, 2015; Fan *et al.*, 2016a) and to define energy prices in the short-term market (Reis *et al.*, 2020). Over the past few years, several studies have investigated the potential use of medium-range ensembles to forecast streamflow in South American basins, both for flood early warning systems and reservoir operation (e.g., Fan *et al.*, 2014; Meller *et al.*, 2014; Raso *et al.*, 2014; Fan *et al.*, 2016a; Fan *et al.*, 2016c; Siqueira *et al.*, 2016a; Casagrande *et al.*, 2017; Tomasella *et al.*, 2019). The common approach of these studies is to force a hydrological model with meteorological predictions resulting from multiple realizations of (one or more) atmospheric models, producing probabilistic outcomes that represent the likelihood of discharge exceeding a certain decision threshold (e.g., for triggering actions or setting operation rules in reservoirs). More recently, ensemble hydrological forecasts have also been assessed at the level of full coverage of SA (Siqueira *et al.*, 2020), motivated by operational applications of continental to global scale forecasting systems around the world (e.g., Thielen *et al.*, 2009a; Alfieri *et al.*, 2013; Bennett *et al.*, 2014; Demargne *et al.*, 2014). Continental to global ensemble forecasting systems are becoming increasingly popular, aiming to deliver hydrological predictions at multiple timescales to support (trans)national forecasting capabilities (Emerton *et al.*, 2016; Lavers *et al.*, 2020).

Even with the use of ensembles, there will be uncertainties that are not accounted for in the issued hydrological forecasts. For instance, numerical weather models are often biased due to the incomplete representation of physical processes, and they can integrate only a finite sample of the possible states of the atmosphere (Buizza *et al.*, 2005; Hamill *et al.*, 2006). Hydrological models, in general, are subject to errors in input data, structure and parameterization (Renard *et al.*, 2010), while those focused on continental to global domains are less calibrated and typically have input data with coarser resolution and large uncertainties (Bierkens, 2015; Sperna Weiland *et al.*, 2015; Siqueira *et al.*, 2018). This causes hydrological ensemble forecasts to fail to provide reliable (i.e., probabilistically unbiased) estimates of the total uncertainty, thus hampering their use for rational decision-making.

Statistical postprocessing is therefore necessary to correct model outputs and improve skill and reliability of forecasts. It can be used either to model errors from individual sources separately before aggregating them into a single predictive distribution (Krzysztofowicz, 1999; Seo *et al.*, 2006; Demargne *et al.*, 2014), or to quantify the total uncertainty by modeling the residual errors of the whole forecasting chain in a lumped fashion (Montanari and Grossi, 2008; Todini, 2008; Reggiani *et al.*, 2009; Weerts *et al.*, 2011; Regonda *et al.*, 2013). In the latter case, hydrological forecasts and corresponding observations are used to fit a statistical model to estimate predictive uncertainty conditionally upon one or more predictors (Krzysztofowicz, 1999; Todini, 2008; Coccia and Todini, 2011; Li *et al.*, 2017), producing probability density functions (PDFs) that must be as sharp as possible, while subject to calibration (i.e., statistical consistency between forecast PDFs and observed values) (Raftery *et al.*, 2005; Gneiting *et al.*, 2007). Statistical postprocessors may also require homogeneous samples of streamflow forecasts collected over a long period of time, and these can be achieved by using retrospective meteorological forecasts of the same atmospheric model cycle (i.e., reforecasts) as inputs to a hydrological model (Hamill *et al.*, 2006; Harrigan *et al.*, 2020). Reforecasts not only increase the chance of including very high or low flow events (Van den Bergh and Roulin, 2016), but also allow for the separation of data into subsets to refine training according to seasonal (e.g., Hemri *et al.*, 2015) or event-based analogs (e.g., Hemri and Klein, 2017).

Initial efforts in statistical postprocessing of hydrological forecasts were made by Krzysztofowicz (1999), who proposed a Bayesian Forecasting System to estimate predictive uncertainty through a deterministic hydrological model. Since then, a plethora of methods have been developed or adapted for this purpose, such as those based on parametric or nonparametric regression (e.g., Weerts *et al.*, 2011; Regonda *et al.*, 2013), Bayesian formulations applied to ensembles (e.g., Todini, 2008; Reggiani *et al.*, 2009), kernel dressing (e.g., Pagano *et al.*, 2013; Verkade *et al.*, 2017), copula-based functions (e.g., Madadgar *et al.*, 2014; Klein *et al.*, 2016), autoregressive approaches (e.g., Bogner and Pappenberger, 2011) and combinations thereof (see Li *et al.*, 2017 for a detailed review). There is no single postprocessing method that outperforms all the others in any case (Herr and Krzysztofowicz, 2015; Li *et al.*, 2017). In addition to its effectiveness, the ideal postprocessing method should be parsimonious and efficient in order to be applied in real time (Seo *et al.*, 2006; Boucher *et al.*, 2015). The Ensemble Model Output Statistics (EMOS) (Gneiting *et al.*, 2005), for instance, is a simple linear regression-based method that has the advantage of using the raw ensemble spread as a predictor of the variance of predictive distributions. The ability to incorporate the ensemble

spread information is a general recommendation for hydrological uncertainty processors (Biondi and Todini, 2018). EMOS was initially designed for postprocessing weather quantities for which the PDF may be normally distributed, such as temperature and pressure (Gneiting *et al.*, 2005), but has undergone adaptations for variables with skewed distributions, like wind speed (e.g., Thorarinsdottir and Gneiting, 2010), precipitation (e.g., Baran and Nemoda, 2016) and streamflow (e.g., Hemri *et al.*, 2015; Hemri and Klein, 2017; Baran *et al.*, 2019; Zhong *et al.*, 2020). Moreover, it has been shown that EMOS has the potential to postprocess ensemble streamflow forecasts not only in locations where data is available, but also along the entire river network by making use of parameter regionalization approaches (Skøien *et al.*, 2016).

As with most statistical postprocessing methods, EMOS applies only for a single forecast quantity, location and lead time. This produces univariate PDFs that are marginally calibrated but do not preserve any spatial or temporal (between lead times) dependencies (Schefzik *et al.*, 2013). In turn, postprocessed predictive distributions should be also given in the form of streamflow ensemble traces to allow their use as inputs for decision support systems, including optimization models for reservoir management, waterway operations, and detailed hydrodynamic models for the prediction of flooded areas (Herr and Krzysztofowicz, 2010; Engeland and Steinsland, 2014; Hemri *et al.*, 2015; Bellier *et al.*, 2018). Realistic forecast trajectories, that is, time series that have correct autocorrelation and are unbiased (Bennett *et al.*, 2016), can be drawn from predictive distributions by using multivariate postprocessing methods that account for dependence structures, such as empirical methods that follow reordering notions like the Schaake Shuffle (Clark *et al.*, 2004) and Ensemble Copula Coupling (ECC) (Schefzik *et al.*, 2013). While the former uses observed data to model realistic spatial and temporal dependencies, ECC relies only on the rank structure of the raw ensemble and has been applied in hydrological postprocessing as a multivariate extension for both EMOS (e.g., Hemri *et al.*, 2015; Schefzik, 2017) and Bayesian Model Averaging (BMA) (e.g., Bellier *et al.*, 2018; Sharma *et al.*, 2019). The ECC approach is very attractive due to its simplicity and ability to handle high dimensionality problems (e.g., large number of locations, lead times), while adding no computational cost beyond the univariate postprocessing (Schefzik *et al.*, 2013).

Most studies regarding statistical postprocessing of (short- to) medium-range hydrological forecasts have been carried out in regions with relatively good availability of real-time hydrometeorological data. Applications typically are limited to a few or a dozen stations in small- to medium-sized basins (up to few thousands of km²) (e.g., Zalachori *et al.*, 2012; Pagano *et al.*, 2013; Roulin and Vannitsem, 2015), but some of them include medium to large

catchment areas (~10 000 km²) (e.g., Hemri *et al.*, 2015; Abaza *et al.*, 2017; Siddique and Mejia, 2017; Sharma *et al.*, 2018) or also very large basins (> ~100 000 km²), the latter usually in the Rhine River in Europe (e.g., Reggiani *et al.*, 2009; Hemri and Klein, 2017; Verkade *et al.*, 2017; Baran *et al.*, 2019). Although the use of hydrological postprocessors has also been reported in continental-scale forecasting systems as in the US (e.g., Demargne *et al.*, 2014), Europe (e.g., Bogner and Pappenberger, 2011; Thielen-del Pozo *et al.*, 2019) and Australia (e.g., Bennett *et al.*, 2014), a comprehensive evaluation of such techniques over a large number of gauge stations, drainage areas and hydrological regimes is not very common in literature. A few postprocessing studies consider these aspects, but are focused on longer timescales (e.g., Woldemeskel *et al.*, 2018), or are restricted to quantification of hydrological uncertainty only (Alizadeh *et al.*, 2020) or evaluation of forecasting skill improvement only (Zsoter *et al.*, 2016).

In SA, however, there is a general lack of studies addressing this topic, despite being a continent with great hydrological and climate diversity. One particular challenge is that countries typically have sparse real-time hydrometeorological networks, often with short time series (Fan *et al.*, 2014; Fan *et al.*, 2015b; Salio *et al.*, 2015; Tomasella *et al.*, 2019), which may place additional constraints on setting up and validating statistical postprocessors in hydrological forecasting systems. Integrating large-scale hydrological models with global precipitation data (e.g., satellite, reanalysis or multiple sources) may overcome some of these limitations because they allow for the production of spatially consistent, streamflow forecasts for the entire river network (Alfieri *et al.*, 2013; Siqueira *et al.*, 2020) and for multiple years in the past (Harrigan *et al.*, 2020), despite the well-recognized large uncertainties of such approaches (Wu *et al.*, 2014; Emerton *et al.*, 2016; Li *et al.*, 2016; Zsoter *et al.*, 2016; Alfieri *et al.*, 2020; Wu *et al.*, 2020). Thus, a question emerges as to what extent statistical postprocessing would enable the obtainment of skillful and informative streamflow forecasts at the continental-scale of SA, that is, forecasts that would translate into proper estimates of predictive uncertainty and also realistic ensemble traces to allow their use by multiple stakeholders. Addressing this question may help to foster probabilistic forecasting with state-of-the-art meteorological and hydrological modeling techniques in SA, where most of the existing systems still make use of pure statistical or deterministic forecasting models for predicting floods and planning the operation of hydropower plants (Fan *et al.*, 2016b; Tucci *et al.*, 2019). In this context, the objective of this study is to investigate how EMOS contributes to the skill and reliability of continental-scale, medium-range ensemble streamflow forecasts in SA, and to address the performance and limitations of ECC in producing forecast trajectories

from EMOS predictive distributions. The analysis is performed across hundreds of locations in SA using a continental hydrological model and reforecasts from the European Center for Medium-Range Weather Forecasting (ECMWF).

The next sections are organized as follows: Section 2 provides information on the study area and observed data. Section 3 describes the methods used to produce ensemble streamflow forecasts, general concepts about EMOS and ECC methods, configurations adopted for postprocessing and strategies of forecast verification. Results are presented in Section 4, while the discussion and main conclusions are offered in Sections 5 and 6, respectively.

4.2. **Study domain and streamflow data**

The study domain encompasses the South American continent. The territory hosts some of the largest basins in the world, such as the Amazon (~5.9×10^6 km²) and La Plata (~3.2×10^6 km²), most of them draining to the Atlantic Ocean as an effect of the N–S oriented Andes Cordillera in the western part of the continent. A particular focus is given to Brazil, which is the largest country by far (almost 50 % of the total land area) and in which the majority of surface water resources in SA are concentrated.

The same observed discharge data as used by Siqueira *et al.* (2018) was selected for this study. These data were collected from many hydrological centers in SA, and consist of daily observed discharge in gauge stations and naturalized flows at reservoir locations for drainage areas larger than 10 000 km² (with few exceptions). Naturalized flows are those that would be observed at hydropower dam locations in the absence of upstream reservoirs and water withdrawals, and are routinely provided by the Brazilian National Water Agency (ANA) and the Brazilian National Electric System Operator (ONS). A visual inspection was carried out to exclude gauge stations affected by reservoir regulation, and only those with more than 10 years of data (not necessarily consecutive) were selected (488 gauges in total). An overview of the political borders, major hydrographic features and spatial distribution of gauge stations is shown in Figure 4.1, while the drainage areas covered by the selected gauge stations are summarized in Table 4.1.

Table 4.1. Characteristics of the gauge stations used in this study.

Drainage area (km²)	Number of gauge stations	% of total
< 20 000	164	33.6 %
20 000 – 50 000	148	30.3 %
50 000 – 100 000	69	14.1 %
100 000 – 300 000	61	12.5 %
300 000 – 500 000	16	3.3 %
500 000 – 1 000 000	21	4.3 %
> 1 000 000	9	1.8 %

Data Providers: ANA (Brazil), DGA (Chile), GRDC (Global), IDEAM (Colombia), INA (Argentina), SENAMHI (Peru and Bolivia), ONS (Brazil), ORE-HyBAM (Amazon and Orinoco Basins).

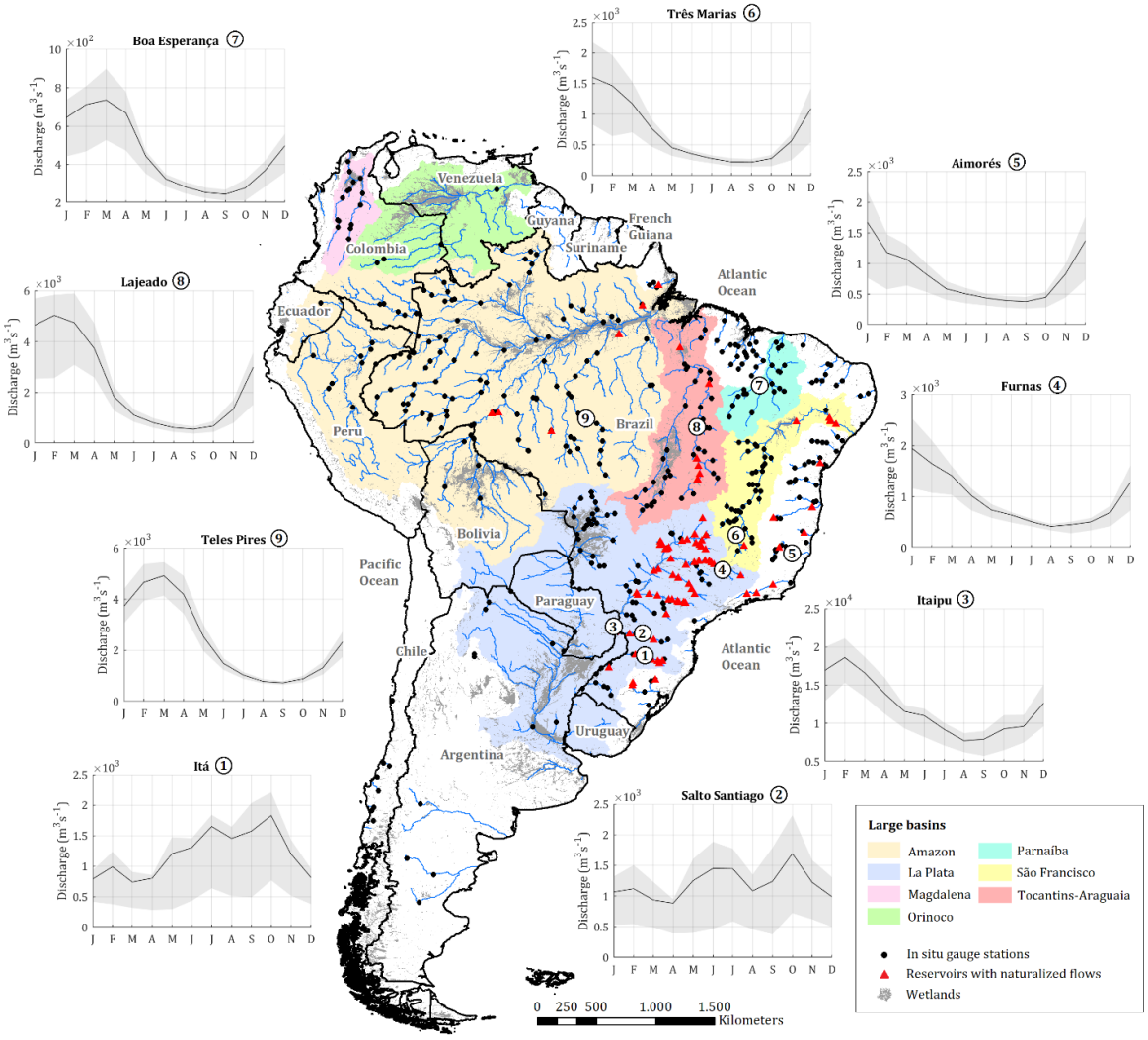

Figure 4.1. General overview of the political borders (thick black lines) and large-scale hydrographic features of SA. Main basins are highlighted in multiple colors, while rivers are shown only for drainage areas > 10 000 km² for visualization purposes. Major wetlands extracted from the GIEMS dataset (Fluet-Chouinard *et al.*, 2015) are also presented in gray. The graphs surrounding the SA domain show the seasonality of (natural) flows at selected reservoir locations, and the shaded gray area represents the interquartile range (25–75 %) of monthly climatological discharges based on naturalized flows.

4.3. Methods

4.3.1. Modeling framework

4.3.1.1. MGB hydrological model

MGB (acronym of *Modelo de Grandes Bacias*) is a conceptual, semi-distributed hydrological model with a history of development focused on South American water issues (Collischonn *et al.*, 2007a) and hydrological processes (Paiva *et al.*, 2013a). It has been applied in many studies related to large SA river basins, including works on the topic of ensemble hydrological forecasting (e.g., Paiva *et al.*, 2012a; Fan *et al.*, 2014; Meller *et al.*, 2014; Fan *et al.*, 2016a; Fan *et al.*, 2016c; Siqueira *et al.*, 2016a; Siqueira *et al.*, 2020). For this study, the continental-scale MGB model developed for the SA domain (hereafter the MGB–SA) was chosen due to its enhanced discharge accuracy compared to global models (Siqueira *et al.*, 2018), aimed at producing streamflow forecasts to meet societal needs.

Regarding the model structure, MGB–SA is discretized into 33 749 unit-catchments (with median, p_5 and p_{95} areas of 327, 85 and 1322 km², respectively), each one containing a river segment with a fixed length equal to 15 km. Unit-catchments are further subdivided into Hydrological Response Units (HRU), taking into account combinations of land use and soil type. Vertical hydrological processes (e.g., soil water budget, energy balance, evapotranspiration) are computed independently for each HRU at a daily time step. Surface, subsurface and groundwater runoff produced at the HRU level are propagated to the unit-catchment main channel using linear reservoirs, and flow routing through drainage networks is computed using an explicit inertial approximation of 1D Saint-Venant equations to deal with hydrodynamic effects associated with lowland rivers and floodplains. For the latter case, MGB–SA uses an adaptive time step (usually 3–4 minutes) to satisfy the Courant–Friedrichs–Lewy (CFL) condition. Snow processes are not represented in the current model structure since the MGB was primarily developed for tropical regions.

MGB–SA uses daily precipitation data from the 0.25º global Multi-Source Weighted Ensemble Precipitation (MSWEP) v1.1 (Beck *et al.*, 2017c) and CRU v.2 long-term monthly means of other climatic variables (temperature, relative humidity, radiation, wind speed and pressure) (New *et al.*, 2002) as meteorological forcing. Calibration was performed manually for the period from 1990 to 2010 using observed data from 604 in situ gauge stations and the model was validated with several remote sensing datasets. It was shown that MGB–SA was able to

reproduce daily discharges satisfactorily over several regions of South America (70 % [55 %] of the gauges with KGE [NSE] > 0.6). Figure 4.2 shows the spatial distribution of model performance (NSE) regarding the locations selected for this study, and further details about model datasets, calibration and performance can be found in Siqueira *et al.* (2018).

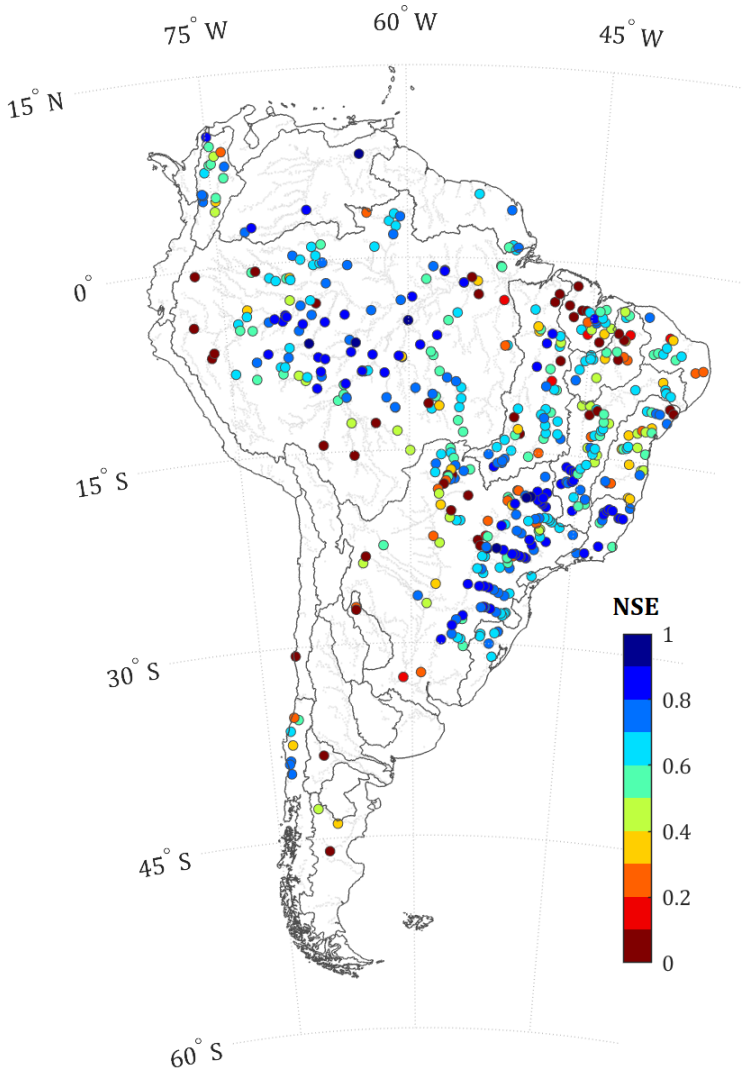

Figure 4.2. Spatial distribution of Nash–Sutcliffe Efficiency (NSE) across the model domain. Main hydrographic regions of SA are highlighted in dark grey.

4.3.1.2. Hydrological forecasting setup

To produce raw ensemble streamflow forecasts, we used precipitation reforecasts from the ECMWF Integrated Forecast System (IFS). The operational medium-range/monthly ensemble forecast component of IFS (ECMWF ENS) consists of a 51-member ensemble (control run + 50 perturbed forecasts) and horizontal resolutions of 16 km for lead times up to day 15 and 36 km onwards. Reforecasts are issued twice a week (on Mondays and Thursdays) for the same calendar day for the previous 20 years, using the same ECMWF ENS operational

model cycle but with a reduced ensemble of 11 members. For instance, the reforecasts issued on March 10, 2016 are 11-member hindcasts produced with initial conditions of March 10, 1996, March 10, 1997, and so forth, until March 10, 2015. ECMWF precipitation reforecasts issued between March 2016 and February 2017 were achieved with a grid of 0.2º × 0.2º resolution, 6 h accumulated intervals and lead times up to 15 days, although we used only the hindcasts from before January 2015 (i.e., 1996–2014) due to the availability of MSWEP v1.1 precipitation. Data were first aggregated from 6 h to daily values and then interpolated to the MGB–SA unit-catchment centroids using the inverse distance squared weighting method. To enable hydrological forecast initialization, a long-term MGB–SA run was performed spanning from January 1990 to December 2014 and model state variables (e.g., soil moisture, volume of water in rivers and floodplains) were saved for each day with available ECMWF reforecast data. As in Siqueira *et al.* (2020), the CRU v.2 monthly means of climatic variables (other than precipitation) used by MGB–SA to compute evapotranspiration in simulation mode were also used as model inputs in the forecast mode.

4.3.2. Postprocessing of raw hydrological ensemble forecasts

Statistical postprocessing was conducted in two stages. Initially, EMOS was applied to transform raw streamflow ensembles into univariate predictive distributions at each location, forecast day and lead time. Afterwards, the ECC method was used to extract forecast trajectories from the EMOS predictive distributions. The postprocessing techniques and their assumptions are detailed in the following sections.

4.3.2.1. Ensemble Model Output Statistics (EMOS)

EMOS is a univariate, nonhomogeneous regression-based method that was proposed by Gneiting *et al.* (2005). The original formulation assumes that predictive densities are Gaussian, and the raw ensemble is a predictor of the variance of forecast errors. For a given forecast variable, location and lead time, the parameters of the normal distribution $N(\mu, \sigma^2)$ are defined by the regression estimate and a linear function of the raw ensemble spread:

$$\mu = a + b_1 x_1 + b_2 x_2 + \cdots + b_M x_M \quad (4.1)$$

$$\sigma^2 = c + d s^2 \quad (4.2)$$

$$s^2 = \frac{1}{M} \sum_{m=1}^{M} (x_m - \bar{x})^2 \quad (4.3)$$

Where μ and σ^2 are, respectively, the mean and variance of the Gaussian predictive distribution; s^2 is the spread of the raw ensemble forecasts; x_m is the forecasted value for the ensemble member m; $\bar{x}$ is the ensemble mean of the raw hydrological forecasts; M is the number of ensemble members; a, b, c and d are parameters (note that b_m represents the weight of a given ensemble member for the regression estimate).

As the raw ensemble members derived by forcing the MGB–SA model with ECMWF reforecasts individually lack distinguishable physical characteristics, they are equally likely and belong to the same exchangeable group (Fraley *et al.*, 2010), that is, they can be assumed to have the same weight. Therefore, the notation of the normal predictive distribution can be written in terms of the ensemble mean according to:

$$N(\mu, \sigma^2) \sim N(a + b\bar{x}, c + ds^2) \tag{4.4}$$

Where $\bar{x}$ is the ensemble mean of the raw hydrological forecasts and N denotes the normal predictive distribution, with mean equal to $a + b\bar{x}$ and variance equal to $c + ds^2$.

The regression estimate of Eq. (4.1) corrects for bias in the ensemble mean, while the non-static variance term in Eq. (4.2) accounts for dispersion errors. According to Gneiting *et al.* (2005), the parameters a, b, c and d of Eq. (4.4) can be fitted through the minimization of the Continuous Ranked Probability Score (CRPS) (Hersbach, 2000), which is also one of the most used verification metrics to assess the performance of hydrological forecasts (Pappenberger *et al.*, 2015b).

While the assumption of Gaussianity applies well for meteorological variables such as temperature and sea-level pressure (Raftery *et al.*, 2005), it may not be applicable to river discharge since the latter typically follows a positive skewed distribution. Therefore, hydrological forecasts and corresponding observations must be transformed to make the distributions as nearly normal as possible. Examples of commonly used transformations in the topic of hydrological postprocessing are the normal quantile transform (e.g., Weerts *et al.*, 2011; Verkade *et al.*, 2017; Bellier *et al.*, 2018), log-sinh (e.g., Wang *et al.*, 2012b; Pagano *et al.*, 2013) and the Box–Cox power transformation (e.g., Duan *et al.*, 2007; Engeland and Steinsland, 2014; Madadgar and Moradkhani, 2014; Hemri *et al.*, 2015; Hemri and Klein, 2017; Qu *et al.*, 2017; Baran *et al.*, 2019). Here the Box–Cox approach was applied according to:

$$h(x) = \begin{cases} \frac{x^{\lambda}-1}{\lambda}, & \lambda \neq 0 \\ \log(x), & \lambda = 0 \end{cases} \quad (4.5)$$

Where *h(x)* is the Box–Cox transformed variable; *x* is the observed/forecasted streamflow; and λ is the Box–Cox parameter.

The optimal λ value for each location can be found through a grid search with a pre-defined range, selecting the value that minimizes the Kolmogorov–Smirnov statistics (e.g., Duan *et al.*, 2007; Hemri *et al.*, 2015), the Shapiro-Wilk test (e.g., Engeland and Steinsland, 2014) or the CRPS value (e.g., Hemri and Klein, 2017; Baran *et al.*, 2019). However, performing such a grid search in a continental domain that comprises a large number of locations is computationally expensive. Furthermore, calibrating λ is not always a good choice since it is very sensitive to medium and low flows (McInerney *et al.*, 2017). Woldemeskel *et al.* (2018) showed that a Box–Cox λ = 0.2 performed reasonably well for monthly and seasonal forecasts across many gauges and different climate regions in Australia. By applying different transformations on discharges using a large set of French catchments, Berthet *et al.* (2020) also suggested a Box–Cox λ = 0.2 as a robust choice for operational flood forecasting. Following the aforementioned studies, we set a fixed value of λ = 0.2 for applying the Box–Cox transformation on observed/forecasted values in all available locations.

EMOS models are fitted to the Box–Cox transformed streamflow forecasts, and the resulting quantiles are back-transformed to finally produce univariate predictive distributions. However, Hemri *et al.* (2015) state that EMOS sometimes produces positive probabilities for unrealistic high and low flows after back-transformation. Therefore, a variant of the truncated EMOS model presented by Thorarinsdottir and Gneiting (2010) was adopted following Hemri and Klein (2017) and Baran *et al.* (2019), in which both left and right tails of the Gaussian distribution are truncated at half of the minimum and two times the maximum observed flow during the hindcast period, respectively. The Cumulative Distribution Function (CDF) *F* of the double truncated Gaussian $N_{\alpha}^{\beta}(\mu, \sigma^2)$ is then described as follows:

$$F(y) = \begin{cases} 0, & \text{for } y \leq \alpha \\ \frac{\Phi\left(\frac{y-\mu}{\sigma}\right)-\Phi\left(\frac{\alpha-\mu}{\sigma}\right)}{\Phi\left(\frac{\beta-\mu}{\sigma}\right)-\Phi\left(\frac{\alpha-\mu}{\sigma}\right)}, & \text{for } \alpha < y < \beta \\ 1, & \text{for } y \geq \beta \end{cases} \quad (4.6)$$

Where *y* denotes the variable to be forecasted, Φ denotes the CDF of the standard normal distribution, α and β are truncation limits corresponding to the half of minimum and two times the maximum observed flow between March 1996 and December 2014, respectively. For simplicity, the double truncated EMOS is referred to hereafter as EMOS.

4.3.2.2. Ensemble Copula Coupling (ECC)

EMOS estimates a continuous predictive distribution for a given forecast variable, lead time and location. Therefore, a multivariate postprocessing method must be also applied in order to produce coherent forecast trajectories. Here we used the ECC technique (Schefzik *et al.*, 2013; Schefzik, 2017) because of its simplicity and low computational burden, which makes it attractive for modeling multivariate dependencies in such a large continental domain. In a nutshell, the ECC inherits the rank order structure from the raw ensemble, with the implicit assumption that the latter is able to represent the correlations between forecasted variables, lead times and locations appropriately.

As this study deals only with river discharge as a forecast quantity, let $k = \{j, l\}$ be a multi-index that summarizes a forecast lead time $j \in \{1, \dots, J\}$ and a location $l \in \{1, \dots, L\}$, and let K be the dimension of the vector consisting of all lead times and locations, i.e., $K = J \times L$. For a given forecast date, the set of K raw ensembles with M members $x_1, \dots, x_M$ are defined as a dependence template $z = \{(x_1^1, \dots, x_M^1), \dots, (x_1^K, \dots, x_M^K)\}$, where the subscript indices $1 \dots M$ are unique member labels that do not change across the J lead times.

Since each univariate EMOS predictive density can be described by a cumulative distribution function (CDF) F_k, the multivariate problem is solved by drawing samples from these distributions and reordering them according to the rank order of the dependence template z^k. By definition, the number of samples derived from each univariate quantity should be equal to the number of elements of z^k, which implies that the multivariate postprocessed ensemble will have the same size M of the raw hydrological ensemble. Schefzik *et al.* (2013) present three variants of the ECC method for the sampling-reordering procedure, namely ECC-R (random sampling), ECC-Q (equally spaced quantiles) and ECC-T (transformation). According to Hemri *et al.* (2015), the T-variant is the most suitable approach since it reduces jumps in the trajectories of predicted discharges, which is particularly important for the case of strongly autocorrelated river flows.

For the ECC-T, a parametric, continuous CDF S_k is fitted to the dependence template z^k and the postprocessed ensemble $\tilde{x}^k = (\tilde{x}_1^k, \ldots, \tilde{x}_M^k)$ is derived by determining to which quantiles of S_k the raw ensemble members correspond before mapping them to the quantiles of EMOS CDF F_k. This is performed after the template z^k is Box–Cox transformed, as the S_k is assumed to be normally distributed (Hemri *et al.*, 2015; Hemri and Klein, 2017; Bellier *et al.*, 2018). The CDF S_k is fitted using maximum-likelihood estimation assuming a Gaussian distribution. Note that the rank dependence of the postprocessed ensemble is automatically preserved according to the dependence template *z*, that is, the reordering step occurs naturally through the quantile mapping procedure of ECC-T (Schefzik, 2017). The postprocessing of hydrological forecasts is summarized in the flowchart presented in Figure 4.3.

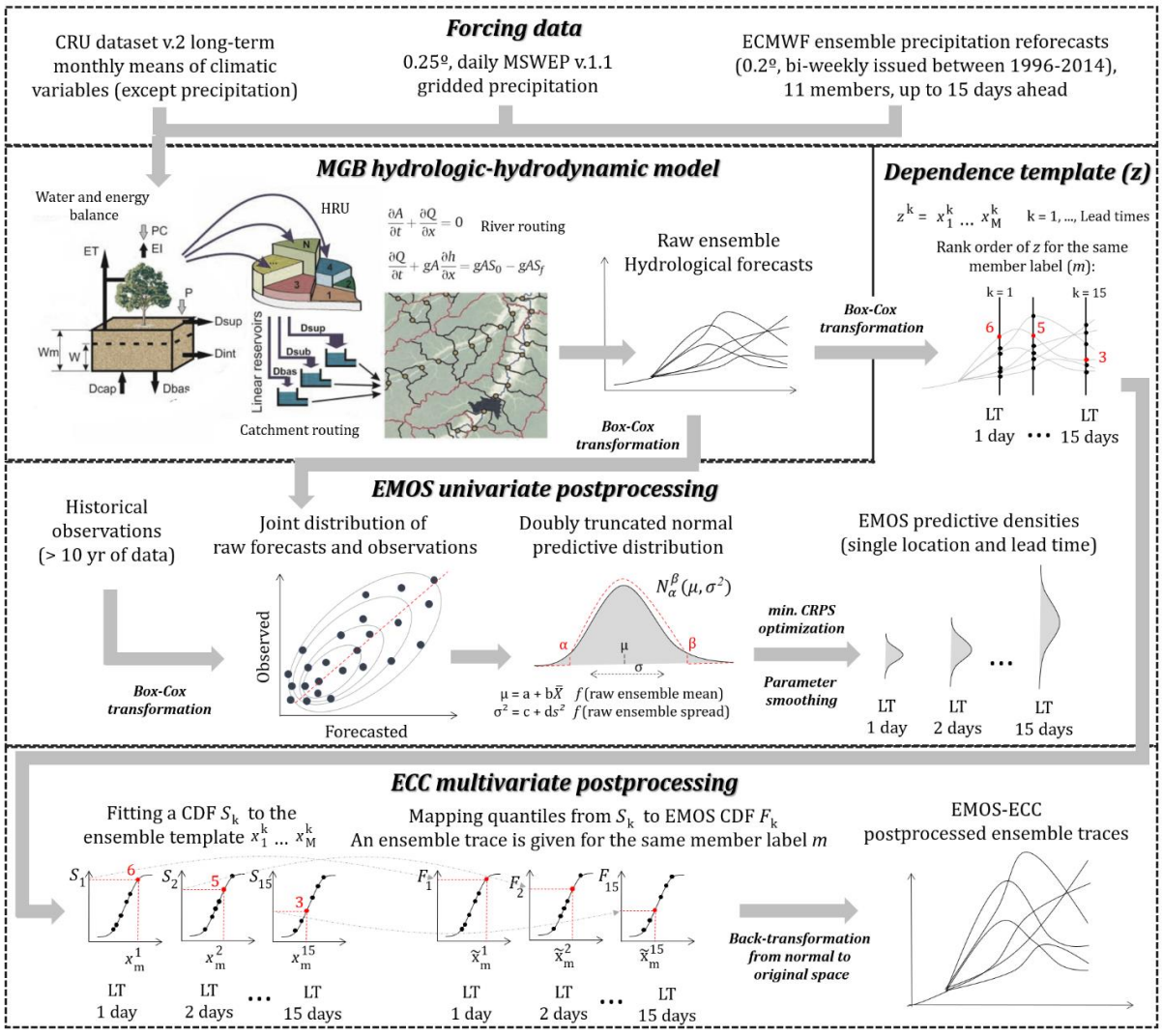

Figure 4.3. Schematic diagram of producing and postprocessing raw hydrological ensemble forecasts.

In cases where the raw ensemble spread is too low, an additional correction is made to avoid unrealistically extreme quantiles by setting the variance of S_k to (Hemri *et al.*, 2015):

$$\sigma_k^2 = \max\left\{\sigma_k^2, \left[h\left((1+d)\bar{x}^k\right) - h\left((1-d)\bar{x}^k\right)\right]^2\right\} \quad (4.7)$$

Where σ_k^2 is the variance of S_k, h denotes de Box–Cox transformation, $\bar{x}^k$ is the raw ensemble mean, k is the index related to a given location and lead time, and d is a parameter to be tuned. While other authors have adopted values of 0.001 (Hemri *et al.*, 2015) and 0.0001 (Bellier *et al.*, 2018) for the d parameter, here d was set to 0.005 based on previous experiences and a sensitivity analysis was performed, since it affects the forecasted ensemble traces and their calibration (supplementary material S.4.1, at the end of this chapter).

4.3.3. Experiment setup

4.3.3.1. Training EMOS models and deriving ensemble forecast trajectories

As most of the rivers of South America have a well-defined seasonal pattern, the EMOS models were trained for each location and lead time using subsets of data according to the season (DJF, MAM, JJA and SON). A leave-one-year-out cross-validation was applied in a similar way to other postprocessing studies (e.g., Fundel and Zappa, 2011; Hemri *et al.*, 2015; Verkade *et al.*, 2017) in order to maximize the verification period and to carry out a robust statistical analysis. For instance, parameters of the EMOS model that correspond to DJF of validation year 2010 were fitted using training data from DJF for all years except the target one (i.e., 2010). In addition, EMOS parameters across lead times were further smoothed using a cubic spline interpolation. This was necessary to reduce undesirable jumps in the quantiles of the marginal predictive distributions between individual lead times (Hemri *et al.*, 2015; Bellier *et al.*, 2018) and was performed before applying the ECC-T to produce forecast trajectories. The same procedure was applied for all seasons and years spanning from March 1996 to December 2014. Finally, postprocessed forecasts resulting from the validation years were merged together in order to cover all the reforecast period. For training the EMOS models, applying parameter smoothing between lead times and deriving forecast trajectories with ECC-T, we used the R software (R Core Team, 2013) with the package called *hydemos* (Klein and Hemri, 2017). Note that data assimilation or autoregressive models were not applied to adjust the initial forecast values prior to the postprocessing step. The objective was to reproduce the simplest operational settings in which real-time observed flows are not readily available to the continental-scale forecasting system.

4.3.3.2. Verification strategy

The general aim of postprocessing is to provide forecasts that are as sharp as possible subject to calibration (Raftery *et al.*, 2005; Gneiting *et al.*, 2007). It may also preserve the predictive skill of raw forecasts (Li *et al.*, 2017) and allow the generation of coherent ensemble traces (Herr and Krzysztofowicz, 2010; Schefzik *et al.*, 2013; Bellier *et al.*, 2018). To evaluate the postprocessing performance, a set of metrics in (geographic) space were analyzed for different lead times and flow conditions, and a visual inspection of forecast hydrographs and graphical measures of forecast attributes was carried out at specific locations. To allow for a direct comparison between EMOS distributions and ensemble streamflow forecasts (i.e., raw and EMOS-ECC-T), 11 members for each forecast day were derived by drawing *M* equally spaced samples from the univariate EMOS predictive CDFs $\left[F_k^{-1}\left(\frac{1}{M+1}\right), F_k^{-1}\left(\frac{2}{M+1}\right), \ldots, F_k^{-1}\left(\frac{M}{M+1}\right)\right]$.

The evaluation of forecast skill is generally performed against benchmarks, that is, alternative forecasts that use simpler strategies of predicting flows, such as climatology or persistence of the last observed discharge. The former is more appropriate for longer lead times since the forecast signal tends to be controlled by the seasonality of flows, whereas the latter is recommended for shorter lead times where the forecast signal is controlled by serial correlation of flows (Pappenberger *et al.*, 2015b; Harrigan *et al.*, 2020). As the study area encompasses multiple catchment characteristics and flow regimes, and because forecast lead times are considered up to 15 days ahead, both climatology and persistence are used here as benchmarks. Discharge climatology was calculated by resampling observed data within the reforecast period (for the target calendar day) and using the leave-one-year-out procedure to exclude data from climatology that correspond to the evaluated year. Persistence was computed by simply assuming the most recent observation available (at the time of issuing a forecast) for all lead times.

Predictive skill can be quantified using scoring rules such as the CRPS (Hersbach, 2000). It summarizes calibration and sharpness of a probabilistic forecast into a single overall score, expressed as a mean of all individual CRPS values:

$$\overline{CRPS} = \frac{1}{N}\int_{-\infty}^{\infty}[F(y) - F_0(y)]^2\,dy \tag{4.8}$$

$$F_0(y) = \begin{cases} 0, & \text{y} \leq \text{observed value} \\ 1, & \text{y} > \text{observed value} \end{cases} \quad (4.9)$$

Where *F(y)* is the CDF of the ensemble forecast *y*; and $F_0(y)$ is the Heaviside step function that equals one when forecast values are greater than the observed value and zero otherwise. $\overline{CRPS}$ is then converted into an overall skill score according to CRPSS = $1 - \frac{\overline{CRPS}_{forecast}}{\overline{CRPS}_{reference}}$, using both daily climatology and persistence of the last observed discharge as reference. For the specific case of persistence (i.e., a deterministic forecast), $\overline{CRPS}$ reduces to the mean absolute error. Maximum skill is achieved when CRPSS = 1.

Forecast calibration (or reliability) is analyzed by means of the Rank Histogram (Anderson, 1996). It is closely related to the Probability Integral Transform (PIT) histogram used to assess the calibration of predictive distributions (Gneiting *et al.*, 2007), with the difference that it applies to the discrete case of ensembles. Rank histograms describe the proportion of observations falling in a given forecast probability interval, each one defined between two consecutive ensemble members. A horizontally flat histogram indicates a well-calibrated ensemble. U-shaped histograms indicate underdispersion, whereas U-inverted ones represent overdispersion. Moreover, histograms with an L-shaped or L-inverted pattern are indicative of positive or negative bias, respectively. The information provided by the rank histogram can be also summarized by the Reliability Index (RI) (Delle Monache *et al.*, 2006), which expresses the deviation from flatness:

$$RI = \sum_{i=1}^{M+1} \left| \xi_i - \frac{1}{M+1} \right| \quad (4.10)$$

Where ξ_i is the frequency of observations in bin *i* and *M* is the number of ensemble members. An RI = 0 would result in perfect calibration.

To provide further details on forecast calibration, we computed the proportion of observations falling within the nominal coverage of the raw ensemble, i.e., the interval between the upper and lower member, which is given by the $\left(\frac{M-1}{M+1}\right) * 100\%$ centered prediction intervals (Baran *et al.*, 2019). For an 11-member ensemble, the nominal coverage refers to the 83.3 % centered prediction intervals that should be matched by the actual ensemble coverage (denoted here by the Coverage Rate, CR):

$$\mathrm{CR} = \frac{C}{NC+C} \tag{4.11}$$

Where *C* is the number of observations falling inside the ensemble range; and *NC* is the number of observations not captured by the ensemble.

Sharpness is a property of the forecasts only and refers to the width of predictive distributions (Gneiting *et al.*, 2007). Sharper forecasts have more concentrated prediction intervals (lower spread in the case of ensembles), and thus greater ability to forecast extreme probabilities near 0% and 100%. Sharpness is given here in terms of an average spread computed as the square root of mean variance (Fortin *et al.*, 2014; Roulin and Vannitsem, 2015):

$$S = \sqrt{\frac{1}{N}\sum_{i=1}^{N}\left[\frac{\sum_{m=1}^{M}\left(x_{m,i}-\bar{x}_i\right)^2}{M}\right]} \tag{4.12}$$

Where *N* is the number of forecasts issued, *M* is the number of ensemble members, $x_{m,i}$ is the streamflow for the ensemble member *m* and forecast day *i*, and $\bar{x}_i$ is the ensemble mean for forecast day *i*. Similarly to CRPS, sharpness can assume the form of a skill score when computed against daily climatology: $\mathrm{SS} = 1 - \frac{S_{forecast}}{S_{climatology}}$. Maximum sharpness skill occurs for an SS = 1.

To investigate whether the individual ensemble traces from EMOS-ECC-T are able to represent the serial dependence of hydrological forecasts, i.e., produce trajectories that are realistic across lead times, the Auto Correlation Function (ACF) of EMOS-ECC-T was compared to the ACF of raw ensemble, as suggested by Bellier *et al.* (2018). Firstly, the forecast values were transformed into series of lag-one differences to remove seasonality and trends. The resulting multiple series samples (*M* ensemble traces × *N* forecast dates) were concatenated to compute ACF but ensuring that pairs from different samples were excluded from the calculation. Moreover, to summarize the ACF into a single score, the area between ACF curves ($\mathrm{ACF}_{\mathrm{Area}}$) was also calculated using a trapezium approach, where an area = 0 indicates perfect match. Similarly to sharpness, the ACF is a property of the forecasts only.

4.4. Results

4.4.1. Forecast hydrographs and EMOS distributions

We start the analysis of hydrological forecasts with a closer look at the corresponding hydrographs and postprocessed predictive distributions. Examples of ensemble streamflow forecasts with lead times up to 15 days ahead produced by the MGB–SA forced with ECMWF reforecasts in selected locations (hydropower reservoirs of the Brazilian National Interconnected System, SIN) and for a particular date are presented in Figure 4.4. Postprocessing results are shown in the form of EMOS probabilities for the centered prediction intervals of 90 % (5–95 %) and 50 % (25–75 %), and also in the form of ensemble traces derived from the predictive distributions of EMOS after applying the ECC-T method. It is worth mentioning that the EMOS quantiles that correspond to the above centered prediction intervals are used here only for plotting purposes, which differ from the 11 equally-spaced quantiles of EMOS that were selected for verification in the later sections. Observed flows for the locations in Figure 4.4 refer to naturalized river flows, while the selected forecast dates represent cases of flood events in which discharges are ≥ 2-year return period flows. Additional graphs of extended forecast time series at these locations are available in the supplementary material S.4.2.

As noted, hydrological behavior varies greatly between locations. Some of these show a rapid rise in the hydrograph (e.g., Itá at Uruguay River, Figure 4.4-1) while others exhibit a slower variation of flows (e.g., Teles Pires at Teles Pires River, Figure 4.4-9). The raw ensemble is able to predict the occurrence of high flows in most cases but tends to partially capture the observed discharges. When looking to the postprocessed forecasts, observations usually fall within the EMOS centered prediction intervals of 5–95 %. Because streamflow forecasts are issued without further correction by data assimilation or autoregressive models, predicted discharges that are close to the forecast initialization day are often displaced in relation to the observed values, notably in Três Marias (São Francisco River, Figure 4.4-6) and Lajeado (Tocantins River, Figure 4.4-8). As a result, the predictive uncertainty estimated by EMOS postprocessing can be relatively large even at the initial lead times. The forecast trajectories obtained with the ECC-T maintain the rank order structure of the raw ensemble, but generally increase the ensemble spread in relation to the latter. In some cases, such as Itá, Salto Santiago (Iguazu River, Figure 4.4-2), Itaipu (Paraná River, Figure 4.4-3), Lajeado and Aimorés (Doce River, Figure 4.4-5), there is a good agreement between the postprocessed forecast trajectories

and the ones from the raw ensemble, but in other locations (e.g., Furnas at Grande River (Figure 4.4-4), Boa Esperança at Parnaíba River (Figure 4.4-7), and Teles Pires) the ensemble traces tend to demonstrate a more distinct behavior.

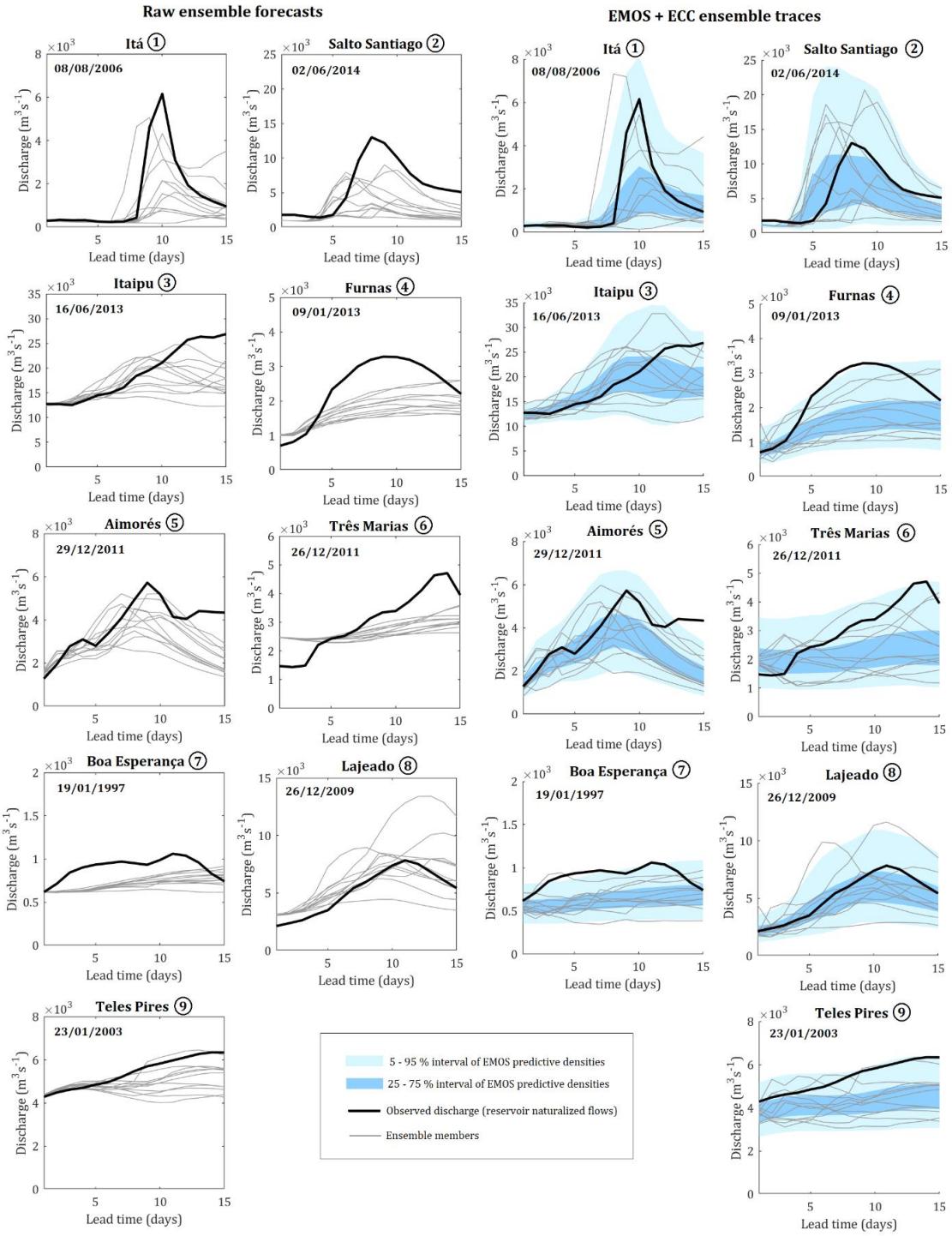

Figure 4.4. Examples of streamflow forecasts issued for selected locations and selected dates in SA (reservoirs of the Brazilian SIN). Forecasts are presented for the raw ensemble (left) and EMOS predictive distributions together with postprocessed ensemble traces derived using the ECC-T (right). Observed discharges and ensemble members are shown in black (thick) and gray (thin) lines, whereas the centered 50 % and 90 % EMOS prediction intervals are presented in dark and light blue colors, respectively. Numbers within circles refer to locations previously shown in Figure 4.1.

4.4.2. Spatial assessment of forecast skill: overall quality and sharpness

In order to assess the forecast skill, the raw ensemble, EMOS and EMOS-ECC-T were compared with the reference forecasts in terms of CRPSS and sharpness skill (SS), considering a lead time of seven days. Figure 4.5 (at the top) shows the results of CRPSS of hydrological forecasts computed against the persistence (pers) of the last observed discharge. The $CRPSS_{pers}$ of raw forecasts has a clear heterogeneous pattern, where skillful predictions are more concentrated in the eastern and southeastern SA. Negative $CRPSS_{pers}$ values are observed mainly in central and western regions of SA, notably in large basins such as the Amazon, Orinoco, Tocantins-Araguaia and Paraguay (west of La Plata), and also along the São Francisco Basin in eastern SA. This indicates that the overall quality of the raw ensemble is lower than the benchmark at these locations, with respect to streamflow forecasts issued for one week ahead. EMOS postprocessing improves the overall skill in relation to the raw ensemble and demonstrates a positive $CRPSS_{pers}$ in eastern SA as well as in most western regions. In addition, the spatial pattern of the overall performance of postprocessed forecasts in SA does not change after the derivation of ensemble traces with the ECC-T method.

When the overall skill is computed against the daily streamflow climatology (Figure 4.5, bottom), the geographical distribution of $CRPSS_{cli}$ values for raw and postprocessed forecasts resembles that found in the case with persistence as the reference. However, clear differences between $EMOS_{cli}$ and $EMOS_{pers}$ are notable in the main stem of large rivers like the Amazon and Paraguay, as well as in the lower Magdalena Basin and Araguaia River (west of the Tocantins-Araguaia Basin).

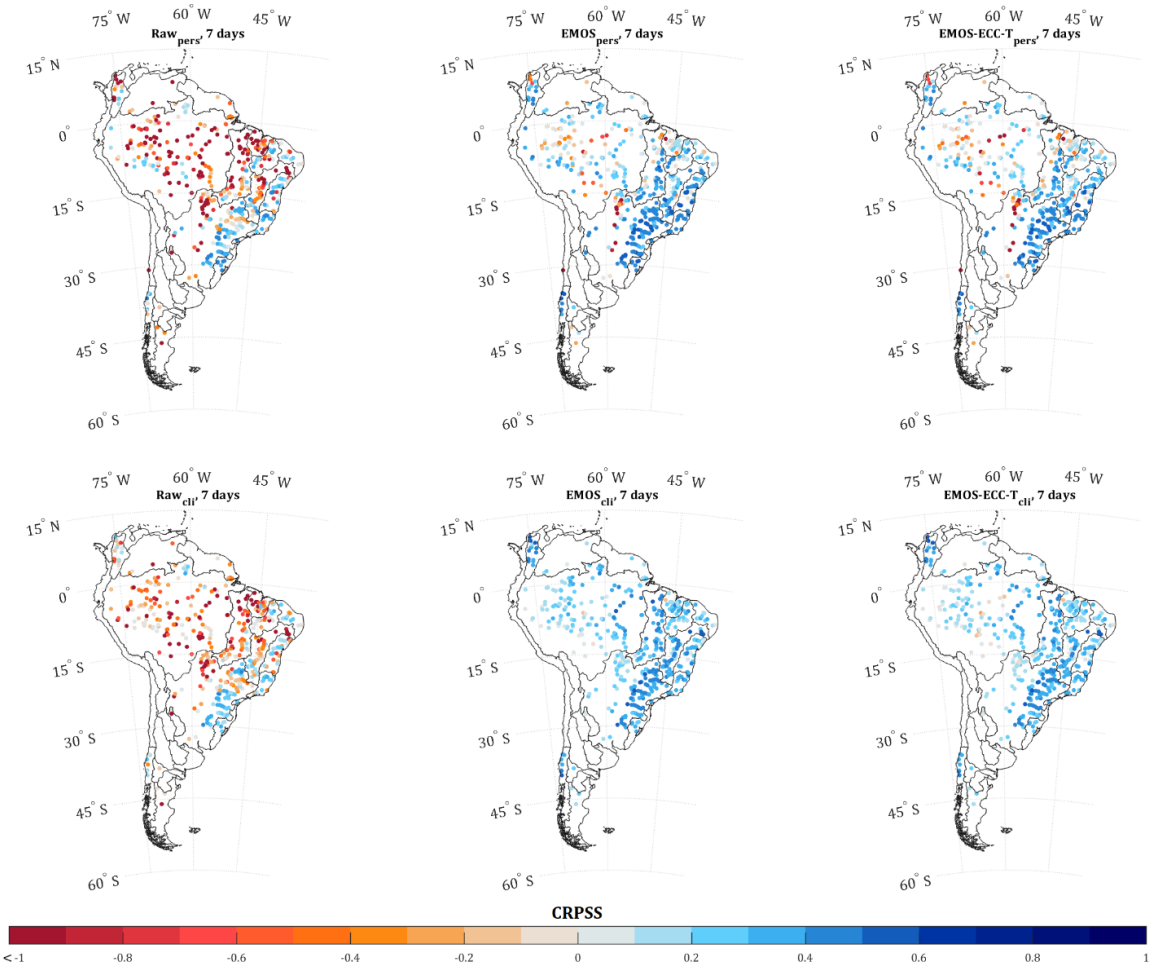

Figure 4.5. CRPSS maps of ensemble streamflow forecasts for a lead time of seven days, using persistency (pers, top) and daily climatology (cli, bottom) as benchmarks. Results are shown for the raw ensemble (left), EMOS univariate postprocessing (center) and EMOS-ECC-T multivariate postprocessing (right).

Figure 4.6 shows the sharpness skill (SS) values spatially distributed over the gauge stations in SA. Unlike CRPSS, forecasts are compared only with daily climatology since a deterministic benchmark such as the persistence does not provide uncertainty information. As expected, the raw ensemble exhibits the highest sharpness (SS generally > 0.6). EMOS postprocessing generally degrades the skill of the raw ensemble, but it still demonstrates greater sharpness than daily climatology. This reduction in skill tends to be larger in some specific regions such as the Amazon, northern SA and western La Plata Basin (e.g., the Paraguay River). Furthermore, the application of ECC-T slightly reduces the sharpness skill of EMOS in most of the gauges, although SS values are higher in locations where the flood rise is very slow (e.g., the main stem of the Amazon).

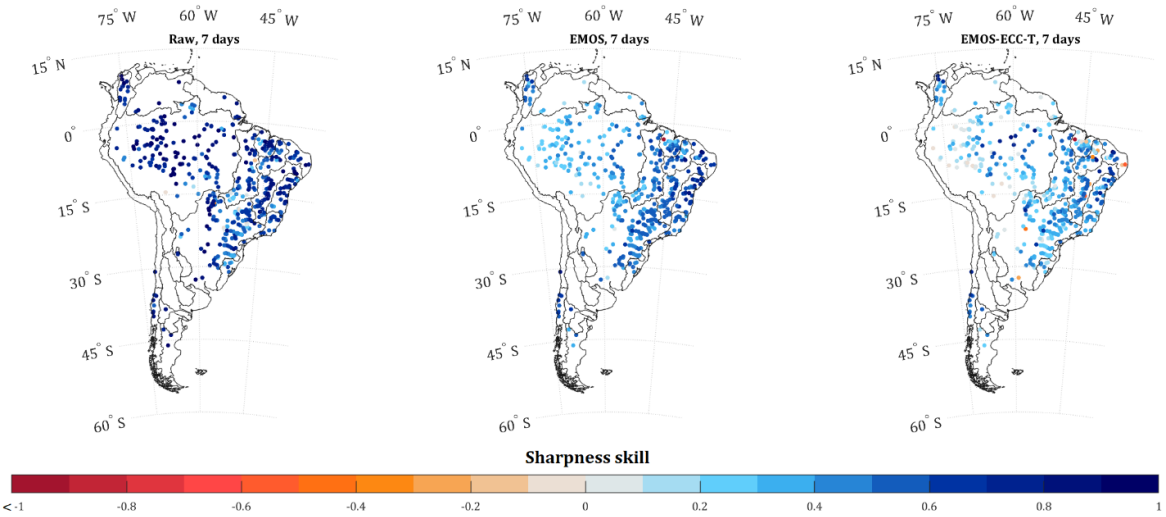

Figure 4.6. Sharpness skill of ensemble streamflow forecasts for a lead time of seven days, computed against daily climatology. Results are shown for the raw ensemble (left), EMOS univariate postprocessing (center) and EMOS-ECC-T multivariate postprocessing (right).

4.4.3. Spatial assessment of forecast calibration

To evaluate forecast calibration, first the rank histograms were plotted for the selected locations considering a lead time of seven days (Figure 4.7). Results obtained for the raw ensemble, EMOS and EMOS-ECC-T are separated by the colored vertical bars in the histograms. Each ensemble interval is represented by a rank, with the tails of the histograms representing the observations lying below the lower (or above the upper) member of the ensemble. RI values that summarize the calibration performance are also shown for each rank histogram. The diagrams clearly show that the frequency of observations at intermediate probabilities is very low in the case of raw ensemble forecasts, that is, the latter are markedly unreliable (with high RI values, ranging between 0.58 and 1.78). In specific cases located in southern Brazil, such as in the Itá and Salto Santiago reservoirs, the rank histograms indicate that raw forecasts are underspread (U-shaped histograms), while in the other analyzed locations there is a tendency of the observations to fall below the lower limit of the ensemble (i.e., a signal of large conditional positive bias, given by the L-shaped histograms). On the other hand, EMOS postprocessing fosters a better calibration of the forecast ensemble, producing rank histograms that are approximately flat (with low values of RI, varying between 0.07 and 0.2) with observed frequencies remarkably close to the perfect reliability line [1/(M+1)] %. Except for Itá and Salto Santiago, the EMOS-ECC-T reduces the improvement gained in calibration in comparison with EMOS, which is highlighted by the higher values of RI (between 0.11 and 0.51).

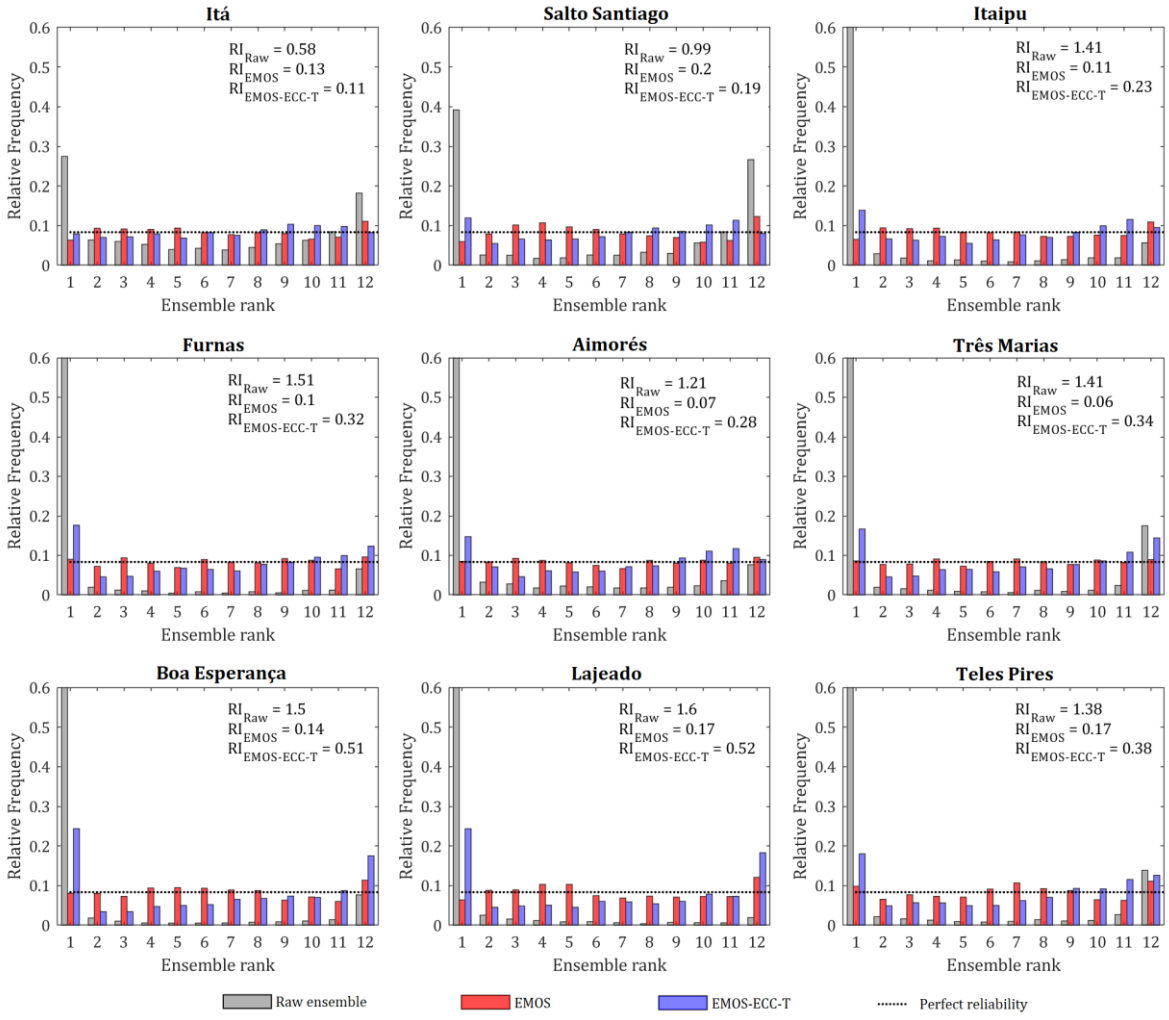

Figure 4.7. Rank histograms for ensemble streamflow forecasts at selected locations and for a lead time of seven days. Raw, EMOS and EMOS-ECC-T forecasts are represented in gray, red and blue, respectively. The black dotted line represents the relative frequency for which perfect reliability is achieved.

Figure 4.8 and Figure 4.9 show, respectively, the values of RI and CR plotted over SA for a lead time of seven days. For the raw ensemble, most of RI values are very large (usually > 1), which indicates that there is little or no agreement between the forecasted probabilities and relative observed frequencies of river discharges. The lack of calibration is reflected in the underestimation of CR values, with the ensemble coverage usually capturing less than 30 % of observations in the verification period. This means that observed values are often lying outside the limits of the ensemble. On the other hand, the statistical consistency of the EMOS postprocessed forecasts previously identified in the rank histograms of Figure 4.7 seems to occur in most of the gauge stations (RI values closer to 0, globally), with the exception of a few locations in Northeast Brazil characterized by intermittent flows. The frequency of observations falling between the upper and lower limits of the ensemble derived from univariate EMOS is also very close to the expected value of 83.3 %. For the case of EMOS-ECC-T, the improvement in forecast calibration is reduced in several gauges when compared with the univariate EMOS

postprocessing. In particular, calibration with EMOS-ECC-T is notably lower in the São Francisco, Tocantins–Araguaia, Parnaíba and northern La Plata (upper Paraguay) Basins (RI between 0.5–1.0 and CR ranging from 50–60 %), and exhibits a poor performance in the main stem of the Amazon (RI > 1.0 and CR < 30 %).

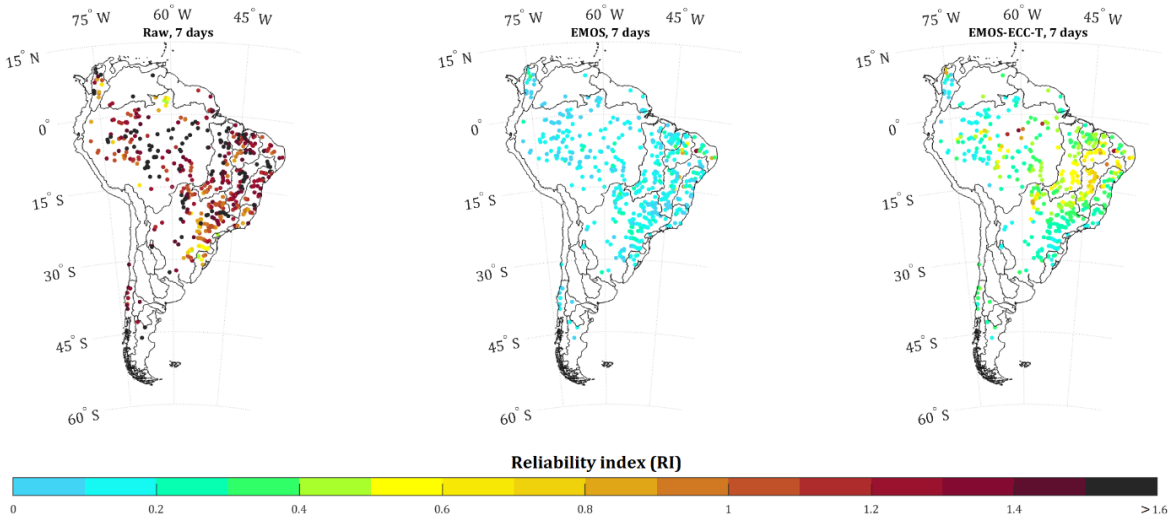

Figure 4.8. RI maps of ensemble streamflow forecasts for a lead time of seven days. Results are shown for the raw ensemble (left), EMOS univariate postprocessing (center) and EMOS-ECC-T multivariate postprocessing (right).

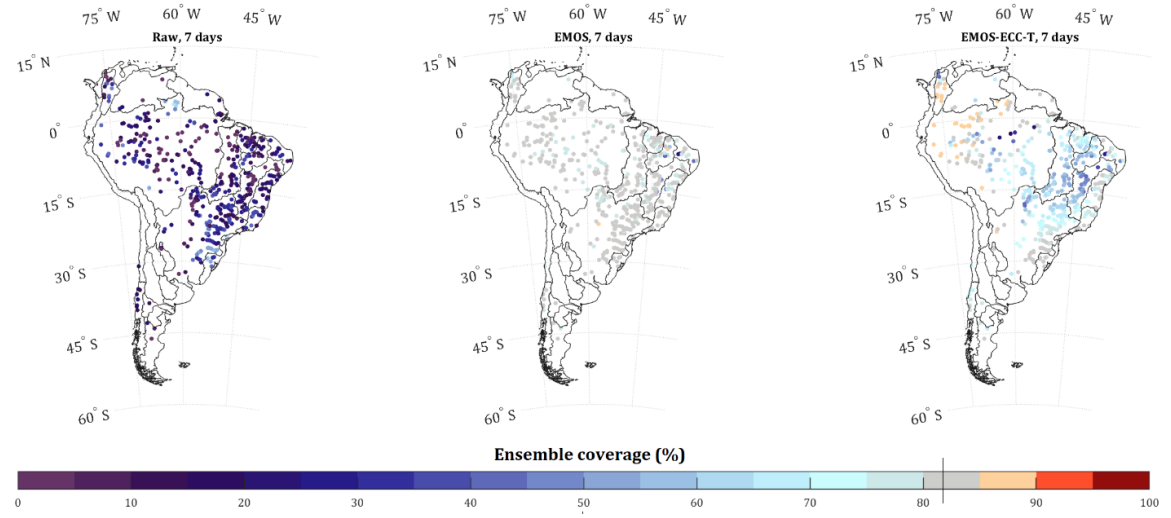

Figure 4.9. Coverage rate (CR) of ensemble streamflow forecasts for a lead time of seven days. Results are shown for the raw ensemble (left), EMOS univariate postprocessing (center) and EMOS-ECC-T multivariate postprocessing (right). The vertical black line in the color bar indicates the coverage of the nominal 83.3 % centered prediction interval (for an ensemble with 11 members).

4.4.4. Forecast performance according to lead time

Figure 4.10 shows the performance of the streamflow forecasts as a function of lead time. Results were plotted in a summarized manner and refer to the median of verifying gauge stations throughout SA. While the raw ensemble shows CRPSS values below the no skill line

over the entire forecast horizon (against climatology) and exhibits overall skill relative to the persistence benchmark only after 10 days ahead, postprocessed forecasts anticipate the latter by approximately six days, also showing positive CRPSS values in relation to climatology (ranging between 0.2 and 0.4). In contrast, the median SS is the highest for the raw ensemble at the 1-day lead time (SS close to 1), but the differences of SS between raw and postprocessed forecasts gradually reduce in the subsequent lead times. Although EMOS degrades the SS compared to the raw ensemble in more than 50 % of the gauges, it outperforms the skill of daily climatology along the entire forecast horizon while providing a well-calibrated ensemble. For example, low values of RI that were identified for one week ahead over multiple gauges in SA (Figure 4.8) are also observed in the other lead times with almost no change in the median (relatively constant RI < 0.2), whereas the corresponding CR is kept systematically close to the nominal coverage of 83.3 %. The application of multivariate ECC-T on EMOS has a small effect on the overall skill measured by the CRPSS (both for climatology and persistence) compared with the univariate postprocessing, but for calibration and sharpness the differences are more apparent and vary with lead time. Performances of EMOS-ECC-T closer to those obtained from univariate EMOS are achieved only more than 10 days in advance, but at the cost of a larger ensemble spread as explained by the lower median SS.

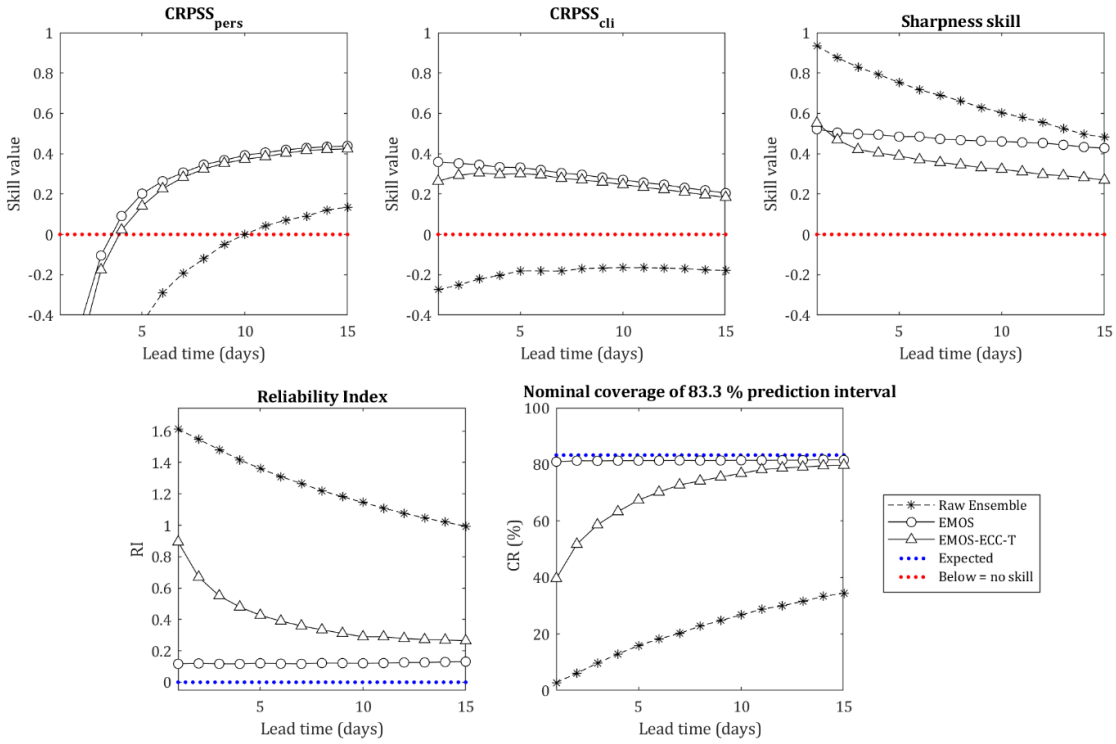

Figure 4.10. Performance metrics of ensemble streamflow forecasts as a function of lead time. Results correspond to the median values of all gauge stations. Values below the red dotted line indicate no skill in relation to persistency (pers) or climatology (cli), whereas the blue dotted line indicates the expected value for RI and CR.

4.4.5. Forecast performance according to flow conditions

Performance metrics for different flow categories at the lead time of seven days are given in the box plots of Figure 4.11. Results are shown for the entire verification period and also for subsets of the verification data conditioned on forecasts, both for low to moderate (< Q_{50}) and high forecasted discharges (> Q_{90} of non-exceedance flows). The analysis was conditioned on forecasts using the ensemble mean as the stratification criterion, that is, the subsets of verification data are given for the cases in which the ensemble mean exceeds or is below its forecast climatological probabilities of 90 % (Q_{90}) and 50 % (Q_{50}), respectively. These climatological probabilities of the ensemble mean were computed using all available forecast dates, and the evaluation was performed separately for each lead time. The forecast-based data stratification is recommended over the observed conditioning since the latter can lead to nonflat histograms for calibrated forecasts (Bellier *et al.*, 2017b).

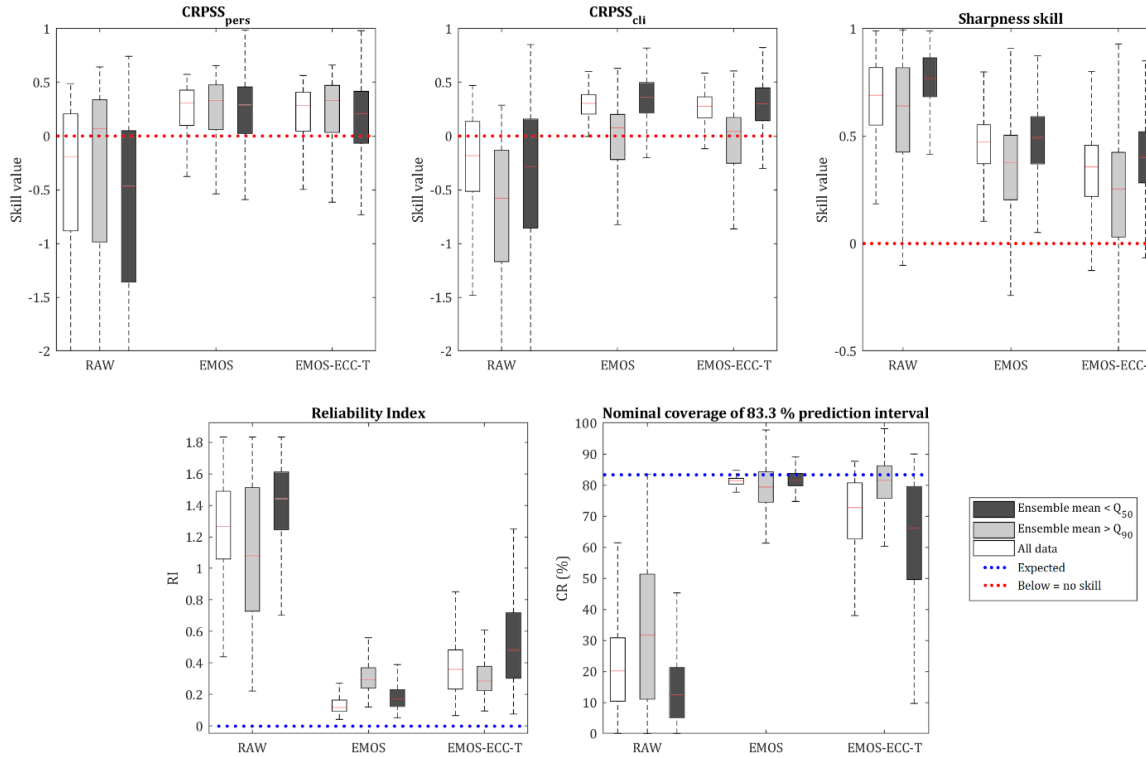

Figure 4.11. Performance metrics conditioned on forecasted flows for a lead time of seven days. Results are given for the entire verification data and subsets of low to moderate (< Q_{50} of non-exceedance flows) and high forecasted discharges (> Q_{90} of non-exceedance flows). Thresholds are derived from the climatological probabilities of forecasted streamflows, considering the ensemble mean as the stratification criterion. Values below the red dotted line indicate no skill in relation to persistency (pers) or climatology (cli), whereas the blue dotted line indicates the expected (optimal) value for RI and CR.

For the case of low to moderate forecasted flows (< Q_{50}), postprocessing results tend to be similar or slightly better than the ones found for the entire verification data, except for

EMOS-ECC-T when looking to calibration. On the other hand, differences of performance are generally more visible for high forecasted discharges (> Q_{90}). For instance, the overall skill of postprocessed ensembles decreases substantially when compared with daily climatology, reaching median values slightly above the no skill line. Despite EMOS and EMOS-ECC-T still exhibiting positive SS values for the > Q_{90} condition in most locations, sharpness is reduced and the ensemble spread becomes closer to that one of climatology. Regarding calibration, the statistical consistency of EMOS reduces while the EMOS-ECC-T increases compared with the entire verification data, and the range of RI values in both cases becomes similar (with median RI around 0.3). The same pattern is observed for the CR, with median values of coverage close to 80 %. Box plots also indicate that over-dispersive forecasts are more likely to occur for the > Q_{90} condition after postprocessing, since more than 25 % of CR values lie above the nominal coverage of 83.3 %.

4.4.6. Evaluation of the ensemble traces derived using ECC-T

In this section we explore the performance of the ECC–T for extracting realistic forecasting trajectories from the EMOS predictive distributions. Figure 4.12 shows the resulting ACF of the lag-one differences of forecasted discharges plotted for the selected locations, both for the raw ensemble (i.e., the reference ACF, expressed by ACF_{Ref}) and EMOS-ECC-T ($ACF_{EMOS\text{-}ECC\text{-}T}$). The agreement between both ACFs is summarized by the area between the curves shown in each diagram. Unlike a metric or graphic measure that evaluates the univariate performance for a single lead time, the ACF_{Area} is an aggregated result for all lead times within the forecast horizon. In some locations, such as the Itá, Salto Santiago and Aimorés reservoirs, $ACF_{EMOS\text{-}ECC\text{-}T}$ and ACF_{Ref} are almost identical (with ACF_{Area} ranging between 0.08 and 0.24). The rapid decrease in ACF in these cases is indicative of larger fluctuations in the predicted flows. In addition, EMOS-ECC-T produces an ACF relatively close to the reference also in Itaipu and Lajeado (ACF_{Area} ~0.8), while larger differences occur in the other analyzed locations (ACF_{Area} ranging between 1.65 and 2.83, respectively in Furnas and Teles Pires). Postprocessed forecast trajectories tend to perform worser in locations for which the raw ensemble exhibits stronger autocorrelations in forecast time series.

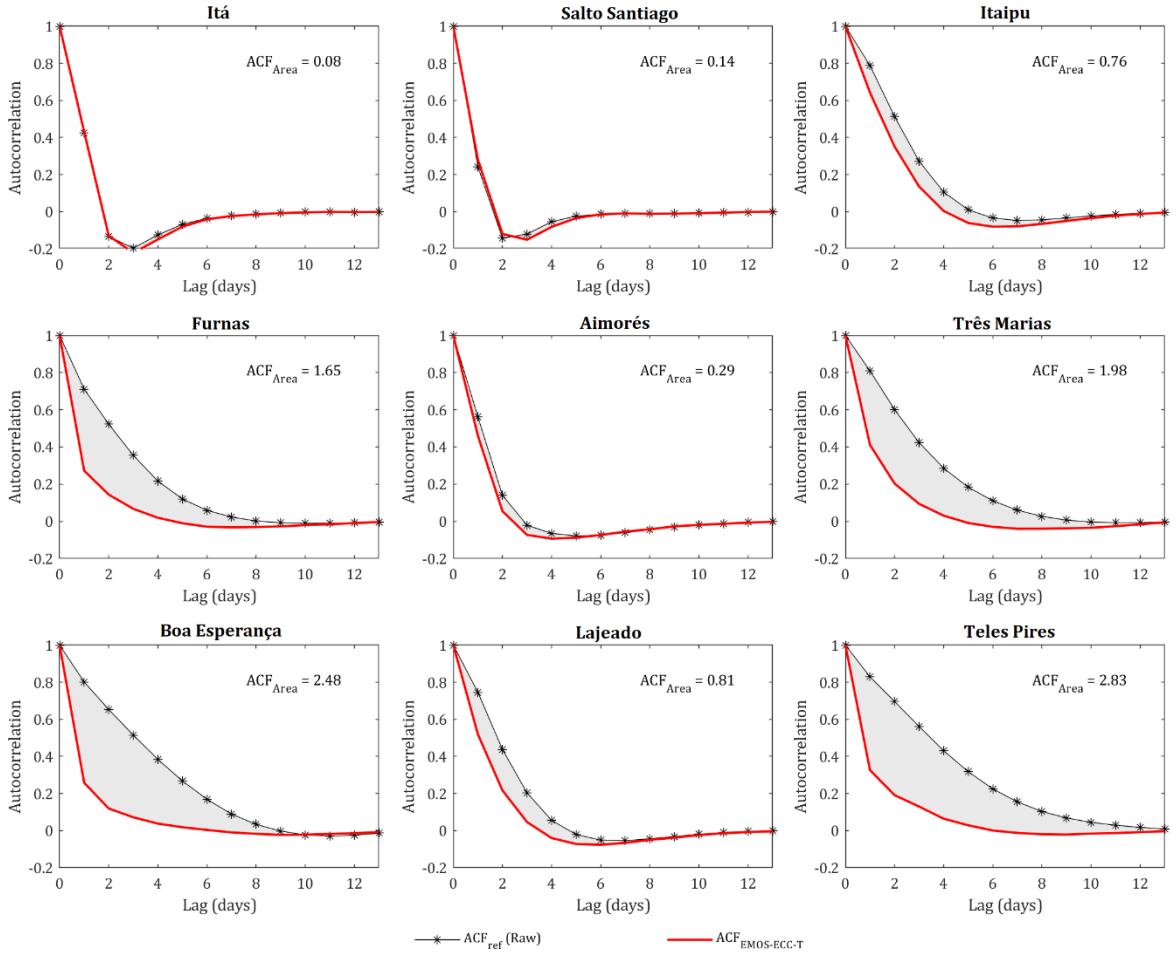

Figure 4.12. Autocorrelation function (ACF) of the lag-one differences of forecasted discharges. The ACF of raw ensemble (reference) and the ACF of EMOS-ECC-T are shown in lines of black and red colors, respectively.

To provide broader insight into the behavior of forecast trajectories derived using ECC-T, the areas between the $ACF_{EMOS\text{-}ECC\text{-}T}$ and ACF_{Ref} curves were plotted for the analyzed gauge stations in SA (Figure 4.13). The spatial distribution of ACF_{Area} shows that EMOS-ECC-T performance varies largely across the continent. For instance, ACF_{Area} values are relatively low in most of La Plata basin (usually in the eastern region drained by the upper Paraná and Uruguay Rivers), generally reaching magnitudes less than 0.5. Similar performances by EMOS-ECC-T are also found in large basins such as Parnaíba and Tocantins (on the eastern side of the Tocantins–Araguaia Basin), except at locations characterized by large reservoirs (e.g., Boa Esperança in Parnaíba Basin). In turn, a low agreement between raw and postprocessed ACF curves (with a very high ACF_{Area}, generally > 2.0) is observed in much of the Amazon Basin and also in areas affected by floodplains where the raw ensemble spread is expected to be low for lead times up to 15 days in advance. This is the case for the Araguaia River (on the western side of Tocantins–Araguaia Basin), upper Paraguay and lower Magdalena.

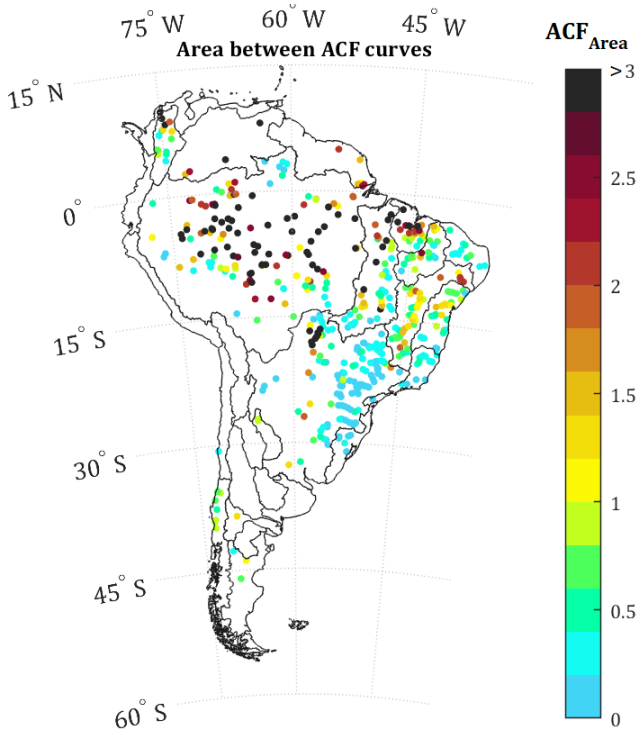

Figure 4.13. Geographical distribution of the area between ACF curves (raw ensemble × EMOS-ECC-T postprocessing) with respect to lag-one differences of forecasted discharges.

To analyze the effect of the raw ensemble spread on EMOS-ECC-T forecast trajectories, the sharpness skill (SS) of both the raw ensemble and EMOS were plotted against the ACF_{Area} (Figure 4.14). As can be clearly observed, gauges with large ACF_{Area} values tend to be concentrated at the top of the diagrams. This means that the autocorrelation in forecast time series is not well depicted by ECC-T when the raw ensemble has very low spread (SS_{Raw} close to 1), at the same time that EMOS has to largely increase dispersion (SS_{EMOS} usually < 0.7). This effect is more pronounced at shorter leads because of the delayed response of streamflow to predicted precipitation, and it undermines the extraction of coherent forecast trajectories, as it favors unrealistic jumps during the quantile mapping procedure of ECC-T.

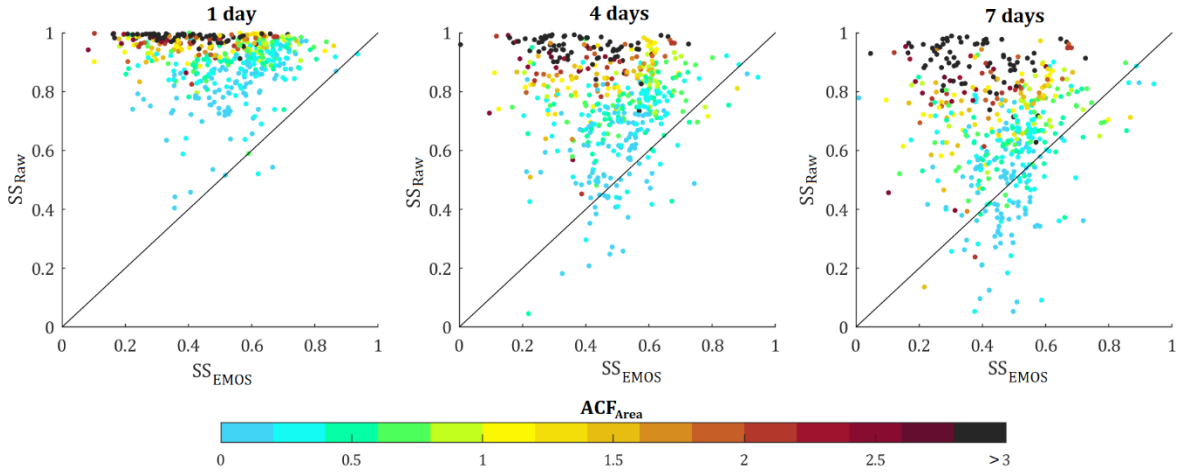

Figure 4.14. Relationship between ACF_{Area} and sharpness skill (SS) for both the raw ensemble and EMOS. SS values are given for lead times of one, four and seven days, while the ACF_{Area} for each gauge station is indicated by the color of the dots.

4.5. Discussion

As shown in the previous sections, raw ensemble streamflow forecasts issued from a continental-scale forecasting system can often lead to lower overall performance than that of simpler alternatives, like daily climatology or persistence forecasts. From a spatial point of view, the lack of skill regarding the raw ensemble was identified in a considerable number of gauge stations located mainly in central to western tropical regions of SA. Negative values of CRPSS were noted also in large basins in such regions, although other studies have shown that forecast skill typically increases with basin size (Pappenberger *et al.*, 2011; Alfieri *et al.*, 2014; Siddique and Mejia, 2017). It should be noted that the assessment of forecast skill is here performed in South American basins that can reach up to hundreds of thousands or even millions of square kilometers, encompassing distinct geographic regions, multiple hydroclimatic features, and flow regimes ranging from highly variable (year-round) to unimodal flood peak regimes. Benchmarks, for instance, may perform better when the seasonality or serial correlation of discharges is strong; thus streamflow forecast skill is expected to be lower in these situations, even in large basins. Forecast skill is also closely linked to the hydrological model performance, and it is likely that CRPSS would increase with catchment area in some of these regions if hydrological initial conditions were more evenly (and well-) estimated across the continent (Siqueira *et al.*, 2020). This is not the case, as simulated discharges perform very differently in space due to limitations in process representation, model calibration and variations in quality of rainfall estimates (MSWEP) used for forecast initialization. In addition, predicted precipitation often dictates the skill of streamflow forecasts, especially at longer lead times. The contribution of skill coming from

ECMWF rainfall prediction has been found to be spatially dependent in SA, exhibiting higher skill in eastern and southeastern regions but lower skill in the Amazon and western areas close to the Andes Cordillera (Medina *et al.*, 2019; Siqueira *et al.*, 2020).

By assessing calibration, we found low ensemble coverage rates compared to the nominal ensemble coverage and large deviations from horizontally flat rank histograms, which clearly indicates that raw streamflow forecasts are far from being samples from the true PDFs, even at longer lead times such as one week ahead. The EMOS postprocessor substantially improved the skill and statistical consistency of raw hydrological forecasts, also leading to narrower uncertainty ranges in relation to climatology in most of the analyzed gauge stations. In some regions, such as the Amazon, northern SA and western La Plata, larger reductions of sharpness skill in relation to other areas were observed after postprocessing. This probably occurs because streamflow forecasts (i) are being affected by the low skill of predicted precipitation (mainly indicated by low $CRPSS_{cli}$ in Figure 4.5, center), or (ii) have almost no spread in the raw ensemble (mainly indicated by low $CRPSS_{pers}$ in Figure 4.5, center). These factors may result in a high frequency of large, random errors in streamflow forecasts after bias correction, consequently leading to a larger increase in the width of EMOS predictive distributions in order to appropriately calibrate forecasts. Furthermore, simulated discharges in these areas are often subject to significant timing errors (Paiva *et al.*, 2013a; Siqueira *et al.*, 2018). Delayed (or advanced in time) flows are expected to contribute to non-systematic errors (e.g., underestimation during rising flows and overestimation during hydrograph recession, or vice-versa), and could be also one of the reasons for the degradation of sharpness skill. It is worth noting that, despite the postprocessed forecasts are generally less sharp than the raw ensembles, the number of locations with $SS_{EMOS} > SS_{Raw}$ tends to increase with lead time (as indicated in Figure 4.14). This means that EMOS can contribute positively to sharpness to some extent, by reducing the average spread of raw forecasts especially at longer leads.

A sample reordering method such as the ECC is an interesting way to extract forecast trajectories from postprocessed distributions. Combining EMOS and ECC techniques for medium-range streamflow forecasting can be promising, especially in some regions of SA such as the La Plata basin. This is important since hydropower in La Plata plays a key role in energy production for many South American countries (Popescu *et al.*, 2012). Our assessment is the first that demonstrates the applicability of EMOS and ECC methods for streamflow forecasting on a very large extent, using approaches and global datasets that are potentially available for less developed regions. Once the parameters of EMOS models are adjusted, predictive

distributions and postprocessed ensemble traces could be easily obtained for hundreds of gauge stations across the SA continent.

Nonetheless, some considerations must be outlined here. The performance of EMOS depends on how close the forecasting errors are normally distributed. Recent studies have shown that data transformations (e.g., Box–Cox or any others) can stabilize the variance of errors in a forecasting context, although normal distributions are difficult to achieve in practice (Berthet *et al.*, 2020). This may be even more difficult when dealing with different hydrological regimes occurring in a large domain such as SA. It was found that, in general, applying the ECC (with the T-sampling scheme) on EMOS predictive densities causes little impact on the overall skill of EMOS. On the other hand, it reduces the calibration obtained from univariate postprocessing, which is consistent with previous findings (Hemri *et al.*, 2015; Bellier *et al.*, 2018). The loss of calibration may be attributed to the sampling levels of ECC-T, which are not equally spaced as they are connected to the raw ensemble. Another important consideration is that the ECC strongly depends on the ability of the model used to simulate the real system (Schefzik *et al.*, 2013). This imposes additional limitations for continental domains (such as SA), since large-scale hydrological models usually have coarse resolutions (regarding model discretization, input data, etc.) and are likely to provide a lower performance than the ones tailored for specific basins. In this context, Fleischmann *et al.* (2020) identified artefacts causing excessive attenuation in simulated flows at large reservoirs (e.g., Três Marias), which can occur not only in MGB–SA but also in any other large-scale model with hydrodynamic routing. This artificially reduces the spread in the raw ensemble and may lead to a lower performance of ECC-T.

As indicated from the experiments, the ability of ECC-T to recover temporal dependencies and derive realistic ensemble traces from EMOS postprocessing vary from one place to another. For instance, substantial differences between the ACF curves of EMOS-ECC-T and raw ensemble were observed in areas such as the Amazon and upper Paraguay. Time series of forecasted streamflow in these regions are more strongly correlated due to longer travel times and slow propagation in rivers, as the flow routing is subject to delay effects caused by floodplain storage processes (Paz *et al.*, 2011; Yamazaki *et al.*, 2011; Paiva *et al.*, 2013a; Pontes *et al.*, 2017; Siqueira *et al.*, 2018). As a result, streamflow predictability in large SA rivers is often dominated by initial hydrological conditions rather than predicted precipitation, even for some weeks ahead (Paiva *et al.*, 2012a). As the predicted rainfall is the only uncertainty source cascaded to the raw streamflow ensemble, the corresponding spread in the aforementioned

cases is expected to be systematically low, which consequently provides little information on EMOS variance. Besides, in ECC-T the quantiles from the raw ensemble are mapped to EMOS predictive distributions, which means that some members may be linked to very low probabilities at low ensemble spread conditions, producing unrealistic jumps in forecast trajectories (Hemri *et al.*, 2015). Increasing the minimum variance of the normal distribution that is fitted to the raw ensemble (S_k) may help to reduce these jumps between lead times, albeit at the cost of additional loss of calibration (see supplementary material S.1). Performing data assimilation prior to EMOS postprocessing would be more appropriate and necessary for narrowing the predictive uncertainty, consequently improving the forecast trajectories.

Finally, both the skill of postprocessed forecasts and the generation of ensemble traces could be further improved by making use of variants of EMOS and ECC methods. One possibility is to fit EMOS models using subsets of training data according to forecast analogs (Hemri and Klein, 2017), which can take advantage of long past hydrological ensemble predictions based on meteorological reforecasts. The use of analog-based training periods has been shown to make the skill of EMOS predictive distributions comparable to those generated by more sophisticated postprocessing techniques like BMA, for example (Baran *et al.*, 2019). Regarding ECC-T, random perturbations could be made to the dependence template to improve the fits of the corresponding CDF *S* in low spread conditions (Bellier et al., 2018). Another option would be to apply trajectory smoothing over ensemble traces produced with ECC-Q (i.e., the equally spaced sampling) instead of using the ECC-T method, which could handle the known strong fluctuations (jumps) of the former while improving the calibration over the T scheme (Bellier *et al.*, 2018). In addition, a temporal component could be introduced into the ECC template by using past data statistics, thus enabling it to account for the autocorrelation of the forecast error between consecutive lead times (Ben Bouallègue *et al.*, 2016). Although testing these variants is beyond the scope of this study, assessing their suitability for a continental-scale forecasting system is also of great interest and could be the subject of future work.

4.6. **Conclusions**

This work provides a comprehensive evaluation of the use of statistical postprocessing on medium-range, ensemble streamflow forecasts (up to 15 days ahead) over South America (SA). Forecasts were produced through a continental scale, hydrologic–hydrodynamic model forced with a global precipitation dataset and reforecasts from the ECMWF Ensemble

Prediction System (EPS). The Ensemble Model Output Statistics (EMOS) method was used to convert the raw ensemble into predictive distributions for each location, forecast day and lead time. Additionally, Ensemble Copula Coupling with the transformation scheme (ECC-T) was applied to derive ensemble traces from EMOS distributions. A set of metrics was used to assess skill, calibration and sharpness of raw and postprocessed forecasts against simpler forecasting alternatives such as daily climatology and persistence, and of the capacity of generating realistic postprocessed forecast trajectories was also evaluated. The assessment was carried out for hundreds of gauge stations spread throughout SA. The main conclusions can be summarized as follows:

- Raw ensemble streamflow forecasts issued by a continental-scale hydrological model in SA do not necessarily offer better results in comparison with simpler alternatives such as daily climatology and persistence of the last observed flows. While raw ensembles may exhibit some skill in southeastern and eastern regions (except São Francisco basin) for one week in advance, generally no skill was found in large basins such as the Amazon, Orinoco, Tocantins–Araguaia and west of La Plata (Paraguay). By applying EMOS postprocessing the forecast skill over climatology improved in most locations up to 15 days ahead, and skill over persistence was generally observed after four days in advance;

- Raw ensemble streamflow forecasts were markedly unreliable in most of the gauge stations, even for lead times of one week ahead (usually less than 30 % of observations were captured by the ensemble). EMOS postprocessing generally increases the spread of raw forecasts and also improves the statistical consistency between forecasted probabilities and observed relative frequencies along the entire forecast horizon. However, EMOS was not able to produce skillful forecasts in large rivers where initial hydrological conditions may largely contribute to streamflow predictability;

- EMOS provided streamflow forecasts that were usually less sharp than the raw ensembles. However, the differences in average spread between both approaches reduced with lead time, with EMOS exhibiting better sharpness skill in several locations at longer leads. In addition, EMOS resulted in skillful predictions (in terms of width of predictive distribution) when compared to discharge climatology;

- Generating ensemble traces from EMOS distributions by applying the ECC-T method caused little impact on the overall skill achieved by univariate postprocessing. However, both sharpness skill and improvement in calibration were reduced in comparison with univariate EMOS (especially at shorter leads), with differences being smaller for increasing lead times;

- When verification was conditioned on high forecasted discharges (ensemble mean > non-exceedance probabilities of 90 %), the overall skill, sharpness skill and also calibration gained with EMOS postprocessing decreased in comparison with the results obtained from the entire verification data;

- While the ability of ECC-T to represent the autocorrelation of forecasted streamflows was variable in space, a relatively good performance was observed mainly in eastern La Plata basin. In general, limitations for generating realistic forecast trajectories were found in rivers for which the raw ensemble spread is very low, and EMOS has to largely increase dispersion, especially at short lead times. For such locations, (more) real-time discharge observations may be required for performing further corrections in order to reduce the width of EMOS predictive distributions.

The findings of this study suggest that skillful, medium-range streamflow forecasts could be achieved at the continental scale of SA even if global precipitation data have to be used to initialize the hydrological model. Future research paths should include assessing the utility of this forecast framework for particular applications (e.g., flood forecast, hydropower reservoir operation). Moreover, a further important step in improving the performance of such forecasts is through data assimilation (DA) of river discharge. Experiments using the MGB–SA model and DA are ongoing (e.g., Wongchuig *et al.*, 2019), and the benefits of implementing DA together with statistical postprocessing will likely be explored in the near future. Of course, given the large domain of interest, performing DA would be a great challenge due to the amount of good quality river discharge observations required, which are often not available in real time. Assimilating other sources of data, such as the ones derived from remote sensing (e.g., radar altimetry, flood extent) (e.g., Paiva *et al.*, 2013b; Wongchuig *et al.*, 2020), can be also a promising way to improve forecasting capabilities in South American countries.

Acknowledgements

The first author would like to acknowledge the Brazilian Coordination for the Improvement of Higher Education Personnel (CAPES) (under grant number 88881.189000/2018-01, CAPES/PDSE - *Programa de Doutorado Sanduíche no Exterior*) and the Brazilian National Council for Scientific Research (CNPq) (under grant numbers 141450/2015 and 422422/2016 - Project: "South America Flood Awareness System – SAFAS") for the financial support. We also acknowledge all the hydrological centers that provided observed discharge data (ANA, ONS, IDEAM, DGA, GRDC, INA, HyBAM, SENAMHIs); Princeton University for the MSWEP precipitation data; and the European Center of Medium-Range Weather Forecast (ECMWF) for making available the reforecast data used in this study. Finally, we thank Jan Verkade for the support given during the development of this work and the two anonymous reviewers for their useful suggestions, which helped us to improve the quality of this manuscript.

Supplementary Material

S.4.1 Sensitivity analysis of the ECC-T "d" parameter

Figure S.4.1 shows the sensitivity of forecast trajectories to the ECC-T "*d"* parameter (ranging from 0.00005 to 0.05), which controls the minimum variance of the normal distribution fitted to the raw ensembles in ECC-T method (Eq. (4.7)). Results are shown for the postprocessed ensemble traces at Três Marias reservoir, where the raw ensemble spread is very low in comparison to EMOS uncertainty. Unrealistic jumps in the ECC-T ensemble traces occur more frequently when lower values are adopted for this parameter.

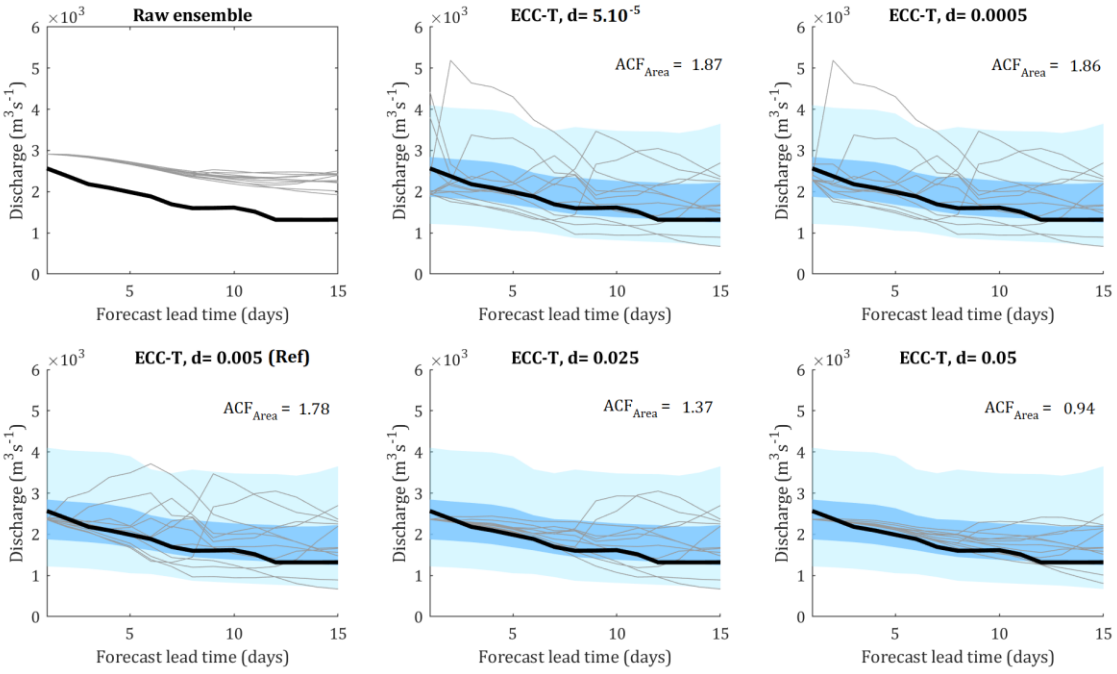

Figure S.4.1. Sensitivity of ECC-T ensemble traces to the "*d*" parameter. EMOS uncertainty is shown for the centered prediction intervals of 90 % (5–95 %) and 50 % (25–75 %), indicated by light and dark blue colors respectively. The analysis is performed taking postprocessed ensemble traces for Três Marias reservoir as example. Reference value for "*d*" is 0.005.

Figure S.4.2 shows the sensitivity of verification metrics to the ECC-T "*d*" parameter. Results for EMOS univariate postprocessing (where ensembles are derived through equally spaced quantiles) are also presented for comparison purposes. Note that there are minor — and often not significant — differences of performance among ECC-T configurations with respect to overall skill ($CRPSS_{pers}$ and $CRPSS_{cli}$), being more visible for sharpness skill and ensemble calibration. Lower *"d"* values lead to improvement in calibration specially at shorter lead times, as explained by lower values of RI and CR close to nominal coverage of the ensemble prediction

intervals (83.3 %), although with a reduction in sharpness skill.

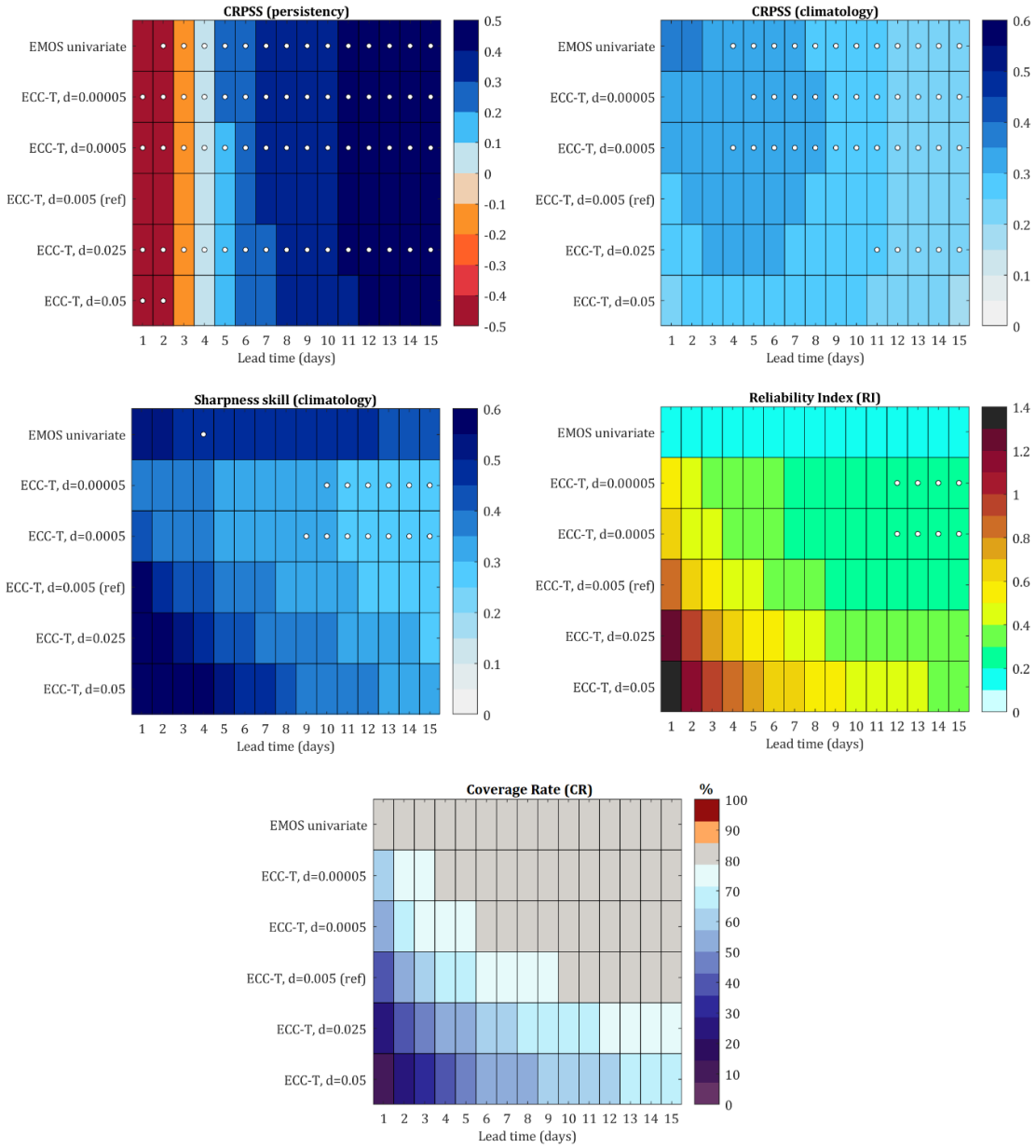

Figure S.4.2. Sensitivity of verification metrics to the ECC-T "*d*" parameter according to lead time. Results are plotted for the median of gauge stations considering the EMOS univariate and EMOS-ECC-T postprocessing with 5 different configurations. White dots indicate that results are not significantly distinguishable (*t*-test, p > 0.05) from the reference EMOS-ECC-T.

Figure S.4.3 shows the sensitivity of the autocorrelation criterion to the ECC-T "*d*" parameter. The relative performance of ECC-T configurations in producing realistic forecast trajectories from EMOS distributions is measured by the area between the ACF curves of raw and postprocessed ensembles, considering forecast time series of lag-one differences. As observed, a better agreement between the ACF curves occurs when higher *d* values are adopted,

and sensitivity is more apparent for d = 0.05 and d = 0.025 (ACF_{Area} < 1 in 84 % and 72 % of the gauges, respectively) in comparison to the other tested configurations (ACF_{Area} < 1 in ~63 % of the gauges for $d \leq 0.005$). Differences of ACF_{Area} between the reference ECC-T parameter (d = 0.005) and $d \leq 0.0005$ are visible for gauges with large ACF_{Area} values, generally > ~2.

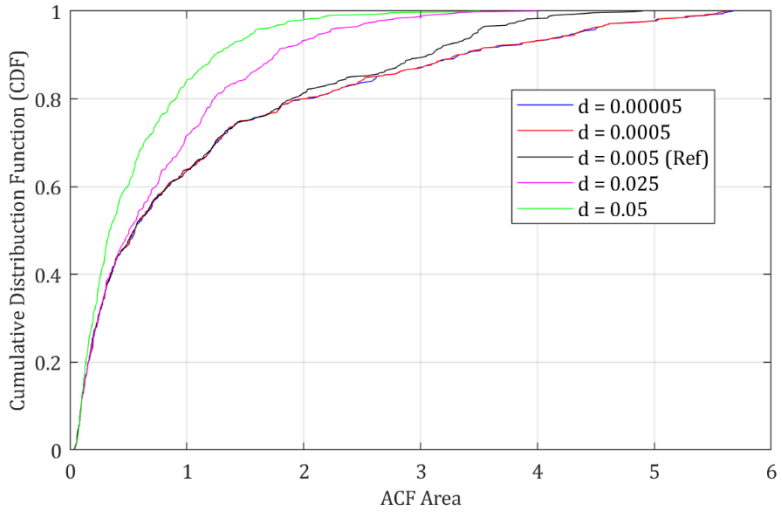

Figure S.4.3. Sensitivity of the autocorrelation criterion to the ECC-T "*d*" parameter. The graph shows the cumulative distribution function (CDF) of the area between the ACF curves (EMOS-ECC-T × raw ensemble) considering all gauge stations.

S.4.2. Extended forecast hydrographs

Figure S.4.4 to Figure S.4.12 show extended time series of streamflow forecasts for the analyzed reservoir locations (Itá, Salto Santiago, Itaipu, Furnas, Aimorés, Três Marias, Boa Esperança, Lajeado and Teles Pires), considering a lead time of 7 days. Forecasts are given in uncertainty ranges and are plotted for the climatology, raw ensemble and EMOS univariate postprocessing. The shaded area in each graph corresponds to the nominal 83.3 % centered prediction intervals. Time series of daily observed flows (black line) are reduced to observations twice a week to match the available dates of ECMWF reforecasts.

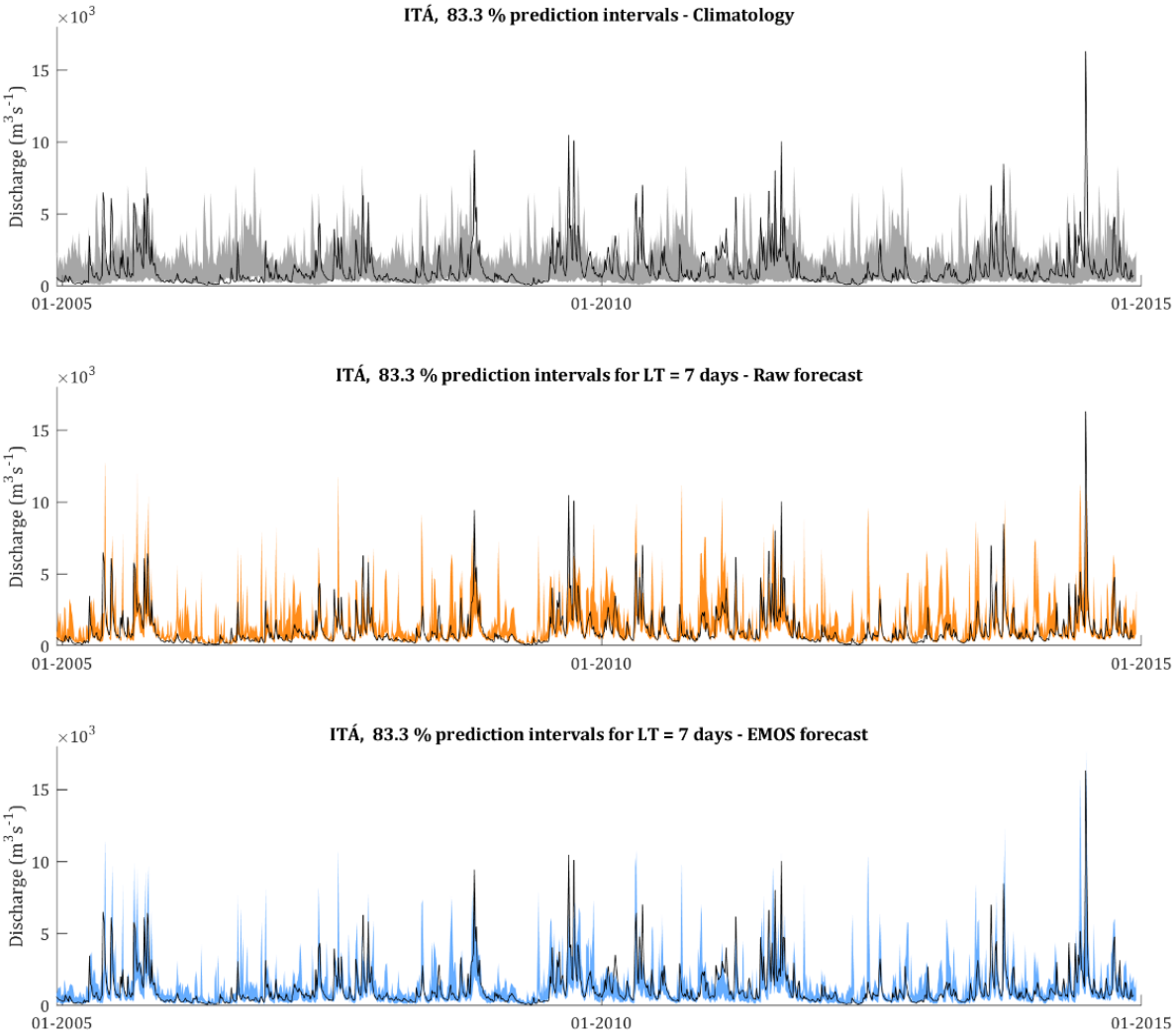

Figure S.4.4. Predictive uncertainty of climatology (top), raw (middle) and EMOS forecasts (bottom) for Itá reservoir (Uruguay River), considering a lead time of 7 days.

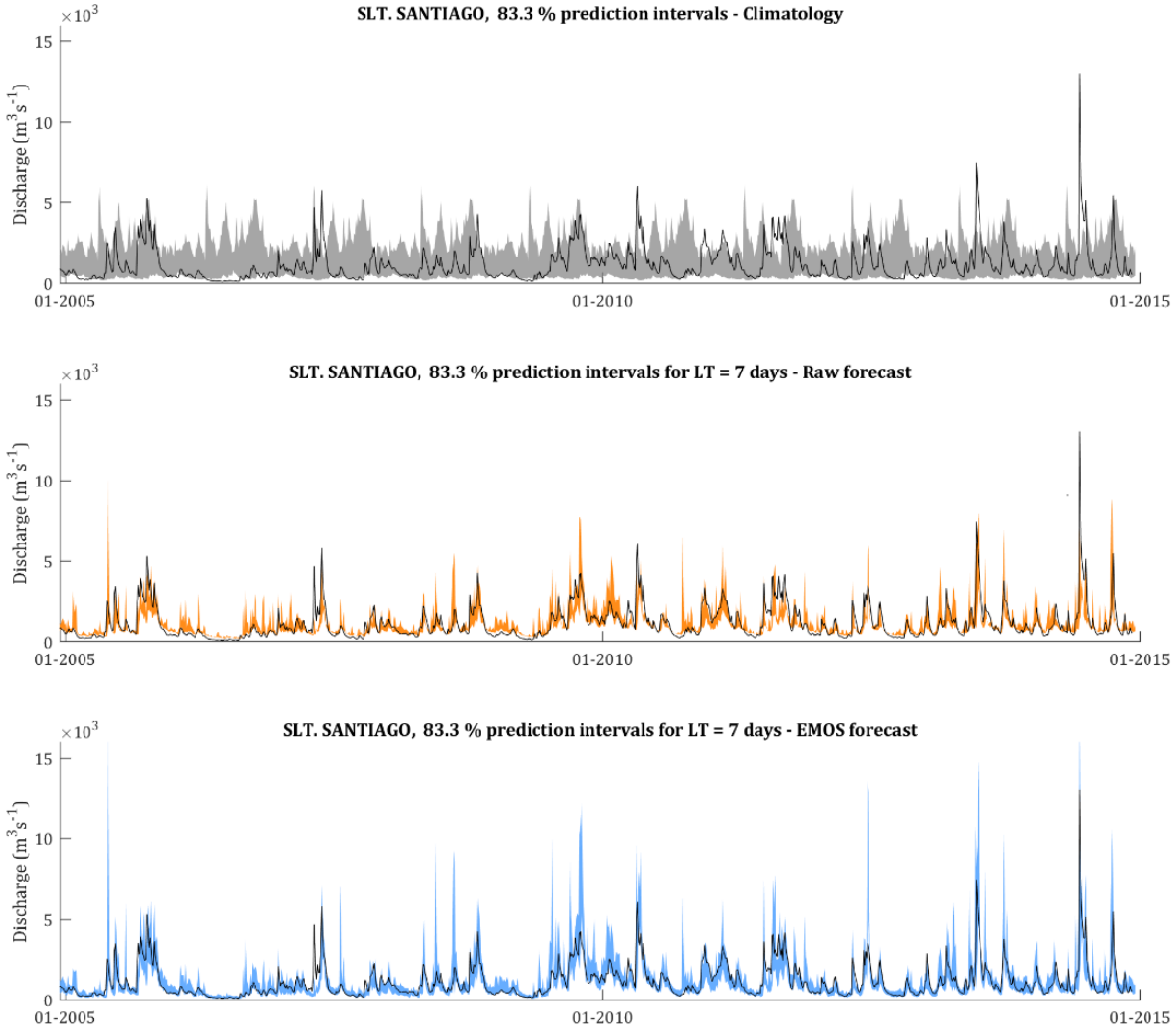

Figure S.4.5. Predictive uncertainty of climatology (top), raw (middle) and EMOS forecasts (bottom) for Salto Santiago reservoir (Iguazu River), considering a lead time of 7 days.

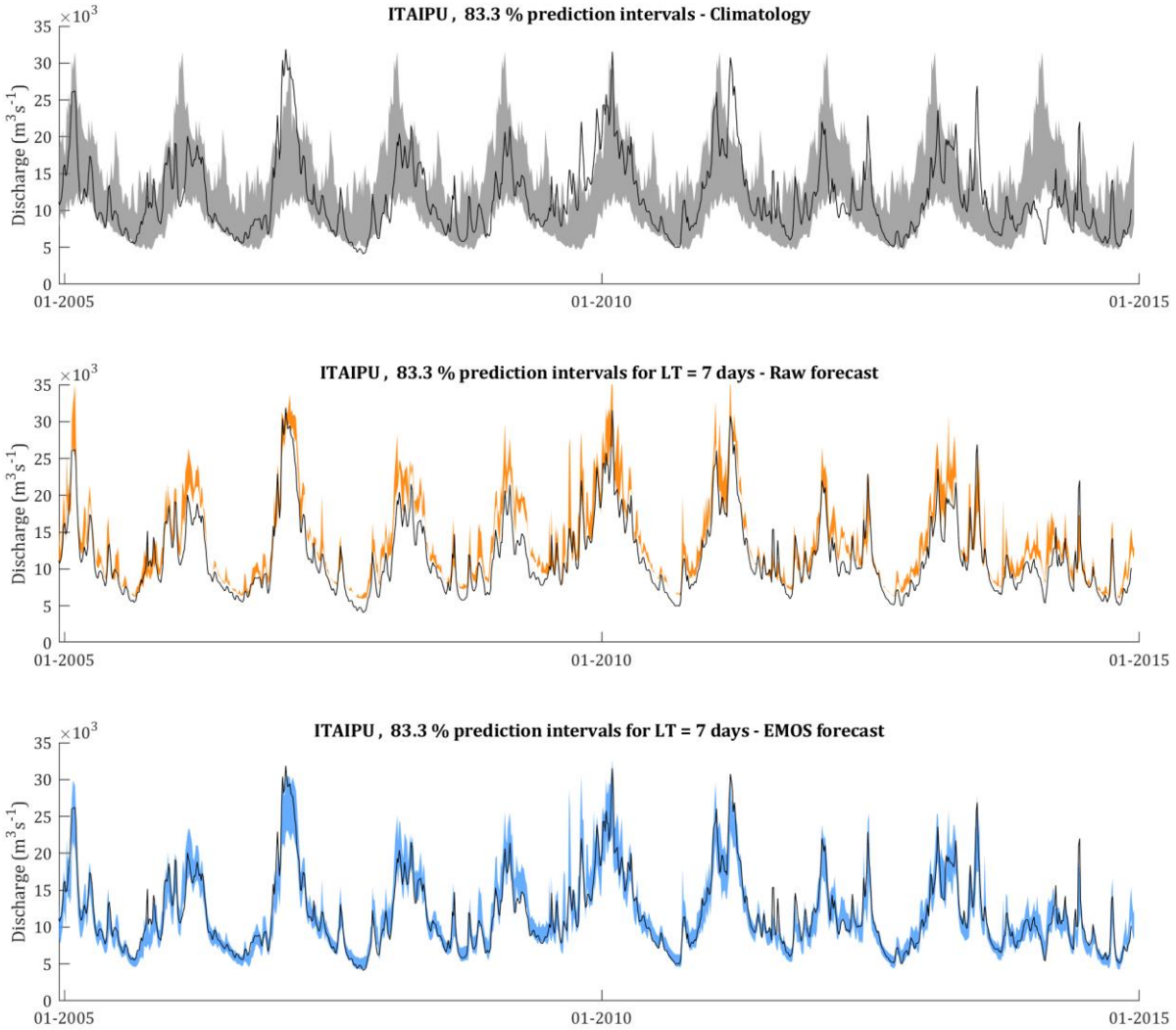

Figure S.4.6. Predictive uncertainty of climatology (top), raw (middle) and EMOS forecasts (bottom) for Itaipu reservoir (Paraná River), considering a lead time of 7 days.

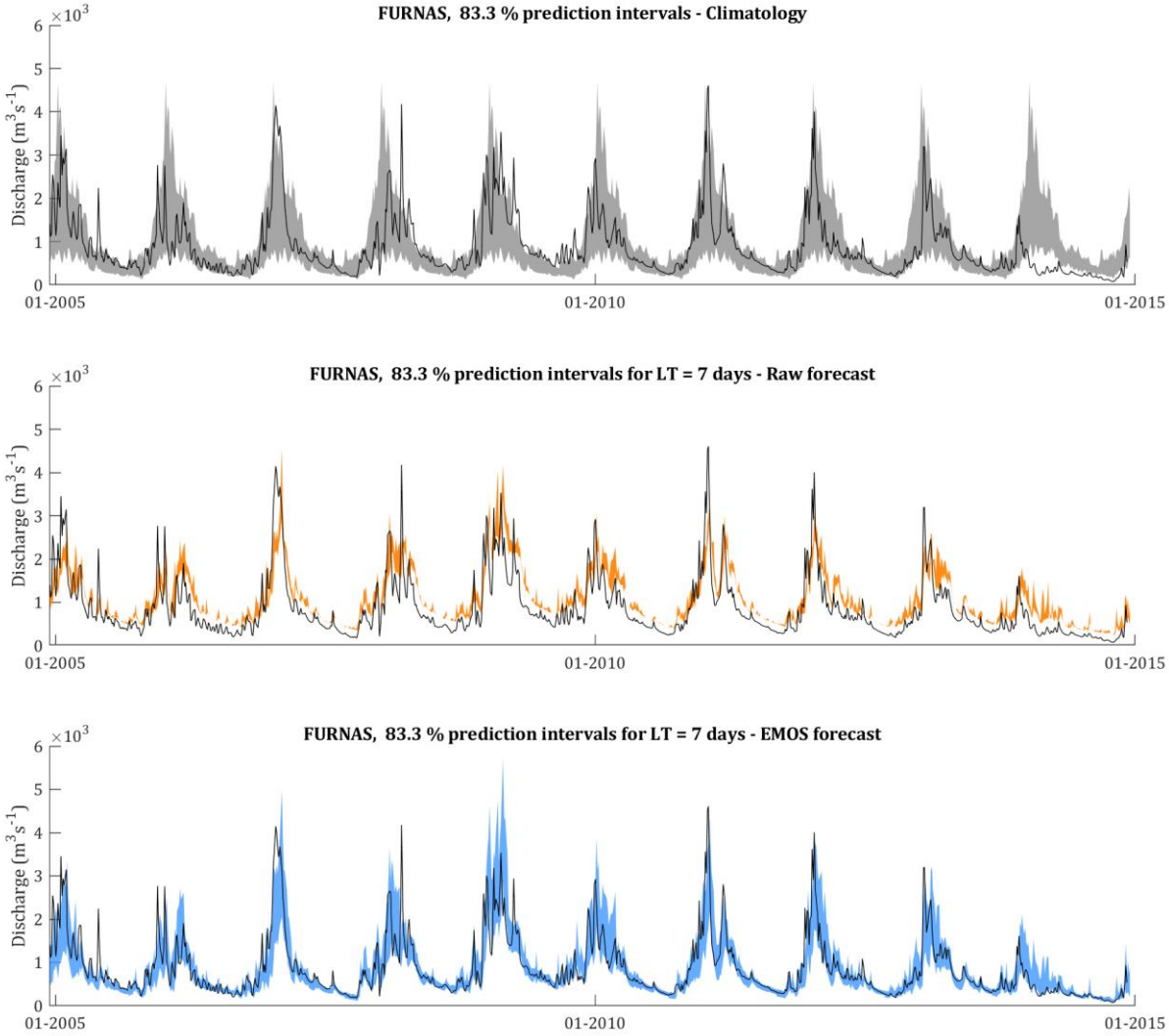

Figure S.4.7. Predictive uncertainty of climatology (top), raw (middle) and EMOS forecasts (bottom) for Furnas reservoir (Grande River), considering a lead time of 7 days.

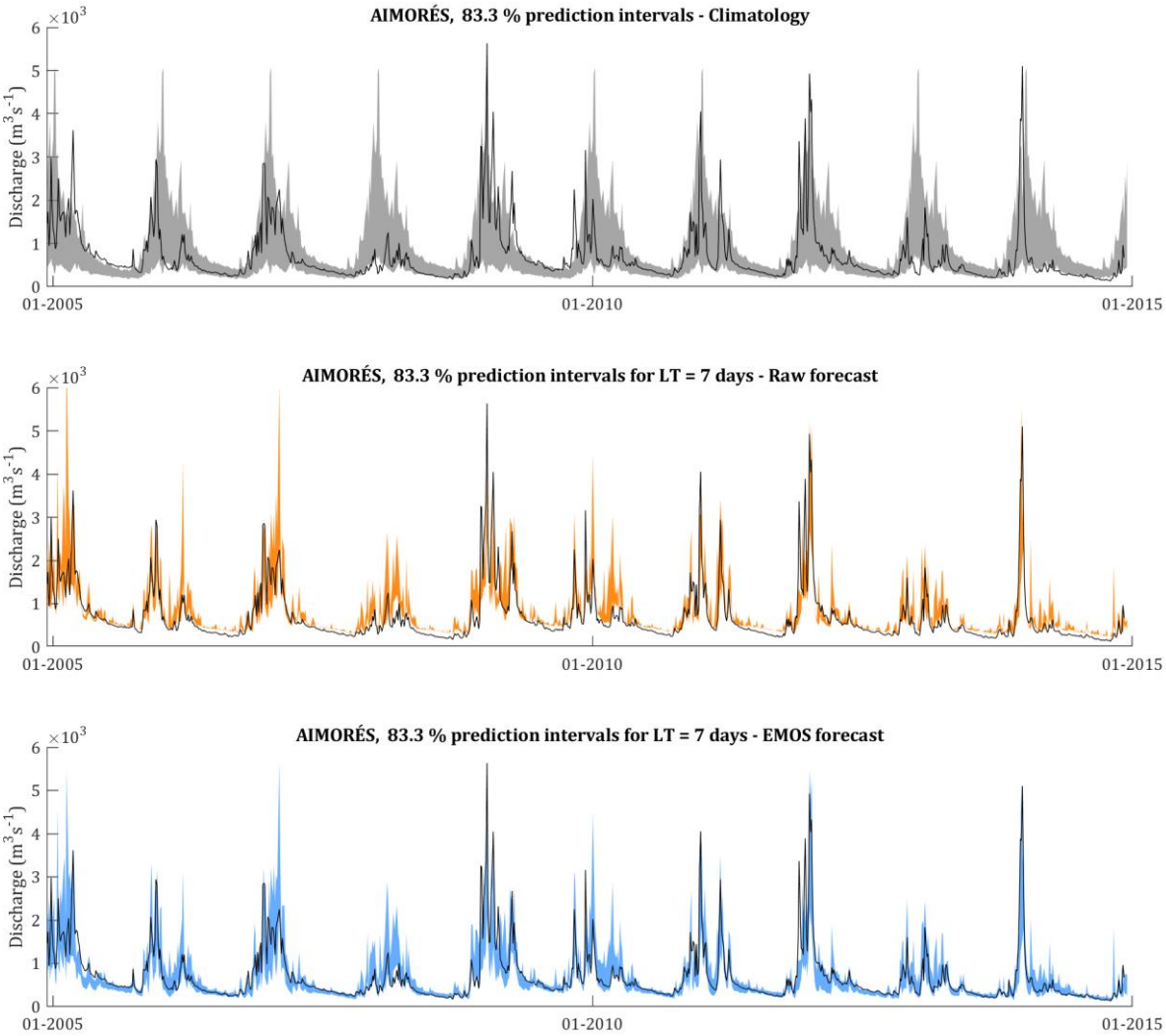

Figure S.4.8. Predictive uncertainty of climatology (top), raw (middle) and EMOS forecasts (bottom) for Aimorés reservoir (Doce River), considering a lead time of 7 days.

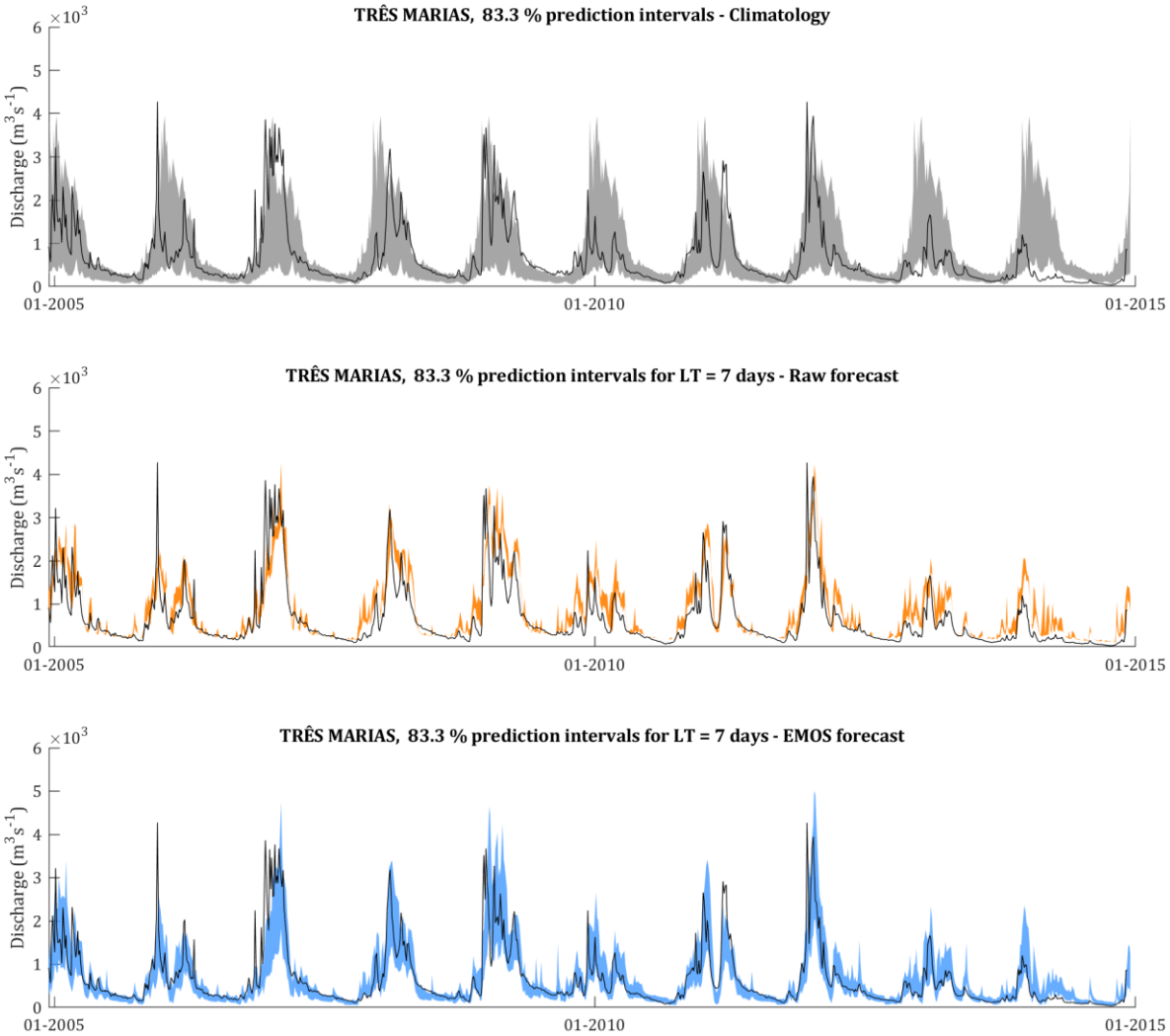

Figure S.4.9. Predictive uncertainty of climatology (top), raw (middle) and EMOS forecasts (bottom) for Três Marias reservoir (São Francisco River), considering a lead time of 7 days.

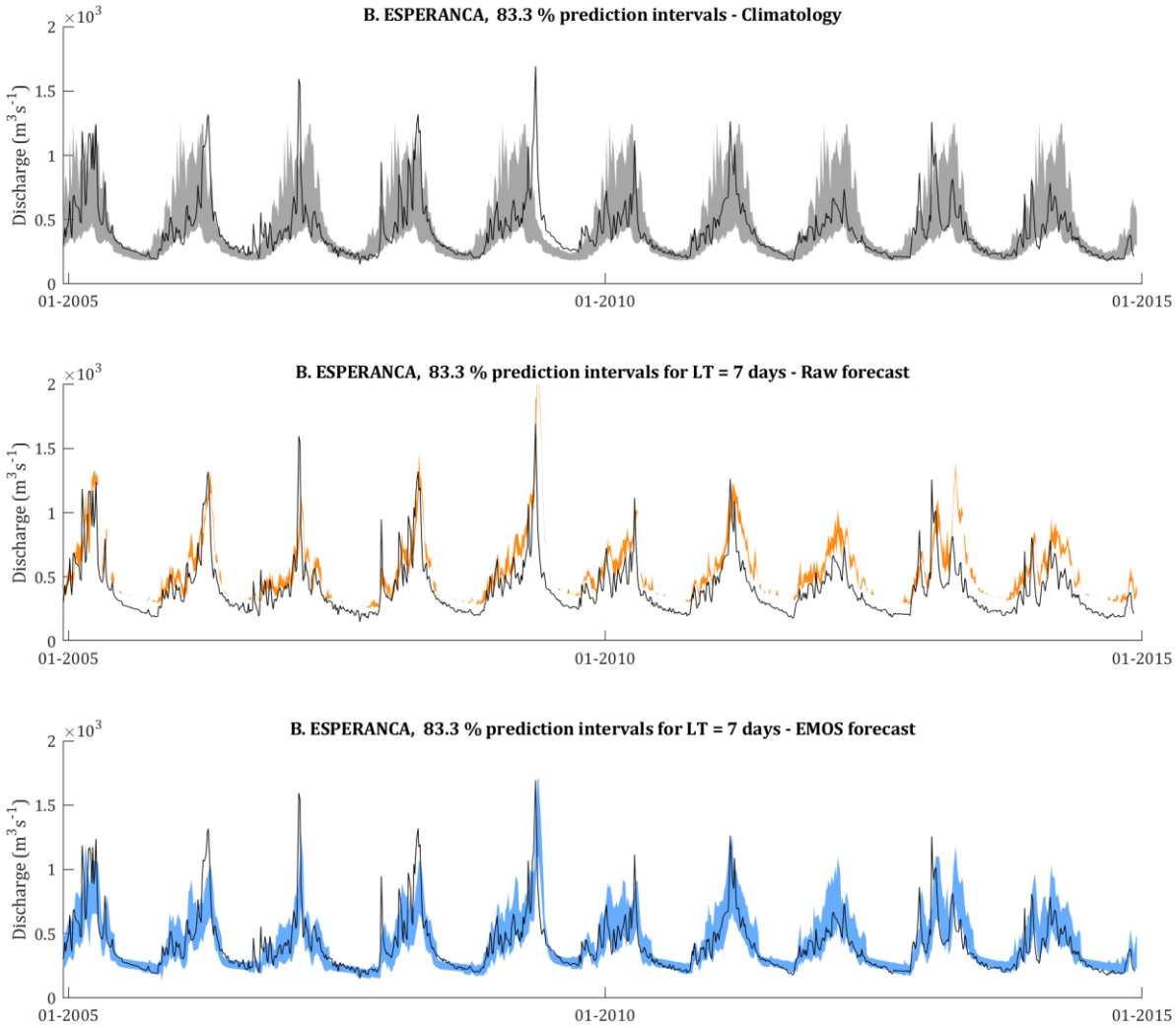

Figure S.4.10. Predictive uncertainty of climatology (top), raw (middle) and EMOS forecasts (bottom) for Boa Esperança reservoir (Parnaíba River), considering a lead time of 7 days.

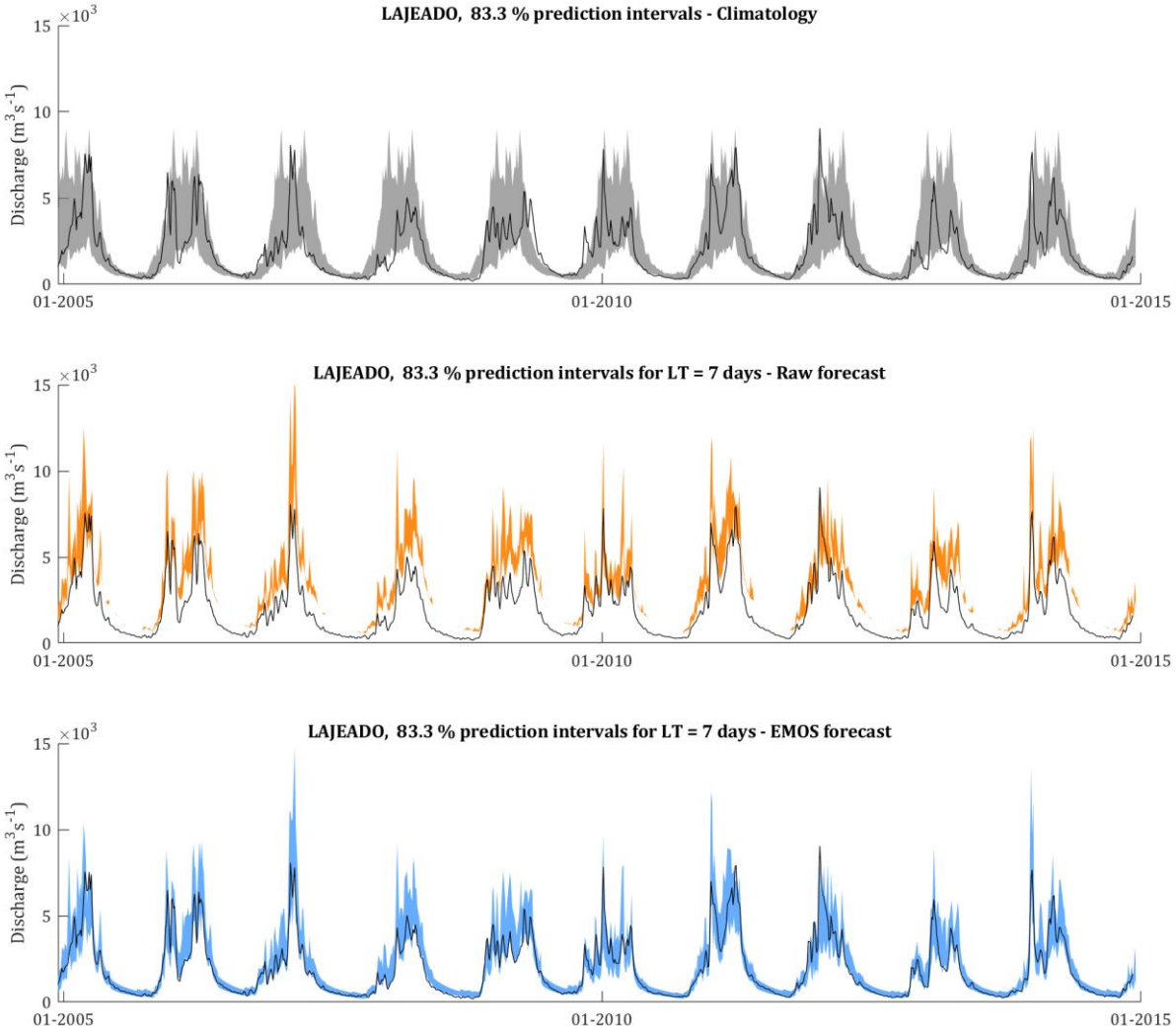

Figure S.4.11. Predictive uncertainty of climatology (top), raw (middle) and EMOS forecasts (bottom) for Lajeado reservoir (Tocantins River), considering a lead time of 7 days.

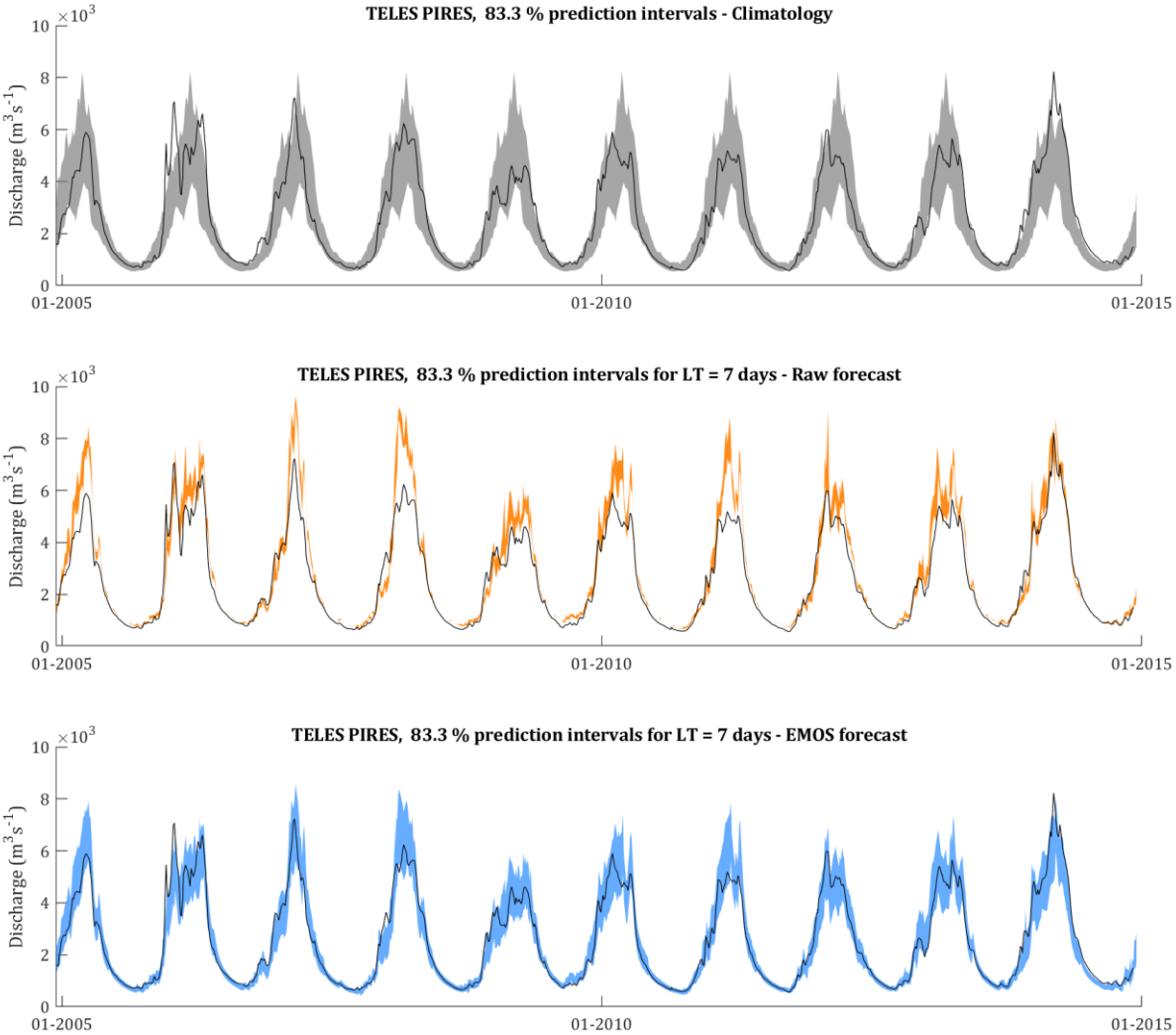

Figure S.4.12. Predictive uncertainty of climatology (top), raw (middle) and EMOS forecasts (bottom) for Teles Pires reservoir (Teles Pires River), considering a lead time of 7 days.

CAPÍTULO 5: Conclusões e recomendações

"In light of knowledge attained, the happy achievement seems almost a matter of course, and any intelligent student can grasp it without too much trouble. But the years of anxious searching in the dark, with their intense longing, their alternations of confidence and exhaustion, and final emergence into light — only those who have experienced it can understand that."

—Albert Einstein

Esta tese de doutorado teve por objetivo estabelecer uma base técnica para a modelagem hidrológica com abrangência da América do Sul e dar contribuições para previsão de vazões em escala continental no horizonte de médio prazo (até 15 dias). As questões técnico-científicas que nortearam esta pesquisa, juntamente com as principais conclusões, limitações e recomendações para trabalhos futuros podem ser elencadas da seguinte forma:

5.1. **Sobre a modelagem hidrológica com abrangência da América do Sul**

Qual o desempenho esperado de um modelo hidrológico-hidrodinâmico continental quanto à representação de variáveis hidrológicas nas diferentes regiões da AS? Como o desempenho das vazões simuladas se compara ao de modelos de escala global na AS?

A fim de preencher esta lacuna existente foi realizada a preparação de um modelo hidrológico–hidrodinâmico para o domínio da América do Sul (MGB–SA). Este modelo foi construído com base em avanços recentes na simulação de grandes bacias sul americanas caracterizadas por extensos rios e planícies de inundáveis (e.g., Amazonas, La Plata), adaptação de técnicas de geoprocessamento para discretização de rios e minibacias, e uso combinado entre bases de dados globais, desde geometria de canais de drenagem até variáveis relacionadas ao ciclo hidrológico extraídas de produtos de sensoriamento remoto e renálises de modelos globais. O modelo foi discretizado com uma área de drenagem mínima de 1000 km² e trechos de rio de comprimento fixo de 15 km, utilizando a base de dados do MSWEP como forçante de precipitação. Esta pesquisa foi pioneira no contexto de modelagem hidrológico–hidrodinâmica totalmente acoplada (balanço hídrico vertical e propagação inercial de vazões) com domínio continental para a AS.

Uma validação extensiva do MGB–SA foi realizada com vazões observadas de diferentes centros hidrológicos da AS, além de séries temporais de níveis (in situ e altimetria por satélite), armazenamento terrestre de água da missão GRACE e evapotranspiração de múltiplas fontes (*Climate Data Record* – CDR). O modelo apresentou resultados satisfatórios em relação a medidas de desempenho na vazão em passo de tempo diário para a escala continental, onde foram observados valores de NSE (KGE) > 0,6 em 55 (70) % das estações analisadas (> 10 000 km²). O desempenho das vazões simuladas foi melhor em grandes rios e regiões úmidas, geralmente com coeficiente de escoamento (RC) entre 0,3–0,6. Por outro lado, o desempenho do modelo foi inferior em regiões de climas mais secos (RC < 0,3), com contribuição significativa de processos de neve (e.g., oeste da Argentina) ou onde a precipitação

possui grande influência da orografia (e.g, Cordilheira dos Andes). Na comparação entre níveis observados e simulados foram obtidos resultados razoáveis, com 50 % dos casos demonstrando diferenças no desvio padrão de amplitude < |30 %|. Adicionalmente, análises efetuadas com dados do GRACE e CDR indicaram que o modelo possui capacidade em representar padrões de sazonalidade e magnitude de evapotranspiração e variações nos estoques de água nas grandes bacias do continente. Estas fontes de dados complementares à vazão se mostraram úteis para mapear potenciais deficiências na estrutura e na calibração do modelo.

As vazões simuladas pelo MGB–SA em passo de tempo diário foram também comparadas àquelas simuladas por modelos globais. Este foi o primeiro estudo que promoveu, com número suficientemente grande de estações, uma intercomparação entre diferentes escalas de modelagem no domínio da AS. Ficou evidente que os modelos globais são bastante limitados em representar as vazões diárias, os quais obtiveram NSE negativos em cerca de 60 % das estações. Tomando-se como base a média dos modelos globais, identificada como a melhor estimativa entre estes, foram encontradas diferenças de viés absoluto > 60 % no leste e nordeste brasileiro, além de diferenças de timing de mais de 20 dias em rios governados por planície como o Amazonas e Paraguai. As diferenças de acurácia para a mediana dos postos também foram consideráveis, equivalendo a 0.91 para NSE e ~0.26 para KGE e log(NSE). As diferenças de desempenho foram em geral menores para regiões úmidas com menor presença de rios de baixa declividade. Adicionalmente, análises com o MGB–SA em configurações alternativas, i.e., com/sem calibração e com/sem propagação hidrodinâmica mostraram que estes dois fatores têm um papel importante para as diferenças observadas entre as escalas de modelagem, porém mesmo a versão não calibrada do MGB–SA (usando um conjunto único de parâmetros para todo o continente) apresentou um desempenho mediano superior ao dos modelos globais. Com base nestes resultados, entende-se que experiências prévias com modelagem regional (e.g., simulação de grandes bacias com diferentes características hidroclimáticas na região de interesse) é um fator chave para impulsionar a aplicação de modelos para maiores escalas.

Alguns aspectos sobre o custo computacional do MGB–SA também devem ser mencionados. Por exemplo, um período de 20 anos de simulação hidrológica com propagação hidrodinâmica na América do Sul leva aproximadamente 35 minutos (~1.75 min/ano) em um computador desktop Intel i9 9900K, de 3,6 GHz com 8 núcleos e 16 *threads*. Portanto, o MGB–SA na sua configuração atual pode ser considerado relativamente eficiente para uma gama de aplicações em escala continental. Salienta-se que o modelo vem atuando como uma importante

ferramenta para a iniciativa denominada SAMEWater (Paiva *et al.*, 2017), que visa estabelecer uma agenda de pesquisa voltada para América do Sul e que trata com diferentes tópicos relacionados a recursos hídricos. Algumas pesquisas com o MGB–SA já foram realizadas e publicadas no decorrer desta tese, dando contribuições em escala continental para o impacto de mudanças climáticas sobre recursos hídricos (Brêda *et al.*, 2020), avaliação da dinâmica e fluxos de sedimentos (Fagundes *et al.*, 2021), compreensão de eventos extremos cheias (Fleischmann *et al.*, 2020), simulação baseada em substituição de vazão em reservatórios (Passaia *et al.*, 2020), além da própria previsão hidrológica em médio prazo que foi abordada no presente trabalho. Outras pesquisas destinadas a avaliar maiores horizontes de previsão (sub-sazonal e sazonal), ou que buscam incorporar técnicas de assimilação de dados observados, também se encontram em fase de desenvolvimento com o MGB–SA.

- **Limitações e recomendações**

Nesta pesquisa foi desenvolvida uma primeira versão do modelo MGB–SA, que embora tenha cumprido o objetivo no contexto deste trabalho, possui diversas características que poderiam ser melhoradas. Por exemplo, a calibração foi realizada de forma manual sem o uso de algoritmos de otimização, associando os parâmetros a regiões delimitadas pela geologia local ao invés de conectá-los a subacias a montante dos postos fluviométricos, tradicionalmente feito em aplicações regionais do MGB (focadas na vazão somente). Archfield *et al.* (2015) argumentam que modelos aplicados na escala continental devem buscar uma representação explicita da variabilidade espacial dos parâmetros e atributos físicos. Nesse sentido, técnicas que visam regionalizar os parâmetros de acordo com características físicas para gerar campos consistentes no espaço (e.g., Samaniego *et al.*, 2017) e que buscam restringir a sua faixa de busca com variáveis do balanço hídrico estimadas a partir sensoriamento remoto (e.g., Rakovec *et al.*, 2016) poderiam ser investigadas buscando tornar mais consistente o procedimento de calibração. Ao mesmo tempo, bases de dados que foram desenvolvidas recentemente poderiam ser utilizadas para aprimorar aspectos hidráulicos do MGB–SA, como largura de rios (e.g., Allen and Pavelsky, 2018), topografia de planície (e.g., Yamazaki *et al.*, 2017) e delineamento de redes de drenagem (Yamazaki *et al.*, 2019).

Quanto à estrutura do modelo, melhorias poderiam ser implementadas para considerar o efeito de reservatórios com alta capacidade de regularização (e.g., em bacias como o Alto Paraná e São Francisco), ou também para considerar pequenos açudes em regiões com menor

disponibilidade hídrica (e.g., Nordeste brasileiro). Técnicas de representação explícita de reservatórios com modelagem hidrodinâmica foram recentemente desenvolvidas e aplicadas com sucesso no modelo MGB (Fleischmann *et al.*, 2019), e poderiam evoluir inclusive para uma aplicação continental. Além disso, atualmente o MGB–SA não conta com um módulo capaz de representar processos que envolvem derretimento e acúmulo de neve. Embora este último seja menos relevante se comparado a regiões como Europa e América do Norte (dada a área predominantemente tropical da AS), há importante contribuição da neve para o escoamento em bacias que drenam os Andes na região das latitudes médias (Pasquini and Depetris, 2007; Rivera *et al.*, 2017). Considerar este processo pode ser útil para compreender o papel da neve nos fluxos hidrológicos nesta escala de aplicação do modelo, como também para viabilizar a aplicação regional do MGB em bacias hidrográficas nas quais este processo pode ser relevante.

Apesar de terem sido exploradas relações entre a acurácia do MGB–SA e alguns aspectos como coeficiente de escoamento e área de drenagem, a relação entre o desempenho do modelo e outras características das bacias deveria ser melhor investigada. A avaliação da acurácia contra assinaturas hidrológicas (McMillan, 2021) e outros fatores como (mudanças no) uso e ocupação do solo, grau de regulação a montante por reservatórios, etc, poderia auxiliar na identificação de elementos relevantes para a modelagem e na quantificação do impacto destes elementos sobre as vazões simuladas. Cabe ressaltar ainda que no presente estudo não foi realizada nenhuma análise sobre potenciais problemas de estabilidade da propagação hidrodinâmica. Entende-se que algumas estratégias utilizadas na tese e que foram avaliadas posteriormente por Fan *et al.* (2021), como a adoção de um valor baixo para o parâmetro α (0.3) relacionado à condição CFL, e o uso de um limitador de Froude para forçar o escoamento em regime subcrítico, estariam contribuindo positivamente para a manutenção da estabilidade numérica do MGB–SA. Apesar de não terem sido detectados sinais de instabilidade do modelo nas vazões simuladas, mesmo para simulações mais longas do MGB–SA em relação ao período utilizado neste trabalho (e.g., Gama *et al.*, 2021), avaliações futuras poderiam ser realizadas para trazer maior clareza quanto a este aspecto.

Notadamente, estender o domínio do modelo MGB — que historicamente possui um foco regional — para um vasto continente como a América do Sul tem como consequência a amplificação das incertezas associadas. Portanto, um dos desafios que devem ser priorizados em trabalhos futuros é a investigação de métodos para estimar a incerteza na simulação hidrológica, a qual deve ser comunicada juntamente com as variáveis de saída (e.g., vazões,

níveis, área inundada, umidade de solo, etc) especialmente quando bases de dados forem desenvolvidas a partir do MGB–SA para amplo acesso do público. A quantificação das incertezas no MGB–SA é um ponto chave para que estimativas hidrológicas produzidas na escala continental possam dar suporte ao gerenciamento de recursos hídricos.

5.2. **Sobre o uso de previsões meteorológicas por conjunto para previsão de vazões em escala continental na América do Sul**

O uso de previsões meteorológicas por conjunto pode contribuir para o ganho de desempenho (destreza) nas previsões de vazão? Como a destreza da previsão varia geograficamente e nas principais bacias da AS? Como a destreza se relaciona com características climáticas e tamanho da bacia?

Na segunda etapa do trabalho, foi investigado o potencial de previsões de precipitação em contribuir para a destreza (*skill*) das previsões de vazão no horizonte de médio prazo (até 15 dias) na AS. Para isso, o modelo MGB–SA foi alimentado com dois cenários de previsão de chuva distintos: (i) previsões por conjunto advindas do modelo atmosférico do *European Center for Medium-range Weather Forecasting* (ECMWF) e (ii) previsões por conjunto geradas a partir de sequências de chuva reamostradas da série histórica (técnica denominada *Ensemble Streamflow Prediction*, ou ESP). As previsões de vazão foram então comparadas contra uma rodada de referência, gerada pela próprio MGB–SA forçado com a chuva observada do MSWEP. Deste modo, os resultados desta investigação proporcionaram uma visão abrangente sobre a destreza potencial das previsões de vazão na AS geradas através do acoplamento entre modelagem atmosférica por conjunto e modelagem hidrológica, simulando uma situação ideal em que este último modelo seria livre de erros.

Em um primeiro momento, observou-se que a chuva prevista do ECMWF apresentou destreza em relação à climatologia de chuva principalmente nas regiões mais ao leste e sudeste da AS. Por outro lado, praticamente não há destreza ao final do horizonte de médio prazo independente da estação do ano, com exceção de algumas áreas na região central do Brasil durante o inverno austral, onde os volumes de chuva são muito baixos. Em relação às previsões de vazão, notou-se que o padrão espacial da destreza foi similar ao da chuva prevista, porém houve um ganho de desempenho geral em relação ao ESP mesmo para antecedências de 15 dias como consequência dos processos de transformação chuva-vazão e propagação ao longo dos rios. Em bacias como o Uruguai, Alto Paraná, São Francisco, Tocantins–Araguaia e Parnaíba,

a destreza geralmente atinge um máximo por volta de 3–4 dias à frente, levando em consideração a mediana dos trechos de rio do modelo MGB–SA, diminuindo com a antecedência da previsão. Para estas bacias, a antecedência em que ocorre máxima destreza tende a aumentar de acordo com a área de drenagem.

No lado oeste da AS, sobretudo nas proximidades da Cordilheira dos Andes, as previsões de vazão baseadas no ECMWF apresentaram pouca ou nenhuma destreza na comparação com o ESP para as antecedências de 5, 10 e 15 dias. Em bacias que drenam (integral ou parcialmente) as áreas Andinas como Magdalena, Orinoco, Madeira e Paraguai, não foi identificado um padrão claro que relaciona área de drenagem e *skill*, uma vez que a destreza da previsão varia geograficamente de acordo com tributário analisado. Além disso, observou-se um viés condicional positivo nestas últimas bacias, onde as previsões de chuva por si só levam a probabilidades previstas consideravelmente maiores do que as frequências observadas (fator geralmente ≥ 2) para os eventos de vazões elevadas (> percentil 90 % de não-excedência da climatologia de vazões). Especificamente sobre a discriminação entre a ocorrência e não ocorrência destes eventos, foi observado maior destreza da previsão principalmente no sul do Brasil, com ganhos de desempenho também nas áreas ao leste da bacia do São Francisco. Por fim, ficou destacado que previsões de vazão baseadas na chuva prevista do ECMWF teriam maior destreza, tanto em termos de qualidade geral quanto capacidade de discriminação, em regiões da AS com clima temperado úmido. Uma possível explicação para a destreza observada neste tipo climátco é a i) baixa previsibilidade a partir da climatologia, devido à menor sazonalidade da precipitação em comparação a outras regiões e; ii) influência de sistemais frontais que podem ser melhor previstos por modelos atmosféricos em relação a eventos de natureza convectiva. É importante ressaltar que estes resultados não implicam que a acurácia ou a capacidade de discriminação de previsões de vazão baseadas em precipitação prevista por conjunto, em termos absolutos, sejam similares àqueles encontrados para a destreza. Os resultados apenas demonstram o ganho de desempenho que poderia ser obtido em relação a alternativas que não fazem uso destas previsões de chuva.

De uma maneira geral, os resultados indicaram que há vantagem em se usar previsões de precipitação por conjunto de modelos atmosféricos (no caso, do ECMWF) para gerar previsões de vazão na escala continental, se comparado ao uso de informações de precipitação baseadas apenas no conhecimento do passado. Um aspecto relevante para a pesquisa nacional é que este desempenho relativo tende a ser melhor no Brasil do que na maioria dos países

vizinhos do continente, o que motiva a realização de estudos que promovam o uso dessas previsões meteorológicas, não só na escala continental como também na escala regional.

- **Limitações e recomendações**

Uma limitação desta pesquisa é que não foi realizada correção de viés na chuva prevista do ECMWF. Entretanto, vale mencionar que a base de dados do MSWEP, apesar de ser um dos melhores produtos de chuva com consistência temporal e espacial (Beck *et al.*, 2017d), possui grandes incertezas. Isso é ainda mais importante no caso da cordilheira dos Andes, devido às elevadas altitudes, grande gradiente climático e insuficiência de estações para capturar a altíssima variabilidade espacial da precipitação (Condom *et al.*, 2020). A baixa cobertura de postos e a influência de processos orográficos para a formação de chuva são, reconhecidamente, fatores limitantes para estimativas por satélite em regiões com topografia complexa (Sun *et al.*, 2018). Por estas razões é esperada uma correlação mais baixa entre a previsão e as estimativas de chuva nestas áreas andinas, o que dificultaria a correção de viés e potencialmente traria menor ganho de desempenho. Cabe ressaltar também que, para correção de viés na escala continental, alguns estudos recentes sugerem que pode ser mais benéfico garantir consistência entre as observações e previsões meteorológicas (e.g., usar reanálise meteorológica como dado observado em tempo (quase) real juntamente com a previsão que é gerada pelo mesmo modelo atmosférico) do que usar chuva observada de uma fonte distinta, mesmo que mais acurada (Crochemore *et al.*, 2020). Pesquisas futuras poderiam investigar aspectos relacionados a estas considerações.

As análises efetuadas permitiram apenas inferir, de um modo geral, sobre a contribuição da chuva prevista para a destreza das previsões de vazão. Esta avaliação poderia ser ainda aprofundada, buscando investigar com mais detalhe as antecedências da previsão em que cada fonte de destreza é dominante (incluindo aquelas do modelo hidrológico). Ainda, sobre a avaliação de destreza na discriminação de ocorrência e não ocorrência de eventos, foram utilizados limiares que correspondem ao percentil 90 % de não-excedência da distribuição climatológica das vazões simuladas. Embora seja uma estratégia comumente adotada para aumentar o número de amostras na análise estatística, estes limiares podem ser relativamente baixos para caracterizar cheias em rios com alta variabilidade de vazões, porém altos no caso de rios onde o pulso da cheia é lento e unimodal. Há, portanto, uma necessidade de avaliar com mais detalhe os limiares utilizados para discriminação entre ocorrência e não ocorrência dos

eventos, bem como a própria sensibilidade das métricas para diferentes comportamentos hidrológicos dos rios sul americanos.

Para estudos que busquem avaliar a contribuição da chuva prevista para a previsão de vazões, especialmente em escalas de tempo maiores como sub-sazonal e sazonal, pode ser interessante utilizar abordagens do tipo ESP condicional. Por exemplo, seria possível reamostrar sequências temporais de chuva do período histórico selecionando apenas anos específicos, visando construir membros do *ensemble* cujas condições do passado seriam semelhantes ao estado atual da atmosfera/clima (e.g., índices ENSO, etc). De maneira similar, técnicas de correção poderiam ser aplicadas às previsões que são baseadas em modelos físicos, levando-se em conta a semelhança entre condições atmosféricas passadas e a presente a partir de um conjunto de previsões retrospectivas (*reforecasts*).

5.3. **Sobre o uso de pós-processamento sobre previsões de vazões por conjunto na escala continental**

Qual é o desempenho esperado de previsões de vazão pós-processadas em relação a previsões por conjunto brutas (cruas), na escala continental? Como o desempenho destas previsões de vazão se compara à de previsões mais simples, como climatologia e persistência das vazões observadas? É possível gerar trajetórias realísticas de previsão de vazão a partir de distribuições preditivas pós-processadas, considerando limitação de dados em tempo (quase) real?

A última etapa do trabalho consistiu em investigar sobre o uso de pós-processamento estatístico nas previsões de vazão por conjunto geradas em escala continental. O modelo MGB–SA foi alimentado por estimativas de chuva da base do MSWEP e *reforecasts* do ECMWF, que são previsões meteorológicas produzidas para muitos anos no passado com uma mesma versão do modelo atmosférico. Sobre as previsões de vazão resultantes foram aplicadas as técnicas (i) *Ensemble Model Output Statistics* (EMOS) para corrigir viés e erros de dispersão do conjunto, resultando em distribuições preditivas condicionais às previsões de vazão brutas e; (ii) *Ensemble Copula Coupling* (ECC) para recuperar a dependência temporal (i.e., ao longo das antecedências) das distribuições preditivas do EMOS. O ECC foi aplicado através de um esquema que mapeia os quantis do conjunto bruto para os quantis das densidades preditivas pós-processadas, denominado *transformation scheme* (ECC-T). Ambas previsões tiveram seus

desempenhos comparados aos da climatologia e persistência das vazões observadas. Este foi um trabalho pioneiro com o EMOS-ECC se considerada a escala espacial avaliada e, diferentemente dos trabalhos realizados na AS sobre previsão de vazão por conjunto baseada em modelagem hidrológica, o primeiro que se propôs a aplicar e avaliar o uso de pós-processamento estatístico para gerar distribuições preditivas condicionais com posterior derivação de trajetórias de previsão.

Através de uma análise de validação cruzada, identificou-se que em mais de 50 % dos postos avaliados e para todas antecedências entre 1 e 15 dias as previsões brutas apresentaram qualidade inferior à climatologia das vazões (i.e., sem destreza). No caso da avaliação destas previsões contra a persistência da última vazão observada, foi verificado que em 50 % das localidades as primeiras apresentaram destreza somente a partir de 10 dias à frente. Também observou-se que a consistência estatística entre as probabilidades previstas e as frequências observadas para as vazões foi muito baixa, para a qual o intervalo máximo do conjunto (entre o membro inferior e o membro superior) sem nenhum tipo de pós-processamento capturou, na mediana dos postos, menos do que 30 % das observações.

A aplicação do EMOS (pós-processamento univariado) permitiu uma melhoria substancial no desempenho das previsões de vazão. Na maioria das localidades avaliadas, as previsões pós-processadas exibiram destreza ao longo de todo o horizonte de médio prazo em relação à climatologia, ao passo que na comparação com a persistência as previsões apresentaram destreza a partir de uma antecedência de 4 dias para a mediana dos postos. Além disso, através do pós-processamento foi possível melhorar substancialmente a confiabilidade das previsões de vazão, isto é, possibilitando uma maior consistência entre as probabilidades do conjunto e as frequências observadas. Em geral, o EMOS teve um custo de ampliar a largura de incerteza em relação àquela estimada pelas previsões brutas, porém geralmente manteve esta banda de incerteza mais estreita (i.e., aguda) do que a distribuição climatológica das vazões observadas. Contudo, em rios cuja previsibilidade tende a ser dominada pelas condições iniciais hidrológicas (e.g., com influência de planícies), o pós-processamento foi menos efetivo para atribuir destreza às previsões de vazão.

O uso da técnica ECC-T (pós-processamento multivariado) possibilitou a extração de séries temporais (trajetórias) de vazão prevista a partir das distribuições preditivas do EMOS. Estas foram analisadas através de um critério de autocorrelação, onde foi observado um desempenho bastante variável para as localidades analisadas. A correlação serial das trajetórias

pós-processadas teve melhor concordância com aquela verificada para as previsões brutas principalmente na região leste da bacia do Prata (e.g., Alto Paraná e Uruguai), o que é um aspecto positivo dado o papel importante desta última para a produção de energia no contexto brasileiro. Por outro lado, as trajetórias de previsão de vazão obtidas com o ECC-T foram menos coerentes em condições de baixo espalhamento do conjunto bruto (e.g., Amazônia), especialmente quando este foi associado a uma grande largura de incerteza estimada pelo EMOS. Em geral, o desempenho do ECC-T foi menor quando a agudeza (*sharpness skill*) das previsões por conjunto brutas e pós-processadas com o EMOS foram, respectivamente, próximo de 1 e < 0.7 na primeira antecedência da previsão.

Quanto ao impacto das trajetórias pós-processadas sobre a qualidade das previsões, notou-se pouca diferença entre a destreza obtida com pós-processamento multivariado e aquela obtida apenas pela aplicação do EMOS, porém houve redução da confiabilidade das previsões principalmente para as antecedências menores, bem como uma tendência de redução de agudeza após a aplicação do ECC-T.

Também foi avaliado o desempenho do pós-processamento para diferentes faixas de vazão prevista. No caso do EMOS, observou-se que para vazões baixas a moderadas (< percentil 50 % de não-excedência) houve um desempenho similar ao verificado para todo o conjunto de verificação tanto para acurácia geral como para consistência estatística, ao passo que para vazões elevadas (> percentil 90 % de não-excedência) houve uma redução geral no desempenho das previsões. Em relação às trajetórias de previsão extraídas do EMOS, notou-se um desempenho superior (inferior) para vazões elevadas (baixas a moderadas) em comparação à análise com todos os dados de verificação.

Por fim, ficou demonstrado que outras fontes de incerteza além daquelas estimadas através da previsão meteorológica não devem ser negligenciadas no processo de geração de previsões de vazão na escala continental, e que o pós-processamento estatístico é uma estratégia viável para levar em conta estas incertezas mesmo para um grande número de localidades. Nesse sentido, os resultados obtidos nesta pesquisa sugerem que é possível obter previsões de vazão na escala continental com destreza e consistência probabilística no horizonte de médio prazo (15 dias), e que ao mesmo tempo sejam capazes de reduzir a incerteza em relação ao histórico de vazões observadas no passado. As técnicas utilizadas neste trabalho se mostraram satisfatórias considerando a limitação de dados em tempo (quase) real e a escala espacial abordada, e demonstram um caminho interessante de como as previsões de vazão geradas

através do acoplamento entre modelagem atmosférica e hidrológica poderiam ser tratadas em termos de estimativa de incerteza e moldadas (i.e., na forma de distribuições preditivas e traços de *ensemble*) para múltiplas finalidades na AS.

- **Limitações e recomendações**

Uma das limitações típicas do pós-processamento estatístico na previsão hidrológica é adoção da premissa de estacionariedade. Isso significa assumir que a correlação estatística entre os dados observados e as previsões brutas no período de ajuste é similar àquela do período de validação (Li *et al.*, 2017). Contudo, alguns estudos têm identificado tendências significativas nas séries de vazões de grande parte dos postos fluviométricos no Brasil (Chagas, 2019) e nas séries de vazões naturalizadas das usinas do SIN (Detzel *et al.*, 2011), o que pode levar a uma redução da efetividade do pós-processamento na estimativa da incerteza preditiva.

Outra limitação importante deste trabalho foi a não atualização ou ajuste das vazões simuladas do modelo hidrológico no instante de início de previsão. O motivo desta escolha foi simular uma condição com a menor necessidade possível de tratamento de dados em tempo real, o que seria mais próximo das condições técnicas atuais para um sistema de previsão de vazões com escala continental para a AS. Por outro lado, espera-se que o uso de técnicas como assimilação de dados ou outras formas de correção de saídas do modelo que façam uso das observações mais recentes possam reduzir a banda de incerteza nos instantes iniciais de previsão, bem como em antecedências maiores no caso de rios com propagação mais lenta. Isto poderia contribuir positivamente para a geração de traços de *ensemble* realísticos em locais onde houve maior discrepância entre as funções de autocorrelação da previsão bruta e pós-processada. Ainda, em um ambiente operacional as correções efetuadas com observações recentes poderiam atenuar, em parte, perdas de desempenho potencialmente associadas à não estacionariedade de vazões. Assim, propõe-se que sejam investigados os potenciais benefícios de uso conjunto entre as técnicas supracitadas e pós-processadores como o EMOS e o ECC em trabalhos futuros.

Um dos *benchmarks* utilizados para avaliar a destreza da previsão gerada pelo MGB–SA foi a persistência da última vazão observada. Este *benchmark* poderia ser substituído por um modelo do tipo autorregressivo (AR) simples, cuja acurácia seria mais dificil de ser superada em locais ou condições específicas (e.g., recessão do hidrograma) para os quais a autocorrelação da série de vazões tende a dominar o sinal da previsão. Este mesmo modelo AR

pode ser usado inclusive para corrigir, isto é, aproximar cada um dos membros de previsão de vazão por conjunto à vazão observada nos instantes iniciais da previsão.

Adicionalmente, algumas limitações foram identificadas no pós-processamento em virtude da propagação inercial do MGB–SA em grandes reservatórios. Nestes casos, há influência da cota da lâmina de água sobre as elevações do MDE e consequente superestimativa da área e volume da planície na curva hipsométrica do modelo, o que por sua vez induz atenuação e atraso nas vazões simuladas. Este efeito tem um impacto direto na qualidade do pós-processamento univariado e na derivação dos traços de *ensemble* com o ECC-T, uma vez que provoca subespalhamento excessivo nas previsões de vazão por conjunto. Tal efeito deve ser removido (e.g., com uma correção artificial na relação cota-área do MGB) antes da geração das previsões cruas, especialmente se vazões naturalizadas forem utilizadas para calibração do EMOS.

Recomenda-se que outros experimentos com pós-processamento sejam realizados em estudos futuros. Sugere-se avaliar o desempenho do EMOS em relação ao número de amostras utilizada para treinamento, por exemplo, utilizando apenas a data de calendário das *reforecasts* ao invés do período trimestral (DJF, MAM...) que foi adotado neste trabalho. Adicionalmente, poderia ser avaliada a sensibilidade dos limites de truncamento para as vazões mínima e máxima na distribuição normal do EMOS, buscando-se adotar valores mais coerentes com os diferentes comportamentos hidrológicos dos rios sul americanos. Métodos estatísticos baseados em análise de frequência de extremos poderiam servir para a definição destes limites de truncamento, muito embora sejam mais sensíveis ao número de anos disponíveis na série de dados observados.

Dentre as fatores importantes relacionados à geração de previsões para um sistema interligado como o SIN está não somente a representação adequada da autocorrelação das séries de vazão prevista, mas também a correlação espacial entre as usinas (Alexandre, 2012). Neste sentido, seria recomendável realizar análises complementares que busquem avaliar se estas correlações no espaço estão sendo adequadamente capturadas. Com relação as trajetórias de previsão, sugere-se uma avaliação mais detalhada para identificar se a sazonalidade vai estar interferindo ou não nas funções de autocorrelação (ACF), mesmo se considerada a diferenciação com lag de 1 dia para as séries de vazão prevista bruta e pós-processada com o ECC.

Também pode ser investigado se existe algum padrão espacial dos parâmetros estimados para o EMOS ao longo da rede de drenagem do MGB–SA, de tal forma que o pós-processamento estatístico possa ser aplicado para gerar distribuições preditivas inclusive em locais sem dados observados. Neste sentido, algumas estratégias estatísticas poderiam ser aplicadas para interpolar os parâmetros do EMOS no espaço, por exemplo, através de abordagens que envolvem inferência Bayesiana e/ou krigagem (e.g., Lima *et al.*, 2021; Skøien *et al.*, 2021). Outras técnicas de pós-processamento univariado, bem como variantes do método ECC, também poderiam ser testadas e comparadas.

Referências

ABAZA, M. et al. On the incidence of meteorological and hydrological processors: Effect of resolution, sharpness and reliability of hydrological ensemble forecasts. **Journal of Hydrology,** v. 555, p. 371-384, 2017.

ABBASPOUR, K. C. et al. A continental-scale hydrology and water quality model for Europe: Calibration and uncertainty of a high-resolution large-scale SWAT model. **Journal of Hydrology,** v. 524, p. 733-752, 2015.

ALEXANDRE, A. M. B. **Previsão de vazões mensais para o Sistema Interligado Nacional utilizando informações climáticas**. 2012. 291 f. Tese (Doutorado em Engenharia Civil) - Departamento de Engenharia Hidráulica e Ambiental, Universidade do Ceará, Fortaleza, 2012.

ALFIERI, L. et al. GloFAS-global ensemble streamflow forecasting and flood early warning. **Hydrology and Earth System Sciences,** v. 17, n. 3, p. 1161-1175, 2013.

ALFIERI, L. et al. A global network for operational flood risk reduction. **Environmental Science and Policy,** v. 84, p. 149-158, 2018.

ALFIERI, L. et al. A global streamflow reanalysis for 1980–2018. **Journal of Hydrology X,** v. 6, p. 100049, 2020.

ALFIERI, L. et al. Evaluation of ensemble streamflow predictions in Europe. **Journal of Hydrology,** v. 517, p. 913-922, 2014.

ALFIERI, L. et al. Operational early warning systems for water-related hazards in Europe. **Environmental Science & Policy,** v. 21, p. 35-49, 2012.

ALFIERI, L. et al. Range-dependent thresholds for global flood early warning. **Journal of Hydrology X,** v. In Press, p. Article 100034, 2019.

ALIZADEH, B. et al. Multiscale Postprocessor for Ensemble Streamflow Prediction for Short to Long Ranges. **Journal of Hydrometeorology,** v. 21, n. 2, p. 265-285, 2020.

ALKAMA, R. et al. Global evaluation of the ISBA-TRIP continental hydrological system. Part I: Comparison to GRACE terrestrial water storage estimates and in situ river discharges. **Journal of Hydrometeorology,** v. 11, n. 3, p. 583-600, 2010.

ALLASIA, D. G. et al. Large basin simulation experience in South America. *In*: IAHS-AISH Publication, 303, 2006**Anais.** p.360-370.

ALLEN, G. H.; PAVELSKY, T. M. Global extent of rivers and streams. **Science,** v. 361, n. 6402, p. 585, 2018.

ALSDORF, D. et al. Spatial and temporal complexity of the Amazon flood measured from space. **Geophysical Research Letters,** v. 34, n. 8, 2007.

ANDERSON, J. L. A method for producing and evaluating probabilistic forecasts from ensemble model integrations. **Journal of Climate,** v. 9, n. 7, p. 1518-1530, 1996.

ANDREADIS, K. M.; SCHUMANN, G. J. P.; PAVELSKY, T. A simple global river bankfull width and depth database. **Water Resources Research,** v. 49, n. 10, p. 7164-7168, 2013.

ANGARITA, H. et al. Basin-scale impacts of hydropower development on the Mompós Depression wetlands, Colombia. **Hydrology and Earth System Sciences,** v. 22, n. 5, p. 2839-2865, 2018.

ANTICO, A.; TORRES, M. E.; DIAZ, H. F. Contributions of different time scales to extreme Paraná floods. **Climate Dynamics,** v. 46, n. 11, p. 3785-3792, 2016.

ARCHFIELD, S. A. et al. Accelerating advances in continental domain hydrologic modeling. **Water Resources Research,** v. 51, n. 12, p. 10078-10091, 2015.

ARNAL, L. et al. Skilful seasonal forecasts of streamflow over Europe? **Hydrology and Earth System Sciences,** v. 22, n. 4, p. 2057-2072, 2018.

ARNELL, N. W.; GOSLING, S. N. The impacts of climate change on river flood risk at the global scale. **Climatic Change,** v. 134, n. 3, p. 387-401, 2016.

BAKKER, M. H. N. Transboundary river floods: examining countries, international river basins and continents. **Water Policy,** v. 11, n. 3, p. 269-288, 2009.

BALSAMO, G. et al. ERA-Interim/Land: a global land surface reanalysis data set. **Hydrol. Earth Syst. Sci.,** v. 19, n. 1, p. 389-407, 2015.

BALSAMO, G. et al. A Revised Hydrology for the ECMWF Model: Verification from Field Site to Terrestrial Water Storage and Impact in the Integrated Forecast System. **Journal of Hydrometeorology,** v. 10, n. 3, p. 623-643, 2009.

BARAN, S.; HEMRI, S.; EL AYARI, M. Statistical Postprocessing of Water Level Forecasts Using Bayesian Model Averaging With Doubly Truncated Normal Components. **Water Resources Research,** v. 55, n. 5, p. 3997-4013, 2019.

BARAN, S.; NEMODA, D. Censored and shifted gamma distribution based EMOS model for probabilistic quantitative precipitation forecasting. **Environmetrics,** v. 27, n. 5, p. 280-292, 2016.

BARROS, V.; CLARKE, R.; DIAS, P. S. Climate change in the La Plata basin. **Publication of the Inter-American Institute for Global Change Research (IAI), São José dos Campos, Brazil**, 2006.

BARTHOLMES, J. C. et al. The european flood alert system EFAS - Part 2: Statistical skill assessment of probabilistic and deterministic operational forecasts. **Hydrology and Earth System Sciences,** v. 13, n. 2, p. 141-153, 2009.

BATES, P. D.; HORRITT, M. S.; FEWTRELL, T. J. A simple inertial formulation of the shallow water equations for efficient two-dimensional flood inundation modelling. **Journal of Hydrology,** v. 387, n. 1-2, p. 33-45, 2010.

BAUGH, C. A. et al. SRTM vegetation removal and hydrodynamic modeling accuracy. **Water Resources Research,** v. 49, n. 9, p. 5276-5289, 2013.

BECK, H. et al. MSWEP: 3-hourly 0.1° fully global precipitation (1979-present) by merging gauge, satellite, and weather model data. *In*: EGU General Assembly Conference Abstracts, 2017a**Anais.** p.18289.

BECK, H. E. et al. Global evaluation of runoff from 10 state-of-the-art hydrological models. **Hydrology and Earth System Sciences,** v. 21, n. 6, p. 2881-2903, 2017b.

BECK, H. E. et al. MSWEP: 3-hourly 0.25º; global gridded precipitation (1979-2015) by merging gauge, satellite, and reanalysis data. **Hydrology and Earth System Sciences,** v. 21, n. 1, p. 589-615, 2017c.

BECK, H. E. et al. Global-scale evaluation of 22 precipitation datasets using gauge observations and hydrological modeling. **Hydrology and Earth System Sciences,** v. 21, p. 6201-6217, 2017d.

BECK, H. E. et al. MSWEP V2 Global 3-Hourly 0.1° Precipitation: Methodology and Quantitative Assessment. **Bulletin of the American Meteorological Society,** v. 100, n. 3, p. 473-500, 2019.

BEIGHLEY, R. E. et al. Simulating hydrologic and hydraulic processes throughout the Amazon River Basin. **Hydrological Processes,** v. 23, n. 8, p. 1221-1235, 2009.

BEIGHLEY, R. E.; GUMMADI, V. Developing channel and floodplain dimensions with limited data: A case study in the Amazon Basin. **Earth Surface Processes and Landforms,** v. 36, n. 8, p. 1059-1071, 2011.

BELLIER, J.; BONTRON, G.; ZIN, I. Using Meteorological Analogues for Reordering Postprocessed Precipitation Ensembles in Hydrological Forecasting. **Water Resources Research,** v. 53, n. 12, p. 10085-10107, 2017a.

BELLIER, J.; ZIN, I.; BONTRON, G. Sample stratification in verification of ensemble forecasts of continuous scalar variables: Potential benefits and pitfalls. **Monthly Weather Review,** v. 145, n. 9, p. 3529-3544, 2017b.

_____. Generating Coherent Ensemble Forecasts After Hydrological Postprocessing: Adaptations of ECC-Based Methods. **Water Resources Research,** v. 54, n. 8, p. 5741-5762, 2018.

BEN BOUALLÈGUE, Z. et al. Generation of Scenarios from Calibrated Ensemble Forecasts with a Dual-Ensemble Copula-Coupling Approach. **Monthly Weather Review,** v. 144, n. 12, p. 4737-4750, 2016.

BENNETT, J. C. et al. A System for Continuous Hydrological Ensemble Forecasting (SCHEF) to lead times of 9days. **Journal of Hydrology,** v. 519, n. PD, p. 2832-2846, 2014.

BENNETT, J. C. et al. Reliable long-range ensemble streamflow forecasts: Combining calibrated climate forecasts with a conceptual runoff model and a staged error model. **Water Resources Research,** v. 52, n. 10, p. 8238-8259, 2016.

BERBERY, E. H.; BARROS, V. R. The hydrologic cycle of the La Plata basin in South America. **Journal of Hydrometeorology,** v. 3, n. 6, p. 630-645, 2002.

BERRY, P. A. M.; GARLICK, J. D.; SMITH, R. G. Near-global validation of the SRTM DEM using satellite radar altimetry. **Remote Sensing of Environment,** v. 106, n. 1, p. 17-27, 2007.

BERTHET, L. et al. A crash-testing framework for predictive uncertainty assessment when forecasting high flows in an extrapolation context. **Hydrol. Earth Syst. Sci.,** v. 24, n. 4, p. 2017-2041, 2020.

BIERKENS, M. F. P. Global hydrology 2015: State, trends, and directions. **Water Resources Research,** v. 51, n. 7, p. 4923-4947, 2015.

BIERKENS, M. F. P. et al. Hyper-resolution global hydrological modelling: what is next? **Hydrological Processes,** v. 29, n. 2, p. 310-320, 2015.

BIONDI, D.; TODINI, E. Comparing Hydrological Postprocessors Including Ensemble Predictions Into Full Predictive Probability Distribution of Streamflow. **Water Resources Research,** v. 54, n. 12, p. 9860-9882, 2018.

BISCHINIOTIS, K. et al. Evaluation of a global ensemble flood prediction system in Peru. **Hydrological Sciences Journal,** v. 64, n. 10, p. 1171-1189, 2019.

BLACUTT, L. A. et al. Precipitation comparison for the CFSR, MERRA, TRMM3B42 and Combined Scheme datasets in Bolivia. **Atmospheric Research,** v. 163, p. 117-131, 2015.

BOGNER, K.; LIECHTI, K.; ZAPPA, M. Post-Processing of Stream Flows in Switzerland with an Emphasis on Low Flows and Floods. **Water,** v. 8, n. 4, p. 115, 2016.

BOGNER, K.; PAPPENBERGER, F. Multiscale error analysis, correction, and predictive uncertainty estimation in a flood forecasting system. **Water Resources Research,** v. 47, n. 7, 2011.

BOUCHER, M.-A.; ROULIN, E.; FORTIN, V. Short-Range Ensemble Forecast Post-processing. *In*: DUAN, Q.;PAPPENBERGER, F.*, et al* (Ed.). **Handbook of Hydrometeorological Ensemble Forecasting**. Berlin, Heidelberg: Springer Berlin Heidelberg, 2018. p.1-25. ISBN 978-3-642-40457-3.

BOUCHER, M. A. et al. A comparison between ensemble and deterministic hydrological forecasts in an operational context. **Adv. Geosci.,** v. 29, p. 85-94, 2011.

BOUCHER, M. A. et al. Exploratory analysis of statistical post-processing methods for hydrological ensemble forecasts. **Hydrological Processes,** v. 29, n. 6, p. 1141-1155, 2015.

BOUCHER, M. A. et al. Hydro-economic assessment of hydrological forecasting systems. **Journal of Hydrology,** v. 416-417, p. 133-144, 2012.

BOUGEAULT, P. et al. The thorpex interactive grand global ensemble. **Bulletin of the American Meteorological Society,** v. 91, n. 8, p. 1059-1072, 2010.

BRAVO, J. M. et al. Coupled Hydrologic-Hydraulic Modeling of the Upper Paraguay River Basin. **Journal of Hydrologic Engineering,** v. 17, n. 5, p. 635-646, 2012.

BRÊDA, J. P. L. F. et al. Climate change impacts on South American water balance from a continental-scale hydrological model driven by CMIP5 projections. **Climatic Change,** v. 159, n. 4, p. 503-522, 2020.

BRÖCKER, J.; SMITH, L. A. Increasing the reliability of reliability diagrams. **Weather and Forecasting,** v. 22, n. 3, p. 651-661, 2007.

BROWN, J. D. et al. Verification of temperature, precipitation, and streamflow forecasts from the NOAA/NWS Hydrologic Ensemble Forecast Service (HEFS): 2. Streamflow verification. **Journal of Hydrology,** v. 519, n. PD, p. 2847-2868, 2014.

BUIZZA, R. et al. Probabilistic predictions of precipitation using the ECMWF Ensemble Prediction System. **Weather and Forecasting,** v. 14, n. 2, p. 168-189, 1999.

BUIZZA, R. et al. A comparison of the ECMWF, MSC, and NCEP global ensemble prediction systems. **Monthly Weather Review,** v. 133, n. 5, p. 1076-1097, 2005.

BUIZZA, R.; LEUTBECHER, M. The forecast skill horizon. **Quarterly Journal of the Royal Meteorological Society,** v. 141, n. 693, p. 3366-3382, 2015.

BUTT, M. A.; MARAGOS, P. Optimum design of Chamfer distance transforms. **IEEE Transactions on Image Processing,** v. 7, n. 10, p. 1477-1484, 1998.

CAI, W. et al. Climate impacts of the El Niño–Southern Oscillation on South America. **Nature Reviews Earth & Environment,** v. 1, n. 4, p. 215-231, 2020.

CALVETTI, L.; PEREIRA FILHO, A. J. Ensemble Hydrometeorological Forecasts Using WRF Hourly QPF and TopModel for a Middle Watershed. **Advances in Meteorology,** v. 2014, p. 484120, 2014.

CAMILLONI, I.; BARROS, V. R. The Paraná River Response to El Niño 1982-83 and 1997-98 Events. **Journal of Hydrometeorology,** v. 1, n. 5, p. 412-430, 2000.

CANDOGAN YOSSEF, N. et al. Skill of a global forecasting system in seasonal ensemble streamflow prediction. **Hydrol. Earth Syst. Sci.,** v. 21, n. 8, p. 4103-4114, 2017.

CARABAJAL, C. C.; HARDING, D. J. ICESat validation of SRTM C-band digital elevation models. **Geophysical Research Letters,** v. 32, n. 22, p. 5, 2005.

CASAGRANDE, L. et al. Early flood warning in the Itajai-Acu River basin using numerical weather forecasting and hydrological modeling. **Natural Hazards,** v. 88, n. 2, p. 741-757, 2017.

CASSAGNOLE, M. et al. Impact of the quality of hydrological forecasts on the management and revenue of hydroelectric reservoirs-a conceptual approach. **Hydrology and Earth System Sciences,** v. 25, n. 2, p. 1033-1052, 2021.

CHAGAS, V. B. P. **Mudanças nos regimes de chuva e vazão no Brasil, de 1980 a 2015**. 2019. 156 f. Dissertação (Mestrado em Engenharia Ambiental) - Programa de Pós-Graduação em Engenharia Ambiental, Universidade Federal de Santa Catarina, Florianópolis, 2019.

CHEN, H. et al. Hydraulic correction method (HCM) to enhance the efficiency of SRTM DEM in flood modeling. **Journal of Hydrology,** v. 559, p. 56-70, 2018.

CHEN, J. L. et al. Patagonia icefield melting observed by gravity recovery and climate experiment (GRACE). **Geophysical Research Letters,** v. 34, n. 22, 2007.

CHRISTOFFERSEN, B. O. et al. Mechanisms of water supply and vegetation demand govern the seasonality and magnitude of evapotranspiration in Amazonia and Cerrado. **Agricultural and Forest Meteorology,** v. 191, p. 33-50, 2014.

CLARK, E. A. et al. Continental Runoff into the Oceans (1950-2008). **Journal of Hydrometeorology,** v. 16, n. 4, p. 1502-1520, 2015.

CLARK, M. et al. The Schaake shuffle: A method for reconstructing space-time variability in forecasted precipitation and temperature fields. **Journal of Hydrometeorology,** v. 5, n. 1, p. 243-262, 2004.

CLOKE, H. L.; PAPPENBERGER, F. Ensemble flood forecasting: A review. **Journal of Hydrology,** v. 375, n. 3-4, p. 613-626, 2009.

CLOKE, H. L. et al. How do i know if I've improved my continental scale flood early warning system? **Environmental Research Letters,** v. 12, n. 4, 2017.

COCCIA, G.; TODINI, E. Recent developments in predictive uncertainty assessment based on the model conditional processor approach. **Hydrology and Earth System Sciences,** v. 15, n. 10, p. 3253-3274, 2011.

COLLISCHONN, W. **Simulação Hidrológica de Grandes Bacias**. 2001. 270 f. Tese (Doutorado em Recursos Hídricos e Saneamento Ambiental) - Instituto de Pesquisas Hidráulicas, Universidade Federal do Rio Grande do Sul, Porto Alegre

COLLISCHONN, W. et al. The MGB-IPH model for large-scale rainfall-runoff modelling. **Hydrological Sciences Journal-Journal Des Sciences Hydrologiques,** v. 52, n. 5, p. 878-895, 2007a.

COLLISCHONN, W. et al. Forecasting River Uruguay flow using rainfall forecasts from a regional weather-prediction model. **Journal of Hydrology,** v. 305, n. 1-4, p. 87-98, 2005.

COLLISCHONN, W. et al. Medium-range reservoir inflow predictions based on quantitative precipitation forecasts. **Journal of Hydrology,** v. 344, n. 1-2, p. 112-122, 2007b.

CONDOM, T. et al. Climatological and Hydrological Observations for the South American Andes: In situ Stations, Satellite, and Reanalysis Data Sets. **Frontiers in Earth Science,** v. 8, n. 92, 2020.

COSTA, A. C.; BRONSTERT, A.; DE ARAÚJO, J. C. A channel transmission losses model for different dryland rivers. **Hydrology and Earth System Sciences,** v. 16, n. 4, p. 1111-1135, 2012.

COSTA, A. C. et al. Analysis of channel transmission losses in a dryland river reach in north-eastern Brazil using streamflow series, groundwater level series and multi-temporal satellite data. **Hydrological Processes,** v. 27, n. 7, p. 1046-1060, 2013.

COSTA, F. S.; MACEIRA, M. E. P.; DAMÁZIO, J. M. Modelos de previsão hidrológica aplicados ao planejamento da operação do sistema elétrico brasileiro. **Revista Brasileira de Recursos Hídricos,** v. 12, n. 3, p. 21-30, 2007.

CROCHEMORE, L.; RAMOS, M.-H.; PECHLIVANIDIS, I. G. Can Continental Models Convey Useful Seasonal Hydrologic Information at the Catchment Scale? **Water Resources Research,** v. 56, n. 2, p. e2019WR025700, 2020.

CROCHEMORE, L. et al. Seasonal streamflow forecasting by conditioning climatology with precipitation indices. **Hydrology and Earth System Sciences,** v. 21, n. 3, p. 1573-1591, 2017.

CROOKS, S. M. et al. From Catchment to National Scale Rainfall-Runoff Modelling: Demonstration of a Hydrological Modelling Framework. **Hydrology,** v. 1, n. 1, p. 63-88, 2014.

CUNGE, J.; HOLLY, F. M.; VERWEY, A. **Practical aspects of computational river hydraulics**. London: Pitman Publishing Ltd., 1980. 420p ISBN 978-0273084426.

DAVID, C. H. et al. River network routing on the NHDPlus dataset. **Journal of Hydrometeorology,** v. 12, n. 5, p. 913-934, 2011.

DAVID, C. H.; YANG, Z. L.; HONG, S. Regional-scale river flow modeling using off-the-shelf runoff products, thousands of mapped rivers and hundreds of stream flow gauges. **Environmental Modelling and Software,** v. 42, p. 116-132, 2013.

DE ALMEIDA, G. A. M.; BATES, P. Applicability of the local inertial approximation of the shallow water equations to flood modeling. **Water Resources Research,** v. 49, n. 8, p. 4833-4844, 2013.

DE ALMEIDA, G. A. M. et al. Improving the stability of a simple formulation of the shallow water equations for 2-D flood modeling. **Water Resources Research,** v. 48, n. 5, 2012.

DE ROO, A. P. J.; WESSELING, C. G.; VAN DEURSEN, W. P. A. Physically based river basin modelling within a GIS: The LISFLOOD model. **Hydrological Processes,** v. 14, n. 11-12, p. 1981-1992, 2000.

DECHARME, B. et al. A new river flooding scheme for global climate applications: Off-line evaluation over South America. **Journal of Geophysical Research-Atmospheres,** v. 113, n. D11, p. 11, 2008.

DELLE MONACHE, L. et al. Probabilistic aspects of meteorological and ozone regional ensemble forecasts. **Journal of Geophysical Research-Atmospheres,** v. 111, n. D24, 2006.

DEMARGNE, J. et al. The Science of NOAA's Operational Hydrologic Ensemble Forecast Service. **Bulletin of the American Meteorological Society,** v. 95, n. 1, p. 79-98, 2014.

DEMARIA, E. M. C. et al. Evaluation of mesoscale convective systems in South America using multiple satellite products and an object-based approach. **Journal of Geophysical Research Atmospheres,** v. 116, n. 8, 2011.

DETZEL, D. H. M. et al. Estacionariedade das afluências às usinas hidrelétricas brasileiras. **Revista Brasileira de Recursos Hídricos,** v. 16, n. 3, p. 95-111, 2011.

DIAS, J. et al. Equatorial waves and the skill of NCEP and ECMWF numerical weather prediction systems. **Monthly Weather Review,** v. 146, n. 6, p. 1763-1784, 2018a.

DIAS, V. S. et al. An overview of hydropower reservoirs in Brazil: Current situation, future perspectives and impacts of climate change. **Water (Switzerland),** v. 10, n. 5, 2018b.

DINKU, T. et al. Evaluating detection skills of satellite rainfall estimates over desert locust recession regions. **Journal of Applied Meteorology and Climatology,** v. 49, n. 6, p. 1322-1332, 2010a.

DINKU, T. et al. Validation and intercomparison of satellite rainfall estimates over Colombia. **Journal of Applied Meteorology and Climatology,** v. 49, n. 5, p. 1004-1014, 2010b.

DIRMEYER, P. A. et al. GSWP-2: Multimodel Analysis and Implications for Our Perception of the Land Surface. **Bulletin of the American Meteorological Society,** v. 87, n. 10, p. 1381-1398, 2006.

DOGULU, N. et al. Estimation of predictive hydrologic uncertainty using the quantile regression and UNEEC methods and their comparison on contrasting catchments. **Hydrol. Earth Syst. Sci.,** v. 19, n. 7, p. 3181-3201, 2015.

DOLL, P.; FIEDLER, K.; ZHANG, J. Global-scale analysis of river flow alterations due to water withdrawals and reservoirs. **Hydrology and Earth System Sciences,** v. 13, n. 12, p. 2413-2432, 2009.

DONNELLY, C.; ANDERSSON, J. C. M.; ARHEIMER, B. Using flow signatures and catchment similarities to evaluate the E-HYPE multi-basin model across Europe. **Hydrological Sciences Journal-Journal Des Sciences Hydrologiques,** v. 61, n. 2, p. 255-273, 2016.

DUAN, Q. Y. et al. Multi-model ensemble hydrologic prediction using Bayesian model averaging. **Advances in Water Resources,** v. 30, n. 5, p. 1371-1386, 2007.

DURR, H. H.; MEYBECK, M.; DURR, S. H. Lithologic composition of the Earth's continental surfaces derived from a new digital map emphasizing riverine material transfer. **Global Biogeochemical Cycles,** v. 19, n. 4, 2005.

DUTRA, E. et al. **Report on the improved Water Resources Reanalysis (WRR-2)**. Deltares, p.94. 2017. (D.5.2)

EISNER, S. et al. An ensemble analysis of climate change impacts on streamflow seasonality across 11 large river basins. **Climatic Change,** v. 141, n. 3, p. 401-417, 2017.

EMERTON, R. et al. Developing a global operational seasonal hydro-meteorological forecasting system: G1oFAS-Seasonal v1.0. **Geoscientific Model Development,** v. 11, n. 8, p. 3327-3346, 2018.

EMERTON, R. E.; STEPHENS, E. M.; CLOKE, H. L. What is the most useful approach for forecasting hydrological extremes during El Niño? **Environmental Research Communications,** v. 1, n. 3, p. 031002, 2019.

EMERTON, R. E. et al. Continental and global scale flood forecasting systems. **Wiley Interdisciplinary Reviews: Water,** v. 3, n. 3, p. 391-418, 2016.

ENGELAND, K.; STEINSLAND, I. Probabilistic postprocessing models for flow forecasts for a system of catchments and several lead times. **Water Resources Research,** v. 50, n. 1, p. 182-197, 2014.

EPE. **Considerações sobre a Expansão Hidrelétrica nos Estudos de Planejamento Energético de Longo Prazo**. Empresa de Pesquisa Energética. Brasília, p.19p. 2018

ERFANIAN, A.; WANG, G.; FOMENKO, L. Unprecedented drought over tropical South America in 2016: Significantly under-predicted by tropical SST. **Scientific Reports,** v. 7, n. 1, 2017.

ESPINOZA, J. C. et al. Rainfall hotspots over the southern tropical Andes: Spatial distribution, rainfall intensity, and relations with large-scale atmospheric circulation. **Water Resources Research,** v. 51, n. 5, p. 3459-3475, 2015.

ESPINOZA, J. C. et al. The extreme 2014 flood in south-western Amazon basin: The role of tropical-subtropical South Atlantic SST gradient. **Environmental Research Letters,** v. 9, n. 12, 2014.

ESPINOZA, J. C. et al. The new historical flood of 2021 in the Amazon River compared to major floods of the 21st century: Atmospheric features in the context of the intensification of floods. **Weather and Climate Extremes,** v. 35, 2022.

ESPINOZA, J. C. et al. The Major Floods in the Amazonas River and Tributaries (Western Amazon Basin) during the 1970-2012 Period: A Focus on the 2012 Flood. **Journal of Hydrometeorology,** v. 14, n. 3, p. 1000-1008, 2013.

ESPINOZA VILLAR, J. C. et al. Spatio-temporal rainfall variability in the Amazon basin countries (Brazil, Peru, Bolivia, Colombia, and Ecuador). **International Journal of Climatology,** v. 29, n. 11, p. 1574-1594, 2009.

FAGUNDES, H. O. et al. Sediment Flows in South America Supported by Daily Hydrologic-Hydrodynamic Modeling. **Water Resources Research,** v. 57, n. 2, p. e2020WR027884, 2021.

FAN, F. M. **Previsão por conjunto de vazões afluentes a reservatórios em grandes bacias hidrográficas brasileiras**. 2015. 424 f. Tese (Doutorado em Recursos Hídricos e Saneamento Ambiental) - Instituto de Pesquisas Hidráulicas, Universidade Federal do Rio Grande do Sul, Porto Alegre, 2015.

FAN, F. M. et al. Um mapa de unidades de resposta hidrológica para a América do Sul. *In*: XXI Simpósio Brasileiro de Recursos Hídricos, 2015a, Brasilia. **Anais.**: ABRH. p.PAP019919.

FAN, F. M. et al. Ensemble streamflow forecasting experiments in a tropical basin: The Sao Francisco river case study. **Journal of Hydrology,** v. 519, p. 2906-2919, 2014.

FAN, F. M. et al. Flood forecasting on the Tocantins River using ensemble rainfall forecasts and real-time satellite rainfall estimates. **Journal of Flood Risk Management,** v. 9, n. 3, p. 278-288, 2016a.

FAN, F. M.; PAIVA, R. C. D.; COLLISCHONN, W. Hydrological Forecasting Practices in Brazil. *In*: ADAMS, T. E. e PAGANO, T. C. (Ed.). **Flood Forecasting: A Global Perspective**. 1ed: Elsevier, v.1, 2016b. p.41-66. ISBN 978-0-12-801884-2.

FAN, F. M. et al. Evaluation of upper Uruguay river basin (Brazil) operational flood forecasts. **Revista Brasileira De Recursos Hidricos,** v. 22, 2017.

FAN, F. M. et al. Performance of Deterministic and Probabilistic Hydrological Forecasts for the Short-Term Optimization of a Tropical Hydropower Reservoir. **Water Resources Management,** v. 30, n. 10, p. 3609-3625, 2016c.

FAN, F. M. et al. Verification of inflow into hydropower reservoirs using ensemble forecasts of the TIGGE database for large scale basins in Brazil. **Journal of Hydrology-Regional Studies,** v. 4, p. 196-227, 2015b.

FAN, F. M. et al. On the discretization of river networks for large scale hydrologic-hydrodynamic models. **RBRH,** v. 26, p. e5, 2021.

FARR, T. G. et al. The Shuttle Radar Topography Mission. **Reviews of Geophysics,** v. 45, n. 2, 2007.

FERRO, C. A. T.; RICHARDSON, D. S.; WEIGEL, A. P. On the effect of ensemble size on the discrete and continuous ranked probability scores. **Meteorological Applications,** v. 15, n. 1, p. 19-24, 2008.

FLEISCHMANN, A. et al. Modeling the role of reservoirs versus floodplains on large-scale river hydrodynamics. **Natural Hazards,** v. 99, n. 2, p. 1075-1104, 2019.

FLEISCHMANN, A. S. et al. Modeling hydrologic and hydrodynamic processes in basins with semi-arid wetlands. **Journal of Hydrology**, 2018.

FLEISCHMANN, A. S. et al. The great 1983 floods in South American large rivers: a continental hydrological modelling approach. **Hydrological Sciences Journal,** v. 65, n. 8, p. 1358-1373, 2020.

FLUET-CHOUINARD, E. et al. Development of a global inundation map at high spatial resolution from topographic downscaling of coarse-scale remote sensing data. **Remote Sensing of Environment,** v. 158, p. 348-361, 2015.

FORTIN, V. et al. Why Should Ensemble Spread Match the RMSE of the Ensemble Mean? **Journal of Hydrometeorology,** v. 15, n. 4, p. 1708-1713, 2014.

FRALEY, C.; RAFTERY, A. E.; GNEITING, T. Calibrating multimodel forecast ensembles with exchangeable and missing members using Bayesian model averaging. **Monthly Weather Review,** v. 138, n. 1, p. 190-202, 2010.

FRAPPART, F. et al. Surface Freshwater Storage Variations in the Orinoco Floodplains Using Multi-Satellite Observations. **Remote Sensing,** v. 7, n. 12, p. 89-110, 2014.

FUNDEL, F.; ZAPPA, M. Hydrological ensemble forecasting in mesoscale catchments: Sensitivity to initial conditions and value of reforecasts. **Water Resources Research,** v. 47, n. 9, 2011.

GAMA, C. H. A.; PAIVA, R. C. D.; COLLISCHONN, W. Reanálise hidrológica: assimilação de dados aplicada à modelagem da América do Sul: resultados preliminares. *In*: XXIV Simpósio Brasileiro de Recursos Hídricos (SBRH), 24, 2021, Belo Horizonte. **Anais.** Porto Alegre: ABRHidro, 2021. p.1-8.

GARCIA, N. O.; MECHOSO, C. R. Variability in the discharge of South American rivers and in climate. **Hydrological Sciences Journal-Journal Des Sciences Hydrologiques,** v. 50, n. 3, p. 459-478, 2005.

GARREAUD, R. D. The Andes climate and weather. **Adv. Geosci.,** v. 22, p. 3-11, 2009.

GARREAUD, R. D.; ACEITUNO, P. Atmospheric circulation and climatic variability. *In*: VEBLEN, T. T.;YOUNG, K. R., *et al* (Ed.). **The physical geography of South America**. 1.ed. Oxford, England: Oxford University Press, 2007. p.45-59.

GARREAUD, R. D. et al. Present-day South American climate. **Palaeogeography Palaeoclimatology Palaeoecology,** v. 281, n. 3-4, p. 180-195, 2009.

GETIRANA, A. et al. Rivers and Floodplains as Key Components of Global Terrestrial Water Storage Variability. **Geophysical Research Letters,** v. 44, n. 20, p. 10,359-10,368, 2017a.

GETIRANA, A. et al. Trade-off between cost and accuracy in large-scale surface water dynamic modeling. **Water Resources Research,** v. 53, n. 6, p. 4942-4955, 2017b.

GETIRANA, A. C. V. Integrating spatial altimetry data into the automatic calibration of hydrological models. **Journal of Hydrology,** v. 387, n. 3-4, p. 244-255, 2010.

GETIRANA, A. C. V. et al. The Hydrological Modeling and Analysis Platform (HyMAP): Evaluation in the Amazon Basin. **Journal of Hydrometeorology,** v. 13, n. 6, p. 1641-1665, 2012.

GETIRANA, A. C. V. et al. Automatic parameterization of a flow routing scheme driven by radar altimetry data: Evaluation in the Amazon basin. **Water Resources Research,** v. 49, n. 1, p. 614-629, 2013.

GETIRANA, A. C. V.; PAIVA, R. C. D. Mapping large-scale river flow hydraulics in the Amazon Basin. **Water Resources Research,** v. 49, n. 5, p. 2437-2445, 2013.

GNEITING, T.; BALABDAOUI, F.; RAFTERY, A. E. Probabilistic forecasts, calibration and sharpness. **Journal of the Royal Statistical Society Series B-Statistical Methodology,** v. 69, p. 243-268, 2007.

GNEITING, T. et al. Calibrated probabilistic forecasting using ensemble model output statistics and minimum CRPS estimation. **Monthly Weather Review,** v. 133, n. 5, p. 1098-1118, 2005.

GOLNARAGHI, M. et al. **Atlas of Mortality and Economic Losses from Weather, Climate, and Water Extremes (1970-2012)**. Geneva, Switzerland: World Meteorological Organization, 2014. 46p ISBN 978-92-63-11123-4.

GONCALVES, H. C.; MERCANTE, M. A.; SANTOS, E. T. Hydrological cycle. **Brazilian Journal of Biology,** v. 71, n. 1, p. 241-253, 2011.

GOSLING, S. N. et al. A comparative analysis of projected impacts of climate change on river runoff from global and catchment-scale hydrological models. **Hydrology and Earth System Sciences,** v. 15, n. 1, p. 279-294, 2011.

GOTETI, G.; FAMIGLIETTI, J. S.; ASANTE, K. A Catchment-Based Hydrologic and Routing Modeling System with explicit river channels. **Journal of Geophysical Research Atmospheres,** v. 113, n. 14, 2008.

GOUWELEEUW, B. T. et al. Flood forecasting using medium-range probabilistic weather prediction. **Hydrol. Earth Syst. Sci.,** v. 9, n. 4, p. 365-380, 2005.

GREUELL, W.; FRANSSEN, W. H. P.; HUTJES, R. W. A. Seasonal streamflow forecasts for Europe - Part 2: Sources of skill. **Hydrology and Earth System Sciences,** v. 23, n. 1, p. 371-391, 2019.

GRIMM, A. M.; TEDESCHI, R. G. ENSO and Extreme Rainfall Events in South America. **Journal of Climate,** v. 22, n. 7, p. 1589-1609, 2009.

GUDMUNDSSON, L. et al. Comparing Large-Scale Hydrological Model Simulations to Observed Runoff Percentiles in Europe. **Journal of Hydrometeorology,** v. 13, n. 2, p. 604-620, 2012.

GUHA-SAPIR, D.; BELOW, R.; HOYOIS, P. **EM-DAT: International disaster database**. Brussels, Belgium: Université Catholique de Louvain 2018.

GUILHON, L. G. F.; ROCHA, V. F.; MOREIRA, J. C. Comparação de métodos de previsão de vazões naturais afluentes a aproveitamentos hidroelétricos. **Revista Brasileira de Recursos Hídricos,** v. 12, n. 3, p. 13-20, 2007.

GUNTNER, A.; BRONSTERT, A. Representation of landscape variability and lateral redistribution processes for large-scale hydrological modelling in semi-arid areas. **Journal of Hydrology,** v. 297, n. 1-4, p. 136-161, 2004.

GUSWA, A. J.; CELIA, M. A.; RODRIGUEZ-ITURBE, I. Models of soil moisture dynamics in ecohydrology: A comparative study. **Water Resources Research,** v. 38, n. 9, 2002.

HADDELAND, I. et al. Multimodel Estimate of the Global Terrestrial Water Balance: Setup and First Results. **Journal of Hydrometeorology,** v. 12, n. 5, p. 869-884, 2011.

HAMILL, T. M.; WHITAKER, J. S.; MULLEN, S. L. Reforecasts: An important dataset for improving weather predictions. **Bulletin of the American Meteorological Society,** v. 87, n. 1, p. 33-46, 2006.

HAMILTON, S. K.; SIPPEL, S. J.; MELACK, J. M. Comparison of inundation patterns among major South American floodplains. **Journal of Geophysical Research-Atmospheres,** v. 107, n. D20, 2002.

HANASAKI, N. et al. A global hydrological simulation to specify the sources of water used by humans. **Hydrology and Earth System Sciences,** v. 22, n. 1, p. 789-817, 2018.

HARRIGAN, S. et al. Daily ensemble river discharge reforecasts and real-time forecasts from the operational Global Flood Awareness System. **Hydrol. Earth Syst. Sci. Discuss.,** v. 2020, p. 1-22, 2020.

HATTERMANN, F. F. et al. Sources of uncertainty in hydrological climate impact assessment: a cross-scale study. **Environmental Research Letters,** v. 13, n. 1, 2018.

HEMRI, S.; KLEIN, B. Analog-Based Postprocessing of Navigation-Related Hydrological Ensemble Forecasts. **Water Resources Research,** v. 53, n. 11, p. 9059-9077, 2017.

HEMRI, S.; LISNIAK, D.; KLEIN, B. Multivariate postprocessing techniques for probabilistic hydrological forecasting. **Water Resources Research,** v. 51, n. 9, p. 7436-7451, 2015.

HERR, H. D.; KRZYSZTOFOWICZ, R. Bayesian ensemble forecast of river stages and ensemble size requirements. **Journal of Hydrology,** v. 387, n. 3-4, p. 151-164, 2010.

_____. Ensemble Bayesian forecasting system Part I: Theory and algorithms. **Journal of Hydrology,** v. 524, p. 789-802, 2015.

HERSBACH, H. Decomposition of the continuous ranked probability score for ensemble prediction systems. **Weather and Forecasting,** v. 15, n. 5, p. 559-570, 2000.

HIRABAYASHI, Y. et al. Global flood risk under climate change. **Nature Climate Change,** v. 3, n. 9, p. 816-821, 2013.

HIRPA, F. A. et al. The Effect of Reference Climatology on Global Flood Forecasting. **Journal of Hydrometeorology,** v. 17, n. 4, p. 1131-1145, 2016.

HOBOUCHIAN, M. P. et al. Assessment of satellite precipitation estimates over the slopes of the subtropical Andes. **Atmospheric Research,** v. 190, p. 43-54, 2017.

HODGES, B. R. Challenges in Continental River Dynamics. **Environmental Modelling & Software,** v. 50, p. 16-20, 2013.

HOPSON, T. M.; WEBSTER, P. J. A 1–10-Day Ensemble Forecasting Scheme for the Major River Basins of Bangladesh: Forecasting Severe Floods of 2003–07. **Journal of Hydrometeorology,** v. 11, n. 3, p. 618-641, 2010.

HOUSTON, J. Variability of precipitation in the Atacama Desert: Its causes and hydrological impact. **International Journal of Climatology,** v. 26, n. 15, p. 2181-2198, 2006.

HOYOS, N. et al. Impact of the 2010-2011 La Nina phenomenon in Colombia, South America: The human toll of an extreme weather event. **Applied Geography,** v. 39, p. 16-25, 2013.

HUANG, S. et al. Evaluation of an ensemble of regional hydrological models in 12 large-scale river basins worldwide. **Climatic Change,** v. 141, n. 3, p. 381-397, 2016.

HUMPHREY, V.; GUDMUNDSSON, L.; SENEVIRATNE, S. I. Assessing Global Water Storage Variability from GRACE: Trends, Seasonal Cycle, Subseasonal Anomalies and Extremes. **Surv Geophys,** v. 37, p. 357-395, 2016.

JACKS, E. et al. **Guidelines on early warning systems and application of nowcasting and warning operations**. World Meteorological Organization p.22. 2010

JANOWIAK, J. E. et al. An evaluation of precipitation forecasts from operational models and reanalyses including precipitation variations associated with MJO activity. **Monthly Weather Review,** v. 138, n. 12, p. 4542-4560, 2010.

JARIHANI, A. A. et al. Where does all the water go? Partitioning water transmission losses in a data-sparse, multi-channel and low-gradient dryland river system using modelling and remote sensing. **Journal of Hydrology,** v. 529, p. 1511-1529, 2015.

JARVIS, A. et al. **Hole-filled SRTM for the globe : version 4 : data grid**: CGIAR Consortium for Spatial Information 2008.

JAUN, S.; AHRENS, B. Evaluation of a probabilistic hydrometeorological forecast system. **Hydrology and Earth System Sciences,** v. 13, n. 7, p. 1031-1043, 2009.

JENSON, S. K.; DOMINGUE, J. O. Extracting topographic structure from digital elevation data for geographic information system analysis. **Photogrammetric Engineering and Remote Sensing,** v. 54, n. 11, p. 1593-1600, 1988.

JOLLIFFE, I. T.; STEPHENSON, D. B. **Forecast verification: a practitioner's guide in atmospheric science**. John Wiley & Sons, 2012. 254 ISBN 1119961076.

JUNK, C. et al. Comparison and Combination of Regional and Global Ensemble Prediction Systems for Probabilistic Predictions of Hub-Height Wind Speed. **Weather and Forecasting,** v. 30, n. 5, p. 1234-1253, 2015.

KALNAY, E. **Atmospheric modeling, data assimilation and predictability**. Cambridge University Press, 2003. 341 ISBN 0521791790.

KAUFFELDT, A. et al. Technical review of large-scale hydrological models for implementation in operational flood forecasting schemes on continental level. **Environmental Modelling & Software,** v. 75, p. 68-76, 2016.

KERR, Y. H. et al. The SMOS soil moisture retrieval algorithm. **IEEE Transactions on Geoscience and Remote Sensing,** v. 50, n. 5 PART 1, p. 1384-1403, 2012.

KIDD, C.; DAWKINS, E.; HUFFMAN, G. Comparison of precipitation derived from the ecmwf operational forecast model and satellite precipitation datasets. **Journal of Hydrometeorology,** v. 14, n. 5, p. 1463-1482, 2013.

KIRCHNER, J. W. Getting the right answers for the right reasons: Linking measurements, analyses, and models to advance the science of hydrology. **Water Resources Research,** v. 42, n. 3, 2006.

KLEIN, B.; HEMRI, S. **R package hydemos - Probabilistic Forecasting using EMOS:** Provides S4 classes and methods for the estimation of the predictive uncertainty of hydrological water level and flow simulations and forecasts using Ensemble Model Output Statistics EMOS p. 2017.

KLEIN, B. et al. Predictive uncertainty estimation of hydrological multi-model ensembles using pair-copula construction. **Water (Switzerland),** v. 8, n. 4, 2016.

KLING, H.; FUCHS, M.; PAULIN, M. Runoff conditions in the upper Danube basin under an ensemble of climate change scenarios. **Journal of Hydrology,** v. 424-425, p. 264-277, 2012.

KOTTEK, M. et al. World map of the Köppen-Geiger climate classification updated. **Meteorologische Zeitschrift,** v. 15, n. 3, p. 259-263, 2006.

KRYSANOVA, V. et al. Intercomparison of regional-scale hydrological models and climate change impacts projected for 12 large river basins worldwide - A synthesis. **Environmental Research Letters,** v. 12, n. 10, 2017.

KRZYSZTOFOWICZ, R. Bayesian theory of probabilistic forecasting via deterministic hydrologic model. **Water Resources Research,** v. 35, n. 9, p. 2739-2750, 1999.

KRZYSZTOFOWICZ, R.; KELLY, K. S. Hydrologic uncertainty processor for probabilistic river stage forecasting. **Water Resources Research,** v. 36, n. 11, p. 3265-3277, 2000.

KUPPEL, S. et al. What does it take to flood the Pampas?: Lessons from a decade of strong hydrological fluctuations. **Water Resources Research,** v. 51, n. 4, p. 2937-2950, 2015.

LANDERER, F. W.; SWENSON, S. C. Accuracy of scaled GRACE terrestrial water storage estimates. **Water Resources Research,** v. 48, p. 11, 2012.

LATRUBESSE, E. M. Large rivers, megafans and other Quaternary avulsive fluvial systems: A potential "who's who" in the geological record. **Earth-Science Reviews,** v. 146, p. 1-30, 2015.

LATRUBESSE, E. M.; STEVAUX, J. C.; SINHA, R. Tropical rivers. **Geomorphology,** v. 70, n. 3-4 SPEC. ISS., p. 187-206, 2005.

LAVERS, D. A. et al. A vision for improving global flood forecasting. **Environmental Research Letters,** v. 14, n. 12, p. 121002, 2019.

LAVERS, D. A. et al. A Vision for Hydrological Prediction. **Atmosphere,** v. 11, n. 3, p. 237, 2020.

LEHNER, B.; DÖLL, P. Development and validation of a global database of lakes, reservoirs and wetlands. **Journal of Hydrology,** v. 296, n. 1-4, p. 1-22, 2004.

LEHNER, B.; GRILL, G. Global river hydrography and network routing: baseline data and new approaches to study the world's large river systems. **Hydrological Processes,** v. 27, n. 15, p. 2171-2186, 2013.

LEHNER, B.; VERDIN, K.; JARVIS, A. New global hydrography derived from spaceborne elevation data. **Eos,** v. 89, n. 10, p. 93-94, 2008.

LEOPOLD, L. B.; MADDOCK, T. J. **The hydraulic geometry of stream channels and some physiographic implications**. U.S. Geological Survey Professional Paper, 252, p.56p. 1953

LEUTBECHER, M. et al. Stochastic representations of model uncertainties at ECMWF: state of the art and future vision. **Quarterly Journal of the Royal Meteorological Society,** v. 143, n. 707, p. 2315-2339, 2017.

LEUTBECHER, M.; PALMER, T. N. Ensemble forecasting. **Journal of Computational Physics,** v. 227, n. 7, p. 3515-3539, 2008.

LI, W. T. et al. A review on statistical postprocessing methods for hydrometeorological ensemble forecasting. **Wiley Interdisciplinary Reviews-Water,** v. 4, n. 6, 2017.

LI, Y. et al. Application of Remote Sensing Data to Constrain Operational Rainfall-Driven Flood Forecasting: A Review. **Remote Sensing,** v. 8, n. 6, p. 456, 2016.

LIEBMANN, B. et al. Submonthly Convective Variability over South America and the South Atlantic Convergence Zone. **Journal of Climate,** v. 12, n. 7, p. 1877-1891, 1999.

LIEBMANN, B. et al. Subseasonal Variations of Rainfall in South America in the Vicinity of the Low-Level Jet East of the Andes and Comparison to Those in the South Atlantic Convergence Zone. **Journal of Climate,** v. 17, n. 19, p. 3829-3842, 2004.

LIMA, C. H. R.; KWON, H.-H.; KIM, Y.-T. A Bayesian Kriging model applied for spatial downscaling of daily rainfall from GCMs. **Journal of Hydrology,** v. 597, p. 126095, 2021.

LININGER, K. B.; LATRUBESSE, E. M. Flooding hydrology and peak discharge attenuation along the middle Araguaia River in central Brazil. **Catena,** v. 143, p. 90-101, 2016.

LÓPEZ LÓPEZ, P. et al. Alternative configurations of quantile regression for estimating predictive uncertainty in water level forecasts for the upper Severn River: a comparison. **Hydrol. Earth Syst. Sci.,** v. 18, n. 9, p. 3411-3428, 2014.

LOPEZ, P. L. et al. Calibration of a large-scale hydrological model using satellite-based soil moisture and evapotranspiration products. **Hydrology and Earth System Sciences,** v. 21, n. 6, p. 3125-3144, 2017.

LORENZ, E. N. Deterministic Nonperiodic Flow. **Journal of Atmospheric Sciences,** v. 20, n. 2, p. 130-141, 1963.

LU, C. et al. Scale-dependent uncertainties in global QPFs and QPEs from NWP model and satellite fields. **Journal of Hydrometeorology,** v. 11, n. 1, p. 139-155, 2010.

LUDWIG, K.; BREMICKER, M. **The water balance model LARSIM – design, content and applications**. Germany: Institut für Hydrologie, Uni Freiburg i, 2006.

LUO, X. Y. et al. Modeling surface water dynamics in the Amazon Basin using MOSART-Inundation v1.0: impacts of geomorphological parameters and river flow representation. **Geoscientific Model Development,** v. 10, n. 3, p. 1233-1259, 2017.

MADADGAR, S.; MORADKHANI, H. Improved Bayesian multimodeling: Integration of copulas and Bayesian model averaging. **Water Resources Research,** v. 50, n. 12, p. 9586-9603, 2014.

MADADGAR, S.; MORADKHANI, H.; GAREN, D. Towards improved post-processing of hydrologic forecast ensembles. **Hydrological Processes,** v. 28, n. 1, p. 104-122, 2014.

MAEDA, E. E. et al. Evapotranspiration seasonality across the Amazon Basin. **Earth System Dynamics,** v. 8, n. 2, p. 439-454, 2017.

MAIDMENT, D. R. **Arc Hydro: GIS for water resources**. Redlands, California: ESRI, Inc., 2002. ISBN 1589480341.

MANTAS, V. M. et al. Validation of TRMM multi-satellite precipitation analysis (TMPA) products in the Peruvian Andes. **Atmospheric Research,** v. 163, p. 132-145, 2015.

MARENGO, J. A.; ESPINOZA, J. C. Extreme seasonal droughts and floods in Amazonia: causes, trends and impacts. **International Journal of Climatology,** v. 36, n. 3, p. 1033-1050, 2016.

MARENGO, J. A. et al. Future change of temperature and precipitation extremes in south america as derived from the precis regional climate modeling system. **International Journal of Climatology,** v. 29, n. 15, p. 2241-2255, 2009.

MARENGO, J. A. et al. Recent developments on the South American monsoon system. **International Journal of Climatology,** v. 32, n. 1, p. 1-21, 2012a.

MARENGO, J. A. et al. The drought of Amazonia in 2005. **Journal of Climate,** v. 21, n. 3, p. 495-516, 2008.

MARENGO, J. A. et al. Extreme climatic events in the Amazon basin. **Theoretical and Applied Climatology,** v. 107, n. 1-2, p. 73-85, 2012b.

MARENGO, J. A.; TORRES, R. R.; ALVES, L. M. Drought in Northeast Brazil—past, present, and future. **Theoretical and Applied Climatology,** v. 129, n. 3-4, p. 1189-1200, 2017.

MARTZ, L. W.; GARBRECHT, J. The treatment of flat areas and depressions in automated drainage analysis of raster digital elevation models. **Hydrological Processes,** v. 12, n. 6, p. 843-855, 1998.

MATEO, C. M. R. et al. Impacts of spatial resolution and representation of flow connectivity on large-scale simulation of floods. **Hydrology and Earth System Sciences,** v. 21, n. 10, p. 5143-5163, 2017.

MATTE, S. et al. Moving beyond the cost-loss ratio: Economic assessment of streamflow forecasts for a risk-Averse decision maker. **Hydrology and Earth System Sciences,** v. 21, n. 6, p. 2967-2986, 2017.

MCINERNEY, D. et al. Improving probabilistic prediction of daily streamflow by identifying Pareto optimal approaches for modeling heteroscedastic residual errors. **Water Resources Research,** v. 53, n. 3, p. 2199-2239, 2017.

MCMILLAN, H. K. A review of hydrologic signatures and their applications. **Wiley Interdisciplinary Reviews: Water,** v. 8, n. 1, 2021.

MEADE, R. H. et al. Backwater effects in the Amazon River basin of Brazil. **Environmental Geology and Water Sciences,** v. 18, n. 2, p. 105-114, 1991.

MEDINA, H. et al. Comparing GEFS, ECMWF, and postprocessing methods for ensemble precipitation forecasts over Brazil. **Journal of Hydrometeorology,** v. 20, n. 4, p. 773-790, 2019.

MEKONNEN, M. M. et al. Sustainability, efficiency and equitability of water consumption and pollution in Latin America and the Caribbean. **Sustainability,** v. 7, n. 2, p. 2086-2112, 2015.

MELLER, A. et al. Previsão de cheias por conjunto em curto prazo. **Revista Brasileira de Recursos Hidricos,** v. 19, n. 3, p. 33-49, 2014.

MELO, D. D. D. et al. Reservoir storage and hydrologic responses to droughts in the Parana River basin, south-eastern Brazil. **Hydrology and Earth System Sciences,** v. 20, n. 11, p. 4673-4688, 2016.

MESINGER, F. et al. An upgraded version of the Eta model. **Meteorology and Atmospheric Physics,** v. 116, n. 3-4, p. 63-79, 2012.

MIRALLES, D. G. et al. Magnitude and variability of land evaporation and its components at the global scale. **Hydrology and Earth System Sciences,** v. 15, n. 3, p. 967-981, 2011.

MIZUKAMI, N. et al. Towards seamless large-domain parameter estimation for hydrologic models. **Water Resources Research,** v. 53, n. 9, p. 8020-8040, 2017.

MIZUKAMI, N. et al. MizuRoute version 1: A river network routing tool for a continental domain water resources applications. **Geoscientific Model Development,** v. 9, n. 6, p. 2223-2228, 2016.

MOLTENI, F. et al. The ECMWF Ensemble Prediction System: Methodology and validation. **Quarterly Journal of the Royal Meteorological Society,** v. 122, n. 529, p. 73-119, 1996.

MONTANARI, A.; GROSSI, G. Estimating the uncertainty of hydrological forecasts: A statistical approach. **Water Resources Research,** v. 44, n. 12, 2008.

MOORE, R. J.; BELL, V. A.; JONES, D. A. Forecasting for flood warning. **Comptes Rendus - Geoscience,** v. 337, n. 1-2, p. 203-217, 2005.

MULLER SCHMIED, H. et al. Sensitivity of simulated global-scale freshwater fluxes and storages to input data, hydrological model structure, human water use and calibration. **Hydrology and Earth System Sciences,** v. 18, n. 9, p. 3511-3538, 2014.

MULUYE, G. Y. Implications of medium-range numerical weather model output in hydrologic applications: Assessment of skill and economic value. **Journal of Hydrology,** v. 400, n. 3, p. 448-464, 2011.

MUÑOZ-SABATER, J. et al. ERA5-Land: A state-of-the-art global reanalysis dataset for land applications. **Earth System Science Data**, in preparation.

NAUMANN, G. et al. Dynamics of socioeconomic exposure, vulnerability and impacts of recent droughts in Argentina. **Geosciences (Switzerland),** v. 9, n. 1, 2019.

NEAL, J.; SCHUMANN, G.; BATES, P. A subgrid channel model for simulating river hydraulics and floodplain inundation over large and data sparse areas. **Water Resources Research,** v. 48, n. 11, 2012.

NEW, M. et al. A high-resolution data set of surface climate over global land areas. **Climate Research,** v. 21, n. 1, p. 1-25, 2002.

NOGUÉS-PAEGLE, J.; MO, K. C. Alternating Wet and Dry Conditions over South America during Summer. **Monthly Weather Review,** v. 125, n. 2, p. 279-291, 1997.

NUNES, L. H. An overview of recent natural disasters in South America. **Meddedelingen der Zittingen (Bulletin des Seances),** v. 57, p. 409-425, 2011.

O'LOUGHLIN, F. E. et al. A multi-sensor approach towards a global vegetation corrected SRTM DEM product. **Remote Sensing of Environment,** v. 182, p. 49-59, 2016.

OLIVEIRA, P. D. et al. The operation of Flood Control in Large Hydroelectric Power Systems – The Brazilian Experience. *In*: IFCM6 - 6th International Conference on Flood Management, 2014a, São Paulo. **Anais.**: ABRH. p.1-11.

OLIVEIRA, P. T. S. et al. Trends in water balance components across the Brazilian Cerrado. **Water Resources Research,** v. 50, n. 9, p. 7100-7114, 2014b.

OLIVEIRA, V. G.; LIMA, C. H. R. Multiscale streamflow forecasts for the Brazilian hydropower system using bayesian model averaging (BMA). **Revista Brasileira de Recursos Hidricos,** v. 21, n. 3, p. 618-635, 2016.

OLSSON, J.; LINDSTRÖM, G. Evaluation and calibration of operational hydrological ensemble forecasts in Sweden. **Journal of Hydrology,** v. 350, n. 1-2, p. 14-24, 2008.

ORME, A. R. Tectonism, climate and landscape change. *In*: VEBLEN, T. T.;YOUNG, K. R., *et al* (Ed.). **The physical geography of South America**. 1.ed. Oxford, England: Oxford University Press, 2007. p.23-44. ISBN 0195313410.

OVANDO, A. et al. Extreme flood events in the Bolivian Amazon wetlands. **Journal of Hydrology: Regional Studies,** v. 5, p. 293-308, 2016.

PAGANO, T. C. et al. Ensemble dressing for hydrological applications. **Hydrological Processes,** v. 27, n. 1, p. 106-116, 2013.

PAGANO, T. C. et al. Challenges of operational river forecasting. **Journal of Hydrometeorology,** v. 15, n. 4, p. 1692-1707, 2014.

PAIVA, R. C. D. et al. Large-scale hydrologic and hydrodynamic modeling of the Amazon River basin. **Water Resources Research,** v. 49, n. 3, p. 1226-1243, 2013a.

PAIVA, R. C. D. et al. On the sources of hydrological prediction uncertainty in the Amazon. **Hydrology and Earth System Sciences,** v. 16, n. 9, p. 3127-3137, 2012a.

PAIVA, R. C. D. et al. On the sources of hydrological prediction uncertainty in the Amazon. **Hydrology and Earth System Sciences,** v. 16, n. 9, p. 3127-3137, 2012b.

PAIVA, R. C. D. et al. Assimilating in situ and radar altimetry data into a large-scale hydrologic-hydrodynamic model for streamflow forecast in the Amazon. **Hydrology and Earth System Sciences,** v. 17, n. 7, p. 2929-2946, 2013b.

PAIVA, R. C. D.; COLLISCHONN, W.; BUARQUE, D. C. Validation of a full hydrodynamic model for large-scale hydrologic modelling in the Amazon. **Hydrological Processes,** v. 27, n. 3, p. 333-346, 2013c.

PAIVA, R. C. D.; COLLISCHONN, W.; TUCCI, C. E. M. Large scale hydrologic and hydrodynamic modeling using limited data and a GIS based approach. **Journal of Hydrology,** v. 406, n. 3-4, p. 170-181, 2011.

PAIVA, R. C. D. D. et al. SAMEWATER: Uma agenda de pesquisa integrada da hidrologia da América do Sul. *In*: XXII Simpósio Brasileiro de Recursos Hídricos (SBRH), 22, 2017, Florianópolis. **Anais.** Porto Alegre: ABRH, 2017. p.1-8.

PAPPENBERGER, F. et al. Cascading model uncertainty from medium range weather forecasts (10 days) through a rainfall-runoff model to flood inundation predictions within the European Flood Forecasting System (EFFS). **Hydrology and Earth System Sciences,** v. 9, n. 4, p. 381-393, 2005.

PAPPENBERGER, F. et al. Global runoff routing with the hydrological component of the ECMWF NWP system. **International Journal of Climatology,** v. 30, n. 14, p. 2155-2174, 2010.

PAPPENBERGER, F. et al. The monetary benefit of early flood warnings in Europe. **Environmental Science and Policy,** v. 51, p. 278-291, 2015a.

PAPPENBERGER, F. et al. How do I know if my forecasts are better? Using benchmarks in hydrological ensemble prediction. **Journal of Hydrology,** v. 522, p. 697-713, 2015b.

PAPPENBERGER, F.; THIELEN, J.; DEL MEDICO, M. The impact of weather forecast improvements on large scale hydrology: analysing a decade of forecasts of the European Flood Alert System. **Hydrological Processes,** v. 25, n. 7, p. 1091-1113, 2011.

PARIS, A. et al. Stage-discharge rating curves based on satellite altimetry and modeled discharge in the Amazon basin. **Water Resources Research,** v. 52, n. 5, p. 3787-3814, 2016.

PARUELO, J. M. et al. The Grasslands and Steppes of Patagonia and the Río de La Plata Plains. *In*: VEBLEN, T. T.;YOUNG, K. R., *et al* (Ed.). **The physical geography of South America**. 1ed. Oxford, England: Oxford University Press, 2007. p.232-248.

PASQUINI, A. I.; DEPETRIS, P. J. Discharge trends and flow dynamics of South American rivers draining the southern Atlantic seaboard: An overview. **Journal of Hydrology,** v. 333, n. 2-4, p. 385-399, 2007.

PASSAIA, O. A. et al. Impact of large reservoirs on simulated discharges of Brazilian rivers. **RBRH,** v. 25, 2020.

PAZ, A. R.; COLLISCHONN, W. River reach length and slope estimates for large-scale hydrological models based on a relatively high-resolution digital elevation model. **Journal of Hydrology,** v. 343, n. 3-4, p. 127-139, 2007.

PAZ, A. R. et al. The influence of vertical water balance on modelling Pantanal (Brazil) spatio-temporal inundation dynamics. **Hydrological Processes,** v. 28, n. 10, p. 3539-3553, 2014.

PAZ, A. R.; COLLISCHONN, W.; LOPES DA SILVEIRA, A. L. Improvements in large-scale drainage networks derived from digital elevation models. **Water Resources Research,** v. 42, n. 8, 2006.

PAZ, A. R. et al. Large-scale modelling of channel flow and floodplain inundation dynamics and its application to the Pantanal (Brazil). **Hydrological Processes,** v. 25, n. 9, p. 1498-1516, 2011.

PECHLIVANIDIS, I. G.; ARHEIMER, B. Large-scale hydrological modelling by using modified PUB recommendations: The India-HYPE case. **Hydrology and Earth System Sciences,** v. 19, n. 11, p. 4559-4579, 2015.

PEDINOTTI, V. et al. Evaluation of the ISBA-TRIP continental hydrologic system over the Niger basin using in situ and satellite derived datasets. **Hydrology and Earth System Sciences,** v. 16, n. 6, p. 1745-1773, 2012.

PEREZ, J. F. et al. From Global to Local: Providing Actionable Flood Forecast Information in a Cloud-Based Computing Environment. **Journal of the American Water Resources Association,** v. 52, n. 4, p. 965-978, 2016.

PLANCHON, O.; DARBOUX, F. A fast, simple and versatile algorithm to fill the depressions of digital elevation models. **Catena,** v. 46, n. 2-3, p. 159-176, 2002.

PONTES, P. R. M. **Modelagem hidrológica e hidrodinâmica integrada da bacia do Prata**. 2016. 194 f. Tese de Doutorado (Doutorado) - Instituto de Pesquisas Hidráulicas, Universidade Federal do Rio Grande do Sul, Porto Alegre, 2016.

PONTES, P. R. M. et al. MGB-IPH model for hydrological and hydraulic simulation of large floodplain river systems coupled with open source GIS. **Environmental Modelling & Software,** v. 94, p. 1-20, 2017.

POPESCU, I. et al. Assessing residual hydropower potential of the La Plata Basin accounting for future user demands. **Hydrol. Earth Syst. Sci.,** v. 16, n. 8, p. 2813-2823, 2012.

POVEDA, G.; MESA, O. J. On the existence of Lloró (the rainiest locality on earth): Enhanced ocean-land-atmosphere interaction by a low-level jet. **Geophysical Research Letters,** v. 27, n. 11, p. 1675-1678, 2000.

POVEDA, G.; WAYLEN, P. R.; PULWARTY, R. S. Annual and inter-annual variability of the present climate in northern South America and southern Mesoamerica. **Palaeogeography, Palaeoclimatology, Palaeoecology,** v. 234, n. 1, p. 3-27, 2006.

QU, B. et al. Multi-Model Grand Ensemble Hydrologic Forecasting in the Fu River Basin Using Bayesian Model Averaging. **Water,** v. 9, n. 2, 2017.

QUEDI, E. S.; FAN, F. M. Sub Seasonal Streamflow Forecast Assessment at Large-Scale Basins. **Journal of Hydrology,** v. 584, p. 124635, 2020.

RAFTERY, A. E. et al. Using Bayesian model averaging to calibrate forecast ensembles. **Monthly Weather Review,** v. 133, n. 5, p. 1155-1174, 2005.

RAHMAN, S. et al. Investigating Spatial Downscaling of Satellite Rainfall Data for Streamflow Simulation in a Medium-Sized Basin. **Journal of Hydrometeorology,** v. 10, n. 4, p. 1063-1079, 2009.

RAKOVEC, O. et al. Improving the realism of hydrologic model functioning through multivariate parameter estimation. **Water Resources Research,** v. 52, n. 10, p. 7779-7792, 2016.

RAMILLIEN, G.; CAZENAVE, A.; BRUNAU, O. Global time variations of hydrological signals from GRACE satellite gravimetry. **Geophysical Journal International,** v. 158, n. 3, p. 813-826, 2004.

RAMOS, M. H. et al. Communicating uncertainty in hydro-meteorological forecasts: mission impossible? **Meteorological Applications,** v. 17, n. 2, p. 223-235, 2010.

RAMOS, M. H.; VAN ANDEL, S. J.; PAPPENBERGER, F. Do probabilistic forecasts lead to better decisions? **Hydrology and Earth System Sciences,** v. 17, n. 6, p. 2219-2232, 2013.

RASO, L. et al. Short-term optimal operation of water systems using ensemble forecasts. **Advances in Water Resources,** v. 71, p. 200-208, 2014.

RAWLS, W. J. et al. Infiltration and soil water movement. *In*: MAIDMENT, D. R. (Ed.). **Handbook of Hydrology**. New York, USA: McGraw-Hill, 1993. p.5.1-5.51. ISBN 9780070397323.

REBOITA, M. S. et al. Regimes de precipitação na América do Sul: uma revisão bibliográfica. **Revista Brasileira de Meteorologia,** v. 25, p. 185-204, 2010.

REGGIANI, P. et al. Uncertainty assessment via Bayesian revision of ensemble streamflow predictions in the operational river Rhine forecasting system. **Water Resources Research,** v. 45, n. 2, 2009.

REGONDA, S. K. et al. Short-term ensemble streamflow forecasting using operationally-produced single-valued streamflow forecasts - A Hydrologic Model Output Statistics (HMOS) approach. **Journal of Hydrology,** v. 497, p. 80-96, 2013.

REICHLE, R. H. et al. Assessment and Enhancement of MERRA Land Surface Hydrology Estimates. **Journal of Climate,** v. 24, n. 24, p. 6322-6338, 2011.

REIS, A. A.; FERNANDES, W. S.; RAMOS, M.-H. Assessing two precipitation data sources at basins of special interest to hydropower production in Brazil. **RBRH,** v. 25, n. 14, p. 1-16, 2020.

RENARD, B. et al. Understanding predictive uncertainty in hydrologic modeling: The challenge of identifying input and structural errors. **Water Resources Research,** v. 46, n. 5, 2010.

RENNO, C. D. et al. HAND, a new terrain descriptor using SRTM-DEM: Mapping terra-firme rainforest environments in Amazonia. **Remote Sensing of Environment,** v. 112, n. 9, p. 3469-3481, 2008.

RESTREPO-COUPE, N. et al. What drives the seasonality of photosynthesis across the Amazon basin? A cross-site analysis of eddy flux tower measurements from the Brasil flux network. **Agricultural and Forest Meteorology,** v. 182, p. 128-144, 2013.

REVILLA-ROMERO, B. et al. Filling the gaps: Calibrating a rainfall-runoff model using satellite-derived surface water extent. **Remote Sensing of Environment,** v. 171, p. 118-131, 2015.

REVILLA-ROMERO, B. et al. Integrating remotely sensed surface water extent into continental scale hydrology. **Journal of Hydrology,** v. 543, p. 659-670, 2016.

RICHEY, J. E. et al. SOURCES AND ROUTING OF THE AMAZON RIVER FLOOD WAVE. **Global Biogeochemical Cycles,** v. 3, n. 3, p. 191-204, 1989.

RIVERA, J. A. et al. Regional aspects of streamflow droughts in the Andean rivers of Patagonia, Argentina. Links with large-scale climatic oscillations. **Hydrology Research,** v. 49, n. 1, p. 134-149, 2018.

RIVERA, J. A. et al. Spatio-temporal patterns of the 2010-2015 extreme hydrological drought across the Central Andes, Argentina. **Water (Switzerland),** v. 9, n. 9, 2017.

ROBERTSON, D. E.; SHRESTHA, D. L.; WANG, Q. J. Post-processing rainfall forecasts from numerical weather prediction models for short-term streamflow forecasting. **Hydrol. Earth Syst. Sci.,** v. 17, n. 9, p. 3587-3603, 2013.

RODELL, M. et al. The Global Land Data Assimilation System. **Bulletin of the American Meteorological Society,** v. 85, n. 3, p. 381-394, 2004.

RODRIGUEZ, E.; MORRIS, C. S.; BELZ, J. E. A global assessment of the SRTM performance. **Photogrammetric Engineering and Remote Sensing,** v. 72, n. 3, p. 249-260, 2006.

ROGERS, D.; TSIRKUNOV, V. **Costs and benefits of early warning systems**. United Nations International Strategy for Disaster Reduction, p.17. 2011

ROMATSCHKE, U.; HOUZE JR, R. A. Extreme summer convection in South America. **Journal of Climate,** v. 23, n. 14, p. 3761-3791, 2010.

ROSALES, J. et al. Ecohydrology of riparian forests in the Orinoco River Basin. **The ecohydrology of South American rivers and wetlands. Special Publication Nº6. IAHS Press. Wallingford, UK**, p. 93-110, 2002.

ROULIN, E. Skill and relative economic value of medium-range hydrological ensemble predictions. **Hydrology and Earth System Sciences,** v. 11, n. 2, p. 725-737, 2007.

ROULIN, E.; VANNITSEM, S. Skill of Medium-Range Hydrological Ensemble Predictions. **Journal of Hydrometeorology,** v. 6, n. 5, p. 729-744, 2005.

ROULIN, E.; VANNITSEM, S. Post-processing of medium-range probabilistic hydrological forecasting: impact of forcing, initial conditions and model errors. **Hydrological Processes,** v. 29, n. 6, p. 1434-1449, 2015.

RUDNICK, H. et al. Flexible connections: Solutions and challenges for the integration of renewables in South America. **IEEE Power and Energy Magazine,** v. 10, n. 2, p. 24-36, 2012.

RUDNICK, H. et al. A delicate balance in South America. **IEEE Power and Energy Magazine,** v. 6, n. 4, p. 22-35, 2008.

SALIO, P. et al. Evaluation of high-resolution satellite precipitation estimates over southern South America using a dense rain gauge network. **Atmospheric Research,** v. 163, p. 146-161, 2015.

SALIO, P.; NICOLINI, M.; ZIPSER, E. J. Mesoscale convective systems over southeastern South America and their relationship with the South American low-level jet. **Monthly Weather Review,** v. 135, n. 4, p. 1290-1309, 2007.

SAMANIEGO, L. et al. Toward seamless hydrologic predictions across spatial scales. **Hydrology and Earth System Sciences,** v. 21, n. 9, p. 4323-4346, 2017.

SANTOS DA SILVA, J. et al. Water levels in the Amazon basin derived from the ERS 2 and ENVISAT radar altimetry missions. **Remote Sensing of Environment,** v. 114, n. 10, p. 2160-2181, 2010.

SATGÉ, F. et al. Assessment of satellite rainfall products over the Andean plateau. **Atmospheric Research,** v. 167, p. 1-14, 2016.

SATYAMURTY, P.; NOBRE, C. A.; DIAS, P. L. S. South America. *In*: KAROLY, D. J. e VINCENT, D. G. (Ed.). **Meteorology of the southern hemisphere**: Springer, 1998. cap. South America, p.119-139.

SCANLON, B. R. et al. Global evaluation of new GRACE mascon products for hydrologic applications. **Water Resources Research,** v. 52, n. 12, p. 9412-9429, 2016.

SCHAAKE, J. C. et al. HEPEX: The hydrological ensemble prediction experiment. **Bulletin of the American Meteorological Society,** v. 88, n. 10, p. 1541-1547, 2007.

SCHEFZIK, R. Combining parametric low-dimensional ensemble postprocessing with reordering methods. **Quarterly Journal of the Royal Meteorological Society,** v. 142, n. 699, p. 2463-2477, 2016.

SCHEFZIK, R. Ensemble calibration with preserved correlations: unifying and comparing ensemble copula coupling and member-by-member postprocessing. **Quarterly Journal of the Royal Meteorological Society,** v. 143, n. 703, p. 999-1008, 2017.

SCHEFZIK, R.; THORARINSDOTTIR, T. L.; GNEITING, T. Uncertainty Quantification in Complex Simulation Models Using Ensemble Copula Coupling. **Statistical Science,** v. 28, n. 4, p. 616-640, 2013.

SCHELLEKENS, J. et al. A global water resources ensemble of hydrological models: the eartH2Observe Tier-1 dataset. **Earth System Science Data,** v. 9, n. 2, p. 389-413, 2017.

SCHELLEKENS, J. et al. The use of MOGREPS ensemble rainfall forecasts in operational flood forecasting systems across England and Wales. **Advances in Geosciences,** v. 29, p. 77-84, 2011.

SCHEUERER, M. et al. A method for preferential selection of dates in the Schaake shuffle approach to constructing spatiotemporal forecast fields of temperature and precipitation. **Water Resources Research,** v. 53, n. 4, p. 3029-3046, 2017.

SCHMIDT, R. et al. Hydrological Signals Observed by the GRACE Satellites. **Surveys in Geophysics,** v. 29, n. 4-5, p. 319-334, 2008.

SCHWANENBERG, D. et al. Short-Term Reservoir Optimization for Flood Mitigation under Meteorological and Hydrological Forecast Uncertainty. **Water Resources Management,** v. 29, n. 5, p. 1635-1651, 2015.

SEIBERT, J.; MCGLYNN, B. L. A new triangular multiple flow direction algorithm for computing upslope areas from gridded digital elevation models. **Water Resources Research,** v. 43, n. 4, 2007.

SEO, D. J.; HERR, H. D.; SCHAAKE, J. C. A statistical post-processor for accounting of hydrologic uncertainty in short-range ensemble streamflow prediction. **Hydrol. Earth Syst. Sci. Discuss.,** v. 2006, p. 1987-2035, 2006.

SHARMA, S. et al. Hydrological model diversity enhances streamflow forecast skill at short- to medium-range timescales. **Water Resources Research,** v. 55, n. 2, p. 1510-1530, 2019.

SHARMA, S. et al. Relative effects of statistical preprocessing and postprocessing on a regional hydrological ensemble prediction system. **Hydrology and Earth System Sciences,** v. 22, n. 3, p. 1831-1849, 2018.

SHUTTLEWORTH, W. J. Evaporation. *In*: MAIDMENT, D. R. (Ed.). **Handbook of Hydrology**: McGraw-Hill, 1993. cap. four, p.1424p. ISBN 978-0070397323.

SIDDIQUE, R.; MEJIA, A. Ensemble streamflow forecasting across the U.S. Mid-Atlantic Region with a distributed hydrological model forced by GEFS reforecasts. **Journal of Hydrometeorology,** v. 18, n. 7, p. 1905-1928, 2017.

SIQUEIRA, V. A. **Previsão de cheias por conjunto em curto a médio prazo: Bacia do Taquari-Antas/RS (in Portuguese)**. 2015. 157 (Master) - Instituto de Pesquisas Hidráulicas, Federal University of Rio Grande do Sul

SIQUEIRA, V. A. et al. Ensemble flood forecasting based on operational forecasts of the regional Eta EPS in the Taquari-Antas basin. **Revista Brasileira de Recursos Hidricos,** v. 21, n. 3, p. 587-602, 2016a.

SIQUEIRA, V. A. et al. Potential skill of continental-scale, medium-range ensemble streamflow forecasts for flood prediction in South America. **Journal of Hydrology,** v. 590, p. 125430, 2020.

SIQUEIRA, V. A. et al. IPH-Hydro Tools: A GIS coupled tool for watershed topology acquisition in an open-source environment. **Rbrh,** v. 21, n. 1, p. 274-287, 2016b.

SIQUEIRA, V. A. et al. Toward continental hydrologic-hydrodynamic modeling in South America. **Hydrology and Earth System Sciences,** v. 22, n. 9, p. 4815-4842, 2018.

SKØIEN, J. O. et al. Regionalization of post-processed ensemble runoff forecasts. **Proc. IAHS,** v. 373, p. 109-114, 2016.

SKØIEN, J. O. et al. On the Implementation of Postprocessing of Runoff Forecast Ensembles. **Journal of Hydrometeorology,** v. 22, n. 10, p. 2731-2749, 2021.

SNOW, A. D. et al. A High-Resolution National-Scale Hydrologic Forecast System from a Global Ensemble Land Surface Model. **Journal of the American Water Resources Association,** v. 52, n. 4, p. 950-964, 2016.

SONG, X. L.; ZHANG, G. J.; LI, J. L. F. Evaluation of Microphysics Parameterization for Convective Clouds in the NCAR Community Atmosphere Model CAM5. **Journal of Climate,** v. 25, n. 24, p. 8568-8590, 2012.

SOOD, A.; SMAKHTIN, V. Global hydrological models: a review. **Hydrological Sciences Journal,** v. 60, n. 4, p. 549-565, 2015.

SPERNA WEILAND, F. C. et al. Significant uncertainty in global scale hydrological modeling from precipitation data errors. **Journal of Hydrology,** v. 529, p. 1095-1115, 2015.

STEFFEN, P. C.; GOMES, J. Clustering of historical floods observed on Iguaçu River, in União da Vitória, Paraná. **Revista Brasileira de Recursos Hidricos,** v. 23, 2018.

STENSRUD, D. J.; BAO, J.-W.; WARNER, T. T. Using Initial Condition and Model Physics Perturbations in Short-Range Ensemble Simulations of Mesoscale Convective Systems. **Monthly Weather Review,** v. 128, n. 7, p. 2077-2107, 2000.

STEVAUX, J. C. et al. Floods in Urban Areas of Brazil. *In*: LATRUBESSE, E. M. (Ed.). **Natural Hazards and Human-Exacerbated Disasters in Latin America: Special Volumes of Geomorphology.** Oxford: Elsevier Science & Technology, v.13, 2009. p.245-266. ISBN 9780444531179.

SU, F. G.; LETTENMAIER, D. P. Estimation of the Surface Water Budget of the La Plata Basin. **Journal of Hydrometeorology,** v. 10, n. 4, p. 981-998, 2009.

SUN, Q. et al. A Review of Global Precipitation Data Sets: Data Sources, Estimation, and Intercomparisons. **Reviews of Geophysics,** v. 56, n. 1, p. 79-107, 2018.

SUNILKUMAR, K. et al. Comprehensive evaluation of multisatellite precipitation estimates over India using gridded rainfall data. **Journal of Geophysical Research,** v. 120, n. 17, p. 8987-9005, 2015.

TAPLEY, B. D. et al. The gravity recovery and climate experiment: Mission overview and early results. **Geophysical Research Letters,** v. 31, n. 9, p. 4, 2004.

TARBOTON, D. G. A new method for the determination of flow directions and upslope areas in grid digital elevation models. **Water Resources Research,** v. 33, n. 2, p. 309-319, 1997.

TAVAKOLY, A. A. et al. Continental-Scale River Flow Modeling of the Mississippi River Basin Using High-Resolution NHDPlus Dataset. **Journal of the American Water Resources Association,** v. 53, n. 2, p. 258-279, 2017.

TEAM, R. C. **A Language and Environment for Statistical Computing. R Foundation for Statistical Computing, Vienna, Austria.** Vienna, Austria 2013.

TESFA, T. K. et al. Scalability of grid- and subbasin-based land surface modeling approaches for hydrologic simulations. **Journal of Geophysical Research,** v. 119, n. 6, p. 3166-3184, 2014.

THIELEN-DEL POZO, J. et al. Medium Range Flood Forecasting Example EFAS. *In*: DUAN, Q.;PAPPENBERGER, F., *et al* (Ed.). **Handbook of Hydrometeorological Ensemble Forecasting**. Berlin: Springer, 2019. p.1261-1277. ISBN 978-3-642-39924-4.

THIELEN, J. et al. The European Flood Alert System - Part 1: Concept and development. **Hydrology and Earth System Sciences,** v. 13, n. 2, p. 125-140, 2009a.

THIELEN, J. et al. Monthly-, medium-, and short-range flood warning: testing the limits of predictability. **Meteorological Applications,** v. 16, n. 1, p. 77-90, 2009b.

THIEMIG, V. et al. A pan-African medium-range ensemble flood forecast system. **Hydrology and Earth System Sciences,** v. 19, n. 8, p. 3365-3385, 2015.

THIREL, G. et al. On the impact of short-range meteorological forecasts for ensemble stream flow predictions. **Journal of Hydrometeorology,** v. 9, n. 6, p. 1301-1317, 2008.

THORARINSDOTTIR, T. L.; GNEITING, T. Probabilistic forecasts of wind speed: ensemble model output statistics by using heteroscedastic censored regression. **Journal of the Royal Statistical Society Series a-Statistics in Society,** v. 173, p. 371-388, 2010.

TIAN, Y.; PETERS-LIDARD, C. D. A global map of uncertainties in satellite-based precipitation measurements. **Geophysical Research Letters,** v. 37, n. 24, 2010.

TODINI, E. The ARNO rainfall-runoff model. **Journal of Hydrology,** v. 175, n. 1-4, p. 339-382, 1996.

_____. A model conditional processor to assess predictive uncertainty in flood forecasting. **International Journal of River Basin Management,** v. 6, n. 2, p. 123-137, 2008.

TOMASELLA, J. et al. Probabilistic flood forecasting in the Doce Basin in Brazil: Effects of the basin scale and orientation and the spatial distribution of rainfall. **Journal of Flood Risk Management,** v. 12, n. 1, 2019.

TRACTON, M. S.; KALNAY, E. Operational Ensemble Prediction at the National Meteorological Center: Practical Aspects. **Weather and Forecasting,** v. 8, n. 3, p. 379-398, 1993.

TRIGG, M. A. et al. Amazon flood wave hydraulics. **Journal of Hydrology,** v. 374, n. 1-2, p. 92-105, 2009.

TUCCI, C. E. M.; BERTONI, J. C. **Inundações urbanas na América do Sul**. Porto Alegre: ABRH, 2003. 150 ISBN 85-88686-07-4.

TUCCI, C. E. M.; CLARKE, R. T. Environmental issues in the la Plata Basin. **International Journal of Water Resources Development,** v. 14, n. 2, p. 157-173, 1998.

TUCCI, C. E. M. et al. Hydropower forecasting in Brazil. *In*: DUAN, Q.;PAPPENBERGER, F., *et al* (Ed.). **Handbook of Hydrometeorological Ensemble Forecasting**: Springer, v.1, 2019. p.1307-1328. ISBN 978-3642399244.

VAN DEN BERGH, J.; ROULIN, E. Postprocessing of medium range hydrological ensemble forecasts making use of reforecasts. **Hydrology,** v. 3, n. 2, 2016.

VAN DER KNIJFF, J. M.; YOUNIS, J.; DE ROO, A. P. J. LISFLOOD: a GIS-based distributed model for river basin scale water balance and flood simulation. **International Journal of Geographical Information Science,** v. 24, n. 2, p. 189-212, 2010.

VAN DIJK, A. I. J. M. et al. Global analysis of seasonal streamflow predictability using an ensemble prediction system and observations from 6192 small catchments worldwide. **Water Resources Research,** v. 49, n. 5, p. 2729-2746, 2013.

VARAS, P. et al. Latin America Goes Electric: The Growing Social Challenges of Hydroelectric Development. **IEEE Power and Energy Magazine,** v. 11, n. 3, p. 66-75, 2013.

VELÁZQUEZ, J. A. et al. Can a multi-model approach improve hydrological ensemble forecasting? A study on 29 French catchments using 16 hydrological model structures. **Advances in Geosciences,** v. 29, p. 33-42, 2011.

VELÁZQUEZ, J. A. et al. An evaluation of the Canadian global meteorological ensemble prediction system for short-term hydrological forecasting. **Hydrol. Earth Syst. Sci.,** v. 13, n. 11, p. 2221-2231, 2009.

VERA, C. et al. The South American low-level jet experiment. **Bulletin of the American Meteorological Society,** v. 87, n. 1, p. 63-77, 2006a.

VERA, C. et al. Toward a Unified View of the American Monsoon Systems. **Journal of Climate,** v. 19, n. 20, p. 4977-5000, 2006b.

VERA, C. S.; VIGLIAROLO, P. K.; BERBERY, E. H. Cold season synoptic-scale waves over subtropical South America. **Monthly Weather Review,** v. 130, n. 3, p. 684-699, 2002.

VERKADE, J. S. **Estimating real-time predictive hydrological uncertainty**. 2015. 179 f. Tese (Doutorado em Engenharia Civil) - Faculty of Civil Engineering and Geosciences, Technisiche Universiteit Delft, Delft, The Netherlands, 2015.

VERKADE, J. S. et al. Estimating predictive hydrological uncertainty by dressing deterministic and ensemble forecasts; a comparison, with application to Meuse and Rhine. **Journal of Hydrology,** v. 555, p. 257-277, 2017.

VERKADE, J. S. et al. Post-processing ECMWF precipitation and temperature ensemble reforecasts for operational hydrologic forecasting at various spatial scales. **Journal of Hydrology,** v. 501, p. 73-91, 2013.

VERKADE, J. S.; WERNER, M. G. F. Estimating the benefits of single value and probability forecasting for flood warning. **Hydrol. Earth Syst. Sci.,** v. 15, n. 12, p. 3751-3765, 2011a.

_____. Estimating the benefits of single value and probability forecasting for flood warning. **Hydrology and Earth System Sciences,** v. 15, n. 12, p. 3751-3765, 2011b.

VIALE, M. et al. Contrasting climates at both sides of the Andes in Argentina and Chile. **Frontiers in Environmental Science,** v. 7, n. May, 2019.

VINUKOLLU, R. K. et al. Multi-model, multi-sensor estimates of global evapotranspiration: climatology, uncertainties and trends. **Hydrological Processes,** v. 25, n. 26, p. 3993-4010, 2011.

VOISIN, N. et al. Application of a Medium-Range Global Hydrologic Probabilistic Forecast Scheme to the Ohio River Basin. **Weather and Forecasting,** v. 26, n. 4, p. 425-446, 2011.

VOROSMARTY, C. J. et al. Extreme rainfall, vulnerability and risk: a continental-scale assessment for South America. **Philosophical Transactions of the Royal Society a-Mathematical Physical and Engineering Sciences,** v. 371, n. 2002, 2013.

WADA, Y.; VAN BEEK, L. P. H.; BIERKENS, M. F. P. Modelling global water stress of the recent past: On the relative importance of trends in water demand and climate variability. **Hydrology and Earth System Sciences,** v. 15, n. 12, p. 3785-3808, 2011.

WAHR, J.; MOLENAAR, M.; BRYAN, F. Time variability of the Earth's gravity field: Hydrological and oceanic effects and their possible detection using GRACE. **Journal of Geophysical Research: Solid Earth,** v. 103, n. B12, p. 30205-30229, 1998.

WANDERS, N. et al. The suitability of remotely sensed soil moisture for improving operational flood forecasting. **Hydrology and Earth System Sciences,** v. 18, n. 6, p. 2343-2357, 2014.

WANG, A. et al. Time scales of land surface hydrology. **Journal of Hydrometeorology,** v. 7, n. 5, p. 868-879, 2006.

WANG, F. et al. Ensemble hydrological prediction-based real-time optimization of a multiobjective reservoir during flood season in a semiarid basin with global numerical weather predictions. **Water Resources Research,** v. 48, n. 7, 2012a.

WANG, L.; LIU, H. An efficient method for identifying and filling surface depressions in digital elevation models for hydrologic analysis and modelling. **International Journal of Geographical Information Science,** v. 20, n. 2, p. 193-213, 2006.

WANG, Q. J. et al. A log-sinh transformation for data normalization and variance stabilization. **Water Resources Research,** v. 48, 2012b.

WATKINS, M. M. et al. Improved methods for observing Earth's time variable mass distribution with GRACE using spherical cap mascons. **Journal of Geophysical Research: Solid Earth,** v. 120, n. 4, p. 2648-2671, 2015.

WEERTS, A. **Global Flood Forecasting Information System (GLOFFIS)**. European Geosciences Union. Vienna, Austria**:** 14017 p. 2018.

WEERTS, A. H.; WINSEMIUS, H. C.; VERKADE, J. S. Estimation of predictive hydrological uncertainty using quantile regression: examples from the National Flood Forecasting System (England and Wales). **Hydrology and Earth System Sciences,** v. 15, n. 1, p. 255-265, 2011.

WERTH, D.; AVISSAR, R. The local and global effects of Amazon deforestation. **Journal of Geophysical Research-Atmospheres,** v. 107, n. D20, 2002.

WERTH, S.; GUNTNER, A. Calibration analysis for water storage variability of the global hydrological model WGHM. **Hydrology and Earth System Sciences,** v. 14, n. 1, p. 59-78, 2010.

WIESE, D. N.; LANDERER, F. W.; WATKINS, M. M. Quantifying and reducing leakage errors in the JPL RL05M GRACE mascon solution. **Water Resources Research,** v. 52, n. 9, p. 7490-7502, 2016.

WIGMOSTA, M. S.; VAIL, L. W.; LETTENMAIER, D. P. A distributed hydrology-vegetation model for complex terrain. **Water Resources Research,** v. 30, n. 6, p. 1665-1679, 1994.

WILKS, D. S. **Statistical methods in the atmospheric sciences**. Academic press, 2011. 676 ISBN 0123850223.

WILKS, D. S. Chapter 3 - Univariate Ensemble Postprocessing. *In*: VANNITSEM, S.;WILKS, D. S., *et al* (Ed.). **Statistical Postprocessing of Ensemble Forecasts**: Elsevier, 2018. p.49-89. ISBN 978-0-12-812372-0.

WMO. **Manual on flood forecasting and warning**. Geneva, Switzerland: World Meteorological Organization, 2011. 142p ISBN 978-92-63-11072-5.

WOLDEMESKEL, F. et al. Evaluating post-processing approaches for monthly and seasonal streamflow forecasts. **Hydrology and Earth System Sciences,** v. 22, n. 12, p. 6257-6278, 2018.

WONGCHUIG, S. C. et al. Assimilation of future SWOT-based river elevations, surface extent observations and discharge estimations into uncertain global hydrological models. **Journal of Hydrology,** v. 590, p. 125473, 2020.

WONGCHUIG, S. C. et al. Hydrological reanalysis across the 20th century: A case study of the Amazon Basin. **Journal of Hydrology,** v. 570, p. 755-773, 2019.

WOOD, A. W.; LETTENMAIER, D. P. A test bed for new seasonal hydrologic forecasting approaches in the western United States. **Bulletin of the American Meteorological Society,** v. 87, n. 12, p. 1699-1712, 2006.

WOOD, E. F. et al. **The upgraded, high-resolution Latin American Flood and Drought Monitor (LAFDM) for improved risk management**. European Geosciences Union**:** 5094 p. 2018.

WOOD, E. F. et al. Hyperresolution global land surface modeling: Meeting a grand challenge for monitoring Earth's terrestrial water. **Water Resources Research,** v. 47, 2011.

WU, H. et al. Real-time global flood estimation using satellite-based precipitation and a coupled land surface and routing model. **Water Resources Research,** v. 50, n. 3, p. 2693-2717, 2014.

WU, H. et al. Automated upscaling of river networks for macroscale hydrological modeling. **Water Resources Research,** v. 47, n. 3, 2011.

WU, W. et al. Ensemble flood forecasting: Current status and future opportunities. **WIREs Water,** v. 7, n. 3, p. e1432, 2020.

YAMAZAKI, D. et al. Adjustment of a spaceborne DEM for use in floodplain hydrodynamic modeling. **Journal of Hydrology,** v. 436-437, p. 81-91, 2012.

YAMAZAKI, D.; DE ALMEIDA, G. A. M.; BATES, P. D. Improving computational efficiency in global river models by implementing the local inertial flow equation and a vector-based river network map. **Water Resources Research,** v. 49, n. 11, p. 7221-7235, 2013.

YAMAZAKI, D. et al. MERIT Hydro: A High-Resolution Global Hydrography Map Based on Latest Topography Dataset. **Water Resources Research,** v. 55, n. 6, p. 5053-5073, 2019.

YAMAZAKI, D. et al. A high-accuracy map of global terrain elevations. **Geophysical Research Letters,** v. 44, n. 11, p. 5844-5853, 2017.

YAMAZAKI, D. et al. A physically based description of floodplain inundation dynamics in a global river routing model. **Water Resources Research,** v. 47, n. 4, 2011.

YAMAZAKI, D. et al. Development of the Global Width Database for Large Rivers. **Water Resources Research,** v. 50, n. 4, p. 3467-3480, 2014.

YAMAZAKI, D.; OKI, T.; KANAE, S. Deriving a global river network map and its sub-grid topographic characteristics from a fine-resolution flow direction map. **Hydrology and Earth System Sciences,** v. 13, n. 11, p. 2241-2251, 2009.

YOUNIS, J.; RAMOS, M.-H.; THIELEN, J. EFAS forecasts for the March–April 2006 flood in the Czech part of the Elbe River Basin—a case study. **Atmospheric Science Letters,** v. 9, n. 2, p. 88-94, 2008.

ZAITCHIK, B. F.; RODELL, M.; OLIVERA, F. Evaluation of the Global Land Data Assimilation System using global river discharge data and a source-to-sink routing scheme. **Water Resources Research,** v. 46, n. 6, 2010.

ZAJAC, Z. et al. The impact of lake and reservoir parameterization on global streamflow simulation. **Journal of Hydrology,** v. 548, p. 552-568, 2017.

ZALACHORI, I. et al. Statistical processing of forecasts for hydrological ensemble prediction: a comparative study of different bias correction strategies. **Adv. Sci. Res.,** v. 8, n. 1, p. 135-141, 2012.

ZAMBRANO-BIGIARINI, M. et al. Temporal and spatial evaluation of satellite-based rainfall estimates across the complex topographical and climatic gradients of Chile. **Hydrology and Earth System Sciences,** v. 21, n. 2, p. 1295-1320, 2017.

ZAPPA, M. et al. Superposition of three sources of uncertainties in operational flood forecasting chains. **Atmospheric Research,** v. 100, n. 2-3, p. 246-262, 2011.

ZARFL, C. et al. A global boom in hydropower dam construction. **Aquatic Sciences,** v. 77, n. 1, p. 161-170, 2015.

ZHANG, Y. et al. A Climate Data Record (CDR) for the global terrestrial water budget: 1984–2010. **Hydrology and Earth System Sciences,** v. 22, n. 1, p. 241-263, 2018.

ZHANG, Y. et al. Evaluating Regional and Global Hydrological Models against Streamflow and Evapotranspiration Measurements. **Journal of Hydrometeorology,** v. 17, n. 3, p. 995-1010, 2016.

ZHAO, F. et al. The critical role of the routing scheme in simulating peak river discharge in global hydrological models. **Environmental Research Letters,** v. 12, n. 7, 2017.

ZHAO, T.; DAI, A. The magnitude and causes of global drought changes in the twenty-first century under a low-moderate emissions scenario. **Journal of Climate,** v. 28, n. 11, p. 4490-4512, 2015.

ZHONG, Y. et al. Probabilistic forecasting based on ensemble forecasts and EMOS method for TGR inflow. **Frontiers of Earth Science,** v. 14, n. 1, p. 188-200, 2020.

ZHOU, X. et al. Benchmarking global land surface models against the observed mean annual runoff from 150 large basins. **Journal of Hydrology,** v. 470-471, p. 269-279, 2012.

ZHU, H. et al. Seamless precipitation prediction skill in the tropics and extratropics from a global model. **Monthly Weather Review,** v. 142, n. 4, p. 1556-1569, 2014.

ZSOTER, E. et al. Building a Multimodel Flood Prediction System with the TIGGE Archive. **Journal of Hydrometeorology,** v. 17, n. 11, p. 2923-2940, 2016.

Anexos

A. Details about the MGB hydrological–hydrodynamic model

Herein, a brief overview of the MGB structure used for hydrological modeling in South America is presented. Basically, this is a semi-distributed model that uses conceptual equations to simulate the terrestrial hydrological cycle, including soil water and energy budget, evapotranspiration, canopy interception, surface, subsurface and groundwater runoff, as well as flow routing along river channels (Figure A.1.1). The following sections describe the main MGB formulations according to the initial model development by Collischonn *et al.* (2007a) and further improvements by Paiva *et al.* (2011), Pontes *et al.* (2017) and Fleischmann *et al.* (2018), including parameters adopted for channel geometry. Methods used for river network discretization are also presented in detail and are based on the documentation by Siqueira *et al.* (2018, supplementary material) and Fan *et al.* (2021).

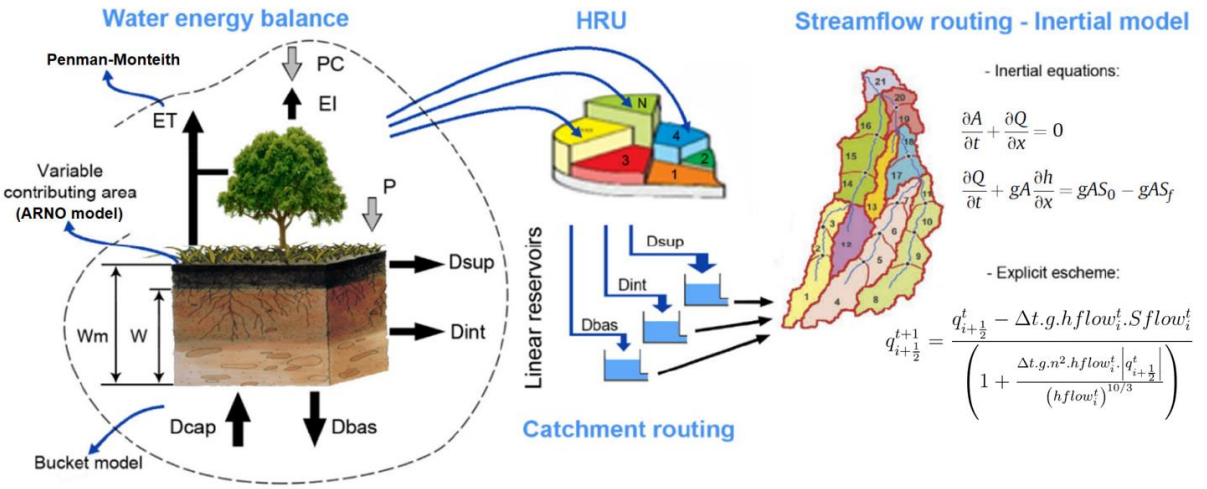

Figure A.1.1. Schematic representation of MGB model general structure.

A.1.1. Water and energy balance

The MGB discretizes the basin into unit-catchments, which are further divided into hydrological response units (HRU) that are usually produced by the combination of soil and land cover maps. Vertical water and energy budgets are computed independently for each HRU of each unit-catchment. Soil water balance is computed considering a single soil layer (bucket model), according to:

$$W_{i,j}^{t} = W_{i,j}^{t-1} + (P_i - ET_{i,j} - Dsup_{i,j} - Dint_{i,j} - Dbas_{i,j} + Dinf_{i,j})\,\Delta t \quad \text{(A_1.1)}$$

Where: *t*, *i* and *j*, are indexes related to time step, unit-catchment and HRU, respectively; *Wm* is the water storage capacity in the soil layer [mm]; *P* is the precipitation that reaches the soil [mm Δt^{-1}]; *ET* is the evapotranspiration from soil [mm Δt^{-1}]; *Dsup* is the surface runoff [mm Δt^{-1}]; *Dint* is the subsurface flow [mm Δt^{-1}]; *Dbas* is the flow to the groundwater reservoir [mm Δt^{-1}]; *Dinf* is the infiltration of flooded areas to the soil [mm Δt^{-1}] and; Δt is the time step for water budget, usually equal to 1 day.

Soil infiltration and runoff are computed based on the variable contributing area concept of the ARNO model (Todini, 1996):

$$Dsup_{i,j} = \Delta t P_i - \left(Wm_j - W_{i,j}^{t-1}\right), for\ y \leq 0 \quad \text{(A_1.2)}$$

$$Dsup_{i,j} = \Delta t P_i - \left(Wm_j - W_{i,j}^{t-1}\right) + Wm_j \left[\left(1 - \frac{W_{i,j}^{t-1}}{Wm_j}\right)^{\frac{1}{b_j+1}} - \frac{\Delta t P_i}{Wm_j\,(b_j+1)}\right]^{b_j+1}, \quad for\ y > 0 \quad \text{(A_1.3)}$$

$$y = \left[\left(1 - \frac{W_{i,j}^{t-1}}{Wm_j}\right)^{\frac{1}{b_j+1}} - \frac{\Delta t P_i}{Wm_j\,(b_j+1)}\right] \quad \text{(A_1.4)}$$

Where *W* is the current soil water storage [mm]; *Wm* is the maximum water storage capacity [mm]; *b* is a parameter that controls the distribution of water storage capacity of the soil [-]; *P* is the precipitation that reaches the soil [mm];

Subsurface flow is obtained using a function similar to the Brooks and Corey unsaturated hydraulic conductivity equation (Rawls *et al.*, 1993):

$$Dint_{i,j} = Kint_j \left(\frac{W_{i,j} - Wz_j}{Wm_j - Wz_j}\right)^{\left(3+\frac{2}{\lambda_j}\right)} \quad \text{(A_1.5)}$$

Where *Kint* is the saturated hydraulic conductivity [mm Δt^{-1}], λ is the soil porosity index [-] and *Wz* is the lower limit below which there is no subsurface flow (W_Z = 0.1Wm).

Percolation from soil layer to groundwater is calculated according to a simple linear relation between soil water storage and maximum soil water storage:

$$Dbas_{i,j} = Kbas_j \left(\frac{W_{i,j} - Wc_j}{Wm_j - Wc_j} \right) \quad \text{(A\_1.6)}$$

Where *Kbas* is a parameter that gives the percolation rate to groundwater in the case of saturated soil [mm Δt^{-1}].

Infiltration from floodplain into soil column is computed as a two–way coupled scheme between hydrological vertical balance and hydrodynamic module (see also (A_1.21)). It is assumed that infiltration rate is linearly dependent on the degree of soil saturation, thus reaching its maximum when soil is completely dry (Fleischmann *et al.*, 2018).

$$D_{inf_i}^t = \frac{A_{fl_i}^t}{A_i} . K_{inf} \left(1 - \frac{W_i^t}{Wm} \right) \quad \text{(A\_1.7)}$$

Where Afl_i is the flooded area at unit-catchment i [km²], A is the unit-catchment area [km²], K_{inf} the infiltration rate that occurs when the whole unit-catchment is flooded and soil is totally dry [mm Δt^{-1}], w is the soil water content and Wm is the maximum soil water storage.

Runoff generated (*Dsup*, *Dint* and *Dbas*) within unit-catchments is routed to the drainage network using three independent linear reservoirs ((A_1.8) to (A_1.10)). For surface and subsurface reservoirs, streamflow releases (Q) are controlled by the time of concentration computed with Kirpich formula similarly to (Ludwig and Bremicker, 2006).

$$Q_{sup_i} = \frac{V_{sup_i}}{Cs \left[3600 \left(0.868 \frac{L_i}{\Delta H_i} \right)^{0.385} \right]} \quad \text{(A\_1.8)}$$

$$Q_{int_i} = \frac{V_{int_i}}{Ci \left[3600 \left(0.868 \frac{L_i}{\Delta H_i} \right)^{0.385} \right]} \quad \text{(A\_1.9)}$$

$$Q_{bas_i} = \frac{V_{bas_i}}{Cb} \quad \text{(A\_1.10)}$$

Where *Vsup*, *Vint* and *Vbas* are the surface, subsurface and groundwater reservoir volumes, respectively [m³]; L_i and ΔH_i are, respectively, the length and the elevation difference of the largest flowpath between unit-catchment border and the main river [m]; *Cs* and *Ci* are

parameters that correct the prior estimate of time of concentration (given by Kirpich formula) [-]; *Cb* is the groundwater residence time, which can be estimated from hydrograph recession considering a long dry period [s].

Precipitation is assumed to be stored in canopy until maximum interception storage capacity is reached, which is determined for each HRU based on the vegetation leaf area index. Energy budget and evaporation from soil, vegetation and canopy to the atmosphere is estimated by the Penman–Monteith equation (Shuttleworth, 1993), using an approach similar to Wigmosta *et al.* (1994):

$$E = \left[\frac{\Delta \left(R_L - G \right) + \rho_a c_p \frac{e_s - e_d}{r_a}}{\Delta + \gamma \left(1 + \frac{r_s}{r_a} \right)} \right] \frac{1}{\lambda \rho_w} \qquad \text{(A\_1.11)}$$

Where E is the potential evaporation rate [m s^{-1}]; R_L is the net radiation [MJ m^{-2} s^{-1}]; *G* is the soil heat flux [MJ m^{-2} s^{-1}]; λ is the latent heat of vaporization [MJ kg^{-1}]; Δ is the gradient of the saturated vapour pressure–temperature function [kPa $ºC^{-1}$]; *A* is the available energy [MJ m^{-2} s^{-1}]; ρa is the air density [kg m^{-3}]; ρ_w is the specific mass of water [kg m^{-3}]; c_p is the specific heat of moist air [MJ kg^{-1} $ºC^{-1}$]; (e_s – e_d) represents the vapor pressure deficit [kPa]; γ is the psychrometric constant [kPa $ºC^{-1}$]; r_s is the surface resistance of the land cover [s m^{-1}] and r_a is the aerodynamic resistance [s m^{-1}].

Firstly, intercepted water is evaporated (*EI*) at the potential rate *E*. The evapotranspiration (*ET*) of the vegetated soil (soil evaporation + plant transpiration) is calculated using (A_1.11), weighted by the remaining evaporative demand ([*E*–*EI*]/*E*) in order to respect the overall energy balance. In addition, *ET* is reduced in situations of water stress, and it is assumed that soil conditions restrict evapotranspiration if current soil water storage is below a threshold value given by $W_L = Wm / 2$. In the range between this limit and the wilting point, surface resistance increases according to:

$$r_s = r_{s_{j,m}} \left(\frac{W_L - W_{wp}}{W_{i,j} - W_{wp}} \right) \qquad \text{(A\_1.12)}$$

Where W_{wp} is the wilting point, equal to 10% of maximum soil capacity (Wm) [mm]; $r_{s_{j,m}}$ is the vegetation-dependent minimum surface resistance, in conditions not affected by soil moisture [s m^{-1}] and m is the month index.

A.1.2. Flow routing (local inertial equation)

Flow in natural channels is governed by 1D full Saint–Venant equations (Cunge *et al.*, 1980), expressed by continuity (A_1.13) and momentum conservation (A_1.14):

$$\frac{\partial A}{\partial t} + \frac{\partial Q}{\partial x} = q, \tag{A_1.13}$$

$$\underbrace{\frac{\partial Q}{\partial t}}_{\text{Local Acceleration}} + \underbrace{\frac{\partial}{\partial x}\left(\frac{Q^2}{A}\right)}_{\text{Convective Acceleration}} + \underbrace{gA\frac{\partial (h+z)}{\partial x}}_{\text{Pressure + Bed gradients}} + \underbrace{\frac{gn^2 |Q| Q}{R_h^{4/3} A}}_{\text{Friction}} = 0 \tag{A_1.14}$$

Where Q is the river discharge [m³ s^{-1}], q is the lateral inflow [m³ s^{-1}], A is the flow cross-section area [m²], h is the flow depth [m], z is the channel bed elevation, relative to a datum [m]; R_h is the hydraulic radius [m], g is the acceleration due to gravity [m s^{-2}], and n is the Manning coefficient [s m$^{-1/3}$].

In order to deal with a wide range of flow conditions, the MGB solves the momentum equation using the local inertial approximation proposed by Bates *et al.* (2010). Using a forward in time finite difference scheme and neglecting the convective acceleration term, the momentum equation can be written as:

$$\frac{Q^{t+1} - Q^t}{\Delta t} + gA\frac{\partial (h^t + z)}{\partial x} + \frac{gn^2 |Q^t| Q^t}{R_h^{4/3} A} = 0 \tag{A_1.15}$$

In (A_1.15), flow variables in the friction term ($|Q^t|Q^t$) are written semi-implicitly ($|Q^t|Q^{t+1}$), which in turn can be rearranged into an explicit form of flow calculation:

$$Q^{t+1} = \frac{Q^t - \Delta t g A \frac{\partial (h^t + z)}{\partial x}}{\left(1 + \frac{\Delta t g n^2 |Q^t|}{R_h^{4/3} A}\right)} \tag{A_1.16}$$

Assuming a rectangular channel and approximating the hydraulic radius with the flow depth (*h*) for wide, relatively shallow rivers, we can divide (A_1.16) by the flow constant width (*B*) to obtain an equation in terms of flow per unit width:

$$q^{t+1} = \frac{q^t - \Delta t g h^t \frac{\partial\left(h^t + z\right)}{\partial x}}{\left(1 + \frac{\Delta t g h^t n^2 |q^t|}{(h^t)^{10/3}}\right)} \qquad \text{(A\_1.17)}$$

The resulting local inertial equation (Bates *et al.*, 2010) plays an important role for large-scale simulations in lowland rivers and floodplains areas, and some advantages over a diffusive wave model (which neglects both acceleration terms) include a better physical representation of shallow water flows, as well as the stability improvement for both large depths and small surface water slopes (De Almeida and Bates, 2013; Yamazaki *et al.*, 2013). Following De Almeida *et al.* (2012) and Neal *et al.* (2012), the explicit finite difference scheme is applied to a "staggered grid", so that flows at interfaces are used to update water depths at the centers of the numerical grid (i.e., centered in space approximation). Therefore, the momentum equation is written at its final form:

$$q_{i+\frac{1}{2}}^{t+1} = \frac{q_{i+\frac{1}{2}}^{t} - \Delta t.g.hflow_i^t.Sflow_i^t}{\left(1 + \frac{\Delta t.g.n^2.hflow_i^t.\left|q_{i+\frac{1}{2}}^t\right|}{\left(hflow_i^t\right)^{10/3}}\right)} \qquad \text{(A\_1.18)}$$

Where: Δt is the routing model time step [s]; $q^t_{\,i+1/2}$ and $q^{t+1}_{\,i+1/2}$ are, respectively, the flow from previous and current time step divided by channel width, at the outlet of unit catchment *i* [m² s^{-1}]; $Sflow_i$ and $hflow_i$ are, respectively, the water surface slope [m m^{-1}] and the effective water depth at the interface between current (*i*) and downstream (*i+1*) unit-catchment [m]. $q^{t+1}_{\,i+1/2}$ must be multiplied by the channel width (B) to compute discharge Q.

Note that indexes *i+1/2* are positions of the numerical grid corresponding to the outlets of unit-catchments, which are defined at grid interfaces. Using a similar approach of Neal *et al.* (2012), *Sflow* and *hflow* are computed as:

$$Sflow_i^t = \frac{\left(h_{i+1}^t + z_{i+1}\right) - \left(h_i^t + z_i\right)}{\Delta x_i} \qquad \text{(A\_1.19)}$$

$$hflow_i^t = max\left[h_{i+1}^t + z_{i+1}; h_i^t + z_i\right] - max\left[z_{i+1}; z_i\right] \quad \text{(A\_1.20)}$$

Where Δx_i is the flow distance, computed as the average between channel lengths L_i and L_{i+1} ($\Delta x_i \approx L_i \approx L_{i+1}$, according to the fixed-length river discretization, see section A.1.3 for more details); h_i and h_{i+1} are the flow depths; z_i and z_{i+1} are the channel bed elevations, respectively, at unit-catchments i and i+1.

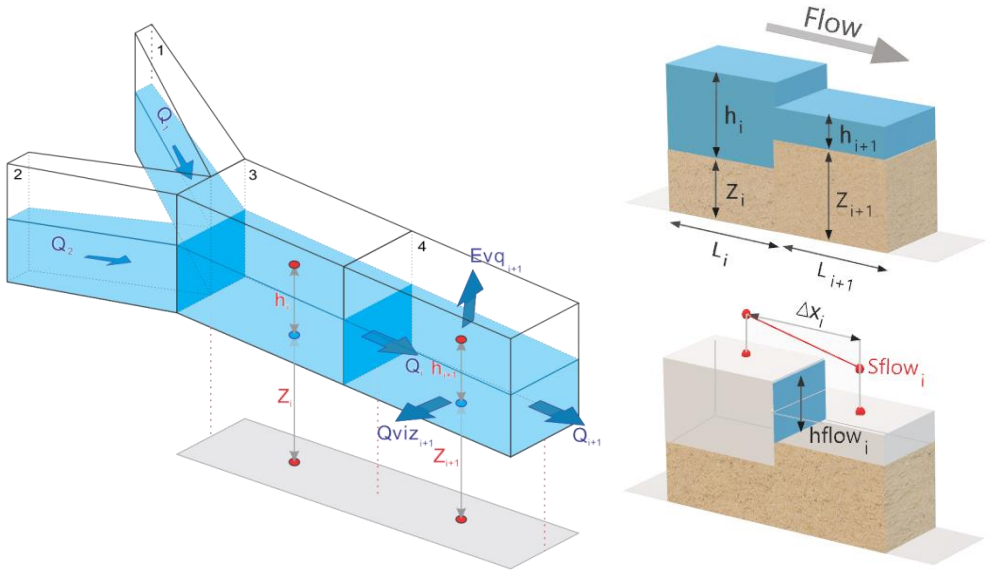

Figure A.1.2. Schematic representation of MGB flow calculation units.

Discharge is computed after solving (A_1.18) and multiplying the q variable by channel width (B), which means that the effective flow area is limited by the rectangular channel geometry. Similar to Yamazaki *et al.* (2011) and Luo *et al.* (2017), water mass is instantaneously exchanged between channel and floodplain when bankfull depth is exceeded, whereas water surface elevation of both storages is assumed equal within a given unit-catchment. Total volume (channel + floodplain) is updated using the continuity equation, expressed in terms of:

$$V_i^{t+1} - V_i^t = \left[\sum Q_{in}^t - \sum Q_{out}^t - \left(Evq_i^t - D_{inf_i}^t\right) A_{fl_i}^t / 1000\right] \Delta t \quad \text{(A\_1.21)}$$

Where V_i is the total volume stored in channel and floodplains, for unit-catchment i [m^3]; Q_{in} and Q_{out} are, respectively, the inflow and outflow discharge of unit-catchment i [$m^3\ s^{-1}$]; Evq_i is the evaporation loss [mm Δt^{-1}] and; $Dinf_i$ is the infiltration from floodplains to soil column [mm Δt^{-1}]. Note in Figure A.1.2 that MGB can also route water in multiple directions

downstream (Q_{viz}) (Pontes *et al.*, 2017), but this configuration is not used in the current South America version.

Evaporation losses are taken into account by assuming flooded area as open water (i.e., $r_s = 0$) and applying the Penman–Monteith equation (A_1.11). Therefore, when flooding occurs in a given unit-catchment, the surface area available for soil water budget is reduced proportionally from each HRU, while rainfall over flooded area produces direct surface runoff.

After solving all V^{t+1} in (A_1.21), these values are used to obtain flow depths by interpolating the water volume at each unit-catchment using channel/floodplain profiles (see section A.1.6 for details). Updated flow depths are then used to recompute both *Sflow* and *hflow* variables using (A_1.19) and (A_1.20), so that flows can be obtained for next time step.

An advantage of the explicit inertial formulation is that model time step is governed by the Courant–Friedrichs–Lewy (CFL) condition. Therefore, the maximum acceptable time step is adaptive and changes according to maximum water depth computed in (A_1.20):

$$\Delta t = \alpha \frac{\Delta x}{\sqrt{g h_{max}}} \tag{A_1.22}$$

Where Δx is the flow distance (according to fixed-length discretization); h_{max} is the maximum flow depth in model domain and α is a coefficient that varies between 0.2–0.7 (Bates *et al.*, 2010). For MGB–SA we adopted an α = 0.3 based on preliminary tests, which were further analyzed and reported by Fan *et al.* (2021).

Despite the CFL condition provides the optimum time step needed for flow computation, some issues can arise especially in rivers with higher slopes, which are expected to produce model instabilities. In cases where supercritical flows occur, a flow limiter (A_1.24) is then invoked to force the Froude number (A_1.23) below to unity, so that model stability can be further enhanced:

$$F = \frac{v}{\sqrt{gh}} = \frac{Q/A}{\sqrt{gh}} < 1 \tag{A_1.23}$$

$$Q \begin{cases} min\left[Q; B\sqrt{hflow^{1.5}g}\right] & for\ \ Q \geq 0 \\ max\left[Q; -B\sqrt{hflow^{1.5}g}\right] & for\ \ Q < 0 \end{cases} \tag{A_1.24}$$

Where F is the Froude number [-]; v is the mean flow velocity [m s^{-1}]; B is the channel width [m]. Note that the flow limiter also considers reverse flows, which can occur due to backwater effects.

A.1.3. Spatial representation of river network in MGB–SA model: definition of unit-catchments by a fixed-length river discretization

One of the key issues for large-scale river routing is to define how the river network is depicted within the model. Partitioning a basin in a regular latitude-longitude cell grid, thus providing a gridded-based network river map, is a very common practice since coupling atmospheric and LSMs, or even LSMs and river routing models, can be easily done with a simple cell-by-cell relationship (e.g., De Roo *et al.*, 2000; Decharme *et al.*, 2008; Zhao *et al.*, 2017). Conversely, large errors in length and slope of rivers, as well as the definition of flow directions over coarse resolution maps, must be treated using upscaling techniques (e.g., Paz *et al.*, 2006; Paz and Collischonn, 2007; Yamazaki *et al.*, 2009; Wu *et al.*, 2011), while a realistic representation of channels and floodplains can be only achieved with a very fine grid cell resolution (Goteti *et al.*, 2008; Lehner and Grill, 2013). A basin can be also divided in several catchments according to its underlying DEM (e.g., Beighley *et al.*, 2009; David *et al.*, 2011; Paiva *et al.*, 2011; Paiva *et al.*, 2013a; Luo *et al.*, 2017) to preserve small-scale topographic features. This approach seems to be more suitable for hydrological models since topography strongly controls surface water storage and movement (Goteti *et al.*, 2008), and a better connectivity of the river system can be ensured by the generation of high-resolution, vector-based network river maps (David *et al.*, 2011; Paiva *et al.*, 2011; Yamazaki *et al.*, 2013).

Currently, there is a strong motivation toward the use of vector-based discretization especially for large-scale modeling, since: (i) it is possible to reduce computational demand due to more flexible computational elements (Beighley *et al.*, 2009; Lehner and Grill, 2013; Yamazaki *et al.*, 2013); (ii) there is a smaller sensitivity of model parameters to its spatial resolution, which can improve model scalability (Tesfa *et al.*, 2014); (iii) gauge-to-reach association becomes easier with a high resolution river network, giving rise to higher societal meaning (David *et al.*, 2013) (iv) it is more suitable for hydro-ecological applications that typically require river-reach scale resolution (Lehner *et al.*, 2008). Because of these benefits, some river routing models are now implementing vector-based river maps for computations also over continental domains, such as RAPID (Tavakoly *et al.*, 2017) and mizuRoute

(Mizukami *et al.*, 2016), as well as for global-scale simulations, for instance, as in HydroROUT (Lehner and Grill, 2013).

An initial step needed to run a hydrological or a river routing model is to derive flow directions from terrain data. For large-scale applications, perhaps the most widely used approach is the deterministic eight-node (D8) method, where the water flow in a given pixel is assigned to a single direction towards the steepest slope among its eight surrounding neighbors (Jenson and Domingue, 1988). Although other approaches were proposed to account for multiple directions and better represent the water movement over terrain (Tarboton, 1997; Seibert and McGlynn, 2007), they can create diffuse and overlapping catchment area boundaries (Jones, 2002). In addition, a pit removal procedure is often applied prior to flow direction in order to produce a "hydrologically corrected" DEM, since the existence of flat regions or single topographical depressions leads to areas without an outlet definition and disconnected drainage patterns (Martz and Garbrecht, 1998; Planchon and Darboux, 2002; Wang and Liu, 2006). Currently, global datasets of flow directions with extensive manual corrections are available at different spatial resolutions (Lehner *et al.*, 2008), which can be suitable for many large scale hydrological and river routing modeling applications.

The sum of pixels along flow direction path originates a flow accumulation matrix, which need to be reclassified in order to define the main channels (i.e., the river network for flow routing). However, depending of the model domain, it is desired to propagate upstream area along the flow directions instead of upstream number of pixels, as individually areas can be quite different from pixel to pixel over large regions (Paz and Collischonn, 2007). Drainage networks are then extracted reclassifying the flow accumulation matrix using a constant area threshold, representing the smallest area in which open channel flow occurs.

One of the commonly procedures to derive catchments is to use well-known GIS packages, for instance, the ArcHydro definitions (Maidment, 2002; Paiva *et al.*, 2011; Yamazaki *et al.*, 2013). In this method, all pixels draining to a given reach belong to a same unit-catchment, while a reach is defined by a river segment between two junctions or between a river source and its downstream junction. However, the resulting river reaches are characterized by a high variability of lengths that are not suitable for hydrodynamic routing. Therefore, we adopted a fixed-length vector river discretization in order to provide even (and predefined) flow distances between unit-catchments, as well as to facilitate coupling of both hydrological and hydrodynamic modules of MGB. Using grids of flow direction, flow

accumulation and river networks, the fixed length discretization can be performed through the following sequence of steps:

A.1.3.1. Step 1 – Marking outlets

The first step is to identify all the intermediate outlet points in the stream network. An "intermediate outlet" refers to the very downstream pixel of a given river reach (i.e., between two junctions), as can be seen in the orange boxes presented in Figure A.1.3a. For each pixel in the flow direction grid, if two or more neighboring pixels are drained to the analyzed one, provided that all of them are over the extracted drainage, then a junction is found. Using a 3 × 3 window centered at this point, the grid positions of nearby upstream draining pixels (i.e., intermediate outlets) are stored together with their respective flow accumulated areas. This procedure is repeated until the entire grid is evaluated, and by the end the positions and accumulated area of basin outlet are also stored in conjunction with the intermediate outlets.

A.1.3.2. Step 2 – Delineating reaches and unit-catchments by a length threshold

The second step is to segment streams using a specific length as a threshold value, thus providing an even distribution of flow distances. For this, grid positions of the intermediate outlets are initially sorted descending according to their flow accumulated area, so the outlet of the main stream is processed at first. Following the schematic presented in Figure A.1.3b, the procedure then starts at the basin outlet point (green square) using a value of accumulated length equal to 0. Tracing in the upstream direction, the length is accumulated pixel by pixel using Euclidean local distances and the Distance Transforms method (Butt and Maragos, 1998; Paz and Collischonn, 2007), and an identifier value (ID) is assigned to each pixel along the flow path to further distinguish between reaches. Whenever the threshold value of distance is exceeded, as highlighted by the break lines in Figure A.1.3b, the ID is increased by one unit and the accumulated length is reset to zero. This procedure must be constantly repeated, but when a junction is found along the current flowpath, the algorithm selects the upstream pixel with the highest accumulated area (blue squares) to keep tracing until the threshold value of length is met. However, if the length threshold is not achieved when the headwater pixel is found, an extension of the drainage network (dashed line in Figure A.1.3b, Figure A.1.3c and Figure A.1.3d) is created following the pixel with the highest upstream accumulated area. In other words, it results in a "dynamic area threshold" for first order streams, but in this case,

length can be lesser than the threshold value once it is topographically limited by headwater catchment boundaries.

After defining all branches in the basin main river, the next intermediate outlet with the highest value of accumulate area is selected (green square) to proceed with the segmentation process, as shown in Figure A.1.3c. However, it is important to mark outlet pixels over the previously segmented flow path as "checked" (white squares). Because the algorithm starts from an intermediate outlet (accumulated length = 0) when tracing in upstream direction, checked pixels must be neglected to avoid redefinition of already processed reaches. Following these constraints, the procedure continues until the entire river network is segmented (Figure A.1.4a).

Finally, all pixels draining to a given reach (i.e., with the same ID) belong to the same unit-catchment, as presented in Figure A.1.4b. The discretization procedure also creates an irregular grid according to topography, despite of the unit-catchment bending at tributaries due to the length threshold constraint.

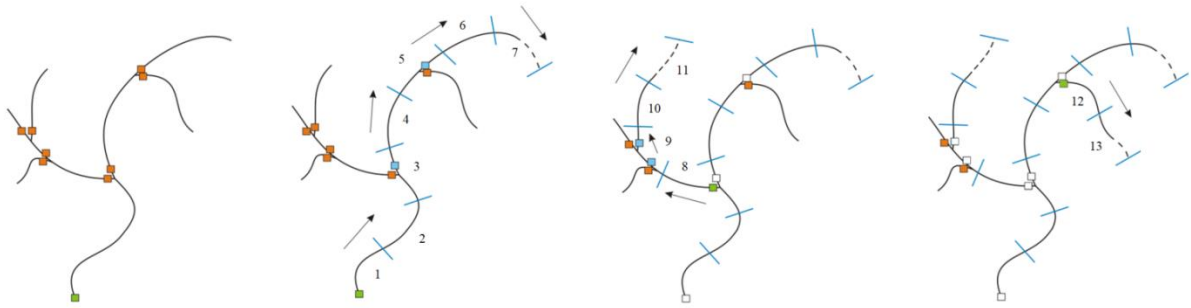

Figure A.1.3. Procedure of delineating reaches by a length threshold value: (a)Marking intermediate (orange squares) and basin outlet (green square) points, (b)Segmentation starting from basin outlet (green square) and junction overpass following outlet pixels with highest accumulated area (blue squares), (c)Segmentation starting from the next intermediate outlet (green square), ranked in descending order of accumulated area. Intermediate outlet pixels located at previously traced flowpaths (white squares) are ignored if selected for starting a new segmentation.

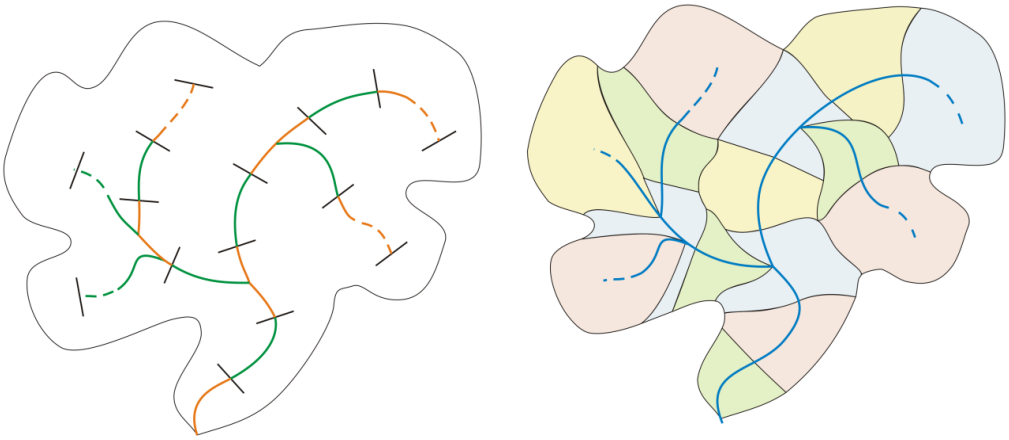

Figure A.1.4. Schematic representation of the resulting fixed-length vector-based discretization: (a)Final river segmentation: river reaches are separated by break lines and distinguished by colors (orange and green) for visualization purposes; (b)All pixels draining to the same river reach correspond to a given unit-catchment.

Figure A.1.5 shows an example of the resulting unit-catchments for MGB–SA, using the above fixed-length discretization approach. Unit-catchments were produced using the flow direction map of HydroSHEDS (Lehner *et al.*, 2008), an upstream area threshold of 1000 km² for river networks and a length threshold of Δx = 15 km. Each unit-catchment centroid represents the location for which precipitation fields are interpolated, as required for the rainfall-runoff module of MGB–SA.

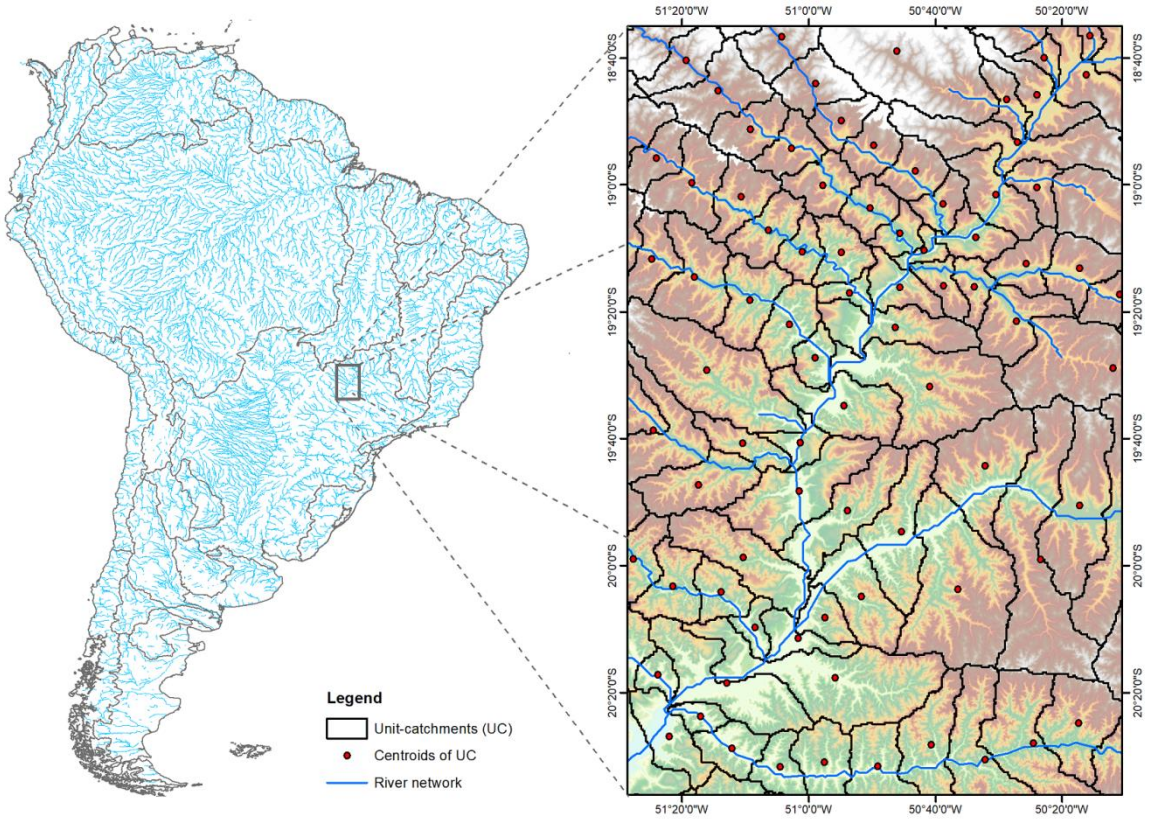

Figure A.1.5. River drainage networks of South America derived from HydroSHEDS flow direction map (Lehner *et al.*, 2008) (left); Unit-catchments defined with a fixed-length river discretization, using a threshold of Δx = 15 km) (right). Red points represent unit-catchment centroids where rainfall is interpolated.

A.1.4. Channel geometry

For the assumption of a rectangular channel, river cross-section geometry is parameterized using downstream hydraulic geometry relationships (HG):

$$W_{bf_i} = aA_i^b \quad \text{(A_1.25)}$$

$$D_{bf_i} = cA_i^d \quad \text{(A_1.26)}$$

Where D_{bf_i} is the bankfull depth [m] for unit-catchment *i*; W_{bf_i} is the channel width [m] for unit-catchment *i*; A_i is the drainage area for unit-catchment *i* [km²]; *a*, *b*, *c* and *d* are fitting parameters, respectively, for river depth and width according to drainage area.

Table A.1.1 and Figure A.1.6 show an overview of channel geometries adopted for South America version of MGB, which were retrieved from literature. It is worth noting that

Paiva *et al.* (2011), Paiva *et al.* (2013a) and Pontes (2016) are past applications of MGB model in Amazon and La Plata basins, respectively.

Table A.1.1. Sources of river geometry parameters (bankfull width and depth) for South American rivers.

Basin/River	Reference	River Geometry	Local adjustments
Amazon main stem (A_d > 2 500 000 km²)	Beighley and Gummadi (2011)	HG based on drainage area	-
Japura, Negro, Solimoes, Xingu and Tapajos	Paiva *et al.* (2013a)	HG based on drainage area	-
Purus and Juruá	Paiva *et al.* (2011)	HG based on drainage area	-
La Plata (Paraná, Paraguay and Uruguay)	Pontes (2016)	*HG based on drainage area (Uruguay and Upper Parana basins) *Widths of main rivers obtained from Satellite imagery (Paraguay and lower Parana basins)	Bermejo River (A_d > 55 000 km²): $W = 270.82\exp(-0.00005 A_d)$ Uruguay River (A_d > 50 000 km²): $W = 0.01A_d^{0.95}$
Other South American Rivers	Andreadis *et al.* (2013)	HG based on mean annual peak flow	Sao Francisco river (A_d> 120 000 km²): D = 12m

A_d = Drainage Area; W = Width; D = Depth;

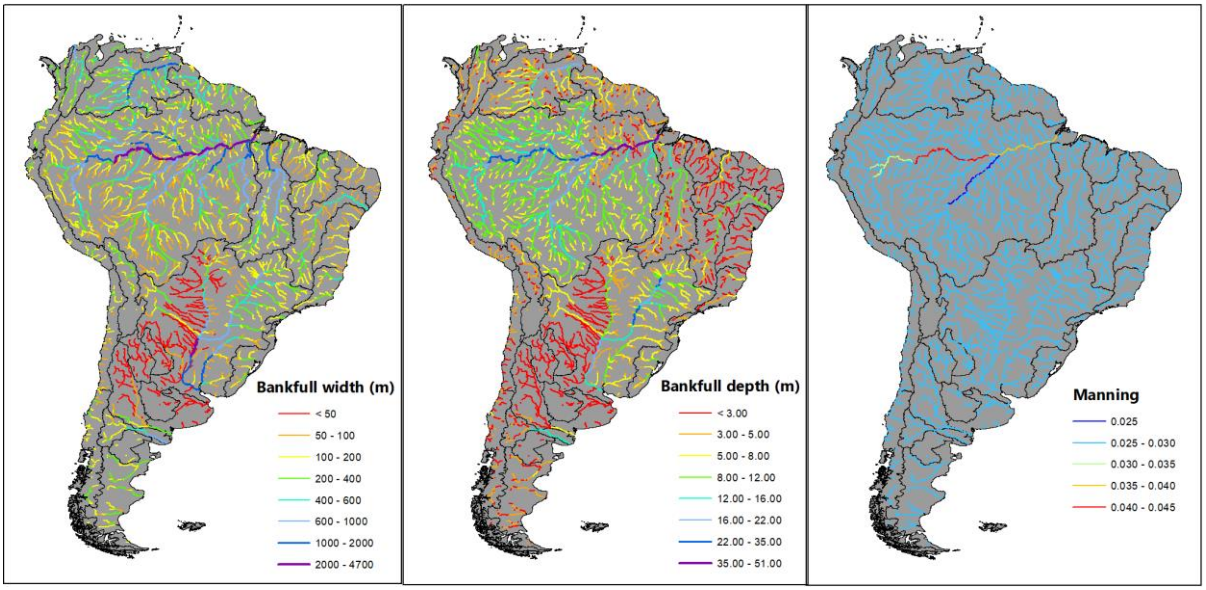

Figure A.1.6. Adopted bankfull width and depth values based on works by (Beighley and Gummadi, 2011), (Andreadis *et al.*, 2013), (Paiva *et al.*, 2011; Paiva *et al.*, 2013a) and (Pontes, 2016). Manning coefficient was globally set to 0.03, with further adjustments based on (Paiva *et al.*, 2013a).

A.1.5. Adjustment of river bed profiles

River bed elevations (z in (A_1.19)) are estimated subtracting the channel depths from the river bank heights derived from a spaceborne DEM (in this case, the Bare-Earth SRTM version 1 DEM from O'Loughlin *et al.* (2016)). However, for large-scale hydrodynamic routing it is essential to reduce noise in river bed profiles to avoid the excess of water leaving channels to the floodplains, especially when coarse resolution (both spatial and vertical) DEMs are used (Paiva *et al.*, 2011; Yamazaki *et al.*, 2012; Chen *et al.*, 2018). Also, noise in river bed profiles are likely to be even more pronounced because of the superposition of HydroSHEDS drainage networks over the Bare-Earth SRTM, since the latter is not hydrologically corrected (for instance, after using a depression-filling correction (e.g., Jenson and Domingue, 1988)).

To handle this, we applied a noise reduction method based on a simple linear regression to obtain smoothed river bank heights. For a given unit-catchment, all DEM pixels located over the river reach of Δx = 15 km (according to fixed-length discretization) are used to adjust a linear regression. River bank height is set as the smoothed elevation associated to the center pixel of the river reach (Figure A 1.7), without modifying DEM original values. Indeed, a larger benefit of the smoothing procedure is expected if a large number of pixels is sampled, i.e., by adopting a larger Δx, albeit this is not a good option due to the potential numerical instabilities associated to flow routing. Figure A.1.8 shows an example of the smoothed bed profile in comparison to the original one extracted from Bare-Earth SRTM (O'Loughlin *et al.*, 2016).

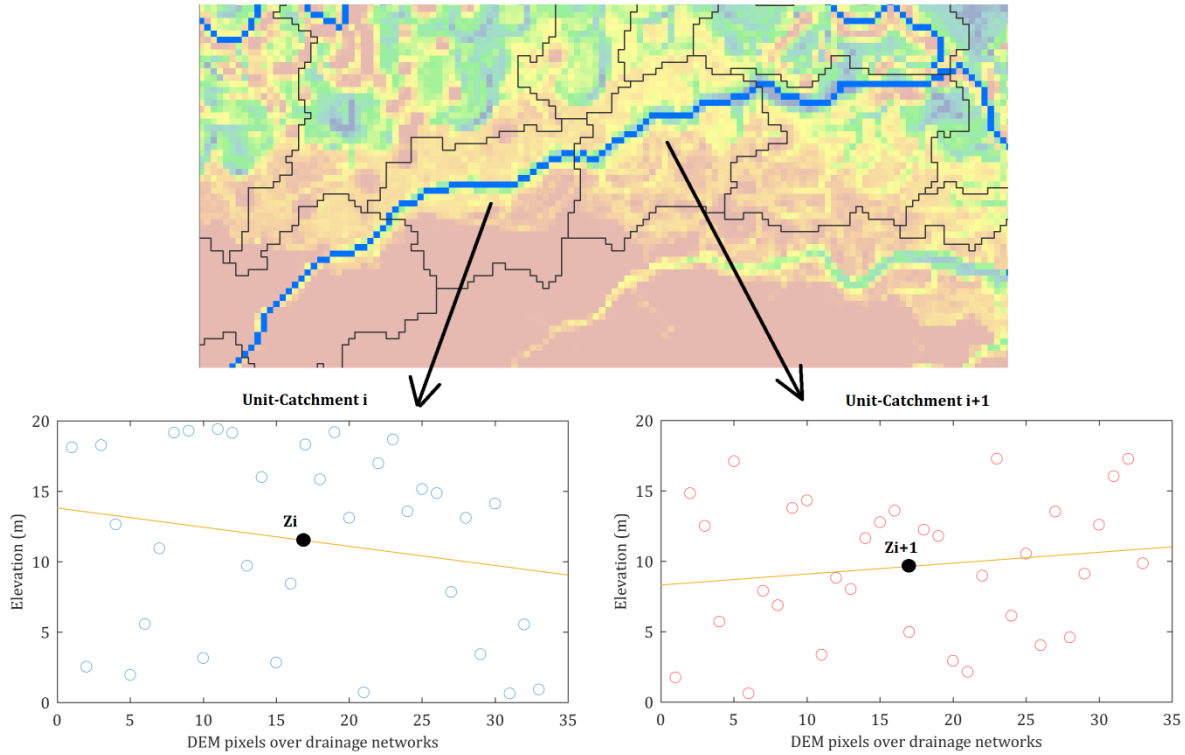

Figure A 1.7. Schematic representation of noise reduction in river bed profiles. Circles represent the elevation of DEM pixels located over river networks, which are used to adjust a linear regression (yellow line) within a same unit-catchment. Pixel numbers are ordered from upstream to downstream, so that bank heights are set in the middle of river reaches using the linear regression slope.

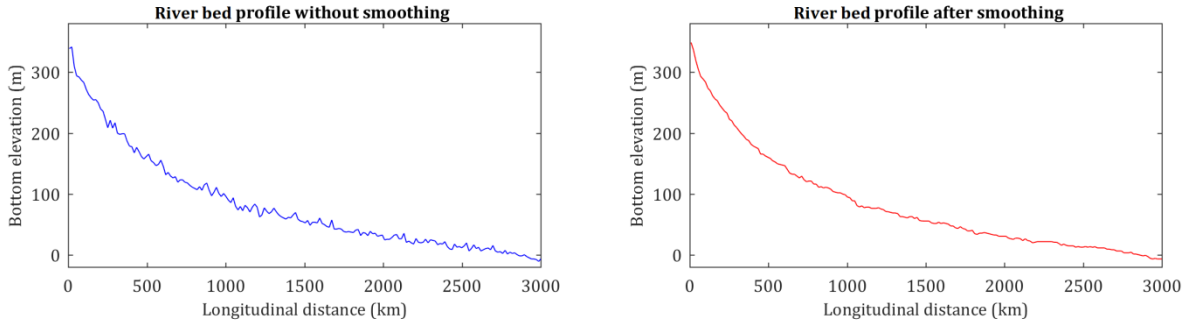

Figure A.1.8. Comparison between non-smoothed (left) and smoothed (right) river bed profile extracted from Bare-Earth SRTM. River profiles in this example were extracted for Purus (380 000 km²) mainstem, a tributary of the Amazon.

A.1.6. Sub-grid (sub- unit-catchment) floodplain topography

In order to represent floodplain inundation, a hypsometric curve relating flow depth, flooded area and water volume stored in both floodplain and channel for a given unit-catchment is derived from its underlying DEM. Regarding the floodplain, concepts of the HAND model (Renno *et al.*, 2008) were adopted to compute water volume emulating the inundation process

from lower to higher elevations (Figure A.1.9), which is the same approach adopted in CaMa-Flood by Yamazaki *et al.* (2013).

In this method, pixels characterized as main channels, i.e., over the drainage network, are initially set as null values defining the interface between channel bank height and floodplain region. The relative elevation between a given floodplain pixel and its nearest downstream channel pixel is computed as the height above channel top bank, which means that the pixel is only inundated if floodplain water level (current flow depth subtracted from channel bankfull depth) is equal or exceeds its respective HAND value. Thus, flooded area is calculated summing the individual areas of inundated pixels for a given HAND value, and volume of water stored in floodplain (plus channel below bankfull depth) is then computed considering vertical increments according to DEM vertical resolution. Figure A.1.10 shows a schematic representation of channel and floodplains (and their parameters) for a given unit-catchment.

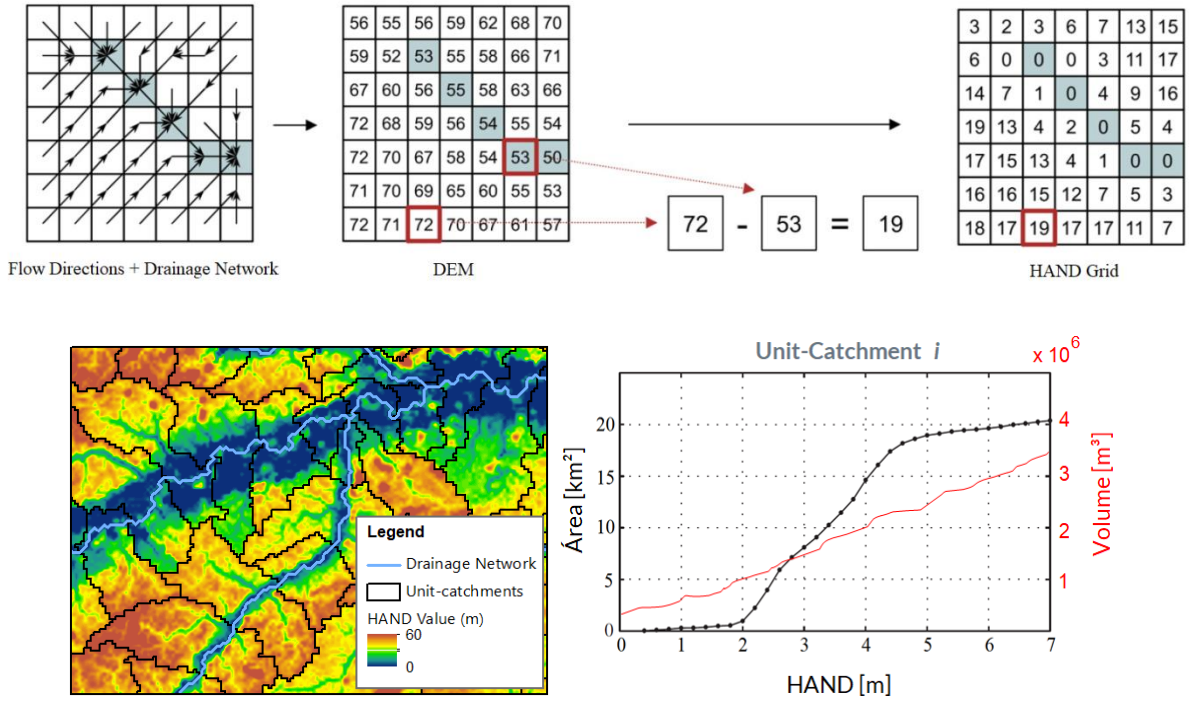

Figure A.1.9. Procedure to compute sub-grid floodplain profile. Top: Derivation of HAND grid using flow directions, DEM and drainage map extracted from a given area threshold. White and shaded cells represent pixels located over floodplain and drainage networks (channel), respectively (adapted from Renno *et al.*, 2008). Bottom: Floodplain area and volume are obtained through vertical increments in the HAND Grid, within a given unit-catchment.

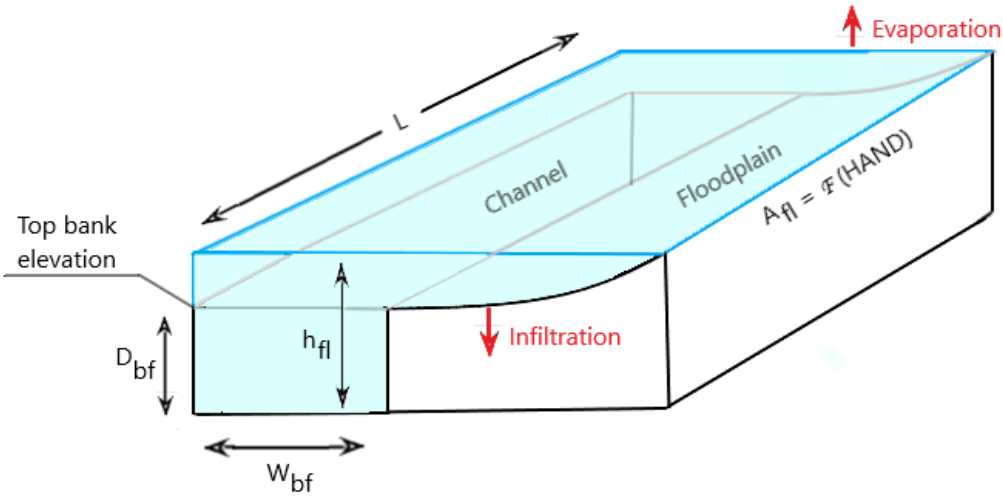

Figure A.1.10. Schematic representation of channel and floodplain within a given unit-catchment. L = Channel length; D_{bf} = Bankfull depth; W_{bf} = Bankfull Width; h_{fl} = Flow depth; A_{fl} = Floodplain area, expressed as a function of HAND value (derived from sub-grid topography).

Following these assumptions, floodplain profiles relating HAND value to flooded area (A_{fl}) and flooded volume (V_{fl}) are defined as:

$$A_{fl}(z,i) = \sum_{\langle y,x\rangle \in S} A\langle y,x\rangle \qquad \text{(A_1.27)}$$

$$V_{fl}(z,i) = W_{bfi} D_{bfi} L_i + \sum_{k=1}^{z} 0.5\left[A_{fl}(k,i) + A_{fl}(k-1,i)\right]\Delta z \qquad \text{(A_1.28)}$$

Where z is the HAND value analyzed [m], i is the unit-catchment analyzed; A_{fl} is the flooded area above channel top bank, for a given HAND and unit-catchment [km²]; V_{fl} is the total water stored in the control volume (channel + floodplains), for a given HAND and unit-catchment [m³], $\langle y,x\rangle$ are the pixel coordinates, located at row y and column x, $A\langle y,x\rangle$ is the pixel surface area [m²], $S = \{\langle y,x\rangle | UC\langle y,x\rangle = i, HAND\langle y,x\rangle \leq z\}$, $UC\langle y,x\rangle$ is the pixel element from the unit-catchment grid; $HAND\langle y,x\rangle$ is the pixel element from the HAND grid [m], Δz is the vertical resolution of the HAND grid, equal to 1 m.

Finally, HAND values in the floodplain profile are further converted to water levels, in such a way that the latter are equivalent to HAND plus bankfull depth. For the submerged part of topography (i.e., inside channel), volume is calculated through the numerical integration of flooded area with flow depth, the former approximated by channel width times river length (Pontes *et al.*, 2017). As previously described in section A.1.2, this enables flow depths to be

derived from stored water volume, by interpolating the channel/floodplain profile for a given unit-catchment.

B. Station list

Below is the list of discharge gauge stations used in this study. Information is related to the data providers, station code, station name, and geographic location. Additional water level data from ANA are related to the same discharge gauge codes of this data provider.

Data Provider	Code	Name	Latitude	Longitude
ANA (Brazil)	'10200000'	'PALMEIRAS DO JAVARI '	-5.133	-72.800
ANA (Brazil)	'10300000'	'SANTA MARIA '	-4.567	-71.417
ANA (Brazil)	'10500000'	'ESTIRÃO DO REPOUSO'	-4.367	-70.933
ANA (Brazil)	'10910000'	'LADÁRIO - JUSANTE '	-4.584	-70.281
ANA (Brazil)	'11400000'	'SÃO PAULO DE OLIVENÇA'	-3.450	-68.750
ANA (Brazil)	'11444900'	'IPIRANGA NOVO '	-2.867	-69.667
ANA (Brazil)	'11450000'	'IPIRANGA VELHO'	-2.983	-69.583
ANA (Brazil)	'11500000'	'SANTO ANTÔNIO DO IÇÁ'	-3.083	-67.933
ANA (Brazil)	'12100000'	'COLOCAÇÃO CAXIAS '	-5.400	-69.000
ANA (Brazil)	'12150000'	'CONCEIÇÃO (EX. ILHA DA NOVA SORTE)'	-4.897	-68.663
ANA (Brazil)	'12180000'	'TANIBUCA'	-4.745	-68.135
ANA (Brazil)	'12200000'	'BARREIRA ALTA '	-4.221	-67.893
ANA (Brazil)	'12240000'	'PORTO SEGURO'	-3.337	-67.492
ANA (Brazil)	'12370000'	'TAUMATURGO'	-8.946	-72.795
ANA (Brazil)	'12500000'	'CRUZEIRO DO SUL '	-7.611	-72.681
ANA (Brazil)	'12520000'	'IPIXUNA'	-7.051	-71.684
ANA (Brazil)	'12550000'	'EIRUNEPÉ - MONTANTE '	-6.684	-69.881
ANA (Brazil)	'12600001'	'TARAUACÁ - JUSANTE'	-8.136	-70.717
ANA (Brazil)	'12640000'	'SERINGAL SÃO FRANCISCO (SANTA HELENA)'	-8.686	-70.551
ANA (Brazil)	'12650000'	'FEIJÓ'	-8.152	-70.368
ANA (Brazil)	'12680000'	'ENVIRA '	-7.428	-70.023
ANA (Brazil)	'12700000'	'SANTOS DUMONT'	-6.440	-68.246
ANA (Brazil)	'12840000'	'GAVIÃO'	-4.839	-66.849
ANA (Brazil)	'12845000'	'VILA BITTENCOURT '	-1.400	-69.417
ANA (Brazil)	'12850000'	'ACANAUI '	-1.817	-66.600
ANA (Brazil)	'12880000'	'ESTIRÃO DA SANTA CRUZ '	-4.321	-65.201
ANA (Brazil)	'13150000'	'ITAPEUÁ '	-4.058	-63.028
ANA (Brazil)	'13180000'	'MANOEL URBANO '	-8.884	-69.268
ANA (Brazil)	'13300000'	'SERINGAL SÃO JOSÉ '	-9.319	-68.718
ANA (Brazil)	'13410000'	'SERINGAL DA CARIDADE '	-9.044	-68.577
ANA (Brazil)	'13600002'	'RIO BRANCO'	-9.976	-67.800

Data Provider	Code	Name	Latitude	Longitude
ANA (Brazil)	'13650000'	'FLORIANO PEIXOTO'	-9.051	-67.368
ANA (Brazil)	'13710001'	'VALPARAÍSO - MONTANTE'	-8.683	-67.400
ANA (Brazil)	'13740000'	'FAZENDA BORANGABA '	-7.550	-67.550
ANA (Brazil)	'13750000'	'SERINGAL FORTALEZA '	-7.717	-66.985
ANA (Brazil)	'13849000'	'JURENÉ'	-8.768	-65.884
ANA (Brazil)	'13880000'	'CANUTAMA '	-6.534	-64.384
ANA (Brazil)	'13886000'	'BACABA '	-6.317	-64.884
ANA (Brazil)	'14110000'	'CUCUÍ '	1.215	-66.853
ANA (Brazil)	'14230000'	'MISSÃO IÇANA '	1.074	-67.595
ANA (Brazil)	'14250000'	'SÃO FELIPE'	0.372	-67.313
ANA (Brazil)	'14260000'	'UARAÇU'	0.477	-69.128
ANA (Brazil)	'14280001'	'TARAQUA '	0.130	-68.539
ANA (Brazil)	'14325000'	'TUMBIRA'	-0.344	-67.536
ANA (Brazil)	'14330000'	'CURICURIARI'	-0.200	-66.801
ANA (Brazil)	'14350000'	'JUSANTE DA CACHOEIRA DO CAJU'	-0.244	-67.016
ANA (Brazil)	'14420000'	'SERRINHA'	-0.482	-64.827
ANA (Brazil)	'14440000'	'POSTO AJURICABA '	0.884	-62.622
ANA (Brazil)	'14450000'	'JALAUACA'	-0.301	-62.762
ANA (Brazil)	'14488000'	'UAICAS '	3.550	-63.169
ANA (Brazil)	'14495000'	'FAZENDA CAJUPIRANGA '	3.438	-61.037
ANA (Brazil)	'14515000'	'FAZENDA PASSARÃO'	3.208	-60.571
ANA (Brazil)	'14680001'	'FÉ E ESPERANÇA '	2.871	-61.441
ANA (Brazil)	'14690000'	'MUCAJAÍ '	2.471	-60.918
ANA (Brazil)	'15030000'	'JATUARANA'	-3.052	-59.678
ANA (Brazil)	'15120001'	'VILA BELA DA SANTÍSSIMA TRINDADE'	-15.008	-59.949
ANA (Brazil)	'15130000'	'PIMENTEIRAS'	-13.480	-61.046
ANA (Brazil)	'15150000'	'PEDRAS NEGRAS'	-12.851	-62.899
ANA (Brazil)	'15250000'	'GUAJARÁ-MIRIM '	-10.793	-65.348
ANA (Brazil)	'15320002'	'ABUNÃ'	-9.703	-65.365
ANA (Brazil)	'15326000'	'MORADA NOVA - JUSANTE'	-9.785	-65.528
ANA (Brazil)	'15550000'	'SANTA ISABEL '	-8.799	-63.711
ANA (Brazil)	'15558000'	'PIMENTA BUENO'	-11.684	-61.192
ANA (Brazil)	'15559000'	'SÍTIO BELA VISTA'	-11.653	-61.215
ANA (Brazil)	'15560000'	'JIPARANÁ '	-10.874	-61.936
ANA (Brazil)	'15580000'	'TABAJARA '	-8.933	-62.054
ANA (Brazil)	'15630000'	'HUMAITÁ '	-7.505	-63.020
ANA (Brazil)	'15670000'	'NOVA ESPERANÇA '	-6.359	-61.766
ANA (Brazil)	'15700000'	'MANICORÉ '	-5.817	-61.302
ANA (Brazil)	'15750000'	'HUMBOLDT'	-10.168	-59.464
ANA (Brazil)	'15795000'	'LEONTINO'	-7.767	-60.567
ANA (Brazil)	'15800000'	'BOCA DO GUARIBA '	-7.708	-60.586

Data Provider	Code	Name	Latitude	Longitude
ANA (Brazil)	'15820000'	'CONCISA '	-9.800	-60.691
ANA (Brazil)	'15828000'	'FAZENDA BOA LEMBRANÇA '	-7.650	-60.833
ANA (Brazil)	'15830000'	'PRAINHA VELHA '	-7.208	-60.650
ANA (Brazil)	'15910000'	'SANTAREM SUCUNDURI'	-6.796	-59.042
ANA (Brazil)	'16205000'	'BASE SIDERAMA - JUSANTE '	-1.683	-58.533
ANA (Brazil)	'16430000'	'GARGANTA'	-0.998	-57.043
ANA (Brazil)	'16460000'	'CARAMUJO'	-1.065	-57.061
ANA (Brazil)	'16480000'	'ALDEIA WAI-WA '	-0.695	-57.975
ANA (Brazil)	'16500000'	'ESTIRÃO DA ANGÉLICA'	-1.101	-57.057
ANA (Brazil)	'17090000'	'BOCA DO INFERNO '	-1.503	-54.873
ANA (Brazil)	'17093000'	'FONTANILHAS'	-11.358	-58.343
ANA (Brazil)	'17095000'	'FAZENDA TOMBADOR '	-11.777	-58.073
ANA (Brazil)	'17120000'	'PORTO DOS GAUCHOS'	-11.536	-57.423
ANA (Brazil)	'17122000'	'RIO DOS PEIXES'	-10.823	-57.726
ANA (Brazil)	'17123000'	'RIO ARINOS'	-10.640	-58.003
ANA (Brazil)	'17200000'	'PORTO RONCADOR '	-13.557	-55.334
ANA (Brazil)	'17210000'	'TELES PIRES '	-12.674	-55.792
ANA (Brazil)	'17280000'	'CACHOEIRÃO '	-11.651	-55.703
ANA (Brazil)	'17300000'	'FAZENDA TRATEX'	-10.956	-55.549
ANA (Brazil)	'17340000'	'INDECO'	-10.113	-55.570
ANA (Brazil)	'17380000'	'JUSANTE FOZ PEIXOTO DE AZEVEDO'	-9.643	-56.018
ANA (Brazil)	'17410000'	'SANTA ROSA '	-8.860	-57.420
ANA (Brazil)	'17420000'	'TRÊS MARIAS'	-7.615	-57.950
ANA (Brazil)	'17430000'	'BARRA DO SÃO MANUEL - JUSANTE'	-7.340	-58.155
ANA (Brazil)	'17500000'	'FORTALEZA '	-6.045	-57.643
ANA (Brazil)	'17650002'	'ACARÁ DO TAPAJÓS'	-4.886	-56.723
ANA (Brazil)	'17675000'	'JARDIM DO OURO'	-6.258	-55.773
ANA (Brazil)	'17730000'	'ITAITUBA '	-4.283	-55.983
ANA (Brazil)	'18200000'	'ARAPARI '	-1.779	-54.397
ANA (Brazil)	'18415000'	'POUSADA MATRINXA '	-13.569	-53.076
ANA (Brazil)	'18436000'	'JUSANTE RIO PRETO'	-10.047	-52.114
ANA (Brazil)	'18460000'	'BOA SORTE '	-6.750	-51.983
ANA (Brazil)	'18500000'	'BOA ESPERANÇA'	-6.719	-51.783
ANA (Brazil)	'18510000'	'SÃO FELIX DO XINGU'	-6.600	-52.050
ANA (Brazil)	'18520000'	'BELO HORIZONTE'	-5.408	-52.902
ANA (Brazil)	'18590000'	'MANOEL JORGE (TERRA PRETA)'	-6.203	-54.074
ANA (Brazil)	'18650000'	'CAJUEIRO'	-5.654	-54.521
ANA (Brazil)	'18700000'	'PEDRA DO Ó'	-4.542	-54.001
ANA (Brazil)	'18850000'	'ALTAMIRA'	-3.212	-52.211
ANA (Brazil)	'18870000'	'ALDEIA BACAJÁ'	-4.916	-51.428
ANA (Brazil)	'19150000'	'SÃO FRANCISCO '	-0.568	-52.569

Data Provider	Code	Name	Latitude	Longitude
ANA (Brazil)	'20050000'	'PONTE QUEBRA LINHA'	-14.978	-48.676
ANA (Brazil)	'20250000'	'CERES (POSTO BIQUINHA)'	-15.309	-49.553
ANA (Brazil)	'20490000'	'COLÔNIA DOS AMERICANOS'	-14.740	-49.064
ANA (Brazil)	'20500000'	'PORTO URUAÇU'	-14.519	-49.042
ANA (Brazil)	'21050000'	'SÃO FELIX (A/B)'	-13.533	-48.138
ANA (Brazil)	'21500000'	'NOVA ROMA (FAZ.SUCURI)'	-13.763	-46.838
ANA (Brazil)	'21600000'	'PONTE PARANÃ'	-13.424	-47.132
ANA (Brazil)	'21650000'	'MONTANTE DA BARRA DO PALMA'	-12.603	-47.861
ANA (Brazil)	'21850000'	'RIO DA PALMA'	-12.416	-47.199
ANA (Brazil)	'21890000'	'BARRA DO PALMA'	-12.603	-47.861
ANA (Brazil)	'21900000'	'PARANÃ '	-12.622	-47.886
ANA (Brazil)	'22150000'	'JACINTO'	-11.981	-48.658
ANA (Brazil)	'22220000'	'PORTO JERÔNIMO - FAZ. PIRACICABA '	-11.759	-47.836
ANA (Brazil)	'22250000'	'FAZENDA LOBEIRA'	-11.533	-48.289
ANA (Brazil)	'22350000'	'PORTO NACIONAL '	-10.704	-48.418
ANA (Brazil)	'22680000'	'JATOBÁ (FAZENDA BOA NOVA) '	-9.995	-47.473
ANA (Brazil)	'22700000'	'NOVO ACORDO'	-9.963	-47.675
ANA (Brazil)	'22900000'	'PORTO REAL'	-9.307	-47.929
ANA (Brazil)	'23100000'	'TUPIRATINS'	-8.392	-48.111
ANA (Brazil)	'23250000'	'GOIATINS'	-7.708	-47.312
ANA (Brazil)	'23300000'	'CAROLINA'	-7.338	-47.473
ANA (Brazil)	'23600000'	'TOCANTINÓPOLIS'	-6.289	-47.392
ANA (Brazil)	'23700000'	'DESCARRETO'	-5.789	-47.469
ANA (Brazil)	'24200000'	'TORIXOREU'	-16.201	-52.550
ANA (Brazil)	'24700000'	'BARRA DO GARÇAS (ARAGARÇAS)'	-15.891	-52.228
ANA (Brazil)	'24800000'	'PERES'	-15.890	-51.853
ANA (Brazil)	'24850000'	'ARAGUAIANA'	-15.738	-51.828
ANA (Brazil)	'24950000'	'MONTES CLAROS DE GOIÁS'	-15.572	-51.634
ANA (Brazil)	'25200000'	'ARUANÃ'	-14.902	-51.082
ANA (Brazil)	'25700000'	'BANDEIRANTES'	-13.690	-50.800
ANA (Brazil)	'25800000'	'JUSANTE DO RIO PINTADO'	-13.561	-50.401
ANA (Brazil)	'25950000'	'LUIZ ALVES'	-13.210	-50.585
ANA (Brazil)	'26015000'	'JUSANTE BARRA DO FORQUILHA'	-12.884	-50.832
ANA (Brazil)	'26050000'	'TORIQUEJE'	-15.249	-53.055
ANA (Brazil)	'26100000'	'XAVANTINA '	-14.672	-52.355
ANA (Brazil)	'26200000'	'TRECHO MÉDIO'	-14.087	-51.696
ANA (Brazil)	'26300000'	'SANTO ANTÔNIO DO LEVERGER'	-12.292	-50.963
ANA (Brazil)	'26350000'	'SÃO FELIX DO ARAGUAIA '	-11.620	-50.663
ANA (Brazil)	'26800000'	'BARREIRA DA CRUZ '	-10.565	-49.934

Data Provider	Code	Name	Latitude	Longitude
ANA (Brazil)	'27500000'	'CONCEIÇÃO DO ARAGUAIA'	-8.269	-49.259
ANA (Brazil)	'28300000'	'XAMBIOÁ '	-6.410	-48.542
ANA (Brazil)	'28850000'	'ARAGUATINS'	-5.634	-48.130
ANA (Brazil)	'29050000'	'MARABÁ '	-5.339	-49.124
ANA (Brazil)	'29100000'	'FAZENDA ALEGRIA'	-5.514	-49.221
ANA (Brazil)	'29200000'	'ITUPIRANGA '	-5.128	-49.324
ANA (Brazil)	'30080000'	'CAPIVARA'	1.071	-51.671
ANA (Brazil)	'30300000'	'SERRA DO NAVIO '	0.901	-52.010
ANA (Brazil)	'30400000'	'PORTO PLATON'	0.708	-51.439
ANA (Brazil)	'31680000'	'FAZENDA MARINGA '	-3.161	-48.099
ANA (Brazil)	'31700000'	'BADAJÓS'	-2.513	-47.768
ANA (Brazil)	'32540000'	'FAZENDA RURAL ZEBU'	-3.341	-46.877
ANA (Brazil)	'32620000'	'ALTO BONITO'	-1.801	-46.316
ANA (Brazil)	'33070000'	'FAZENDA VARIG'	-4.213	-46.495
ANA (Brazil)	'33080000'	'ALTO ALEGRE'	-3.665	-45.842
ANA (Brazil)	'33190000'	'PINDARÉ-MIRIM '	-3.661	-45.458
ANA (Brazil)	'33250000'	'BARRA DO CORDA '	-5.500	-45.243
ANA (Brazil)	'33260000'	'SANTA VITÓRIA'	-5.106	-44.961
ANA (Brazil)	'33281000'	'PEDREIRAS II'	-4.567	-44.600
ANA (Brazil)	'33286000'	'SÃO LUIZ GONZAGA'	-4.383	-44.667
ANA (Brazil)	'33290000'	'BACABAL '	-4.219	-44.765
ANA (Brazil)	'33333000'	'ITAIPAVA'	-5.144	-45.795
ANA (Brazil)	'33365000'	'FAZENDA SABESA'	-4.538	-45.326
ANA (Brazil)	'33380000'	'ARATOI GRANDE'	-3.770	-45.218
ANA (Brazil)	'33480000'	'COLINAS'	-6.019	-44.243
ANA (Brazil)	'33530000'	'MONTEVIDEU'	-5.337	-43.884
ANA (Brazil)	'33550000'	'CAXIAS'	-4.865	-43.358
ANA (Brazil)	'33590000'	'CODÓ '	-4.458	-43.875
ANA (Brazil)	'33630000'	'COROATA'	-4.128	-44.128
ANA (Brazil)	'33680000'	'CANTANHEDE'	-3.628	-44.379
ANA (Brazil)	'33780000'	'NINA RODRIGUES'	-3.459	-43.899
ANA (Brazil)	'34020000'	'ALTO PARNAÍBA'	-9.113	-45.926
ANA (Brazil)	'34040000'	'FAZENDA PARACATI'	-8.281	-45.667
ANA (Brazil)	'34040500'	'FAZENDA PARACATI II'	-8.271	-45.668
ANA (Brazil)	'34060000'	'RIBEIRO GONÇALVES'	-7.567	-45.254
ANA (Brazil)	'34070000'	'SÍTIO DO VELHO'	-7.381	-44.827
ANA (Brazil)	'34090000'	'FAZENDA BANDEIRA'	-7.391	-44.614
ANA (Brazil)	'34170000'	'SÃO FÉLIX DE BALSAS'	-7.068	-44.813
ANA (Brazil)	'34251000'	'CRISTINO CASTRO II'	-8.793	-44.206
ANA (Brazil)	'34270000'	'BARRA DO LANCE'	-7.248	-43.643
ANA (Brazil)	'34470000'	'SANTA CRUZ DO PIAUÍ'	-7.190	-41.770
ANA (Brazil)	'34471000'	'SANTA CRUZ DO PIAUÍ II'	-7.189	-41.770

Data Provider	Code	Name	Latitude	Longitude
ANA (Brazil)	'34480000'	'FAZENDA TALHADA'	-6.973	-42.106
ANA (Brazil)	'34571000'	'SÃO FRANCISCO DO PIAUÍ'	-7.233	-42.544
ANA (Brazil)	'34600000'	'FRANCISCO AYRES'	-6.625	-42.698
ANA (Brazil)	'34750000'	'FAZENDA BOA ESPERANÇA'	-5.223	-41.738
ANA (Brazil)	'34760000'	'FAZENDA CARNAIBA'	-5.714	-42.100
ANA (Brazil)	'34770000'	'PRATA DO PIAUÍ'	-5.666	-42.214
ANA (Brazil)	'34789000'	'FAZENDA CANTINHO II'	-5.203	-42.697
ANA (Brazil)	'34879500'	'LUZILÂNDIA'	-3.454	-42.370
ANA (Brazil)	'34940000'	'ESPERANTINA'	-3.903	-42.230
ANA (Brazil)	'34980000'	'TINGUIS'	-3.724	-41.974
ANA (Brazil)	'35275000'	'SOBRAL'	-3.689	-40.341
ANA (Brazil)	'36070000'	'SÍTIO PATOS'	-6.521	-39.639
ANA (Brazil)	'36160000'	'IGUATU'	-6.373	-39.293
ANA (Brazil)	'36290000'	'ICÓ'	-6.406	-38.867
ANA (Brazil)	'36320000'	'JAGUARIBE'	-5.901	-38.632
ANA (Brazil)	'36390000'	'PEIXE GORDO'	-5.229	-38.199
ANA (Brazil)	'36580000'	'MORADA NOVA II'	-5.121	-38.444
ANA (Brazil)	'37410000'	'SÍTIO VASSOURAS'	-6.729	-37.794
ANA (Brazil)	'37470000'	'JARDIM DE PIRANHAS '	-6.378	-37.353
ANA (Brazil)	'37710150'	'SÍTIO ACAUA II'	-5.616	-36.891
ANA (Brazil)	'38860000'	'BODOCONGO'	-7.528	-36.000
ANA (Brazil)	'38880000'	'GUARITA'	-7.334	-35.373
ANA (Brazil)	'38895000'	'PONTE DA BATALHA'	-7.130	-35.048
ANA (Brazil)	'40070000'	'PONTE DO CHUMBO'	-19.776	-45.479
ANA (Brazil)	'40100000'	'PORTO DAS ANDORINHAS'	-19.279	-45.286
ANA (Brazil)	'41650002'	'PONTE DO LICÍNIO - JUSANTE'	-18.673	-44.194
ANA (Brazil)	'41818000'	'SANTO HIPÓLITO (ANA/CEMIG)'	-18.306	-44.226
ANA (Brazil)	'41990000'	'VÁRZEA DA PALMA'	-17.595	-44.714
ANA (Brazil)	'42395000'	'SANTA ROSA'	-17.255	-46.473
ANA (Brazil)	'42690001'	'PORTO DA EXTREMA'	-17.030	-46.014
ANA (Brazil)	'42750000'	'CAATINGA '	-17.143	-45.880
ANA (Brazil)	'42930000'	'PORTO DO CAVALO '	-17.031	-45.539
ANA (Brazil)	'42980000'	'PORTO ALEGRE'	-16.907	-45.383
ANA (Brazil)	'43200000'	'SÃO ROMÃO '	-16.373	-45.070
ANA (Brazil)	'43429998'	'ARINOS - MONTANTE'	-15.924	-46.109
ANA (Brazil)	'43670000'	'VILA URUCUIA '	-16.133	-45.742
ANA (Brazil)	'43880000'	'SANTO INÁCIO'	-16.281	-45.414
ANA (Brazil)	'43980002'	'BARRA DO ESCURO '	-16.268	-45.237
ANA (Brazil)	'44200000'	'SÃO FRANCISCO'	-15.949	-44.868
ANA (Brazil)	'44290002'	'PEDRAS DE MARIA DA CRUZ'	-15.610	-44.395
ANA (Brazil)	'44500000'	'MANGA'	-14.757	-43.932
ANA (Brazil)	'44670000'	'COLÔNIA DO JAIBA'	-15.343	-43.676

Data Provider	Code	Name	Latitude	Longitude
ANA (Brazil)	'44950000'	'BOCA DA CAATINGA'	-14.783	-43.538
ANA (Brazil)	'45210000'	'LAGOA DAS PEDRAS'	-14.283	-44.409
ANA (Brazil)	'45260000'	'JUVENÍLIA '	-14.260	-44.152
ANA (Brazil)	'45298000'	'CARINHANHA'	-14.304	-43.763
ANA (Brazil)	'45480000'	'BOM JESUS DA LAPA'	-13.257	-43.435
ANA (Brazil)	'45910001'	'SANTA MARIA DA VITÓRIA '	-13.397	-44.199
ANA (Brazil)	'45960001'	'PORTO NOVO'	-13.291	-43.909
ANA (Brazil)	'46035000'	'GAMELEIRA'	-12.869	-43.380
ANA (Brazil)	'46105000'	'PARATINGA'	-12.697	-43.226
ANA (Brazil)	'46150000'	'IBOTIRAMA'	-12.183	-43.223
ANA (Brazil)	'46295000'	'PONTE BR-242'	-12.245	-42.764
ANA (Brazil)	'46360000'	'MORPARÁ '	-11.558	-43.283
ANA (Brazil)	'46550000'	'BARREIRAS'	-12.153	-45.009
ANA (Brazil)	'46610000'	'SÃO SEBASTIÃO'	-11.979	-44.877
ANA (Brazil)	'46650000'	'TAGUA'	-11.721	-44.502
ANA (Brazil)	'46675000'	'FAZENDA MACAMBIRA'	-11.611	-44.157
ANA (Brazil)	'46790000'	'FORMOSA DO RIO PRETO '	-11.051	-45.197
ANA (Brazil)	'46830000'	'IBIPETUBA'	-11.006	-44.524
ANA (Brazil)	'46870000'	'FAZENDA PORTO LIMPO'	-11.236	-43.949
ANA (Brazil)	'46902000'	'BOQUEIRÃO'	-11.355	-43.846
ANA (Brazil)	'47900000'	'ABREUS'	-10.010	-40.695
ANA (Brazil)	'48860000'	'FLORESTA'	-8.609	-38.577
ANA (Brazil)	'50169000'	'PONTE SE-302'	-10.621	-37.751
ANA (Brazil)	'50169500'	'CAMINHO DO RIO'	-10.639	-37.698
ANA (Brazil)	'50191000'	'FAZENDA BELÉM'	-10.943	-37.347
ANA (Brazil)	'50465000'	'QUEIMADAS'	-10.973	-39.633
ANA (Brazil)	'50494000'	'AMBRÓSIO'	-10.998	-39.224
ANA (Brazil)	'50520000'	'PONTE EUCLIDES DA CUNHA'	-11.060	-38.837
ANA (Brazil)	'50540000'	'CIPÓ'	-11.098	-38.513
ANA (Brazil)	'50591000'	'FAZENDA TRIANON'	-11.664	-37.936
ANA (Brazil)	'50595000'	'USINA ALTAMIRA'	-11.735	-37.803
ANA (Brazil)	'51240000'	'ITAETÉ '	-12.993	-40.961
ANA (Brazil)	'51280000'	'IAÇU'	-12.762	-40.214
ANA (Brazil)	'51330000'	'FAZENDA SANTA FÉ'	-12.516	-39.848
ANA (Brazil)	'51350000'	'ARGOIM '	-12.586	-39.522
ANA (Brazil)	'51460000'	'PONTE RIO BRANCO'	-12.233	-39.046
ANA (Brazil)	'52264000'	'TOCADAS'	-14.109	-41.429
ANA (Brazil)	'52265000'	'ROÇADOS'	-14.113	-41.414
ANA (Brazil)	'52270000'	'SANTO ANTÔNIO '	-14.096	-41.292
ANA (Brazil)	'52404000'	'AREIÃO'	-14.031	-40.983
ANA (Brazil)	'52405000'	'LAGOA DO TAMBURI'	-13.878	-40.896
ANA (Brazil)	'52570000'	'JEQUIÉ'	-13.864	-40.081

Data Provider	Code	Name	Latitude	Longitude
ANA (Brazil)	'52680000'	'IPIAÚ'	-14.140	-39.687
ANA (Brazil)	'52695000'	'VAPOR'	-14.209	-39.546
ANA (Brazil)	'52831000'	'UBAITABA - JUSANTE'	-14.319	-39.328
ANA (Brazil)	'53540001'	'VEREDA DO PARAÍSO (SUDENE)'	-15.494	-41.450
ANA (Brazil)	'53620000'	'CÂNDIDO SALES'	-15.513	-41.237
ANA (Brazil)	'53630000'	'INHOBIM'	-15.340	-40.933
ANA (Brazil)	'53650000'	'ITAMBÉ '	-15.248	-40.631
ANA (Brazil)	'53880000'	'FAZENDA NANCY'	-15.604	-39.517
ANA (Brazil)	'53950000'	'MASCOTE'	-15.559	-39.308
ANA (Brazil)	'54150000'	'PORTO MANDACARU'	-16.679	-42.486
ANA (Brazil)	'54195000'	'BARRA DO SALINAS'	-16.618	-42.309
ANA (Brazil)	'54390000'	'PEGA'	-16.860	-42.348
ANA (Brazil)	'54500000'	'ARAÇUAÍ'	-16.850	-42.063
ANA (Brazil)	'54530000'	'ITIRA'	-16.761	-42.003
ANA (Brazil)	'54580000'	'ITAOBIM'	-16.568	-41.503
ANA (Brazil)	'54710000'	'JEQUITINHONHA'	-16.428	-41.014
ANA (Brazil)	'54780000'	'JACINTO'	-16.139	-40.307
ANA (Brazil)	'54950000'	'ITAPEBI'	-15.948	-39.524
ANA (Brazil)	'55699998'	'NANUQUE - MONTANTE'	-17.841	-40.381
ANA (Brazil)	'55960000'	'BOCA DA VALA'	-18.651	-40.089
ANA (Brazil)	'56425000'	'FAZENDA CACHOEIRA D"ANTAS'	-19.994	-42.674
ANA (Brazil)	'56539000'	'CACHOEIRA DOS ÓCULOS - MONTANTE'	-19.777	-42.476
ANA (Brazil)	'56719998'	'CENIBRA'	-19.328	-42.398
ANA (Brazil)	'56825000'	'NAQUE VELHO'	-19.188	-42.423
ANA (Brazil)	'56850000'	'GOVERNADOR VALADARES '	-18.883	-41.950
ANA (Brazil)	'56920000'	'TUMIRITINGA'	-18.971	-41.639
ANA (Brazil)	'56948005'	'RESPLENDOR - JUSANTE'	-19.343	-41.246
ANA (Brazil)	'56994500'	'COLATINA'	-19.531	-40.623
ANA (Brazil)	'58974000'	'CAMPOS - PONTE MUNICIPAL'	-21.753	-41.300
ANA (Brazil)	'60040000'	'FAZENDA SÃO DOMINGOS'	-18.103	-47.695
ANA (Brazil)	'60510010'	'ENGENHEIRO AMORIM'	-17.036	-47.941
ANA (Brazil)	'60544990'	'PIRES DO RIO - ME'	-17.328	-48.239
ANA (Brazil)	'60545000'	'PIRES DO RIO '	-17.327	-48.239
ANA (Brazil)	'60680000'	'PONTE MEIA PONTE'	-18.339	-49.611
ANA (Brazil)	'60772000'	'FAZENDA SANTA MARIA'	-17.981	-50.247
ANA (Brazil)	'60798000'	'MAURILÂNDIA'	-17.974	-50.337
ANA (Brazil)	'60805000'	'PONTE SUL GOIANA'	-18.071	-50.172
ANA (Brazil)	'60907000'	'FAZENDA RONDINHA'	-19.083	-50.648
ANA (Brazil)	'61145000'	'MACAIA '	-21.145	-44.914
ANA (Brazil)	'61855000'	'FAZENDA BELA VISTA '	-20.909	-48.089
ANA (Brazil)	'61902000'	'PORTO FERREIRA'	-21.842	-47.475

Data Provider	Code	Name	Latitude	Longitude
ANA (Brazil)	'61912000'	'PONTE GUATAPARA'	-21.502	-48.041
ANA (Brazil)	'61915000'	'PASSAGEM'	-21.017	-48.177
ANA (Brazil)	'61915005'	'PASSAGEM'	-21.019	-48.181
ANA (Brazil)	'61925000'	'PONTE JOAQUIM JUSTINO'	-20.454	-48.450
ANA (Brazil)	'63002000'	'SÃO JOSÉ DO SUCURIU'	-19.965	-52.219
ANA (Brazil)	'63003100'	'PORTO GALEANO'	-20.094	-52.160
ANA (Brazil)	'63350100'	'ÁGUA CLARA'	-20.444	-52.899
ANA (Brazil)	'63390000'	'ESTRADA QUEIROZ'	-20.889	-52.355
ANA (Brazil)	'63950280'	'FAZENDA BARRA GRANDE'	-21.574	-53.618
ANA (Brazil)	'63955000'	'DELFINO COSTA'	-21.614	-53.051
ANA (Brazil)	'63970000'	'FAZENDA BURITI'	-21.662	-52.866
ANA (Brazil)	'64390000'	'PORTO SANTA TEREZINHA'	-23.123	-50.450
ANA (Brazil)	'64482000'	'TELÊMACO BORBA'	-24.359	-50.595
ANA (Brazil)	'64501000'	'PORTO LONDRINA'	-23.650	-50.883
ANA (Brazil)	'64506000'	'CHACARA ANA CLAÚDIA'	-23.283	-50.967
ANA (Brazil)	'64507000'	'JATAIZINHO ANA/CESP'	-23.251	-50.982
ANA (Brazil)	'64611000'	'RETIRO GUARUJÁ'	-21.901	-54.054
ANA (Brazil)	'64614000'	'FAZENDA IPACARAI'	-21.956	-53.768
ANA (Brazil)	'64617000'	'IVINHEMA '	-22.383	-53.529
ANA (Brazil)	'64655000'	'UBÁ DO SUL'	-24.042	-51.623
ANA (Brazil)	'64689005'	'TAPIRA JUSANTE'	-23.231	-53.052
ANA (Brazil)	'64693000'	'NOVO PORTO TAQUARA'	-23.198	-53.304
ANA (Brazil)	'64795000'	'PONTE DO PIQUIRI'	-24.517	-53.167
ANA (Brazil)	'64820000'	'PORTO FORMOSA'	-24.200	-53.333
ANA (Brazil)	'64830000'	'BALSA SANTA MARIA '	-24.166	-53.736
ANA (Brazil)	'65220000'	'FLUVIÓPOLIS'	-26.019	-50.593
ANA (Brazil)	'65310000'	'UNIÃO DA VITÓRIA '	-26.228	-51.080
ANA (Brazil)	'66015000'	'PORTO ESTRELA'	-15.326	-57.226
ANA (Brazil)	'66070004'	'CÁCERES (DNPVN) '	-16.063	-57.688
ANA (Brazil)	'66090000'	'DESCALVADOS'	-16.733	-57.748
ANA (Brazil)	'66120000'	'PORTO CONCEIÇÃO'	-17.143	-57.359
ANA (Brazil)	'66250001'	'ROSÁRIO OESTE '	-14.834	-56.414
ANA (Brazil)	'66255000'	'ACORIZAL'	-15.204	-56.367
ANA (Brazil)	'66260001'	'CUIABÁ '	-15.616	-56.109
ANA (Brazil)	'66280000'	'BARÃO DE MELGAÇO'	-16.192	-55.966
ANA (Brazil)	'66340000'	'PORTO CERCADO (EX-Retiro Biguacal) '	-16.500	-56.333
ANA (Brazil)	'66360000'	'SÃO JOÃO'	-16.944	-56.632
ANA (Brazil)	'66370000'	'ILHA CAMARGO'	-17.057	-56.586
ANA (Brazil)	'66450001'	'RONDONÓPOLIS'	-16.479	-54.651
ANA (Brazil)	'66460000'	'ACIMA DO CÓRREGO GRANDE'	-16.608	-55.206
ANA (Brazil)	'66470000'	'SÃO JOSÉ DO BORIRÉU'	-16.921	-56.223

Data Provider	Code	Name	Latitude	Longitude
ANA (Brazil)	'66600000'	'SÃO JERÔNIMO '	-17.201	-56.008
ANA (Brazil)	'66650000'	'SÃO JOSÉ DO PIQUIRI'	-17.291	-56.385
ANA (Brazil)	'66710000'	'POUSADA TAIAMÃ (Ex-Porto Jofre)'	-17.368	-56.773
ANA (Brazil)	'66750000'	'PORTO ALEGRE'	-17.623	-56.965
ANA (Brazil)	'66800000'	'AMOLAR'	-18.039	-57.489
ANA (Brazil)	'66810000'	'SÃO FRANCISCO '	-18.394	-57.391
ANA (Brazil)	'66870000'	'COXIM '	-18.508	-54.761
ANA (Brazil)	'66895000'	'PORTO DA MANGA'	-19.258	-57.235
ANA (Brazil)	'66910000'	'MIRANDA'	-20.241	-56.396
ANA (Brazil)	'66941000'	'PALMEIRAS (JANGO)'	-20.448	-55.428
ANA (Brazil)	'66945000'	'AQUIDAUANA '	-20.459	-55.781
ANA (Brazil)	'66950000'	'PORTO CIRIACO'	-19.697	-56.281
ANA (Brazil)	'67100000'	'PORTO MURTINHO'	-21.700	-57.891
ANA (Brazil)	'67170000'	'SÃO CARLOS'	-22.224	-57.304
ANA (Brazil)	'71550000'	'PASSO CARU'	-27.538	-50.860
ANA (Brazil)	'72300000'	'PASSO DO VIRGILIO'	-27.501	-51.714
ANA (Brazil)	'73010000'	'MARCELINO RAMOS '	-27.461	-51.904
ANA (Brazil)	'73550000'	'PASSO CAXAMBU'	-27.171	-52.868
ANA (Brazil)	'74100000'	'IRAÍ'	-27.190	-53.265
ANA (Brazil)	'74800000'	'PORTO LUCENA '	-27.854	-55.023
ANA (Brazil)	'75550000'	'GARRUCHOS'	-28.183	-55.643
ANA (Brazil)	'75780000'	'PASSO SÃO BORJA '	-28.630	-56.039
ANA (Brazil)	'76310000'	'ROSÁRIO DO SUL '	-30.243	-54.916
ANA (Brazil)	'76500000'	'JACAQUA'	-29.686	-55.194
ANA (Brazil)	'76560000'	'MANOEL VIANA '	-29.596	-55.481
ANA (Brazil)	'76800000'	'PASSO MARIANO PINTO '	-29.308	-56.055
ANA (Brazil)	'77150000'	'URUGUAIANA '	-29.748	-57.089
ANA (Brazil)	'81350000'	'IPORANGA'	-24.585	-48.591
ANA (Brazil)	'83800002'	'BLUMENAU'	-26.918	-49.065
ANA (Brazil)	'85642000'	'PASSO SÃO LOURENÇO'	-30.009	-53.016
ANA (Brazil)	'85900000'	'RIO PARDO'	-29.996	-52.374
ANA (Brazil)	'86460000'	'MONTE CLARO'	-29.033	-51.517
ANA (Brazil)	'86470000'	'PONTE DO RIO DAS ANTAS'	-29.045	-51.567
ANA (Brazil)	'86510000'	'MUÇUM'	-29.166	-51.868
ANA (Brazil)	'86720000'	'ENCANTADO'	-29.234	-51.854
ANA (Brazil)	'87905000'	'PASSO DO MENDONÇA'	-31.010	-52.053
DGA (Chile)	'09140001-4'	'ALMAGRO'	-38.785	-72.952
DGA (Chile)	'10122001-K'	'BALSA SAN JAVIER'	-39.778	-72.990
DGA (Chile)	'05748001-7'	'CABIMBAO'	-33.724	-71.557
DGA (Chile)	'03450001-0'	'CIUDAD COPIAPO'	-27.369	-70.341
DGA (Chile)	'08141001-1'	'COELEMU'	-36.467	-72.694
DGA (Chile)	'08334001-0'	'COIHUE'	-37.550	-72.593

Data Provider	Code	Name	Latitude	Longitude
DGA (Chile)	'07383001-K'	'FOREL'	-35.410	-72.212
DGA (Chile)	'07359001-9'	'LAS BRISAS'	-35.617	-71.768
DGA (Chile)	'04558001-6'	'PANAMERICANA'	-30.667	-71.533
DGA (Chile)	'09437002-7'	'THEODORO SCHMIDT'	-39.020	-73.089
GRDC (Global Runoff Data Centre)	'330830'	'APAIKWA'	6.380	-60.380
GRDC (Global Runoff Data Centre)	'384410'	'D J SADE'	0.523	-79.415
GRDC (Global Runoff Data Centre)	'384440'	'LA CAPILLA'	-1.696	-79.996
IDEAM (Colombia)	'11057010'	'TAGACHI'	6.217	-76.717
IDEAM (Colombia)	'11057020'	'SAN ANTONIO PADUA'	6.283	-76.767
IDEAM (Colombia)	'21237010'	'NARIÑO AUTOM'	4.383	-74.850
IDEAM (Colombia)	'21237020'	'ARRANCAPLUMAS'	5.183	-74.717
IDEAM (Colombia)	'23037010'	'PTO SALGAR AUTOM'	5.467	-74.667
IDEAM (Colombia)	'23157080'	'MALDONADO'	7.200	-73.933
IDEAM (Colombia)	'23167010'	'PENAS BLANCAS'	6.950	-73.950
IDEAM (Colombia)	'23187280'	'SITIO NUEVO'	7.833	-73.800
IDEAM (Colombia)	'25027050'	'MARGENTO'	8.033	-74.950
IDEAM (Colombia)	'25027270'	'LAS FLORES'	8.117	-74.783
IDEAM (Colombia)	'25027330'	'PENONCITO'	8.983	-73.950
IDEAM (Colombia)	'25027640'	'TRES CRUCES'	8.700	-74.517
IDEAM (Colombia)	'25027940'	'TACAMOCHO'	9.483	-74.800
IDEAM (Colombia)	'26167070'	'IRRA'	5.267	-75.683
IDEAM (Colombia)	'26187110'	'LA PINTADA AUTOM'	5.733	-75.600
IDEAM (Colombia)	'26207030'	'PTE IGLESIAS'	5.817	-75.700
IDEAM (Colombia)	'26237050'	'PTE PESCADERO'	7.083	-75.700
IDEAM (Colombia)	'26237100'	'OLAYA'	6.650	-75.817
IDEAM (Colombia)	'26247030'	'APAVI'	7.483	-75.333
IDEAM (Colombia)	'29037020'	'CALAMAR'	10.250	-74.917
IDEAM (Colombia)	'31097010'	'GUAYARE'	3.967	-67.817
IDEAM (Colombia)	'32097010'	'MAPIRIPAN'	2.867	-72.167
IDEAM (Colombia)	'32107010'	'PTO ARTURO'	2.583	-72.700
IDEAM (Colombia)	'37057040'	'ANGELITOS LOS'	7.000	-71.100
IDEAM (Colombia)	'37057060'	'PTE INTERNACIONAL'	7.083	-70.767
IDEAM (Colombia)	'38017030'	'RONCADOR'	5.883	-67.567
IDEAM (Colombia)	'44137020'	'GUAQUIRA'	-0.333	-74.033
IDEAM (Colombia)	'44137080'	'PTO LAS BRISAS'	-0.583	-72.467
IDEAM (Colombia)	'44157010'	'MERCEDES LAS'	-0.533	-72.167
IDEAM (Colombia)	'44157030'	'MARIA MANTECA'	-1.400	-70.600
IDEAM (Colombia)	'44167020'	'STA ISABEL'	-1.133	-71.100
IDEAM (Colombia)	'44187010'	'PTO CORDOBA'	-1.267	-69.733
IDEAM (Colombia)	'44187030'	'BACURI'	-1.234	-69.470

Data Provider	Code	Name	Latitude	Longitude
IDEAM (Colombia)	'44197020'	'VILLAREAL'	-1.300	-69.617
INA (Argentina)	'1453"	'CARMENSA'	-35.185	-67.726
INA (Argentina)	'0693'	'POZO SARMIENTO'	-23.217	-64.200
INA (Argentina)	'2602'	'EL COLORADO'	-26.334	-59.362
INA (Argentina)	'3223'	'PUEBLO ANDINO'	-32.673	-60.866
INA (Argentina)	'2207'	'LOS ALTARES'	-43.889	-68.398
INA (Argentina)	'3249'	'RUTA NACIONAL Nº 168'	-31.661	-60.602
INA (Argentina)	'1801'	'PICHI MAHUIDA'	-38.821	-64.981
INA (Argentina)	'3803'	'PASO LUCERO'	-28.994	-58.561
INA (Argentina)	'3821'	'LOS LAURALES'	-29.757	-59.217
INA (Argentina)	'1219'	'EL ENCON'	-32.225	-67.807
INA (Argentina)	'1452'	'CANALEJAS'	-35.169	-66.495
INA (Argentina)	'2824'	'RUTA PROVINCIAL Nº 039'	-46.724	-69.593
INA (Argentina)	'3265'	'AUTOPISTA'	-32.393	-60.941
INA (Argentina)	'3004'	'ROSARIO DEL TALA'	-32.308	-59.077
INA (Argentina)	'2211'	'GUALJAINA'	-42.654	-70.439
INA (Argentina)	'0686'	'FINCA AGROPECUARIA'	-25.162	-64.105
INA (Argentina)	'0695'	'EL QUEBRACHAL'	-25.344	-64.046
INA (Argentina)	'3231'	'RUTA PROVINCIAL Nº 32'	-28.491	-59.388
INA (Argentina)	'3804'	'PASO LEDESMA'	-29.846	-57.675
INA (Argentina)	'2004'	'PASO DE INDIOS'	-38.532	-69.413
INA (Argentina)	'2401'	'PUERTO BERMEJO'	-26.926	-58.507
INA (Argentina)	'2606'	'PUERTO PILCOMAYO'	-25.420	-57.651
INA (Argentina)	'0631'	'LA PAZ'	-22.378	-62.523
INA (Argentina)	'0804'	'SUNCHO CORRAL'	-27.950	-63.433
INA (Argentina)	'0810'	'CANAL DE DIOS'	-25.630	-63.949
INA (Argentina)	'0811'	'RUTA PROVINCIAL Nº 092 - AÑATUYA'	-28.503	-62.881
INA (Argentina)	'3126'	'RUTA PROVINCIAL Nº 070'	-31.491	-60.781
INA (Argentina)	'0470'	'RUTA PROVINCIAL Nº 323'	-27.133	-65.316
INA (Argentina)	'0016'	'CAIMANCITO'	-23.733	-64.467
INA (Argentina)	'0471'	'RUTA PROVINCIAL Nº 157'	-27.336	-65.317
INA (Argentina)	'2297'	'LOS MOLINOS'	-45.991	-69.500
INA (Argentina)	'3339'	'SANTA FE - LA GUARDIA'	-31.630	-60.678
INA (Argentina)	'3340'	'FLORENCIA'	-28.029	-59.225
INA (Argentina)	'0637'	'SAN TELMO'	-22.571	-64.240
ONS (Brazil)	-	'A. VERMELHA'	-19.863	-50.346
ONS (Brazil)	-	'A.A. LAYDNER'	-23.210	-49.230
ONS (Brazil)	-	'A.S. LIMA'	-22.153	-48.753
ONS (Brazil)	-	'AIMORÉS'	-19.498	-41.024
ONS (Brazil)	-	'B. COQUEIROS'	-18.722	-51.003
ONS (Brazil)	-	'B. ESPERANCA'	-6.754	-43.563
ONS (Brazil)	-	'BAGUARI'	-19.022	-42.125

Data Provider	Code	Name	Latitude	Longitude
ONS (Brazil)	-	'BARRA BONITA'	-22.519	-48.534
ONS (Brazil)	-	'BARRA GRANDE'	-27.780	-51.192
ONS (Brazil)	-	'CACHOEIRA DOURADA'	-18.504	-49.490
ONS (Brazil)	-	'CACU'	-18.532	-51.149
ONS (Brazil)	-	'CAMPOS NOVOS'	-27.604	-51.327
ONS (Brazil)	-	'CANA BRAVA'	-13.402	-48.143
ONS (Brazil)	-	'CANOAS I'	-22.941	-50.517
ONS (Brazil)	-	'CANOAS II'	-22.938	-50.251
ONS (Brazil)	-	'CAPIM BRANCO I'	-18.789	-48.149
ONS (Brazil)	-	'CAPIM BRANCO II'	-18.659	-48.437
ONS (Brazil)	-	'CAPIVARA '	-22.655	-51.357
ONS (Brazil)	-	'CHAVANTES'	-23.128	-49.733
ONS (Brazil)	-	'COARACY NUNES'	0.903	-51.259
ONS (Brazil)	-	'COMP PAF'	-9.396	-38.202
ONS (Brazil)	-	'CORUMBÁ I'	-17.988	-48.532
ONS (Brazil)	-	'CORUMBÁ III'	-16.788	-47.935
ONS (Brazil)	-	'CURUÁ-UNA'	-2.812	-54.299
ONS (Brazil)	-	'D. FRANCISCA'	-29.449	-53.285
ONS (Brazil)	-	'DARDANELOS'	-10.159	-59.453
ONS (Brazil)	-	'EMBORCAÇÃO'	-18.452	-47.985
ONS (Brazil)	-	'ESTREITO'	-20.151	-47.280
ONS (Brazil)	-	'ESTREITO TOCANTINS'	-6.589	-47.466
ONS (Brazil)	-	'FOZ CHAPECÓ'	-27.139	-53.044
ONS (Brazil)	-	'FOZ DO AREIA'	-26.010	-51.666
ONS (Brazil)	-	'FOZ DO RIO CLARO'	-19.117	-50.646
ONS (Brazil)	-	'FUNIL (Paraiba do Sul)'	-22.529	-44.568
ONS (Brazil)	-	'FUNIL (Grande)'	-21.143	-45.036
ONS (Brazil)	-	'FURNAS'	-20.669	-46.318
ONS (Brazil)	-	'GARIBALDI'	-27.626	-50.985
ONS (Brazil)	-	'IBITINGA'	-21.759	-48.991
ONS (Brazil)	-	'IGARAPAVA'	-19.989	-47.756
ONS (Brazil)	-	'ILHA DOS POMBOS'	-21.852	-42.608
ONS (Brazil)	-	'IRAPÉ'	-16.738	-42.575
ONS (Brazil)	-	'ITÁ'	-27.277	-52.382
ONS (Brazil)	-	'ITAIPU '	-25.408	-54.587
ONS (Brazil)	-	'ITAPARICA'	-9.144	-38.312
ONS (Brazil)	-	'ITAPEBI'	-15.966	-39.593
ONS (Brazil)	-	'ITAÚBA'	-29.261	-53.236
ONS (Brazil)	-	'ITUMBIARA'	-18.407	-49.099
ONS (Brazil)	-	'JAGUARA'	-20.023	-47.434
ONS (Brazil)	-	'JUPIÁ '	-20.776	-51.627
ONS (Brazil)	-	'LAJEADO'	-9.757	-48.372

Data Provider	Code	Name	Latitude	Longitude
ONS (Brazil)	-	'M. DE MORAES'	-20.286	-47.064
ONS (Brazil)	-	'MACHADINHO'	-27.527	-51.790
ONS (Brazil)	-	'MARIMBONDO'	-20.303	-49.198
ONS (Brazil)	-	'MASCARENHAS'	-19.500	-40.918
ONS (Brazil)	-	'MAUA'	-24.062	-50.706
ONS (Brazil)	-	'MIRANDA'	-18.910	-48.041
ONS (Brazil)	-	'MONTE CLARO'	-29.031	-51.521
ONS (Brazil)	-	'MOXOTO'	-9.358	-38.208
ONS (Brazil)	-	'NOVA AVANHANDAVA '	-21.119	-50.201
ONS (Brazil)	-	'NOVA PONTE'	-19.133	-47.697
ONS (Brazil)	-	'OURINHOS'	-23.068	-49.838
ONS (Brazil)	-	'P. AFONSO'	-9.416	-38.208
ONS (Brazil)	-	'P. CAVALO'	-12.584	-38.998
ONS (Brazil)	-	'P. COLOMBIA'	-20.124	-48.572
ONS (Brazil)	-	'P. PRIMAVERA'	-22.476	-52.959
ONS (Brazil)	-	'PASSO SÃO JOÃO'	-28.142	-55.052
ONS (Brazil)	-	'PEIXE ANGICAL'	-12.235	-48.386
ONS (Brazil)	-	'PIRAJÚ'	-23.154	-49.380
ONS (Brazil)	-	'PROMISSÃO'	-21.296	-49.783
ONS (Brazil)	-	'RETIRO BAIXO'	-18.878	-44.781
ONS (Brazil)	-	'ROSANA'	-22.600	-52.869
ONS (Brazil)	-	'SALTO'	-18.808	-51.171
ONS (Brazil)	-	'SALTO CAXIAS'	-25.543	-53.498
ONS (Brazil)	-	'SALTO OSÓRIO'	-25.538	-53.009
ONS (Brazil)	-	'SAMUEL'	-8.751	-63.454
ONS (Brazil)	-	'SANTO ANTÔNIO'	-8.797	-63.952
ONS (Brazil)	-	'SÃO SALVADOR'	-12.808	-48.238
ONS (Brazil)	-	'SÃO SIMÃO'	-19.018	-50.499
ONS (Brazil)	-	'SEGREDO'	-25.790	-52.112
ONS (Brazil)	-	'SERRA DA MESA'	-13.834	-48.305
ONS (Brazil)	-	'SERRA FACÃO'	-18.046	-47.675
ONS (Brazil)	-	'SLT. SANTIAGO'	-25.629	-52.615
ONS (Brazil)	-	'SLT. VERDINHO'	-19.143	-50.754
ONS (Brazil)	-	'SOBRADINHO'	-9.430	-40.827
ONS (Brazil)	-	'STA CECILIA'	-22.481	-43.839
ONS (Brazil)	-	'STA CLARA'	-17.896	-40.202
ONS (Brazil)	-	'STO ANT JARI'	-0.641	-52.507
ONS (Brazil)	-	'TAQUARUÇU'	-22.544	-52.000
ONS (Brazil)	-	'TELES PIRES'	-9.349	-56.779
ONS (Brazil)	-	'TRÊS IRMÃOS'	-20.669	-51.300
ONS (Brazil)	-	'TRÊS MARIAS'	-18.215	-45.259
ONS (Brazil)	-	'TUCURUÍ'	-3.832	-49.643

Data Provider	Code	Name	Latitude	Longitude
ONS (Brazil)	-	'VOLTA GRANDE'	-20.033	-48.222
ONS (Brazil)	-	'XINGÓ'	-9.620	-37.793
ORE-HyBam	'10064000'	'BORJA'	-4.470	-77.548
ORE-HyBam	'10080900'	'FRANCISCO DE ORELLANA'	-0.473	-76.983
ORE-HyBam	'10099800'	'NAZARETH'	-4.121	-70.036
ORE-HyBam	'10100000'	'TABATINGA'	-4.250	-69.933
ORE-HyBam	'13870000'	'LABREA'	-7.252	-64.800
ORE-HyBam	'14100000'	'MANACAPURU'	-3.308	-60.609
ORE-HyBam	'14710000'	'CARACARAI'	1.821	-61.124
ORE-HyBam	'14840000'	'MOURA'	-1.456	-61.633
ORE-HyBam	'15275100'	'RURRENABAQUE'	-14.445	-67.534
ORE-HyBam	'15400000'	'PORTO VELHO'	-8.737	-63.920
ORE-HyBam	'15860000'	'BORBA'	-4.897	-60.025
ORE-HyBam	'17050001'	'OBIDOS'	-1.947	-55.511
ORE-HyBam	'17730000'	'ITAITUBA'	-4.283	-55.983
ORE-HyBam	'30030000'	'LANGA TABIKI'	4.986	-54.437
ORE-HyBam	'30055000'	'SAUT MARIPA'	3.802	-51.885
ORE-HyBam	'40800000'	'CIUDAD BOLIVAR'	8.143	-63.607
SENAMHI/Peru	'10043000'	'PICOTA'	-6.955	-76.369
SENAMHI/Peru	'10043600'	'CHAZUTA'	-6.578	-76.129
SENAMHI/Peru	'10046000'	'PUCALLPA'	-8.382	-74.522
SENAMHI/Peru	'10070500'	'SAN REGIS'	-4.507	-73.920
SENAMHI/Peru	'10074800'	'REQUENA'	-5.010	-73.820
SENAMHI/Peru	'10075000'	'TAMSHIYACU'	-4.003	-73.161
SENAMHI/Peru	'10082800'	'NUEVO ROCAFUERTE'	-0.916	-75.396
SENAMHI/Peru	'10086800'	'BELLAVISTA'	-3.487	-73.084
SENAMHI/Bolivia	'15230200'	'PUERTO VILLAROEL'	-16.836	-64.799
SENAMHI/Bolivia	'15233000'	'CAMIACO'	-15.334	-64.866
SENAMHI/Bolivia	'15242000'	'PUERTO SILES'	-12.804	-65.003
SENAMHI/Bolivia	'15250010'	'GUAYARAMERIN'	-10.812	-65.343
SENAMHI/Bolivia	'15289800'	'MIRAFLORES'	-11.108	-66.411
SENAMHI/Bolivia	'15290000'	'PENAS AMARILLAS'	-11.550	-66.667
SENAMHI/Bolivia	'15292000'	'RIBERALTA'	-11.000	-66.078
SENAMHI/Bolivia	'15295500'	'CACHUELA ESPERANZA'	-10.538	-65.572
SENAMHI/Bolivia	'15312000'	'EL SENA'	-11.470	-67.237